Modeling and Stability Analysis of Nine Phase Induction Machine for Hybrid Generation System

by

Taiwo Samuel Ajayi

B.Eng, M.Sc(Elect)

A thesis presented in fulfilment of the requirements

for the degree of Doctor of Philosophy

Wind Energy and Control Centre

Deparment of Electronics and Electrical Engineering

University of Strathclyde, Glasgow

G1 1XW

April 26, 2024

Dedication

I dedicate this thesis to Almighty God, my mum Deborah Ajayi and my late Dad Zacchaeus Ajayi Ibitolu, through them, I draw my first breath of life.

I dedicate this thesis to Habibatu Ajayi and my Children: Bryan,Isabella and Michelle.

Abstract

A model for a nine-phase induction machine using the method of natural variables was studied. A general model which combines the model of a nine-phase induction machine, converter systems and battery energy system is developed. Steady state equations from this model were derived and studied. Approaches to series and parallel converter configurations to voltage source were investigated. Stability analysis of wind turbine system for nine phase, three phase and DFIG induction generator was conducted and reported. New findings show the stability boundary of each respective machine.

In addition, a novel analytical approach to determine the leakage winding inductance of a multi-phase induction machine was investigated for a symmetric and asymmetric nine phase induction machine, using the multiple $d - q$ and vector space decomposition as basis of comparison for the two-machine configuration, an issue commonly overlooked in the scientific literature. On an elaborated scale, the leakage inductance for different inductance subspace of the multiple-phase induction machine for each modelling approach was derived.

The interrelation of the machine pitch factor, leakage inductance of the top and bottom conductor of a double layer windings in a multiphase induction machine, and how these variables affect the leakage flux, a component which is the cause of losses in the $x - y$ subspace of a multi-phase induction machine is investigated and findings discussed. A new metric based on per unit for quantifying the flux density contribution from each winding set of a multiple-set phase induction machine that is simple, intuitive, and well-defined for both motoring and generating mode is also presented. Graphical plots, which show different expected contributions from different machine windings operational scenarios are included and analysed.

List of Symbols

d_i: i_{th} d-axis component

q_i: i_{th} q-axis component

ξ: disposition angle between winding set of asymmetrical Induction machine

θ_r: rotor angle

θ: synchronous angle

ω_r: rotor electrical speed in $rads^{-1}$

ω: synchronous speed in $rads^{-1}$

ω_g: Load point synchronous speed in $rads^{-1}$

n_r: number of rotor bars

v_{qdsi}: stator qds voltage for the ith stator set

v_{qdr}: rotor qdr voltage

i_{qdsi}: stator qds current for the ith stator set

i_{qdr}: rotor qdr current

λ_{qdsi}: stator qds flux linkage for the ith stator set

λ_{qdr}: rotor qdr flux linkage

$a_i b_i c_i$: phase projection notations for specific set of three phase windings

λ_s: stator flux linkage magnitude

λ_{si}: i^{th} stator flux linkage magnitude for the ith stator set

L_{lsi}/L_{lr}: leakage inductance for specific stator set and leakage inductance for rotor

L_{lm}: mutual inductance between winding set

L_m: magnetising inductance

T_s: Transformation matrix for the stator i^{th} set

T_{rr}: Transformation matrix for the rotor

Chapter 0. List of Symbols

T_e: electromagnetic torque

T_{e_i}: i^{th} electromagnetic torque for i^{th} set stator winding

T_r: reactive torque

T_{r_i}: i^{th} reactive torque for i^{th} set stator winding

$\dot{x}$: first derivative of the variable 'x'

$\mathbb{R}$: The real number

$\mathbb{M}$ smooth manifold

$\mathbb{C}$ subspace for defined vector plane

List of Abbreviations

GHG: Green house gases

NECPs: National Energy and Climate Plans (NECPs)

WECS: Wind Energy Conversion System

DG: Distributed generation

DES: Distributed energy system

DFIG: Doubly fed induction machine

MMF: Magneto-motive force

9P6T: Nine Phase Six Terminal

WF: Winding Function

V2G: Vehicle to grid

VSI: Voltage source inverter

VSD: Vector space decomposition

MS: Multi-stator

IRFOC: Indirect rotor flux-oriented control

PWM: Pulse width modulation

CBPWM: carrier-based pulse width modulation

SVPWM: Space vector pulse width modulation

SISO: Single input single output

MIMO: Multiple input multiple output

TF: Turn function

WF: Winding function

IOL: Input-Output Linearization

IODC: Input-Output decoupling control

Chapter 0.   List of Abbreviations

VC: Vector Control

2D: two dimension

$9T_{9asy3}$: Nine phase with isolated neutral transformation matrix

T_{9asy1}: Nine phase with single neutral transformation matrix

Contents

Contents

Contents

Contents

Contents

List of Figures

xiii

List of Figures

List of Figures

List of Figures

List of Figures

List of Tables

Acknowledgements

I would like to acknowledge a lot of contributors to these my research work. Firstly, I give God the glory for seeing me through the years of this PhD research. He alone gives health, wisdom, understanding and directions. I will also want to appreciate my supervisor, Prof. Olimpo Anaya-Lara with a heart that can accommodate nations. His quality of decision for my PhD to see the light of the day is highly acknowledge. I want to thank him for his patience, thoughtful guidance and thought provoking discussions in the course of this research work. I want to thank you for your promising approach to meet my needs in times of difficulty. Thank you for the training, as well as granting me this marvelous and strenuous learning experience. In your words *"I want to see you happy and succeeding, you have the vision of your future self"*. Your support charge me up and makes this research interesting and a strong contender in publish similar works in the area of this research. To this, I say I am grateful.

I want to dedicate this work to my parents and my siblings for their prayers, in the course of this work. To my Dad Zacchaeus Ajayi Ibitolu, whom I miss dearly, Death could not allow you to see this day, that I stand to defend my years of toil of this research work. I know you will be proud in heaven, for this success. To my mum, I do appreciate you for your doggedness, your steadfast prayers right from my childhood to present, to see that I succeed. You are highly appreciated and honoured mum. To my siblings Mrs Florence Thomas, Mary Ajirenike and Femi Ajayi, you are highly appreciated for all your prayers.

I wish to use this medium to recognize and thank my wife, Habibatu Ajayi and my wonderful kids: Bryan, Isabella and Michelle, for their great forbearance and good humour to give me the courage, when the spirit is down to pen down ideas, during

the course of this research, you are a God sent to give me all the moral support from conception of my initiative to start this PhD journey, till this end today. To my wife, I appreciate and acknowledge all you efforts and support to the family. I owe you alot for helping to restrain my kids from distracting me in my study room. God bless you for me.

I want to thank Dr. Raphael Pena Alzola, for his tutorial lessons on power electronics, helpful discussion and support during the course of my PhD and all through the Covid 19 pandemic. Your tutorial lessons helped me alot. I want to also thank Dr. David Campos for their immense support and Prof. Khaled Ahmed, for his encouragement. Not forgetting to thank my supportive friends; Dr. Adedayo Asaolu, and Dr. Fyali Jibji-Bukar, Dr. Isaac Owusu, with whom we share our PhD journey experiences via walking to city centre to unwind the stress. My thanks goes to Dr. Philip Adams for his supports and advice. You all are appreciated.

I also want to use this opportunity to appreciate Prof. Olorunfemi Ojo, My Msc supervisor. Your mentee is forever grateful for all your efforts and supports in shaping me to be a good researcher. God bless you so much. I also want to thank members and staff of Department of Electrical Engineering, Ahmadu Bello University Zaria, Nigeria. I want to thank all friends and well wishers for all their effort, space constraint will not allow me to list your names. But take these from me, you all have been part of the success today, and you are greatly acknowledged.

Lastly, I wont forget to appreciate and thank the petroleum Technology Development Fund (PTDF), Abuja Nigeria for sponsoring me to go for a PhD studies at University of Strathclyde, Wind and Energy Control group. I can't thank you less for all your efforts, morally, financially to me and several of my colleagues you sponsored across the UK institutions. I join thousands of them you have sponsored in the past and present, to say a big thank you.

In my closing remark, for this section, thank you, Department of Electronics and Electrical Engineering, University of Strathclyde for the rigorous training for all the years of the PhD studies. Thank you all.

Chapter 0.   Acknowledgements

Chapter 1

Introduction

Research on multiple-phase electric machines and drives systems is creating solutions for the energy transformation from electro-mobility systems to power generation systems. The interest in multiple-phase induction machines as the preferred choice of power conversion has grown in the past decade, as intense analysis and experimentation in the recent past have proven its viability. Presently, the world craves for a clean, affordable energy supply, while cutting down on the carbon footprint and ensuring a net carbon zero reduction to about 21.2 gigaton by year 2050 [1, 2]. Different topologies of multi-phase induction machines have been deployed in different application areas: wind energy conversion system [3], ship propulsion [4], hybrid electric vehicle [5, 6], more electric aircraft [7], elevator [8] e.t.c. The world is paying a lot more attention to wind electricity now, so isolated power grids (IPGs) powered by wind turbines are commonly used to meet the electricity needs of sparsely populated and industrialised regions because they cut down on high-voltage tranmission line building costs and transmission congestion between regions.

Multiple-phase induction machines are becoming more and more integrated into the application areas in the opening synopsis to this chapter, as electric machines with multiple winding sets offer the possibilities of more flexible energy conversions consisting of multiple interconnected non linear units such as power electronic converters, renewable energy sources unit e.t.c. These strong interactions between these interfaced units greatly complicate inherent system's characteristics and further change the stud-

ied system dynamics. This leads to poor control performances and compromises the entire system operations. To ensure a robust operation of the connected multi-phase induction machine to power electronic units, it is important to recognize these inherent characteristics that could lead to mal-operation. The usual studied subjects of interest, include machine design, steady-state and transient performance study, performance limitations, voltage or power regulation schemes among others [9–11].

It is generally believed that the accuracy of the design features of these key components, can be improved through the successive modeling refinement. With a focus of these salient features, this thesis seeks to investigate the modeling of a nine-phase induction machine and it sub assembly. The approach seeks to model the multiple set windings using the method of *natural variable technique*. The study investigates modeling of a nine phase induction machine, model of a converter/rectifier system, battery energy system and a load. Variations in the inherent system characteristics of this studied system over feasible operating regions are studied and analyzed. Stability analysis of variant induction machine model was studied. Figure 1.1 shows the benefit of multiple-phase induction machine.

Figure 1.1: Benefit of Multiphase Electric Machines.

1.1 Problem Statement

In a time characterised by the advancement of technology and the quest for environmentally-friendly energy alternatives, the impact of electrical engineering on our global landscape is increasingly significant. In the realm of electrical energy conversion, multiphase induction machines are recognised as enduring fixtures. These machines exhibit exceptional efficiency in the conversion of electrical power to mechanical work and vice versa [12]. The indispensability of these machines across diverse industries, ranging from manufacturing to renewable energy generation, can be attributed to their remarkable adaptability.

Electric machines with multiple set of three phase windings have been an inclusive electromagnetic component part demonstrated to be vital promising solution for meeting the net zero carbon footprint target. From HEV, Ship propulsion, wind energy conversion systems and multi-directional power flow systems. This multiple phase electric machines when included in DG systems or distributed energy systems (DES) with other sources of energy, offer great energy support, exchanging the energy between sources and the load. DES are highly supported by the global renewable energy drive as most DES especially in off-grid applications are renewables-based. DES can employ a wide range of energy resources and technologies and can be grid-connected or off-grid. Renewable technologies, contributing to most of the global distribution generation, are becoming efficient, flexible in terms of deployment, and economically competitive with conventional energy systems. Multiple phase induction machine use as a generator or motor with other energy sources is becoming an active area of research. Researchers have examined distributed generation from various perspectives [13]. Gomes *et al* [14], for example have explored the role of distributed generation systems in potential future electricity scenarios. Recently, it has been shown [15] that additional compatibility conditions are required to ensure good multi-directional power flow in an integrated multi-drives systems consisting of a nine phase induction machine. Here, an Induction machine, used with a starter alternator was used to demonstrate the viability of prototype capabilities for multi-directional power flow, where all solutions obtained

must satisfy a power sharing strategy. For multi-directional power control using smart electric vehicle charging stations, interfaced to EV battery, energy storage systems [16] has shown that the system they built can handle a variety of dc sources including different energy sources. Abdullah *et al* [17] emphasize a utilization of double winding six phase induction machine winding sets for efficient multi-directional power control. The stability of renewable energy sources connected to multiport interface systems was exemplified in [18]. In all these work the issues pertinent to effect of leakage inductance arising from coupling of the windings for symmetrical and asymmetrical configurations and issues of stability of the multiple phase induction machine was not discussed. The intermediate situation arising from highly coupled sub-windings handling was brought forward in the work of [19]. Such solution candidate presented by their work neither accounted for the relationship of the leakage inductance and pitch factors for the two known winding configurations(i.e symmetrical and asymmetrical) of multiple- phase induction machine, and the potential impact of the low leakage inductance in the high frequency subspace, drawing inferences as to which of the winding configuration offers the least current flow in the high frequency subspace. In addition, their airgap flux distribution.

This thesis undertakes a comprehensive modeling into this study, examining crucial elements of this intricate terrain. The primary focus of this research is dedicated to the thorough modelling and investigation of the stability of multiphase induction machines in hybrid systems. Simultaneously, it addresses a persistent problem that has adversely affected the operational efficiency of these devices, namely the issue of leakage inductance.

1.2   Aim and Objectives

1.2.1   Aim

The study gives detailed insight in to new approach of modeling the leakage inductance of multiple phase induction machine configure for two winding configurations (i.e symmetrical and asymmetrical). Knowledge gained from this study will help designers

and manufacturers understand the stability of multiple phase induction machine in comparison with other known conventional three phase induction machine, and to quantitatively and qualitatively select a modeling approach that best minimize the circulating current in the $x - y$ subspace, which can help improve the efficiency of the multiple phase induction machine.

1.2.2 Objectives

The research objectives have been meticulously defined to achieve this aim.

1) To develop a comprehensive model for the systems, which are dynamic state entities combining multiphase induction machines, rectifiers, battery energy systems, inverters, and load systems. The model should accurately represent their dynamic states and clearly show the link from one subsystem model to another.

2) To use the natural variable technique to model the system equations for the studied nine phase induction machine.

3) To carry out comprehensive steady-state analysis on the dynamic states of the system model equations and hence establish a steady-state equation relation connecting the systems.

4) To compare by performing a stability analysis on three phase induction machine, nine phase induction machine and DFIG wind turbine system. This understanding will help to predict stability of the system.

5) To conduct analytical field analysis studies on a nine-phase induction machine and determine the magnetic field distribution contribution for each winding set. This will help achieve balanced operation without saturating the core material. Both symmetrical and asymmetrical windings will be considered and compared.

6) To develop an algorithm to determine the inductance of a nine-phase induction machine based on Turn function and winding function approach

7) To conduct a comprehensive analysis of leakage inductance in multiple-phase induction machines. Leakage inductance is a pervasive issue in these machines, and understanding its causes, distribution patterns, and ramifications on machine performance is crucial.

This analysis will provide insights into the nature of leakage inductance for symmetrical and asymmetrical winding nine-phase induction machine and to justify suppressing the circulating current in the $x_i - y_i$ subspace and its impact on machine operation.

8) To compare symmetrical and asymmetrical induction machine topologies using various modeling techniques. The goal is to identify the topology that minimizes circulating currents, which are worsened by leakage inductance.

1.3   Research Scope

This research focuses on modeling and stability analysis of multiphase induction machines wind turbine system in hybrid systems using natural variable techniques. It uses real and reactive power, electromagnetic torque, reactive torque,and square of the magnitude of the stator flux as system variables. The model equations developed for the wind turbine system and multiple phase induction machine, are used to check the stability of the model. The study explore the flux distribution in the airgap for aymmetrical and symmetrical multiple phase induction machine. The study also focuses on the challenges of leakage inductance in multiple-phase induction machines and examines symmetrical and asymmetrical machine topologies using multiple modeling techniques.

1.4   Research Limitation

The research focuses on multiple-phase induction machines in specific hybrid system configurations, but different designs and architectures may have different results. Implementing the strategies in large-scale industrial applications may face practical limitations. The research aims to provide comprehensive insights, but may not cover every operational scenario or system configuration.

1.5   Thesis Contributions

This research makes significant contributions in the field of hybrid systems, specifically focusing on stability analysis of wind turbine system of variant induction machine and

the role of multiphase induction machines. The use of the natural variable technique comes with great simplicity to system equations using vector space decomposition approach, as the multiple $d - q$ approach comes with great complexities in the developed model equations. The study also delves into steady-state analysis, of multiple phase induction machine providing valuable insights for system engineers.

Great effort to exploit the flux distribution in the air-gap of two winding configurations (i.e symmetrical and asymmetrical) of multiple-phase induction machine as a function of peak air-gap flux density was analyzed. Compelling contour plot results shows their peak flux variations differ.

For the first time, the relationship between mutual leakage induction, pitch factors, and current from other sets in the multiple $\alpha - \beta$ frame is derived for a nine-phase induction machine. A graphical comparison and investigation of the relationships between the two machine types (symmetrical and asymmetrical) are conducted.

The research also investigates an un-discussed phenomenon of leakage inductance for symmetrical and asymmetrical induction machine, exploring its causes, distribution, and implications on machine performance. Additionally, a comparative analysis of symmetrical and asymmetrical induction machine topologies is conducted using multiple modeling techniques, offering guidance for machine designers and manufacturers. Overall, this research aims to enhance the efficiency, reliability, and practicality of hybrid systems in various applications, benefiting both academia and the industrial sector.

1.6   Chapter overview

This thesis is divided into seven chapters outlined in the following form:

Chapter 1: Introduction

This chapter sets the stage by introducing the research problem, highlighting the integration of multiphase induction machines into hybrid systems and the challenges it poses, especially related to stability and leakage inductance.

The research objectives and significance outlines the research objectives, emphasizing the aim to model system stability and mitigate leakage inductance issues. It also discusses the significance of the research in the context of electrical engineering and the broader

Chapter 1. Introduction

industrial landscape.

The scope and limitations of the research are defined, emphasizing the focus on specific system configurations and the challenges associated with scalability. Last part of this chapter provides a preview of the contributions expected from the research, including advancements in stability analysis, innovative modeling techniques, and insights into leakage inductance mitigation.

Chapter 2: Background and Literature Review

This chapter starts by providing a comprehensive overview of multi-phase induction machines, their operation, and their significance in various application areas. Next, various modeling techniques relevant to the research, including multiple-phase machine model equations, $d - q$ models, and the vector space decomposition(VSD) model was elaborated. Moreover, concept of hybrid systems, discussing their components, benefits, and the challenges associated with their design and operation are included. A brief review explores leakage inductance in multi-phase induction machines, its causes, and its implications on machine performance. A thorough review of existing literature on topics related to stability analysis, modeling approaches, and leakage inductance mitigation sets the context for the research.

Chapter 3: Modeling Hybrid Systems This chapter focuses on the development of a comprehensive model for hybrid systems, encompassing multiphase induction machines, rectifiers, battery systems, inverters, and loads. The modeling approach is explained in detail, emphasizing the challenges and complexities involved. The application of the natural variable technique is discussed, showcasing how real and reactive power, electromagnetic torque, reactive torque and square of the magnitude of stator flux variables are used in the model equation. Also, steady-state analysis within hybrid systems is shown.

Chapter 4: The dynamic state equations of the system are transformed into state space form, enabling systematic exploration of system behavior and dynamics. Stability boundary analysis on the wind turbine system was carried out for different topologies of wind turbine generator systems. Steady state equation of the system are developed and the relationship between variables of interest established.

9

Chapter 1. Introduction

Chapter 5: Field Analysis of two winding topology of multiple phase induction machine is studied. First, the chapter carries out an mmf analysis on a nine phase induction machine, and clearly shows how multiple-phase induction machine improve mmf waveform magnitude. Next two machine winding configuration (symmetrical and asymmetrical) for nine-phase induction machine in terms of their airgap flux density was derived. Flux density map as each of the winding flux are varied is shown for both machine winding configurations and conclusion is then given on what to take note of when both machine configuration are been deployed for an operation

Chapter 6: This chapter starts by discussing the determination of multiple-phase induction machine inductance based on turn function and winding function approach. An algorithm is then developed to determine the turn function and winding function of the nine-phase induction machine. Next, a comprehensive analysis of leakage inductance ascribed to multiphase induction machines is then developed. The derived analysis investigates and establish relationships of the leakage inductances in terms of the pitch factor, top and bottom leakage inductances and mutual inductances for different subspaces of the nine phase induction machine. More so, a comparative analysis of symmetrical and asymmetrical induction machine topologies, an un-discuss issues in the open literature is presented, utilizing multiple modeling techniques. The goal is to determine which amongst the modeling topologies minimizes circulating currents, exacerbated by leakage inductance.

Chapter 7: This chapter delves into a comprehensive discussion of the research findings, drawing connections between stability analysis and leakage inductance mitigation. The implications of the research findings for practical applications in industries are explored, showcasing how the research contributes to the field of electrical engineering. The chapter concludes by summarizing the key findings, contributions, and their broader significance.

Future Work This chapter identifies potential avenues for future research, including enhancements to modeling techniques, further exploration of hybrid system components, and advanced leakage inductance mitigation strategies.

1.7 Publications

1.7.1 Contribution to conference

- T. S. Ajayi and O. Anaya-Lara,"Modeling, Analysis of Current Trajectories of a Nine Phase Induction Machine for Regenerative Capabilities," 2019 IEEE PES/IAS PowerAfrica, Abuja, Nigeria, 2019, pp. 1-4, doi: 10.1109/PowerAfrica46609.2019.9078671.

- T. S. Ajayi, G. Adam, D. C. Gaona and O. Anaya-Lara, "Determination of an Asymmetrical Nine Phase Induction Machine Stator and Rotor Inductances Using Winding Function Approach," 2023 IEEE Workshop on Electrical Machines Design, Control and Diagnosis (WEMDCD), Newcastle upon Tyne, United Kingdom, 2023, pp. 1-6, doi: 10.1109/WEMDCD55819.2023.10110904.

1.7.2 Contribution to Journal

- T. S. Ajayi, G. Adam, D. C. Gaona and O. Anaya-Lara, "Comprehensive Comparison of Multiple-Phase Induction Machine leakage Inductance evaluation for current suppression based on Multiple $d - q$ and Vector Space Decomposition approach" ***to be Submitted*** to IEEE transaction on Magnetics Journal.

- T. S. Ajayi, G. Adam, D. C. Gaona and O. Anaya-Lara, "Modeling and Comprehensive Steady state Analysis of a Nine phase Induction Machine rectifier and battery energy storage system ***to be Submitted*** to Energies Journal Special Issue on"Mathematical Modelling and Numerical Analysis in Electrical Engineering" in Mathematics (IF = 2.4, ISSN 2227-7390)

Chapter 2

Literature Review

In today's world, variable-speed applications make extensive use of three-phase drives in a variety of different industries. However, a large number of new electric drive applications are investigating the usage of machines with more than three phases. This multiple phase induction machine of various types: induction and permanent magnet machines types are usually implemented in the same stator slots, of the electric machine. The flagship of this novel machines has added confidence to how they are studied. This is being done for a variety of reasons, including enhanced fault tolerance, lower inverter power rating per phase, and so on. This chapter offers a comprehensive presentation of the technique for modelling a machine as well as the models that come from that procedure for any number of phases. A review of related and similar works with respect to multiphase induction machine inverter-supplied or generator inverter drive systems that include sinusoidal magneto-motive force distribution is discussed. In addition to that, it provides a comprehensive summary of various converter connection topologies interfaced to these multiphase machines, current control methodologies, winding alterations for meaningful applications and stability criterion for the multiple set winding machine. The chapter concludes, by highlighting the idea and problems this thesis addresses. Through out this thesis, the synonym **'nine'** phase induction machine and **'tri-three'** phase induction machine will be used interchangeable to mean the same thing.

Chapter 2. Literature Review

2.1 Introduction

The advent of power electronics devices and its application, which eliminated the technical hurdles impeding the early development of multiple set winding induction machines and its related control systems, significantly improved the research study into multiphase induction machines. The development of power electronics systems and devices has made it possible to create converters with any phase number greater than three. Power electronic devices have continuously changed the methods and approaches to numerous new circuit topologies and drives, resulting from evolving electrical energy sources and cutting-edge multiphase electric machines [20–22]. Recently, there has been a major increase in interest in the applications of multiphase induction machines for hybrid electric vehicles. [23, 24], more electric aircraft [25, 26], ships electric drive system [27–29], wind energy conversion system [30, 31]. The authors in [32–34] give a comprehensive review of multiphase electric machine and various application areas. Modeling knowledge in the field of multi-phase induction machine research is quite mature and saturated in this day and age; however, new innovative topological winding configurations deployed to these novel electric machines, as well as ingenious topological winding application, have revolutionised the interest of researchers in the field, in order to determine to what extent the multiple phase (or multiple winding set) induction machine windings could be use for beneficial applications. Such progress has put forward a new machine winding layout, as well as intermediate energy sources circuit re-modification to achieve outstanding benefits. It appears, however, that the applications of this new fashioned topologies of machine windings have not been well exploited. Most studies have often been limited to single and three phase systems. To the knowledge of the author, publications which discuss innovative use of multiple set windings for technical and economic benefit to extract or redistribute power in certain application of interest are limited.

Nine phase induction machine belongs to the class of multiphase induction which has gained prominence in many published work [17, 35, 36]. Most studies of multiphase induction machine deal mainly with different model approaches to study the dynamic

and steady state analysis of the machine equation [37–40]. The concept of having the stator of synchronous electric machine to co-share two set of three phase windings in the same stator frame was first reported by Alger in 1920 [41]. About four decades later, experimental viability of a five phase machine was investigated by [42]. It was further exemplify with sound mathematical background by the work of [43, 44]. The aim of [42] was believe to elevate the power capability of large synchronous generators. Since then, various modeling technique such as multiple $d - q$ technique [5, 45], complex vector modeling [46–48], and vector space decomposition(VSD) [49–53], have been adopted to model higher phase order (symmetrical and asymmetrical windings) including multiple set windings for jointed and dis-jointed neutral electrical machines. Figure 2.1, shows magnetic axis projection of nine phase induction machine symmetrical and asymmetrical induction machine, for jointed and dis-jointed neutral point. Also, indicative in the Figure 2.1, (a),(b), is the geometric angular separations between each winding sets, as distributed round the stator slots.
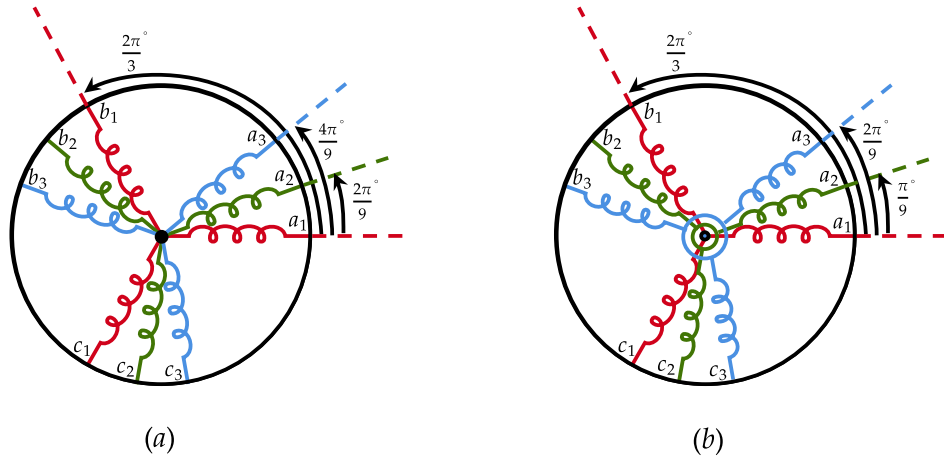
Figure 2.1: Nine Phase Induction machine (a) Symmetrical nine phase induction machine with single neutral point and phase separation between three phase windings sets to be 40° (b) Asymmetrical winding induction machine with isolated neutral point and phase separation between three phase winding sets to be 20°

Having multiple sets of windings co-sharing the same stator result in the following effects: increase mutual coupling between windings [54, 55], increase circulating

current [56, 57], fault tolerance during operation [58, 59], in addition, torque or power segmentation [60, 61], resulting from contribution from each winding sets. Figure 2.3 shows a typical structural stator interactions and that of the rotor.
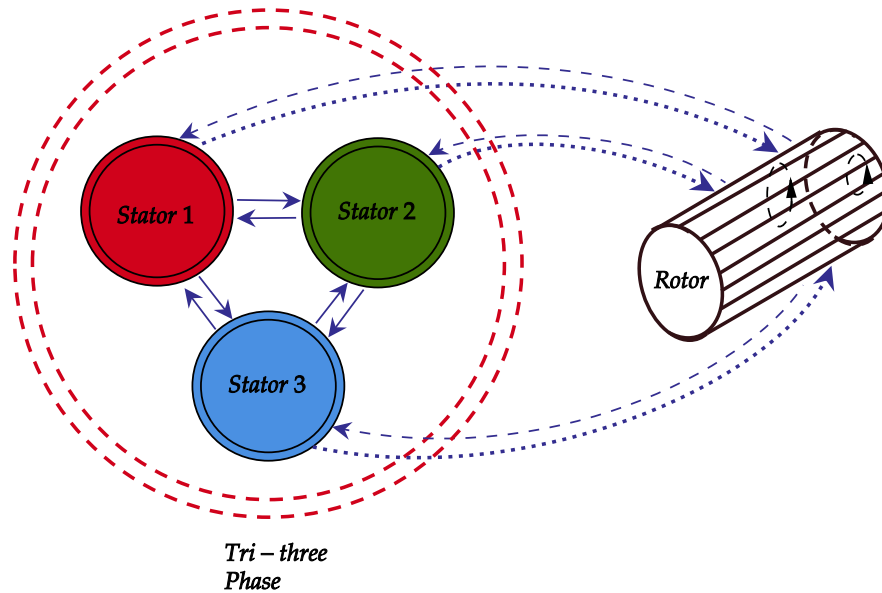
Figure 2.2: Tri-three phase Induction Machine Magnetic Coupling.

2.2   Modeling

Two popular modeling approaches used for modeling higher phase order electric machines namely: (i) *double dq approach* and (ii) *Vector space decomposition*. The choice of these approaches depends on decoupling methodology to decouples machine variables, current control methodology and ease of use.

2.2.1   Multiple dq Set Modeling

The multiple dq approach, also known as **multi-stator** approach happens to be the earlier approach to modeling of higher phase induction machine. The conceptual idea was borrowed from the modeling of a three phase induction machine. The multi-stator approach provides a framework for examining the sub-motor models that make up a multiphase induction machine as a whole. With respect to electric machine modeling

of multiple set of three phase windings, The multi-stator approach model, however, did not elaborate enough on harmonic sequences involving fifth, seventh,... harmonics for isolated neutral topology, as opposed to VSD which clearly makes this obvious after transforming the multiple phase model equations into $\alpha\beta, x_i - y_i$. and zero 0^+0^- sequence subspaces. The popular space vector and $dq0$ models of traditional three-phase machines have been transformed to fit a generic $n-$ phase machine. To accommodate the increased number of degrees of freedom, extra space planes were included.

The following assumptions: *uniform airgap, uniformly distributed stator windings, saturation neglected, negligible inter bar current of the cage rotor*, as applies to three-phase induction machine coupled magnetic circuit approach will be adopted when modeling multi-phase induction machine [62, 63].

- **Stator Voltage Equation for the winding *set 1,2,3* and Rotor Voltage Equation:**

The model equations in the phase variable form for each three-phase winding set are:

$$
\begin{cases}
v_{abcs1} = r_s i_{abcs1} + p\lambda_{abcs1} \\[1ex]
v_{abcs2} = r_s i_{abcs2} + p\lambda_{abcs2} \qquad where, \ p = \frac{d}{dt} \\[1ex]
v_{abcs3} = r_s i_{abcs3} + p\lambda_{abcs3} \\[1ex]
v_{1,2...n_r} = r_{1,2...n_r} i_{1,2...n_r} + p\lambda_{1,2...n_r}
\end{cases}
\tag{2.1}
$$

- **Flux Linkage Equation for the winding set 1,2,3 in Real Variable form:**

The flux linkage equation for the three set of three phase windings in phase variable form can be separated to several parts for ease of analysis and add up together. For the sake of completeness, each stator winding set total flux for that stator set λ_{jsk}, where the subfix 's' denote stator, $k = 1, 2, 3$ denote the index for the stator sets and $j = abc$, will be flux part due to its own stator current, flux part due to mutual coupling to other stator circuit set and flux part due to mutual coupling with the rotor circuit. n_r, is the

number of rotor bar. Without loss of generality, the expression for the flux linkage in compact form:

- Stator flux equation in condense phase variable form

$$\lambda_{jsk} = \sum_{q=1}^{3} L_{jskjsq} \cdot i_{jsq} + L_{jsk} \cdot \sum_{v=1}^{n_r} i_{rv} \ , \forall \ j = abc, \ k = 1, 2, 3 \qquad (2.2a)$$

- rotor flux equation in phase variable form

$$\lambda_{rv..n_r} = \sum_{q=1}^{3} L_{rjsq} . i_{jsq} + L_r . i_{rv..n_r} \ , \forall \ j = abc, \ v = 1..n_r \qquad (2.2b)$$

The flux equation listed in Equation 2.2a and 2.2b contain inductance matrices for each winding sets and that of the rotor.

2.2.2 Transformation Matrices

The studied asymmetrical tri-three phase induction generator under consideration in this thesis have isolated neutral points, and the mutual inductance between the stator and rotor are angle dependent, this is true for all induction machine. It is a matter of fact to apply a decoupling transformation matrix to the phase variable equations in Equation (2.1), Equation (2.2a) and (2.2b) to remove this dependency on the rotor angle, taking into account the disposition angle between the three phase winding sets. This change of variable transformation transforms the phase variable equation to $dq0$ reference frame, which makes it easier to carry out simulation study on the machine without recourse to equation dependent on rotor angle. For the system discussed in this chapter, the transformation for which the amplitude is preserved on both frames is done in the rotor reference frame. For the three-stator winding set, the reference frame is given as:

- Stator transformation

$$T_s\left(\xi\right) = \frac{2}{3} \begin{bmatrix} \cos(\theta - \xi) & \cos(\theta - \xi - \beta) & \cos(\theta - \xi + \beta) \\ \sin\left(\theta - \xi\right) & \sin\left(\theta - \xi - \beta\right) & \sin\left(\theta - \xi + \beta\right) \\ \frac{1}{2} & \frac{1}{2} & \frac{1}{2} \end{bmatrix}, \ \forall, \ \xi = 0, \frac{\pi}{9}, \frac{2\pi}{9} \text{ and } \beta = \frac{2\pi}{3}$$

$$(2.3a)$$

17

- The inverse Clarke transform Matrix is given by:

$$T_s^{-1}(\xi) = \begin{bmatrix} \cos(\theta - \xi) & \sin(\theta - \xi) & 1 \\ \cos(\theta - \xi - \beta) & \sin(\theta - \xi - \beta) & 1 \\ \cos(\theta - \xi + \beta) & \sin(\theta - \xi + \beta) & 1 \end{bmatrix}, \ \forall, \ \xi = 0, \frac{\pi}{9}, \frac{2\pi}{9} \text{ and } \beta = \frac{2\pi}{3} \quad (2.3\text{b})$$

Likewise,

- rotor transformation

$$T_{rr}(\theta_r) = \frac{2}{n_r} \begin{bmatrix} \cos(\theta - \theta_r) & \cos\left((\theta - \theta_r) - \frac{2\pi}{n_r}\right) & \cdots & \cos\left((\theta - \theta_r) - \frac{2(n_r-1)\pi}{n_r}\right) \\ \sin(\theta - \theta_r) & \sin\left((\theta - \theta_r) - \frac{2\pi}{n_r}\right) & \cdots & \sin\left((\theta - \theta_r) - \frac{2(n_r-1)\pi}{n_r}\right) \\ \frac{1}{2} & \frac{1}{2} & \cdots & \frac{1}{2} \end{bmatrix}$$

$$(2.3\text{c})$$

Finally, after going through this mathematical rigour, the dq equation for the multi-stator approach in simplified form alongside the mechanical equation is hereby:

$$\begin{cases} v_{qdsi} = r_{si}i_{qdsi} + p\lambda_{qdsi} - j\omega\lambda_{qdsi} \\ v_{qdr} = r_r i_{qdr} + p\lambda_{qdr} - j(\omega - \omega_r)\lambda_{qdr} = 0 \end{cases} , \forall \ i \ = \ 1, 2, 3 \quad (2.4)$$

For a squirrel-cage rotor, note:, $v_{qr} = v_{dr} = 0$.

$$\begin{cases} \lambda_{qdsi} = L_{ls}i_{qdsi} + L_{lm}\sum_{i=1}^{3} i_{qdsi} + L_m \sum_{i=1}^{3}(i_{qdsi} + i_{qdr}) \\ \lambda_{qdr} = L_{lr}i_{qdr} + L_m \sum_{i=1}^{3}(i_{qdsi} + i_{qdr}) \end{cases} \quad (2.5)$$

$$T_e = \frac{3}{2}\left(\frac{P}{2}\right)\left(\frac{L_m}{L_r}\right)\left[\lambda_{dr}\sum_{i=1}^{3}(i_{qsi}) - \lambda_{qr}\sum_{i=1}^{3}(i_{dsi})\right] \quad (2.6)$$

$$\frac{d\omega_r}{dt} = \frac{1}{J}(T_e - T_L) \quad (2.7)$$

2.2.3 Vector Space Decomposition

The modeling approach is one of the highly published modeling method used for modeling higher order electric machine (i.e., multiphase and multiple $n-$ phase electric machine), where in most circumstances n could be group of $3, 5....$ sets of three phase

18

windings, sharing same stator slots. Multiphase machine modeling using various modeling approaches have been reported in [53]. However, some author argue that, VSD seems better for multiple phase control. This is because of the ease with which the multiple phase electric machine model in the phase variable form are decomposed into decoupled $2D$ orthogonal sub-spaces: the (α, β), (x_i, y_i) and the zero $(0^-, 0^+)$ sequence model [49, 64, 65]. while, other authors are confident multiple dq present the best approach to control the machine windings independently. Vector space decomposition is an extension of classical reference frame transformations, so as to accommodate machine with multiple set of phases while accounting for the sequence harmonic components. The mathematical technique can be used to model multiple set induction machines. The technique involves decomposing the machine's variables into orthogonal components that can be analyzed separately. The orthogonal components arise from the decomposition using the vector space decomposition, which involves breaking down the machine's variables into different frequency component subspaces. These subspace components are orthogonal because they are at $90°$ angles to each other and can be analyzed independently. Table 2.1 shows the mapping of different harmonics in decoupled subspaces of higher order phases [66].

Table 2.1: Harmonic mapping into different planes using VSD transformation for multiphase systems ($k = 0, 1, 2, 3 \ldots, m = 1, 3, 5 \ldots$) [56]

Plane	5-Phase	6-Phase	7-Phase	9-Phase
$\alpha - \beta$	$10k \pm 1$ $(1, 9, 11 \ldots)$	$12k \pm 1$ $(1, 13, 25 \ldots)$	$14k \pm 1$ $(1, 13, 15 \ldots)$	$18k + 1$ $(1, 19, 37 \ldots)$
$x_1 - y_1$	$10k \pm 3$ $(3, 7, 13 \ldots)$	$6m \pm 1$ $(5, 7, 17 \ldots)$	$14k \pm 5$ $(5, 9, 19 \ldots)$	$18k + 17,$ $8m \pm 4$ $(5, 13, 17 \ldots)$
$x_2 - y_2$	-	-	$14k \pm 7$ $(3, 11, 17 \ldots)$	$9k \pm 2$ $(7, 11, 25 \ldots)$
Zero sequence	$5(2k + 1)$ $(5, 15, 25 \ldots)$	$3(2k + 1)$ $(3, 9, 15 \ldots)$	$7(2k + 1)$ $(7, 21, 35 \ldots)$	$3(2k + 1)$ $(3, 9, 15 \ldots)$

The method of vector space decomposition (VSD) [52], was first proposed by T.A. Lipo to address higher phase order machine. The first criteria are to transform these equations to multiple 2D subspaces. The first of this subspace ($\alpha - \beta$) is responsible

for the electromechanical energy conversion. The intermediate subspace $(x_i - y_i)$ is not useful, as it not responsible for torque production. The last subspace $(0^+ 0^-)$ is the zero-sequence subspace, and the current in this subspace, does not flow, if the neutral point of the winding sets is isolated. The VSD can be interpreted as making the subspaces orthogonal to each other after the transformation which decouples the machine equation. A fundamental property of the first subspace is that it is the only part coupled to the rotor. This is shown in the VSD model in [67]. The other decoupled subspace after the fundamental subspaces is not coupled to the rotor. The voltages in these other subspaces are dependent on the leakage inductance of the subspaces. This accounts for the high current flow in the subspaces which amount to losses. Usually, the current in this subspace is driven to zero using controllers [68–70]. In some circumstances, it has been used as additional degree of freedom for *fault tolerant* operation and *power sharing* between winding sets in multiphase induction machine [60, 71]. In the VSD scheme stated above, it is only the fundamental component part of the subspace $(\alpha - \beta)$, that is further transformed to $(d - q)$ using the *rotational* transformation, since that is the part that is responsible for electromechanical conversion.

In contrast to other modeling technique like the multiple $(d - q)$ approach [72], phase variable approach [73] or complex vector approach [48], the VSD, approach in some parlance, gives a modest, and simplistic approach of obtaining the decoupled orthogonal subspaces of a complete multiphase machine model, in a single step, revealing the relationships between the stator-rotor coupling and that with non-torque or flux producing components which is not evident in other modeling approaches. In the VSD presented by T.A. Lipo [52], it was earlier used to model a nine-phase synchronous machine. A modification to the VSD transformation has been applied to accommodate for both symmetric and asymmetric machines with or without isolated neutral [74]. The complex vector approach is like the VSD approach, except that each subspace in the VSD is fused into complex vector parameter, that hold the information of a pair subspace. The essence of this extra effort is to further shrink or compress the transformation matrix into a better compact form. Both the VSD and complex vector form have the same transformation functions. Both transformations are combined to achieve same

decoupling aim, as reported in published work [75, 76].

Using the same phase variable equation shown in Equation (2.1) , Equation(2.2a) and Equation(2.2b), the nine-phase phase-variable equation of the induction machine can be transformed into a set of 2D decoupled sub-spaces. Substituting flux linkage Equation(2.2a),Equation(2.2b) in to the Equation (2.1), and applying the nine phase transformation matrix in (A1.3) to the resulting equation result in the set of decoupled VSD equations in their respective stationary reference frame:

- The $\alpha - \beta$ component voltage of the decoupled model.

$$
\begin{bmatrix} v_\alpha \\ v_\beta \\ 0 \\ 0 \end{bmatrix} = \begin{bmatrix} R_s + L_s \frac{d}{dt} & 0 & L_m \frac{d}{dt} & 0 \\ 0 & R_s + L_s \frac{d}{dt} & 0 & L_m \frac{d}{dt} \\ L_m \frac{d}{dt} & \omega_e L_m & R_r + L_r \frac{d}{dt} & \omega_e L_r \\ -\omega_e L_m & L_m \frac{d}{dt} & -\omega_e L_r & R_r + L_r \frac{d}{dt} \end{bmatrix} \begin{bmatrix} i_\alpha \\ i_\beta \\ i_{r\alpha} \\ i_{r\beta} \end{bmatrix} \qquad (2.8a)
$$

- The $x - y$ component voltage of the decoupled model.

$$
\begin{bmatrix} v_{xj} \\ v_{yj} \end{bmatrix} = \begin{bmatrix} R_s + L_{ls} \frac{d}{dt} & 0 \\ 0 & R_s + L_{ls} \frac{d}{dt} \end{bmatrix} \begin{bmatrix} i_{xj} \\ i_{yj} \end{bmatrix} , \ \forall \ j = 1, 2 \qquad (2.8b)
$$

- The zero sequence $0_1, 0_2, 0_3$ component voltage part of the decoupled model.

$$
v_{zj} = \left(R_s + L_{ls} \frac{d}{dt} \right) i_{zj} , \ \forall \ j = 1, 2, 3 \qquad (2.8c)
$$

Where, for nine phase, $L_m = (\frac{n}{2})M$, L_m is the magnetising inductance, n is the number of phases, M is the peak magnetising inductance, L_{ls} is the leakage inductance, R_s is the stator resistance, R_r is the rotor resistance, L_s, L_r are the stator and rotor self inductances, both expressed as $L_s = L_m + L_{ls}$, $L_r = L_m + L_{lr}$, ω_e is the synchronous speed of the applied excitation.

Applying *rotational* transformation matrix Equation (2.9) to Equation (2.8a)

$$
D_s = \begin{bmatrix} \cos\theta_s & \sin\theta_s & & & \\ -\sin\theta_s & \cos\theta_s & & & \\ & & 1 & & \\ & & & \ddots & \\ & & & & 1 \end{bmatrix}, \ D_r = \begin{bmatrix} \cos\beta & \sin\beta & & & \\ -\sin\beta & \cos\beta & & & \\ & & 1 & & \\ & & & \ddots & \\ & & & & 1 \end{bmatrix} \ \forall, \ \beta = \theta_s - \theta_r
$$

$$(2.9)$$

Where, θ_s is the instantaneous angular position of the $d-$axis with respect to the magnetic axis of phase 'a_1' of the stator in Figure 2.1. The angle θ_r is the incremental rotor angle. The rotational angle β transforms the rotor variables to the arbitrary $d-q$ reference frame. Therefore, the VSD $d-q$ equations in the arbitrary reference frame, resulting from the transformation of Equation (2.9):

$$
\begin{bmatrix} v_{ds} \\ v_{qs} \\ 0 \\ 0 \end{bmatrix} = \begin{bmatrix} R_s + L_s\frac{d}{dt} & -\omega L_s & L_m\frac{d}{dt} & -\omega L_m \\ \omega L_s & R_s + L_s\frac{d}{dt} & \omega L_m & L_m\frac{d}{dt} \\ L_m\frac{d}{dt} & -(\omega-\omega_r)L_m & R_r + L_r\frac{d}{dt} & -(\omega-\omega_r)L_r \\ (\omega-\omega_r)L_m & L_m\frac{d}{dt} & (\omega-\omega_r)L_r & R_r + L_r\frac{d}{dt} \end{bmatrix} \times \begin{bmatrix} i_{ds} \\ i_{qs} \\ i_{dr} \\ i_{qr} \end{bmatrix} \quad (2.10)
$$

The stationary, rotor and the synchronous reference frame can be obtained from equation (2.10) by substituting $\omega = 0$, for *stationary* reference frame, $\omega = \omega_r$, for *rotor* reference frame, $\omega = \omega_s$, for *synchronous* reference frame. For a nine-phase induction machine, with isolated neutral and no asymmetries in the winding, the expression in Equation (2.8c) is neglected and Equation (2.8b), driven to zero, and only the controller for the fundamental expression of (2.8a) suffice. However, if asymmetries are present in the machine windings, a controller build around Equation (2.8b) is combined with the controller built around Equation (2.8a) to compensate for the asymmetries.

The electromagnetic torque equation is:

$$
T_e = \frac{P}{2}L_m\left(i_{dr}i_{qs} - i_{ds}i_{qr}\right) \tag{2.11}
$$

$$
T_e - T_m = J\frac{d\omega_m}{dt} \tag{2.12}
$$

2.2.4 VSD vs Multi-Stator approach

Combining VSD with a multi-stator technique has the practical advantage of recovering concealed information about the machine currents that was lost when VSD was used alone to decouple the current into orthogonal subspaces. The relative importance of the two approaches depends on the problem to be addressed with each method. The multi-stator approach gains wide use in the analysis of multiphase induction machine before the development of vector space decomposition by Thomas Lipo [52, 77]. The former assumes the machines can be independently controlled. The nine-phase induction machine model equations considered in these thesis are quite involved. At first, one feel overwhelmed by complexity of equation. However, the choice of an approach that suits, makes it easier to obtain solutions.

It can be reasoned that the VSD makes analysis simpler. The VSD model of the multiple-phase induction when compared to the multi-stator approach (i.e multiple $d - q$) is that, the sequence harmonics of the model subspaces are included in the transformation matrix which decouples the machine model, into many 2D orthogonal subspaces. By this transformation, all sequence harmonics are considered without leaving out the details, as it was in multi-stator approach.

The multi-stator approach gives up on information regarding the machine sequence harmonic subspace, as only the fundamental component is considered. The VSD model led to a simpler decoupled model without giving up any information about the harmonics of the machine as will be obtained using multi-stator approach. The multiphase machine model elaborated in simple form can be modeled in harmonic sub spaces using appropriate transformation [55, 78–82].

After the model undergoes a transformation to the proper sequence plane using VSD or another well-established transformation, the obtained equation in these various subspace are used to draw the equivalent circuit of the multiple-phase induction machine. It is proven in the study by Abdel-khalik *et al* that despite the introduction of a new subspace, their assumption in their analysis was that the stator resistances remain constant. However, the harmonic sequence number for each subspace must be taken into account when calculating the magnetising inductance and the rotor-referred-to-stator

characteristics [83, 84].

2.3   Review of Related Works

The modeling of multiphase induction machine in published literature works is saturated, and has long been used successfully. However, new possibilities are being explored, to reconfigure the machine for some technical benefits. There are cache of works discussing topological re-organisation of electric machine windings. This new winding re-modification on a general note, has been adjudged a promising contender to symmetric and asymmetric winding induction machine in terms of the measuring indices: *torque density*, *phase current quality*, *stator winding simplicity* and *fault tolerant capability*. Great breakthrough have been sustained in rewinding a three phase induction machine to a five phase induction machine [85]. A review and important developmental strides is the application of winding structural re-modification of three phase induction machine operated as a generator was reported by the work of [86]. There are also reports of multiple phase induction machine used in some form of series cascaded connections of two or more motors by [67, 87, 88], ingenious re-modification for onboard integrated charger by [89–93], reconfiguration from nine phase machine to six terminal phase machine by [51, 94, 95], modification in the control due to structural unbalances by [96, 97], modeling and control of open phases of multiphase induction machine by [98, 99], progresses exploring additional degree of freedom of multiphase induction machine by [100], and the current trajectory of multiple set windings induction machine based on possibilities of using one or more of the winding sets as a generator, and other remaining windings as a motor reported in [101]

These referenced papers are key to the novelty to be brought about by this thesis. Each of these works will be reviewed one after the other in terms of similarity of purpose to the present discussion and the relation with the present work as discussed in this thesis. Sood *et al*, in a thorough analyses of the work presented in [86] reported an ingenious approach of using active switches, see Figure 2.3, connected across the terminals of a

three-phase induction generator with the aim of regulating the output voltage of the induction generator by controlling the machine excitation (by extension reactive power), through a set of switches connected across the machine terminals, controlled in a fashion as to apply sequential short circuit across the machine terminal, that also serves as point of common connection to load.
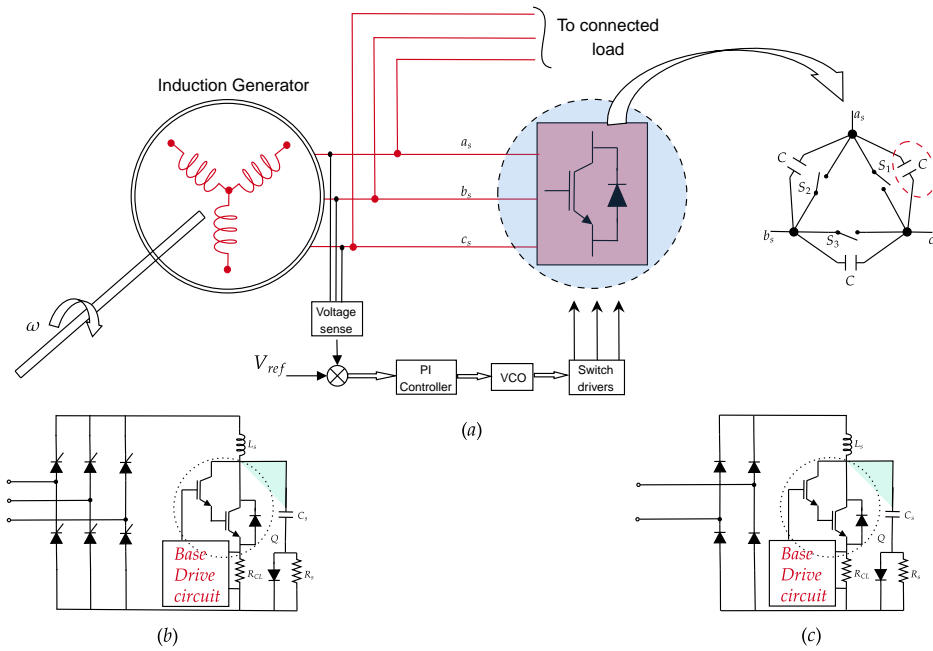
Figure 2.3: Rotating Switch Induction Generator(a) Circuit topology switch Control signals (b) Three phase base drive circuit for rotating short at machine terminal.(c) Single phase base drive circuit for rotating short at machine terminal

The switching actions of these switches connected across the machine terminal during operation results in changes in circuit topology and consequently, the effect results in rotating short circuits been applied at some pre-defined instances of time across the terminals of the machine windings. The findings in the work showed an added knowledge in the excitation control of three phase induction generator without a *dc link inverter* as well as reduction of voltage distortion over a wide control range of the rotating short circuits applied to the generator terminals.

Chapter 2. Literature Review

Extending the idea of using multiple winding induction machine for some technical benefit of achieving high power application, was the possibility of using two or more asymmetrical multiphase induction machine cascaded in series and fed by one single inverter was presented in [67, 87]. In the reported work, the authors, utilize the additional degree of freedom presented by multiple phase induction machine to achieve an independent control of four series connected and cascaded machines: Three of out of these machines is an asymmetrical nine phase induction machine, and the last connected machine is a three phase machine. Figure 2.4, shows the topology presented by the authors.
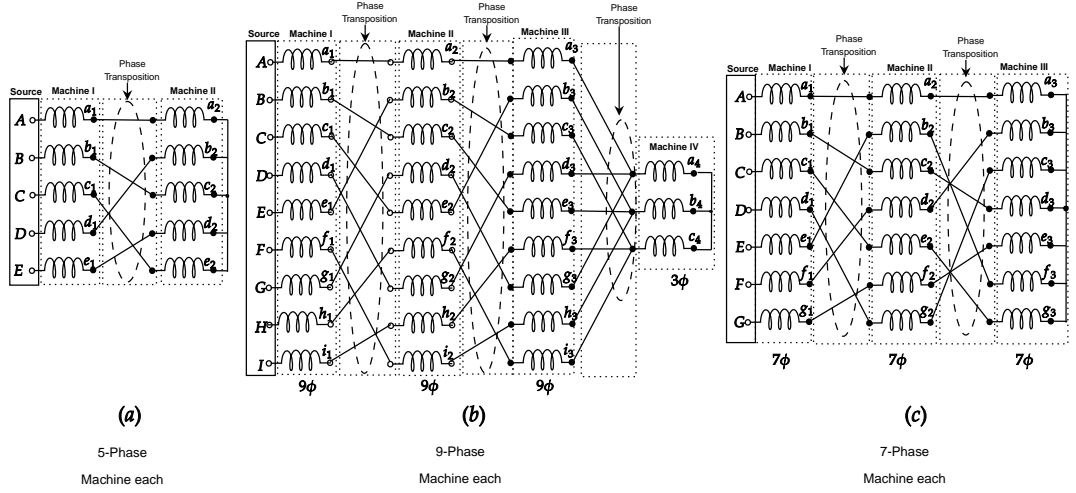
Figure 2.4: Multiple Phase Machine Modification for Multi-motor drive (a) Set of two five phase induction machine connection (b) Set of three Nine phase induction machine connections and three phase induction machine termination (c) Set of three seven phase induction machine connections

In achieving the defined objective in the paper, the model of the machine was first obtained. Next a transformation matrix based on vector space decomposition (VSD) approach of [52, 77], was then applied to develop the decoupled control ideology. The decoupled control strategy was designed such that $d - q$ component of one machine is automatically routed to be the $x - y$ components of the next machine, following an orderly phase transposition mapping. This action makes the other machines not to contribute to air gap flux and torque production. By this, the control action is instituted

26

to achieve an independent vector control. However, improved reliability and the benefits of incremental addition to the torque (by proxy increase power) by harmonic injection using this approach is lost.
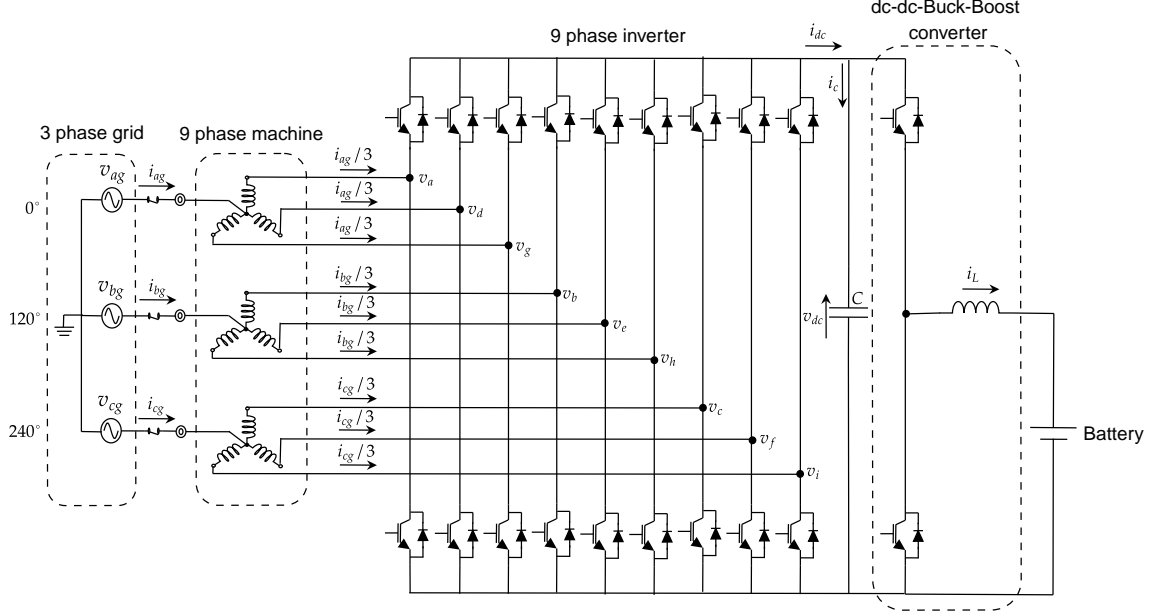
Figure 2.5: Onboard Nine Phase Battery Charger

Another reported innovative alteration to an asymmetrical nine phase induction machine for on board battery charging system for electric vehicle systems without hardware reconfiguration was reported in the work of [102, 103]. Figure 2.5, depict the circuit topology employed by the authors. The conceptual idea in the work was to utilize the common degree of freedom of multiphase- induction machine, such that, three sets of three phase windings, phase shifted from each other by $(\pi/9)°$ are connected to a three phase source via each neutral point connection, for the gains of fast charging of an onboard battery charging system for an electric vehicle. Three analytical cases were investigated for *charging, vehicle to grid (V2G)*, and *propulsion* respectively. During the *charging mode*, the current through phases of each multiple set windings, been 1/3 each of the current of the connected three phase source, and are equally controlled

27

to ensure the mmf balance for each three phase set machine winding sum up to zero (i.e *no torque production*). See Figure 2.6 and Table 2.2 for the analysis. This is so, because geometrically, each winding set angular dispositions between phases is 120°, however, the current flow from the neutral point of each winding sets, divided amongst the phases of each set are the same. Hence, no phase shift exist in them based on the retrofit winding topology adopted here, and so, no mmf exit in the core, a condition required during charging.
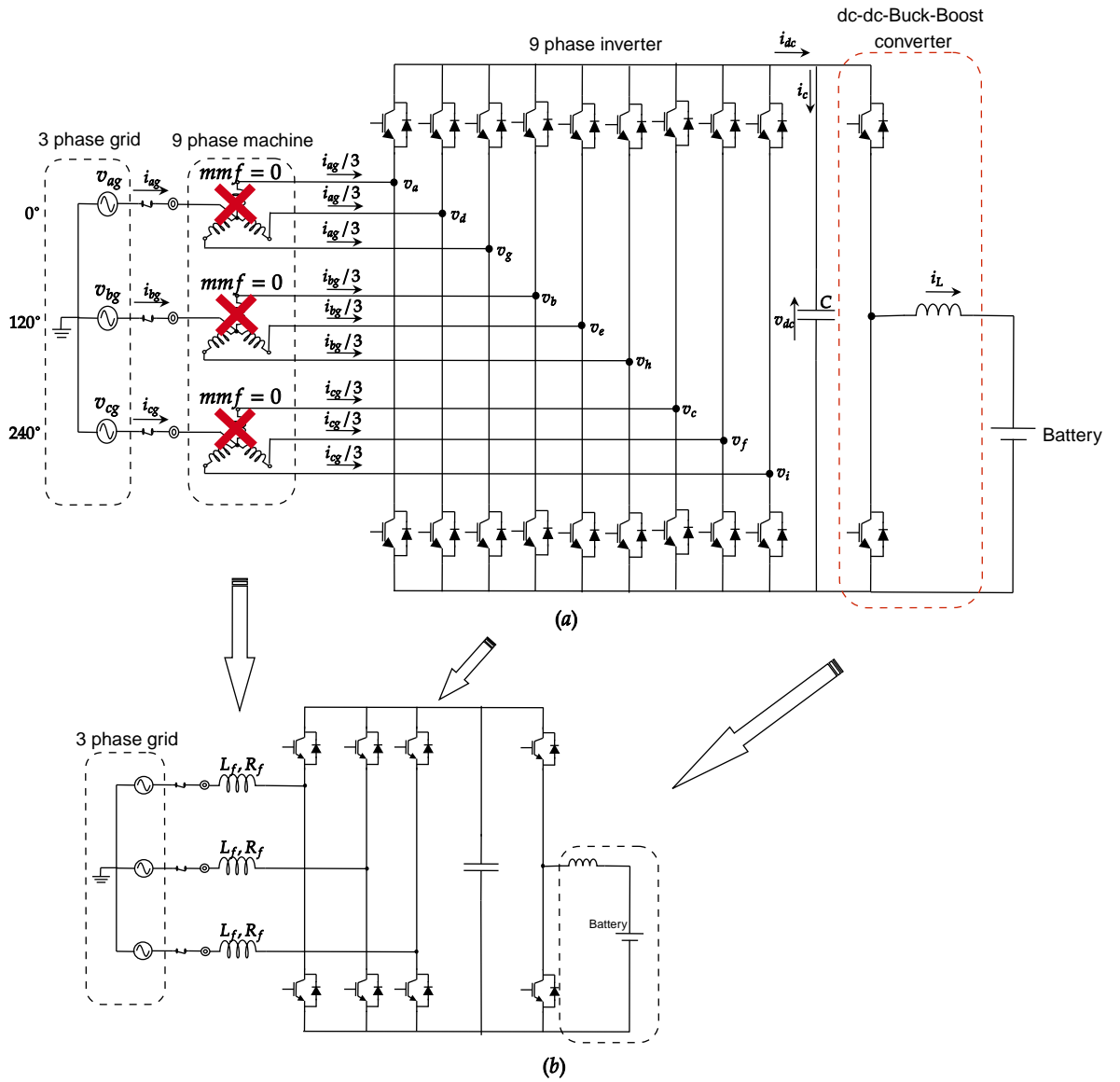
Figure 2.6: (a)Onboard Nine Phase Battery Charger mmf Balance for charging and V2G Mode (b) Reduce equivalent circuit of (a)

The current i_{ag}, i_{bg}, i_{cg} from a three-phase source each, flow through the provided neutral of each set of three phase windings, assuming equal number of turns for each machine. These currents are divided equally in their respective phases windings of each set as shown in Figure 2.5. Therefore there is no phase shift for the currents in the phase windings of a particular set. There fore the MMF analysis for the winding set 1 can be briefly determined. Taking the first winding set as an example in Table 2.2.

Table 2.2: MMF Analysis of first winding set 1 of nine phase Induction machine

Current	WF	MMF	MMF Analysis
$\frac{i_{ag}}{3}\cos wt$	$N\sin\theta$	$\frac{i_{ag}}{3}N\cos wt\sin\theta$	$\frac{i_{ag}}{6}N\left(\sin(A)+\sin(B)\right)$
$\frac{i_{ag}}{3}\cos wt$	$N\sin(\theta-\beta)$	$\frac{i_{ag}}{3}N\cos wt\sin(\theta-\beta)$	$\frac{i_{ag}}{6}N\left(\sin(A-\beta)+\sin(B-\beta)\right)$
$\frac{i_{ag}}{3}\cos wt$	$N\sin(\theta+\beta)$	$\frac{i_{ag}}{3}N\cos wt\sin(\theta+\beta)$	$\frac{i_{ag}}{6}N\left(\sin(A+\beta)+\sin(B+\beta)\right)$

In Table 2.2, $A = \omega t + \theta$, $B = \omega t - \theta$, N, is the turn function of the windings, $\beta = 120°$.

In the V2G mode [104], the machine windings are used as filter to remove unwanted harmonic which is coupled to the grid system. The control is designed to achieve unity power factor to connected load based on the adopted grid oriented control methodology and also, ensure no torque production during this phase. In this mode, the mmf sum up to zero, i.e (all expressions of column 4 in table 2.2, $\sum$ (**mmf analysis**)=**0**. This analysis is shown in table 2.2, supports the action that no torque is produce when the windings is retrofitted for charging and V2G mode of operation.
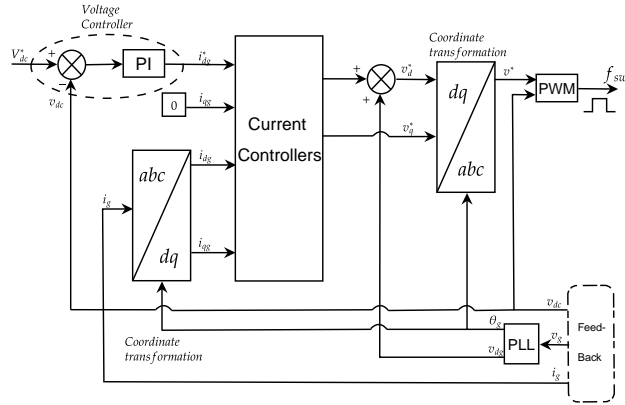
Figure 2.7: On board Battery Charger control algorithm

In the propulsion mode operation, the electromechanical energy component $\alpha\beta$ resulting from decoupled nine-phase machine equations subspaces are used for torque

production (i.e., propulsion), based on field-oriented control concept, while the other subspaces $x_i y_i$ are used as additional degree of freedom as well presented in the work of [21]. Other related work which supported and reported similar approach are well documented in [105–107]. Figure 2.7, shows a controller system designed for the charging mode control of the reduced equivalent circuit of Figure 2.6(b).

A novel strategy for modifying a nine-terminal, nine-phase induction machine to mimic the features of a six-phase, six-terminal machine was reported in the work of [51, 94, 95]. In the report, a nine phase asymmetrical induction machine windings terminals is reconnected in some fashion as to obtain a six terminal(six phase) induction machine, as shown in Figure 2.8. The aim of the authors in [51], was to have an equivalent circuit of the proposed novel machine, to exhibit the operational characteristics of six phase, six terminal induction machine. The phase-variable model of the new machine was obtained. A re-modified vector space decomposition transformation matrix was then used to decompose the machine equation into sequence component subspaces (i.e $\alpha\beta, x_i y_i, 0^-$). The new machine model was then compared to a conventional six phase induction machine model, and these brought about 11% torque density improvement. Post-fault analysis was then carried out on the machine based on selected operational modes: maximum torque and minimum loss. Their result shows a reduction in copper loss by 25% and reduction of 14% compared to rated conditions, when operated based on the maximum torque and minimum loss concept. In all these, however, there was no basic mathematical model to substantiate this claim. Figure 2.8, shows a 9P6T induction machine winding layout.
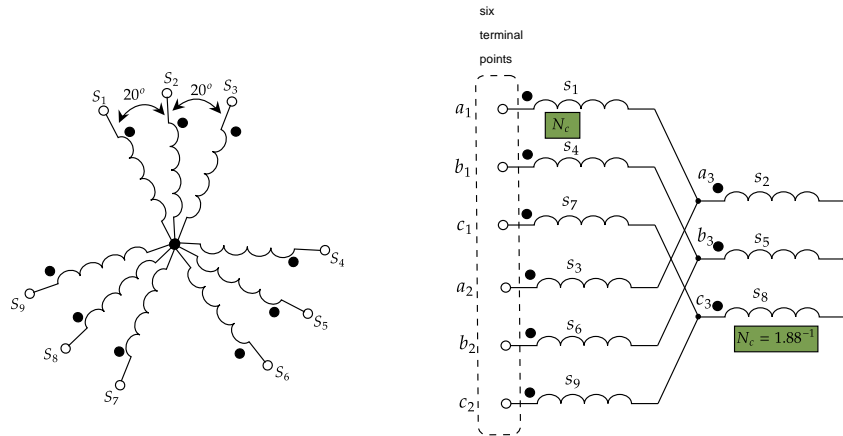
Figure 2.8: Nine Phase Six Terminal Machine

2.3.1   Fault Tolerant Operations

Fault tolerant abilities of multiphase induction machine gives it an edge over the conventional three phase system in terms of faults. In the event of fault in one or two sections of the multiphase machine or converter system, the specific faulted section can be disconnected from the entire power loop without disrupting the operations of the system. Except that, the machine will have to be de-rated, by re-configuring its control architecture to reduce losses caused by asymmetric operations to the barest minimum [108–110]. The converter system in a multiphase machine system is more vulnerable to open circuit and short circuit fault in the upper and lower active switches than fault in machine windings according to [111, 112]. Machine or converter performance drops drastically when a faulty phase(s) occur, consequences of which is torque oscillations, distorted current and voltage waveforms and aberrant heating of the drive system.

Ripples in the torque or current due to loss of a phase can be compensated for using $x - y$ current control from the machine or converter model. The controller for the $x - y$ current control is imposed to compensate the asymmetries in the machine operation due to faulty phase or converter asymmetries while ensuring smooth airgap mmf during pre-fault and postfault operations. This is the basic idea of fault tolerant operations of

multiphase machine.

It is crucial that machines have fault tolerance, or the ability to continue functioning despite the presence of a defect. The machine's performance in these conditions should be optimised for efficiency, with power losses and torque ripple kept to a minimum. When a fault occurs in a multiphase system, the commonest thing is that, the machine loose it specific control capabilities. It may be necessary to reduce the multiphase machine's capacity; nevertheless, a fault-tolerant system may handle this situation gracefully. A great deal of research in this field has been documented in publications such as [113, 114]. In the works of [113], the authors implemented their proposed fault tolerant control of a five phase induction machine pushing the fault testing limits on the stator winding connections in the following configuration study: *star*, *pentagon* and *pentagram* connections. The analysis of the MMF waveform shows distorted current waveform , the torque ripple is amplified, losses are incurred, and the efficiency of the multiphase machine is decreased when a failure occurs in any one or more phase. With regards to the idea on fault tolerant concept on multiphase electric machines, the works of [114], adopted a novel concept on a DFIG. Here, rather than having three phase wound rotor, and three phase stator, the reliability of the system can be improve upon by having the rotor wound for five phase and the stator winding three phase. A fault tolerant analysis was carried out on the machine, to test the viability of their control solution to lost of one or more phase on the rotor windings. The experimental results agrees with results from simulation studies. Exploiting the degree of freedom (i.e. phase breaking) available from the un-faultered phases requires research into the load limit on the machine shaft. The idea of control is to properly regulate the remaining healthy phases to achieve maximum torque output while minimising copper loss. Copper losses may be kept to a minimum while yet allowing for continuous operations under a larger derating factor when the optimal copper loss is used. Therefore, from the point of view of post fault control, its been reported that asymmetrical electrical machines with isolated neutral offers better phase voltage and current THDs compared to that with multiple phase induction machine with single neutral point [115].

2.3.2 Modulating techniques

Having transform the multiphase machine dynamic model equations into orthogonal subspaces, using the vector space decomposition technique, the flux and torque $\alpha\beta$ component of the machine are completely decoupled from the rest of the orthogonal subspaces, i.e the $x_i - y_i$ and 0^+0^- subspace. So, it becomes easier to control specific variable in the machine decoupled model. For example, controlling the α part of the current regulates the machine flux. Likewise, controlling the β component of the machine current regulates the torque. To realize this aim requires a robust modulating technique. Modulating techniques relating to three phase system have been extensively reported in literature and justifiable extended to cover higher phase order machines [66, 116]. Clearly, the mostly reported modulating technique is the carrier-based pulse width modulation (CBPWM) technique and Space vector pulse width modulation (SVPWM). These modulating techniques have been extended to the control of multiphase machines in a similar fashion as in a three-phase machine. The CBPWM and SVPWM signals are used to drive active switches in a two or three level voltage source converter in a drive system. The works of [117] have reported that having more than three phases notably influence the PWM converter control of multiphase machines. As the number of the multiphase system increases, the development of the PWM technique becomes quite involve because of the number of subspaces to be controlled. The CBPWM technique involves modulating a reference signal at low frequency and comparing it with a carrier signal at high frequency to generate train of pulses use to drive the switches on an $n-$ level voltage source converter. The SVPWM technique on the other hand, involves sectorial analysis and synthesis of the switching states of space vectors so as to maximize dc bus utilization. The number of switching states using SVPWM technique is reported to have increase as the number of converter leg increase, in developing a multiphase voltage source inverter (VSI) [118, 119]. The more the switching states, the more the complexity of developing the proper space vectors for the PWM. For example, an $n-$ phase multiphase machine, with a three-level converter, will have 3^n switching states. Because of the computational intensity in determining the appropriate space vector sectors and their respective dwell times, it have been concluded by the authors

of [120–122] that CBPWM was better and easier to implement than SVPWM. This is judging by the ease with which the CBPWM can be developed and extended to accommodate more phase leg in the converter PWM development. The multiphase voltage source converter can be made to operate in the linear and over modulation regions by meeting certain modulating criteria as detailed in the works of [123, 124]. By pushing the boundaries of the modulating signal (i.e amplitude) compared to the carrier signal beyond unity, lead to a condition known as pulse dropping in the PWM control circuitry. A condition which cause the appearance of lower order harmonics at the output of the converter and the dc bus connected to the converter not fully utilized. This problem has been solved by adding a zero-sequence component to the modulating signal to suppress the harmonics and improve dc bus utilization by 15.47% for three phase system and about 5% for five phase system [125]. As a conclusion in this section, the both schemes i.e CBPWM or SVPWM have their merits, and picking one over the other relies on factors like the need for *good waveform quality*, *high dynamic performance*, *low switching loss*, and a *straightforward implementation.*

2.3.3 Current Control

Multiphase induction machine can be wound for concentrated windings [126, 127], or wound for distributed windings [128]. Analysis and performance evaluations for a six-phase induction machine regarding the concentrated winding and distributed windings have been elaborated in the works of [129]. In the concentrated winding topology, the phase windings are concentrated in the slots and not distributed. On the other hand, a distributed winding multiphase induction generator, which is the focus of this thesis have k sets of three phase winding sets arranged in the slots of the stator. The neutral point of the multiphase winding sets can be connected together (i.e. symmetrical windings) or isolated (i.e. asymmetrical windings) to achieve certain design objectives. The number of phases in a multiphase machine with isolated neutral can be obtained based on the expression (phase number $= 3k$). Where $k = 1$ for three phases, $k = 2$ for six phases, $k = 3$ for nine phase system.

Developing control architecture for multiphase machine is important, so as to ensure

decoupled control and balanced current sharing amongst three phase winding sets. Accordingly, control of multiphase machine can be approached from the type of controller and the frame of reference (i.e synchronous or stationary) the controller operates, to control the multiphase machine pertinent variables. Existing dq control in literature have been used to ensure decoupled control of three phase electric machine flux and torque. The I_d is used to control the machine flux and the I_q is used to control the torque. This idea is also achieving the same purpose in multiphase machine. Except that, for multiphase machine, the degree of freedom has increased, so one pair of dq control as in a three phase is insufficient. In the available literature, in some quarters, multiple dq control plane has been used to achieve control of multiphase machine [130]. On the other hand, the VSD control approach have an edge over the multiple dq in that, a unified control of the multiple three winding sets in multiphase machine is achieved [64,65,131]. However, while unified control of the multiple three phase winding sets is achieved, information regarding control of the individual winding sets is lost. Fortunately, reference [60] have derived an equation to correlate the control of the individual winding sets with the unified control, so that the current in the individual windings which is lost in the unified control to be determined.

Each isolated neutral three phase windings sets in the multiphase induction machine will require pairs of current controllers operated either in the stationary reference frame (i.e $\alpha\beta$ control) as reported by [132] or synchronous reference frame (i.e dq control) as reported by [133]. In contrast to one pair of controllers (dq for flux and torque control) for a three phase induction machine as reported in the works of [134], the other two pairs of current controllers ($x - y$) in multiphase induction machine are recognized as a corrective measure to compensate for the winding asymmetries in the multiphase machine.

The work by authors of [69] investigates a five-phase induction machine with current control in the rotating reference frame. With close loop current control and no speed or position control, they claim that asymmetry in the machine windings, in a multiphase induction machine system and also dead time effect in the PWM inverter, introduces unwanted waveform in the machine current steady state waveform. A modify current

loop control was then developed to cope with these unwanted low order stator harmonics in the steady state current waveform. Results from the modification scheme compensated for the imbalance of the fundamental as well as the low order harmonics in the current waveform.

Great flexibility in current sharing have been achieved in a twelve phase induction motor drives reported in the work [17, 135]. Their claim was that the degree of freedom presented by multiphase machine allows better management of the stator current sharing using multiple three phase winding sets. In fact, it was emphasized that the role of the $x - y$ current in the machine model was to create an unbalance compensation so that the stator of the fundamental frequency does not appear in the $x - y$ subspace. Indirect rotor flux-oriented (IRFOC) control has been the control choice for multiphase induction generator. An example of such control technique has been reported in the works of [136, 137]. Such control technique requires aligning the rotor flux vector to the $d-$ axis in the synchronous reference frame to enable the decoupled control of the machine flux and torque. The authors of [69], have at first investigated the current control issues of a five-phase induction machine with sinusoidal magneto-motive force distribution and without any asymmetries in the machine windings. Only the dq plane in this case is excited at the fundamental frequency, no excitation in the $x - y$ plane. The investigation was carried further in the same paper to study the challenges posed by asymmetry and inverter dead time effect of the PWM inverter on the current waveform. The obtained profile harmonics of the stator voltages, current or flux linkage in the stationary reference frame were mapped into the $\alpha\beta$ and $x - y$ plane.

The strategy adopted to mitigate the flow of $x - y$ current harmonics due to the asymmetry, was to use a modified current controller scheme to compensate for this asymmetries or imbalances in the machine and dead-time effect in the inverter. The current control schemes use two pairs of current controllers and based on a rotational transformation matrix rotates the pair of $x - y$ current in the synchronous reference frame as in the dq reference frame. They, however, justify through experimental investigation that their proposed technique in the synchronous reference frame was better in suppressing imbalances caused due to asymmetry and inverter dead time

effect. However, The work by the authors of [70] also implemented a new modified transformation matrix to mitigate the $x - y$ current in a six-phase induction generator system. Two pairs of controllers operated in the synchronous reference frame was used to control the wind generator machine flux and torque as well as asymmetries introduced in the wind generator. As it is evidently proved [69] that conventional control with one pair of controllers is not satisfactory. More convincing explanation was also reported in the works of [70]. In the same vain, the authors of [133] in their conclusions, stress that machine or converter asymmetry in the current waveform depends on the type of asymmetry and eliminations and evaluations is based on the choice of transformation matrix. An in-depth analysis and experimental investigations of the current control for a six phase induction motor drives based on different controllers to remedy the $x - y$ current is reported in works of [138]. An agreement to the works of [133] was also shown in the analysis of [138], where the authors claimed that the asymmetric current are of fundamental frequency. So, cases of control solutions to mitigate the asymmetries can be made by rotating the $x - y$ current in the synchronous, anti-synchronous or best achieve the two in both directions reference frame.

2.3.4 Current sharing between three phase sets

An easy to follow flow chart to create a VSD matrix for an asymmetrical and symmetrical machine have been reported in the works of [53]. Their derivation of the VSD was based on the usual assumption of sinusoidal winding distribution, balance machine winding, uniform air-gap and magnetic linearity of the core. Power sharing within the three-phase winding set of a multiphase machine is important in order to balance the individual dc link voltage of the connected converter in an asymmetrical multiphase machine as reported in the works of [71]. Their central connection in the work is to establish balanced power sharing through imposition of $x - y$ current in the $x - y$ plane. When a phase is lost or loss of three phase winding set is faulted, the control algorithm will have reconfigured it control properties to accommodate these events and ensure a balance dc link voltage. In another simulation studies reported in [108], a novel transformation matrix transforms the model equation and also ensure controlled power sharing between

the winding set through use of multiple dq and with VSD technique. Three PI regulators were used to achieve the control objectives. One PI regulator was used to regulate the voltage in the synchronous reference frame and the remaining two was used for $x - y$ current control in the stationary reference frame. Their simulation result shows that arbitrary current sharing between winding sets of the studied multiphase machine, when the two winding sets are arbitrary set, have no impact on the torque or flux of the machine when operated in the motoring or generating mode. The same work by the same authors was taking further on a nine-phase machine. Power sharing is realizable by imposing $x - y$ current at fundamental frequency. This is achieved by defining a current sharing strategy which defines in a simple ratio controlled current set for each three phase windings in the synchronous reference frame, to enable power sharing without affecting the machine torque and flux.

2.3.5   Converter connections configuration possibilities

Series or parallel configurations of $n-$ leg voltage source converter, connected to a three-phase winding sets of multiphase induction generator in WECS, is to enhance power exchange from machine side to grid and grid side to machine. This impact on the overall dynamic performance of the dc link. To achieve an elevated dc link voltage, the converters depending on the number of three phase sets, are connected in series [74]. The advantage of this converter series connection type is that it enables the splitting of medium voltage connection at the grid side, thus reducing the size of the transformer used to step up the voltage to the grid. However, the connection downside of the series connection type is that when open circuit fault occurs, fault tolerant capabilities of the converter system is degraded.

Another connection type with improve dynamic performance of the dc link is the parallel connection type of three phase converter [139]. Here, each converter dc link with inputs from the multiphase machine are stacked together and connected to a common dc point. The connection type promotes an asymmetric connection and operations proposed in this research work, with improve fault tolerant operation than the series connection type, due to the modularize connection of the stack $n-$ level voltage source
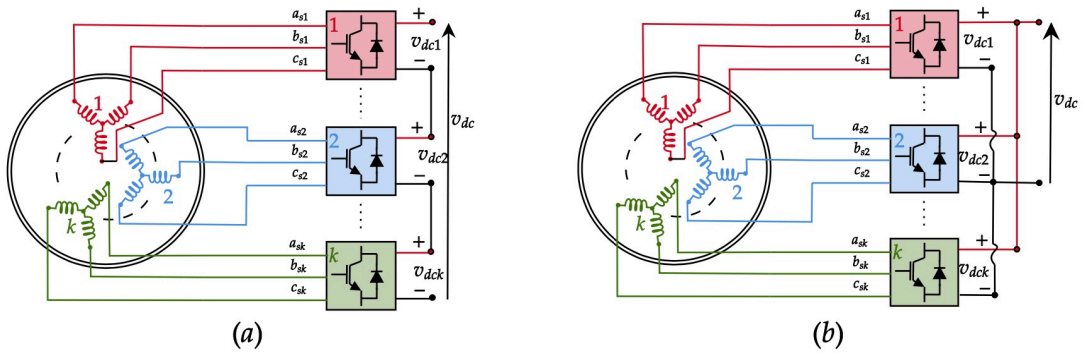
Figure 2.9: Converter connection possibilities to multiple phase machine (a) Series converter connection (b) Parallel converter connection

converter. Meanwhile, research work which combine the advantages of the two types of connection type for a robust fault tolerant operation have been elaborated in the works of [140]. Figure 2.9, shows the converter connection possibilities connected to a multiphase induction machine.

2.3.6 Control of multiphase machine active and reactive power

The objective of controlling active and reactive power delivered to the grid in a wind energy conversion system is to decoupled control of the wind generator excitation flux and torque. Control of multiphase machine using vector space decomposition technique have been reported in the works of [60, 71, 108, 141]. The vector space decomposition has the advantage of mapping the machine model equations into harmonics planes of $\alpha\beta$, $x_i - y_i$, $0^+, 0^-$ which are orthogonal to each other. Figure show a typical control structure for a nine phase induction machine using an indirect rotor flux field oriented control.

With $\alpha\beta$ been the only fundamental flux and torque producing components, the remaining is the harmonics and zero sequence components. The VSD technique profiles the machine model equations (flux, current or voltage) into orthogonal planes of harmonic components thus making the control of the machine specific harmonics caused by asymmetry a lot easier. Aside these advantages, it minimizes the stress involved in seeking control solution of the machine equations when compared with the solutions offered by multiple dq technique which require elaborate voltage decoupling terms.
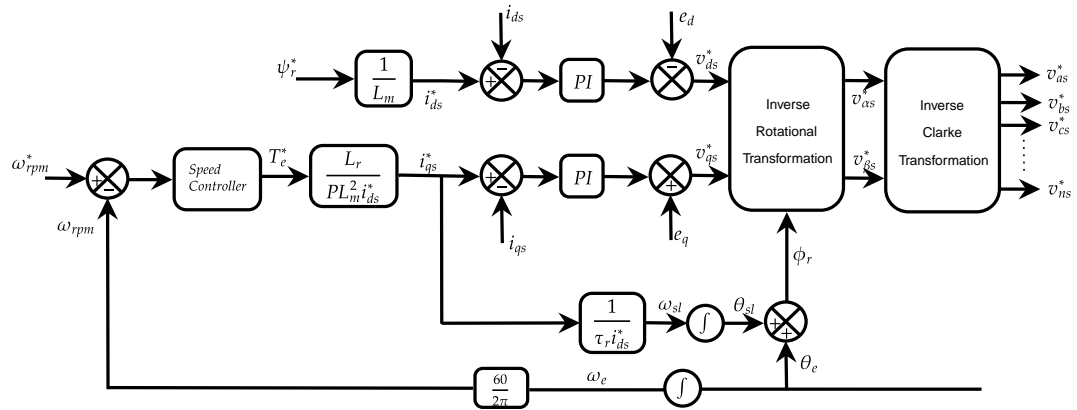
Figure 2.10: Extended indirect rotor flux orientation
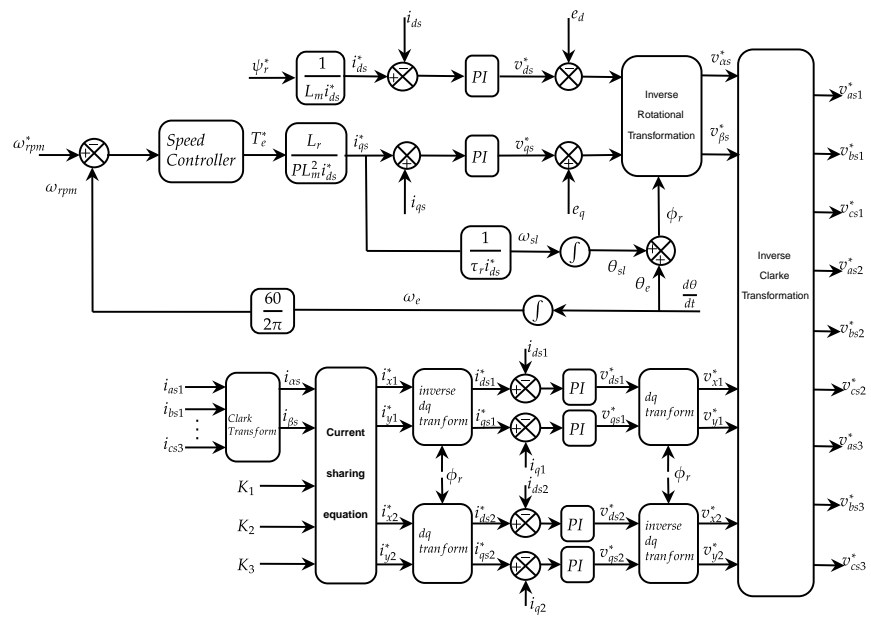
Figure 2.11: Extended indirect rotor flux orientation

2.3.7   Decoupling Control for Induction Machine

Multiphase-induction machines are widely used in various industrial applications due to their robustness, reliability, and cost-effectiveness. However, controlling these machines

41
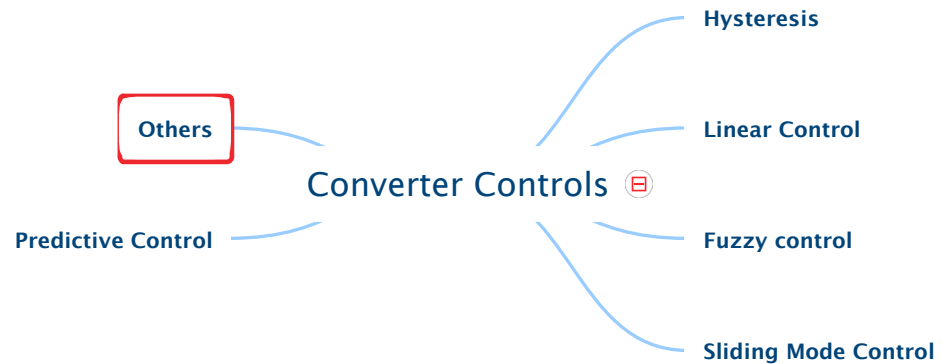
Figure 2.12: Converter Controls types

can be a challenging task due to their inherent nonlinearity, cross-coupling effects, and parameter variations. Decoupling control is an effective technique to improve the performance of multiphase induction machines by separating the control of each phase and reducing the cross-coupling effects between them.

The decoupling control of multiphase induction machines can be achieved using various control strategies, including *vector control*, *direct torque control*, and *model predictive control*. Vector control is a widely used control strategy that decouples the stator and rotor variables and controls the machine using the stator current and voltage components in the dq reference frame. The vector control strategy uses a proportional-integral (PI) controller to regulate the stator current components in the dq reference frame and achieve the desired electromagnetic torque and flux.

Direct torque control on the other hand is another control strategy that decouples the stator and rotor variables and controls the machine using the stator current and voltage components in the dq reference frame. The direct torque control strategy uses a hysteresis band controller to switch the stator voltage components in the dq reference frame and achieve the desired electromagnetic torque and flux. The hysteresis band

controller compares the actual and reference values of the electromagnetic torque and flux and switches the stator voltage components to maintain them within a predefined hysteresis band.

Model predictive control is a more advanced control strategy that uses a mathematical model of the machine to predict its future behavior and optimize the control inputs to achieve the desired performance. Model predictive control decouples the stator and rotor variables and controls the machine using the stator current and voltage components in the dq reference frame. The model predictive control strategy uses an optimization algorithm to solve a cost function that minimizes the deviation of the predicted and desired values of the electromagnetic torque and flux.

2.4 Review of Similar Works

The section covers review of works by other authors and thus far progress from this field, and mathematical basis to establish model conditions and criteria.

2.4.1 Switching Network

Switching network is discontinuous and nonlinear, and the integrated switches in any converter topology are usually operated based on switching function technique on the constraint of voltage source or capacitor in circuit at hand cannot be shorted, equally a current source or inductor cannot be open, else, KVL and KCL will be violated. Three-phase PWM converters operate using this switches on account of this constraints. This converters are operated at relatively high frequency of frequency range $20kHz - 100kHz$ for converters below $100kW$ range. Figure 2.13 show the different converter topologies: dc-dc,dc–ac,ac–dc,ac–ac. which in that other are define as *conversion, inversion,rectification and cyclo-conversion.*. All this transformation are based on switching electronic power converter systems used for transforming electrical energy from one level to another at the load through controlled switching processes. All of the conversion techniques that have been itemized employ a variety of power semi-
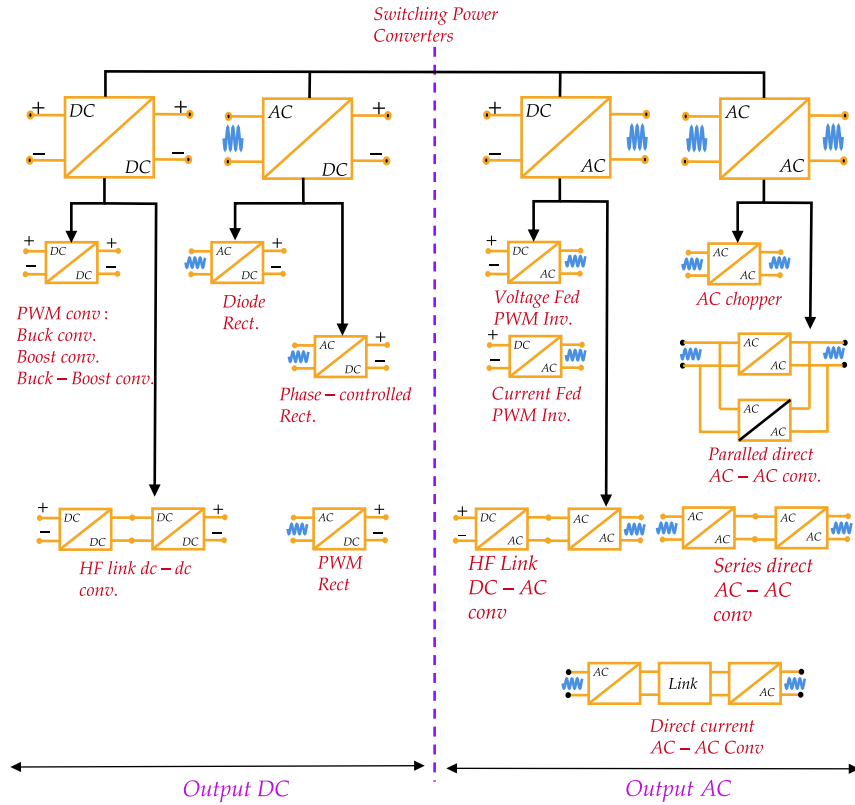
Figure 2.13: Switching Power converter types

conductor devices. Among the devices used in single-phase and three-phase conversion are thyristors, diodes, IGBTs, SiC, GaN, and so on.

The most converter design objectives is to reduce as possible the reactive components. This results to significant improvement in waveform quality and closed-loop performance, to meet modeling and control design. Figure 2.14 represent a switching circuit development model for a boost or voltage source inverter. The line voltages between node points $a - b, b - c, c - a$ and the phase current relations in terms of i_{dc} is shown in the table below the switching circuit model. The voltage and the current relations have been represented compactly in equations (2.13). These equations have been developed based on switching function technique, $s_i = s_{ip} = 1 - s_{in}$, $\forall \, i \in \{a, b, c\}$ arising from the different switch positions represented in the square dash line.

44
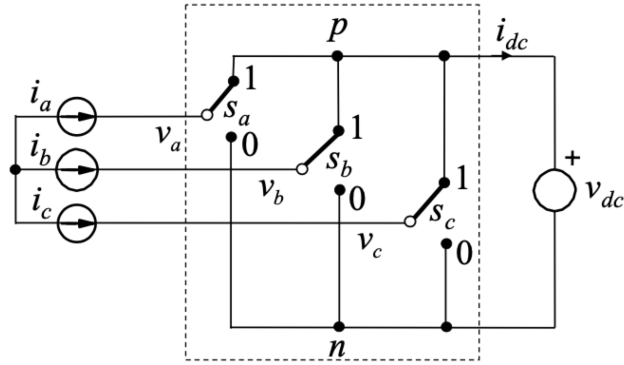
s_a	s_b	s_c	s_a-s_b	s_b-s_c	s_c-s_a	i_{dc}	v_{ab}	v_{bc}	v_{ca}
0	0	0	0	0	0	0	0	0	0
0	0	1	0	-1	1	i_c	0	$-v_{dc}$	v_{dc}
0	1	0	-1	1	0	i_b	$-v_{dc}$	v_{dc}	0
0	1	1	-1	0	1	i_b+i_c	$-v_{dc}$	0	v_{dc}
1	0	0	1	0	-1	i_a	v_{dc}	0	$-v_{dc}$
1	0	1	1	-1	0	i_a+i_c	v_{dc}	$-v_{dc}$	0
1	1	0	0	1	-1	i_a+i_b	0	v_{dc}	$-v_{dc}$
1	1	1	0	0	0	$i_a+i_b+i_c$	0	0	0

Figure 2.14: Switching model development

$$
\begin{bmatrix} v_{ab} \\ v_{bc} \\ v_{ca} \end{bmatrix} = \begin{bmatrix} s_a - s_b \\ s_b - s_c \\ s_c - s_a \end{bmatrix} v_{dc} = \begin{bmatrix} s_{ab} \\ s_{bc} \\ s_{ca} \end{bmatrix} v_{dc} \; , \quad i_{dc} = \begin{bmatrix} s_a & s_b & s_c \end{bmatrix} \cdot \begin{bmatrix} i_a \\ i_b \\ i_c \end{bmatrix} \quad (2.13)
$$

Where: The switching functions; $s_{ab} = s_a - s_b$, $s_{bc} = s_b - s_c$, $s_{ca} = s_c - s_a$ are defined based on the interval $s_{ip}, s_{in} \in \{0,1\}$. The voltages; $v_{ab} = v_a - v_b$, $v_{bc} = v_b - v_c$, $v_{ca} = v_c - v_a$ is the voltage across points ab, bc and ca.

2.5   Three Phase Series and Parallel Rectifier Converter Connections

Boost rectifiers are distinguished by their capacity for bi-directional current flow, which has contributed to their rise in popularity in recent years alongside the use of parallel and series-connected converters. In [142–144], this characteristic, in addition to the
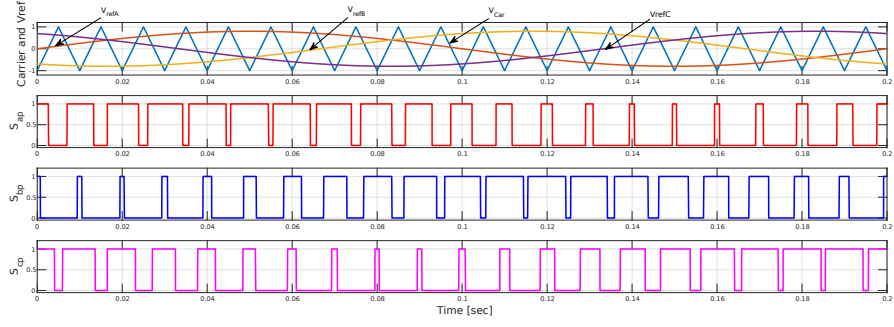
Figure 2.15: Carrier based PWM signal Switching function graph: The comparison of three phase sinusoidal reference signals (V_{refA},V_{refB},V_{refC}) with carrier signal V_{Car} translated to the switching pulses;S_{ap},S_{bp},S_{cp}. which are switching pulses applied to the upper switches of the converter in Figure (2.14).

rectifier model, is subjected to an in-depth analysis. Both the 2-port circuit model for steady-state study and the dq circuit model for analysing transient response and open-loop dynamic stability are used in the process of deriving the model of the three-phase boost rectifier. The first method uses the 2-port circuit model, while the second method uses the dq circuit model.
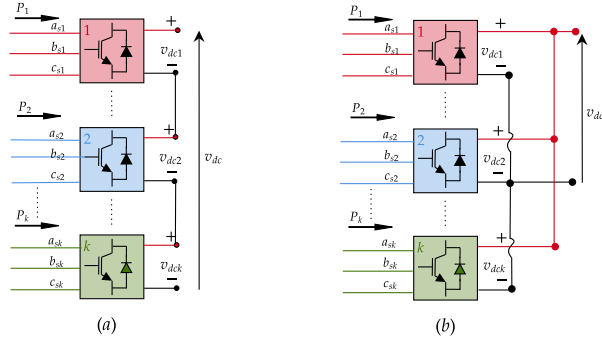
Figure 2.16: Converter connection topologies (a) Series connection (b) Parallel connection

The technology of three-phase rectifiers is thoroughly examined in [145], encompassing strategies for attaining unity power factor operation and reducing current harmonics. The control of a system comprising a vector-controlled three-phase induction machine, a cascaded three-phase rectifier system, a battery energy system, and an inverter is the subject of this thesis. The necessity for parallelizing converters has been underscored as a means to attain objectives such as optimal dynamic performance, diminished

harmonics, and increased power. Nevertheless, the linearization method presented in reference [146–148] for reducing harmonics with a solitary rectifier is not without its stability concerns. Nonetheless, harmonic distortion can be reduced while power can be increased by operating numerous converters in parallel.

2.6   Leakage Inductance in Multiple Phase Induction Machine

Leakage inductance has recently emerged as a significant challenge in multiple-phase induction machines. This phenomenon is identified as the root cause of exceptionally high current circulating within the $x - y$ subspace of multiple sets of induction machines, as analyzed through the vector space decomposition modeling approach. This issue arises due to the low impedance within this subspace. In the multiple $d - q$ approach, leakage inductance is combined to represent the cross interaction of the leakage field among multiple three-phase windings that share the same stator slots. It's worth noting that this leakage inductance, as per the vector space decomposition approach, has been observed to vary from one subspace to another, denoted as $x_i - y_i$ for all $i = 1, 2...n$ [57].

Leakage inductances of this subspace are known not to contribute to electromechanical energy conversion; instead, they only lead to losses. To reduce the high current flow within this subspace, increasing the inductance for a given harmonic excitation has been proposed. This approach allows for the minimization of current in the subspace. However, it's important to note that increasing the inductance of this subspace has been reported to decrease the average torque of the multiphase induction machine.

A study conducted by [149] aimed to investigate the impact of stator leakage mutual inductance in a dual-stator multiphase induction machine, considering a geometric shift of $30°$ between windings. Using the multiple $d - q$ approach to model their machine, two scenarios were examined concerning the mutual leakage inductance between the two stator winding sets that share the same stator slots: one with $(L_{lm} \neq 0)$ and the other without $(L_{lm} = 0)$ mutual leakage inductance. The results indicated that with $(L_{lm} \neq 0)$, the simulation reached a steady state more quickly compared to the scenario

without ($L_{lm} \neq 0$). Additionally, the current magnitude in the scenario with ($L_{lm} \neq 0$) was higher than in the scenario without ($L_{lm} = 0$). This work effectively accounted for the impact of mutual leakage inductance on the studied machine. However, it did not propose an approach to minimize the circulating current resulting from this mutual leakage inductance.

Minimizing such currents due to leakage inductance has been approached from a control perspective following the work of [133, 150]. In order to satisfy the machine torque control requirements for multiphase induction machine, the current in the $x_i - y_i$ plane and the 0^+0^- plane must be driven to zero, using proportional resonant controller [151, 152] or synchronous reference frame controller [153], for single neutral configurations. Likewise $x_i - y_i$ current driven to zero alone, if the machine configuration was for isolated neutral. The controllers to drive the $x_i - y_i$ current to zero, are tuned to suppressed specific harmonics of interest for any phase number of multiphase induction machine. The authors of [154] investigate different winding configurations of a six phase induction machine i.e dual three phase (D3P), symmetrical six phase (S6P), asymmetrical six phase (A6P). The investigation was to extract the parameter and same time under study the performance of these different configurations. Results show that A6P present a higher mutual leakage inductance, based on the configuration equivalent impedance when compared to other machine configurations, which is believe will suppress the current in the $x_i - y_i$ subspace. However, their work did not show an elaborate detailed mathematical analysis arriving at such conclusions. Another approach of suppressing the leakage inductance was that proposed from geometric relations of the stator slot. The authors in [155] believe that by increasing the stator slot depth, and adopting fractional slot winding via optimization of the phase position adjustment, reduction of the $x_i - y_i$ current is possible due to increase leakage inductance. This approach shows great feat in mitigating the current unbalances in asymmetric winding induction machine. However, the machine efficiency is scarified at the expense of increase stator inductance.

2.7   Leakage Inductance Determination Approach

The methodologies used for estimating parameters of multiphase machines share similarities with those employed for three-phase machines. These methods rely on specific equivalent circuits, with the Vector Space Decomposition (VSD) model being commonly utilized. The VSD model [156, 157], decomposes a multiphase machine into distinct equivalent circuits representing various vector subspaces, such as the $(\alpha - \beta)$, $(x - y)$, and zero-sequence (0^+0^-) subspaces. Researchers have successfully applied the VSD approach to six-phase induction machines [158].

In addition to the standard no-load and locked-rotor tests used for three-phase machines, the estimation of parameters in multiphase machines requires consideration of stator and rotor leakage inductances (denoted as L_{ls} and L_{lr}) to separate them from measured locked-rotor impedance. These leakage inductances, along with other parameters, play a critical role in the efficient control of multiphase induction machines.

Flux leakage resulting from leakage inductance is often viewed negatively, but it can have useful applications [159]. Leakage inductance significantly impacts voltage transients, power losses, voltage regulation, and electromagnetic interference (EMI) in PWM AC drive systems, making it an important consideration. By effectively managing and maximizing leakage inductance, system performance, efficiency, and reliability can be improved [160].

The leakage reactance, can be decomposed into constituent parts.

$$X_{ls1} = X_{sl2} = \underbrace{X_l}_{non\ slot} + \underbrace{X_{lT} + X_{lB}}_{top\ and\ bottom} + \underbrace{k_{sp}(p)X_{lTB}}_{top\ and\ bottom\ Mutual} \tag{2.14}$$

These reactances represent magnetic field phenomena associated with the leakage field of the windings. Their primary function is to induce an electromotive force (EMF) of the leakage EMF type in the winding.

Analytical calculation of leakage fluxes in multiphase induction machines is complex and requires detailed expressions to demonstrate the interrelation of leakage fluxes (and by extension, leakage inductance) between phase windings of the same three-phase group

and between different three-phase winding groups within the same stator slot. A novel approach presented in a recent study involved incorporating circular coils, distinct from the three-phase stator windings, at each end of the end winding region [161] . These coils captured and processed the induced voltage from leakage flux through external circuitry, providing information about the leakage flux in the motor. While this approach showed promise, it poses challenges for induction machines with limited space for additional coil windings.

When extending the research according to [162] to higher-order and odd-phase-number induction machines, several aspects require further elaboration. Firstly, it is necessary to determine the leakage equation for multiphase asymmetric induction machines. If the leakage inductance or flux equation derived in the [162] serves as a justification, it should be noted that the generalization is not unique, as the approach only covers asymmetrical induction machines and does not address symmetrical types induction machine. Secondly, understanding the relationship between the original phase current, the reflected current from other winding sets, and the winding pitch factors in the multiphase two-axis model is crucial. This information should be provided in detail, including the interactions, although it is expected to be derived in later section, chapter 6. Finally, the derived expression can be used to accurately compute the slot leakage inductance of multiphase induction machines using the $\alpha - \beta$ plane, instead of the modified VSD plane proposed in previous work.

The primary physical processes occurring in induction machines are related to the fundamental field harmonic ($h = 1$). Therefore, the self-inductance of the phase, along with the mutual inductance due to other phases for the fundamental wave, plays a leading role in terms of value and significance.

2.7.1   Effect of Mutual Leakage Inductance in the $d - q$ frame

Leakage flux must be included in the magnetic modeling of an induction motor because it significantly influences motor performances. For a three phase induction machine, this flux reduces rotor currents as well as the stator currents that induce the rotor current. However, in multiple set induction machine, this present a challenge, as

this leakage flux from the leakage inductance component in the multiphase induction machine model is the cause of exceptional high current in the $x_i - y_i$ and zero sequence subspace. Modeling a multiple-phase induction machine is significantly more complex compared to a three-phase induction machine. This complexity arises from the numerous interactions between different stator sets, stator phases, and the rotor, involving mutual inductances and mutual leakage inductance. Mutual leakage inductance originates from the flux components that do not pass through the air gap but instead couple the phase windings of other stator sets located within the same stator slots or compartment. In most analyses, the mutual leakage inductances between different sets of windings in a multiple-phase induction machine are often neglected [77] , despite their challenging impact. The influence of mutual leakage inductance on the Vector Space Decomposition (VSD) model of a six-phase machine, based on coil pitch, was examined in a previous study by Djafar *et al* [57].

In their work, [162] introduced a simple yet effective method to address the issue of mutual leakage inductance in induction machines with multiple-phase windings. They established a relationship between the double $d - q$ model and the VSD model for a six-phase induction machine. However, the works by Hang Chen *et al* and a recent study by [163], which share similar literature foundations regarding the mutual leakage inductance between winding stator sets, implemented in the same stator slots, did not discuss the effect of mutual leakage inductance on pitch factors and interactions caused by current flowing in other stator sets within the same stator compartment for *symmetrical* and *asymmetrical* induction machines with higher orders or odd numbers of phases. This relationship has not been established in the reviewed works, regarding this two winding configurations. Furthermore, the harmonics analysis takes into account the influence of pitch constraints to minimize the current in the $x_i - y_i$ subspace, as demonstrated in the study by [163].

The problem of high current circulation in the $x - y$ subspace have received much attention in published work in relation to multiple phase induction machine. First there was model of multiphase induction machine [164, 165], in which details of the leakage inductance was largely ignored. Next a brief matrix relations, which partitioned the

leakage inductance into constituent components was only mentioned by Hang Chen *et al*(2013). The purpose was to show the relation of the leakage inductance as it relates with machines of a six phase type.

Recently, a great deal of research has address the problem of low impedance of the higher order sequence harmonics, using control design [150, 166], winding pattern [167]. These rely on useful methodological approach in minimizing this losses. However, in applying those methods to practical problems, several difficulties appear. In particular, the existence of cross coupling inductance. Furthermore, the analysis takes into account the influence of pitch constraints to minimize the current in the $x_i - y_i$ subspace, as demonstrated in the study by [163].

When conducting leakage inductance analysis, it is important to consider the separation of leakage inductance and mutual leakage inductance between windings in a different manner in order to gain a clearer understanding of subspace inductance. The subsequent analysis will provide further insights into this matter.

2.7.1.1 Review of Effect of Leakage Inductance in the $\alpha - \beta$ frame for six Phase machine

- The stator leakage inductance for winding set 1 and 2

$$\begin{bmatrix} [\lambda_{ls1}] \\ [\lambda_{ls2}] \end{bmatrix} = \begin{bmatrix} [L_{ls} + M_{lss11}] & [M_{lss12}] \\ [M_{lss21}] & [L_{ls} + M_{lss11}] \end{bmatrix} \times \begin{bmatrix} [i_{s1}] \\ [i_{s2}] \end{bmatrix} \tag{2.15}$$

Let's consider a six-phase machine where i_{s1} and i_{s2} represent the balanced three-phase current flowing through winding set 1 and set 2, respectively. The leakage flux of winding set 1 and 2 can be denoted as λ_{ls1} and λ_{ls2}, respectively. Furthermore, the mutual inductance $\left[M_{lssii} \right]$, with $i = 1, 2$, characterizes the magnetic influence resulting

from the current flow in winding set 1 and 2, respectively.

$$[L_{ls}] = \begin{bmatrix} L_t + L_b & 0 & 0 \\ 0 & L_t + L_b & 0 \\ 0 & 0 & L_t + L_b \end{bmatrix}, [i_{s1}] = [i_{a1} \; i_{b1} \; i_{c1}]^T, \; [i_{s2}] = [i_{a2} \; i_{b2} \; i_{c2}]^T$$

(2.16)

The inductance of the upper and lower conductors within a slot are represented by L_t and L_b, respectively, in this equation. The mutual inductance between the upper and lower conductors in the stator slot, taking into account the pitch factor, and the magnetic flux resulting from the current i_{s1}, can be described as:

$$[M_{lss11}] = [M_{lss22}] = 2M_{tb} \begin{bmatrix} k_1 & k_2 & k_2 \\ k_2 & k_1 & k_2 \\ k_2 & k_2 & k_1 \end{bmatrix}$$

(2.17)

$$[M_{lss12}] = [M_{lss21}] = 2M_{tb} \begin{bmatrix} k_3 & -k_3 & 0 \\ 0 & k_3 & -k_3 \\ -k_3 & 0 & k_3 \end{bmatrix}$$

(2.18)

The mutual inductance M_{tb} between the upper and lower layers is affected by coefficients $k1$, $k2$, and $k3$, which depend on the coil pitch and can be obtained from the specified reference [57] and the most recent from [163].

$$[T_{3-i}] = \sqrt{\frac{2}{3}} \begin{bmatrix} \cos(\theta) & \cos(\theta + 120) & \cos(\theta - 120) \\ \sin(\theta) & \sin(\theta + 120) & \sin(\theta - 120) \\ \frac{1}{\sqrt{2}} & \frac{1}{\sqrt{2}} & \frac{1}{\sqrt{2}} \end{bmatrix} \forall \; i = 1, 2$$

(2.19)

$$[\theta = 0°, 30°]$$

Applying separate decoupling transformations, denoted as $[T_{3-1}]$ for winding 1 and $[T_{3-2}]$ for winding 2, to the variables in equations (6.35)–(6.36) as discussed in references [162,163], results in the leakage inductance expressions for the $(\alpha - \beta)$ and zero sequence (0^+0^-) subspaces in the clark transform domain.

- Leakage inductance in the $\alpha\beta$ subspace

$$L_t + L_b + 2M_{tb} (k_1 - k_2) \tag{2.20}$$

- Leakage inductance in the zero (0^+0^-) sequence subspace

$$L_t + L_b + 2M_{tb}(k_1 + 2k_2) \tag{2.21}$$

- Mutual Leakage inductance

$$2\sqrt{3}\, M_{tb}k_3 \tag{2.22}$$

According to the findings of Hang Chen et al., the mutual inductances between the top and bottom conductors within the same slot are present in all subspaces, namely $\alpha\beta$ and 0^+0^-. However, it should be noted that the mutual inductance coupling has no impact on the zero sequence (0^+0^-) subspace with respect to the other sets of windings.

2.8   Stability Analysis

The study on the stability of multiphase induction machines integrated with hybrid energy systems is under researched, but it is crucial for understanding dynamic systems and how system parameters or controllers influence model system stability [168]. Stability is an expanded topic that transcends and cut across all fields of engineering. Figure 2.17 shows the simple typical criteria for representing the stability of a system.

The stability criterion in *S–plane* for continuous time system states that all poles must lie in the left hand plane in Figure 2.17(a). The stability criterion for the *Z–plane* for discrete time systems states that all the poles must lie within the unit circle, see Figure 2.17(b). The poles of the closed loop transfer function are the same as the roots of the system characteristics equations and system stability is determined by the roots. There are many methods of testing the stability of a system [169–171]. These thesis will only discuss eigen value approach of finding the stability of a system of equations.
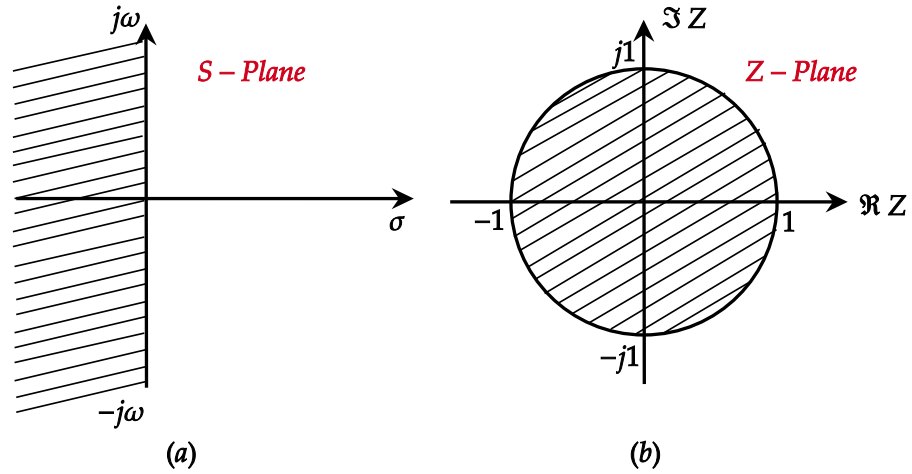
Figure 2.17: Stability criterion (a)*S-Plane* (b)*Z-Plane*.

2.8.1 Stability determination through Eigen value analysis

The stability of the system is determined by the behaviour of eigenvalues in close proximity to these stability boundaries, which can be changed by adjustments made to system parameters. Ensuring stability necessitates the essential feature of maintaining a system's reaction within acceptable thresholds in the presence of perturbation. A system is considered stable if its response deviates from an operational state within prescribed limitations. Otherwise, it is categorised as unstable.

Stability of a system can be investigated using algebraic or graphical means. This thesis adopt the two approach to find the stability of the developed system equations. Given a system of equations in matrix form, written as in equation 2.23, the approach of the stability of the system can be found by calculating the eigen values directly instead of the characteristic equation approach given in the previous section. To evaluate the stability of a system, the series of coupled system equations are drawn together and arrange into a compact form. The system equation can be compactly represented into the form:

$$\dot{\mathbf{x}} = f(\mathbf{x}, \mathbf{u}) \tag{2.23}$$

Where x and u are the vectors with respect to the state and the input variables, which are defined as $x = [x_1, x_2, x_3, ...x_n]^T$, $u = [, u_2, u_3...u_n]^T$. The steady state equations are
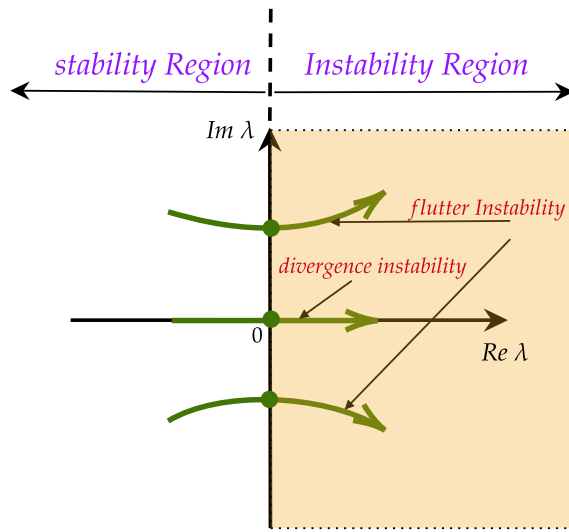
Figure 2.18: Stability criterion based on Eigen approach

then obtained from equation (2.23), by setting the equation $\dot{\mathbf{x}} = 0$, (i.e $f(\mathbf{x}, \mathbf{u}) = 0$). Moving forward, a steady state equation which relates and connects variables of the system is developed, which will be use to find the small signal equations for finding the stability of the system.

2.8.1.1 Small Signal Stability Analysis

The dynamic model equation of the multiple phase induction machine and the connecting systems can be represented in the form of equation (2.24).

Expanding equation (2.23) into a familiar equation, we have:

$$\dot{\mathbf{x}} = A\mathbf{x} + B\mathbf{u} \tag{2.24}$$

Where A is an $n \times n$ matrix describing each system variable equation, B matrix sets of input function. To find the small signal equation, it is thought that each variable in the nonlinear system equations' in equation (2.24) has a steady state component and a small-time changing component i.e $(x = x_o + \Delta x)$. Once the equations have been changed and the second-order parts have been ignored, the linear equations in the

perturbation variables are shown below in state space compact form as:

$$\Delta \dot{\mathbf{X}} = A\Delta\mathbf{X} + B\Delta\mathbf{U} \tag{2.25}$$

In equation (2.25), $\Delta\mathbf{X}=[\Delta x_1, \Delta x_2, ... \Delta x_n]^T$ and $\Delta U = [\Delta U_1, \Delta U_2 ... \Delta U_n]^T$, and quantities assign with subscript "0" in the expanded matrix A and B of the system equation are the steady state values , before perturbation. According to [172], the stability can be found based on the assumption the equation (2.25), is linear and time invariant. It is possible to use the principles of linear system control in order to calculate the eigenvalues and transmission zeros of the system. The dominating eigenvalue is a measure of how far the system is from becoming unstable, while the transmission zeros are a measure of how well the system can withstand disturbances and how tightly its components are coupled. The following equation can be used to derive the eigenvalues (λ) of the perturbation equations:

$$|\lambda I - A| = 0 \tag{2.26}$$

The stability and instability regions are predicted by the characteristic equation (2.26) which is given by the matrix A in (2.25). The eigenvalue locations for a particular operating condition can be obtained by solving (2.26)

2.9 Conclusions

The evolution of multiphase induction machines, particularly the emergence of novel nine-phase machines, has been a significant development in the field of electric drives. These machines, which integrate different types of induction and permanent magnet technologies within the same stator slots, have brought about several advantages, including improved fault tolerance and reduced inverter power ratings per phase, and lots more. The chapter has provided a comprehensive overview of the modeling techniques and related research in this area, spanning various converter connection topologies, current control methodologies, winding configurations, leakage inductance and stability criteria.

Chapter 2. Literature Review

In summary, the research presented in this literature review highlights the growing interest in exploring the potential of multiphase induction machines, particularly nine-phase machines, and the various modeling techniques employed to understand their behavior. The field continues to evolve, offering opportunities for innovative winding configurations and applications that can benefit various industries.

Chapter 3

Modeling of Studied system

3.1 Introduction

Hybrid systems are becoming more popular for efficient and sustainable energy solutions, because they can integrate many energy sources and storage technologies. This chapter explores hybrid systems and develops a complete model that includes numerous components essential to their operation. Multiphase induction machines, rectifiers, battery systems, inverters, and loads are important. We will explain the modelling method and the challenges of developing and analysing such systems.

3.2 Studied System

Figure 3.1 shows the schematic of the studied system. In order to effectively choose a suitable methodology for assessing a given system under study, it is imperative to take into account the mathematical framework of the system's units and the potential impact this may have on the chosen approach.
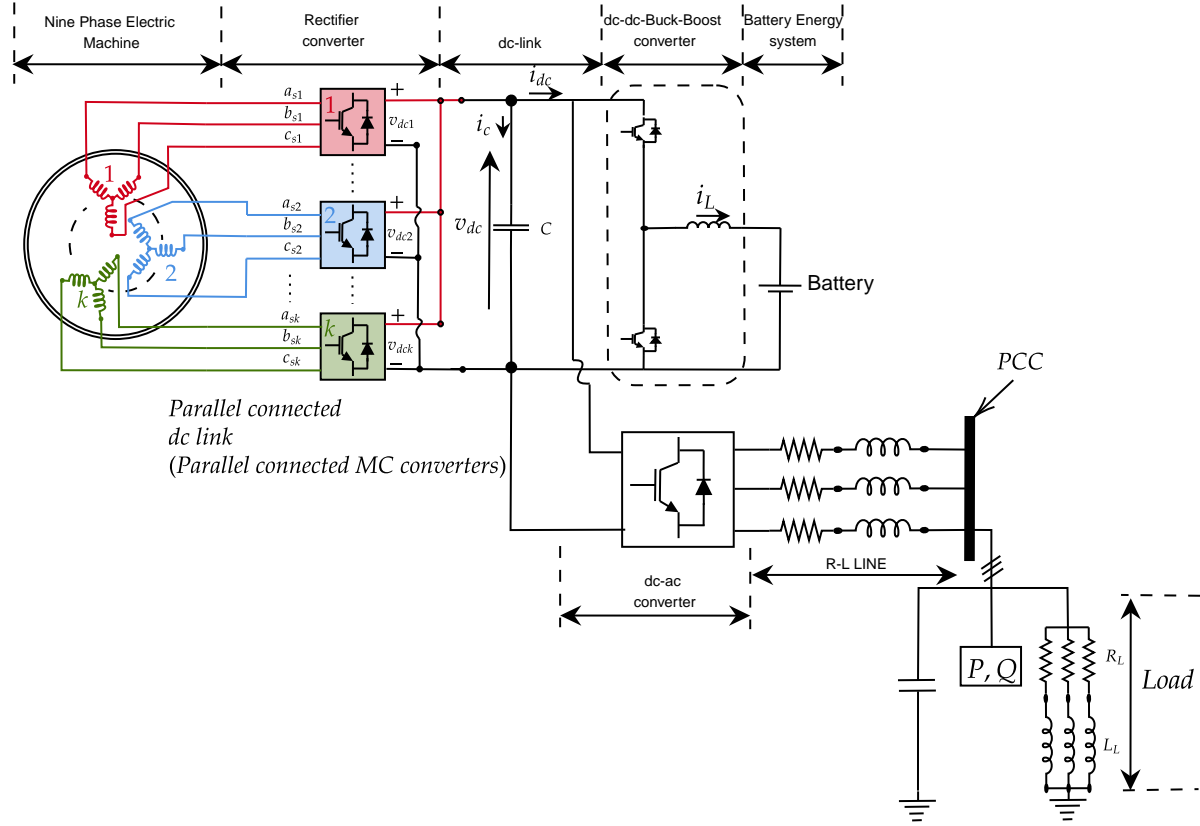
Figure 3.1: Studied System Description

3.2.1 Nine phase Machine side model based on Multiple $q - d$ set

The nine phase induction machine in the $d - q$ condense model is given by:

$$
\begin{cases}
v_{qdsk} = r_{sk}i_{qdsk} + p\lambda_{qdsk} - j\omega\lambda_{qdsk} \\
v_{qdr} = r_r i_{qdr} + p\lambda_{qdr} - j(\omega - \omega_r)\lambda_{qdr} = 0
\end{cases}
\quad for \ k = 1,2,3 \qquad (3.1)
$$

For a squirrel cage rotor, note:, $v_{qr} = v_{dr} = 0$.

$$
\begin{cases}
\lambda_{qdsk} = L_{ls}i_{qdsk} + L_{lm} \sum\limits_{j=1}^{3} i_{qdsj} + L_m \sum\limits_{j=1}^{3} (i_{qdsj} + i_{qdr}) \\
\lambda_{qdr} = L_{lr}i_{qdr} + L_m \sum\limits_{j=1}^{3} (i_{qdsj} + i_{qdr})
\end{cases}
\qquad for \; k = 1, 2, 3 \qquad (3.2)
$$

$$
T_e = \frac{3}{2} \left(\frac{P}{2} \right) \left(\frac{L_m}{L_r} \right) \left[\lambda_{dr} \sum\limits_{k=1}^{3} (i_{qsk}) - \lambda_{qr} \sum\limits_{k=1}^{3} (i_{dsk}) \right]
\qquad (3.3)
$$

$$
\frac{d\omega_r}{dt} = \frac{1}{J} (T_e - T_j) \,, \text{the subscript } j = \begin{cases} L, \; \forall \; \text{Motor Operation} \\[2mm] m, \; \forall \; \text{Generator Operation} \end{cases}
\qquad (3.4)
$$
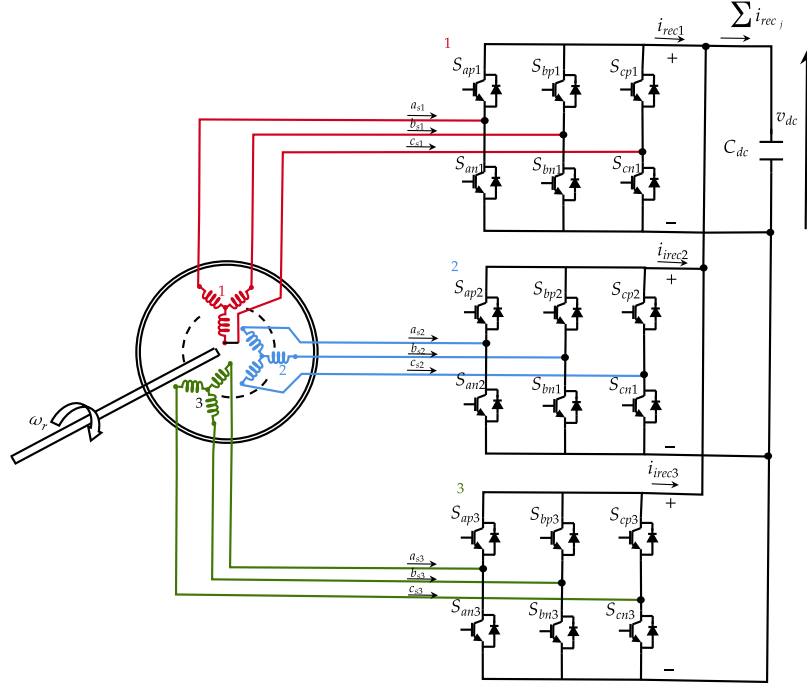
Figure 3.2: Nine Phase Induction Machine Rectifier system Description

The expression in equation (3.1)-(3.4) are defined: v_{qdsk} is the $d - q$ voltage at the terminal of the nine phase induction machine. v_{qdr} is the induction machine rotor voltage, for squirrel cage induction machine this expression $v_{qdr} = 0$. r_{sk}, r_r are the resistances for stator set and rotor resistance, λ_{qdsk} and λ_{qdr} are the stator and rotor flux

linkages, whose expression for each stator winding set has been mathematically defined based on equation (3.2). The parameters $L_m, L_{lm}, L_{ls}, L_{lr}$ are the magnetising, mutual inductance between winding set, stator leakage inductance and rotor leakage inductance respectively. i_{qdsk} is the $q - d$ current flow in the windings of each stator winding sets, i_{qdr} is the current flow in the rotor circuit. ω and ω_r is speed at arbitrary reference frame and rotor speed. T_e and T_L, is the electromagnetic torque and load torque. P is the number of poles of the induction machine. J is the moment of inertial and $p = \frac{d}{dt}$. Since the rectifier outputs are connected together, then we say $v_{dc1} = v_{dc2} = v_{dc3} = v_{dc}$

3.2.2 Rectifier Converter side model

The rectifier converter model in the abc reference frame is:

$$v_{is} = \frac{v_{dc}}{2} \left(2S_{ip} - 1\right), \; j = 1, 2, 3, i = a_j, b_j, c_j, \; S_{ip} \in \{0, 1\} \tag{3.5}$$

Where $v_{is} = [v_{a_j} v_{b_j} v_{c_j}]^T$, are the voltages at the terminal of the multiple-phase induction machine. v_{dc} is the dc link voltage. S_{ip} is the switching function of the converters interfaced to the terminals of the multi-phase induction machine, taking values $S_{ip} \in \{0, 1\}$. The constraint equation for each converter system is $S_{ip} + S_{in} = 1$. The subscript 'ip' denotes specific phase upper switch '**on**' and subscript 'in' denoting lower switch of each converter off. Taking the fundamental component of the switching function, the switching function of the first fundamental component is:

$$S_{ij} = \frac{1}{2} \left(1 + m_{ij}\right); i = a, b, c; j = p, n \tag{3.6}$$

Transforming equation (3.5) into $q - d$ reference frame, using equation (2.3a), setting $\omega = \omega_e$, knowing that $\frac{d\theta}{dt} = \omega$ and considering the shift between the winding sets.

$$v_{qdsk} = T(\xi)v_{is} \tag{3.7}$$

$$[v_{qsk} \; v_{dsk}]^T = \frac{v_{dc}}{2} \left[\begin{array}{cc} m_{qsk} & m_{dsk} \end{array} \right]^T = T_s(\xi = 0)S_{ij} \quad k = 1, 2, 3 \tag{3.8}$$

Chapter 3. Modeling of Studied system

Where:

m_{qsk}, m_{dsk} are the modulating signal, of the rectifier converter system.

3.2.3 dc–link Capacitor side model

The schematic for the dc link is as shown in Figure 3.3
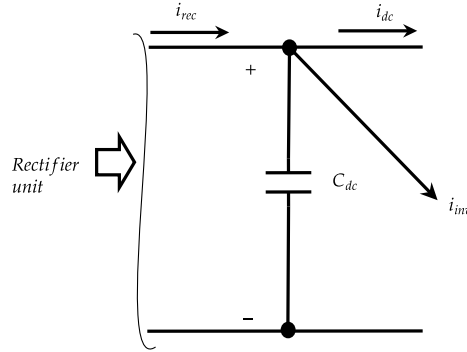
Figure 3.3: dc-link circuit configuration

Writing the dc link capacitor current.

$$Cpv_{dc} + i_{inv} + i_{dc} = \sum_{k=1}^{3} S_{jpk} i_{jsk}, \quad j = a, b, c \tag{3.9}$$

Transforming the equation into the $q - d$ reference frame.

$$Cpv_{dc} + i_{inv} + i_{dc} = \frac{3}{4} \left(m_{qs1} i_{qs1} + m_{ds1} i_{ds1} + m_{qs2} i_{qs2} + m_{ds2} i_{ds2} + m_{qs3} i_{qs3} + m_{ds3} i_{ds3} \right) \tag{3.10}$$

Re-writing the equation in condense form is:

$$Cpv_{dc} = \frac{3}{4} \sum_{k=1}^{3} \left(m_{qsk} i_{qsk} + m_{dsk} i_{dsk} \right) - i_{inv} - i_{dc} \tag{3.11}$$

Where: The rectifier current, $i_{rec} = \frac{3}{4} \sum_{k=1}^{3} \left(m_{qsk} i_{qsk} + m_{dsk} i_{dsk} \right)$, expressed in terms of the input $q - d$ current from the nine phase machine side and modulation indexes of the rectifier.

3.2.4 Bi-directional dc–dc Buck Boost Converter side model

The dc-dc converter model operation is derived based on switching function approach. The boost converter has two mode of operation. During the first mode of operation, the upper switch is turned on and off based on a defined pulse width modulated signal applied to the gate upper switch. The lower switch completely off during this mode, as it is not needed during this mode. During this operation, The voltage of the battery at the input of the dc-dc converter is bucked down to voltage slightly above the battery nominal volatge. The battery is charged through the inductor'L' and energy is dumped into the battery. During this period, the converter operation is in buck mode.
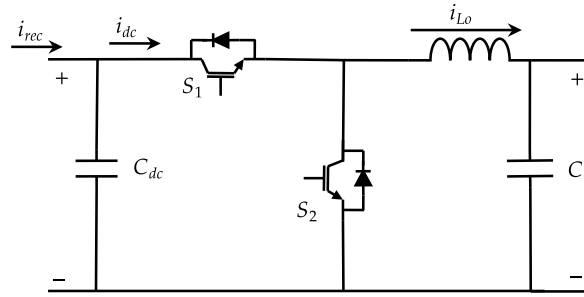
Figure 3.4: Bi-directional Converter System

During the boost mode, energy is returned to the dc link via the upper switch body diode. Here, only the lower switch is turned on and off in a pre-determined pulse width modulated signal fashion. So, for a bulk converter system, the relation between the output and input voltage can be express as, $d = \frac{v_{out}}{v_{in}}$ [173]. where d is the duty ratio for the bulk operation. The model equation for this mode is giving by

$$
\begin{cases}
L_o p i_{Lo} = d v_{dc} - v_b \\
i_{dc} = d i_{Lo}
\end{cases}
\tag{3.12}
$$

where:

L_o is the inductance of the connecting point between the bi-directional converter and the battery. v_b is the battery, i_{Lo} is the current through the inductor L_o.

3.2.5   Battery side model

The battery energy system model used in this schematic is shown in Figure 3.5.
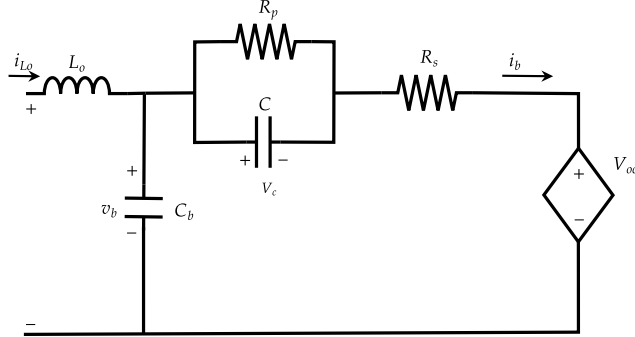
Figure 3.5: Battery Energy System

The battery energy system included in the subsystem can be represented by the following model equations:

$$C_b p v_b = i_{Lo} - i_b \tag{3.13}$$

$$C p v_c = i_b - \frac{v_c}{R_p} \tag{3.14}$$

$$pSoC = \frac{i_b}{q_{\max}} \tag{3.15}$$

$$v_b = v_c + i_b R_s(\text{SoC}) + V_{oc}(\text{SoC}) \tag{3.16}$$

$$
\begin{aligned}
V_{oc}(\text{SoC}) &= A_1 e^{-B_1 SoC} + C_1 + DSoC + ESoC^2 + FSoC^3 \\
R_s(\text{SoC}) &= A_2 e^{-B_2 SoC} + C_2 \\
R_p(\text{SoC}) &= A_3 e^{-B_3 SoC} + C_3
\end{aligned}
\tag{3.17}
$$

Where:

The terms $A_1, A_2, A_3, B_1, B_2, B_3, C_1, C_2, C_3, D, E, F$ in the equation are battery constant, defined by [174]. V_{oc} is the open circuit voltage of the battery R_p, R_s, C are battery parameters

3.2.6 dc–ac Converter side and R-Line side model

The dc–ac converter model in the *abc* frame is obtained using the model equation below. The equation is obtained by writing KVL equations around the output of the inverter and point of common coupling.
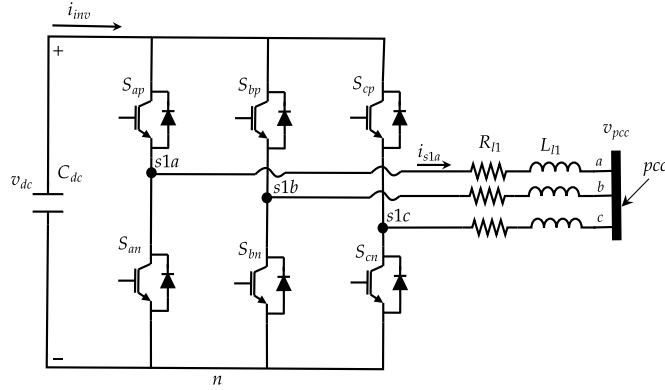
Figure 3.6: Inverter transmission line system

$$\begin{cases} v_{s1a} = v_{pcc_a} + L_{l1}pi_{s1a} + R_{l1}i_{s1a} \\ v_{s1b} = v_{pcc_b} + L_{l1}pi_{s1b} + R_{l1}i_{s1b} \\ v_{s1c} = v_{pcc_c} + L_{l1}pi_{s1c} + R_{l1}i_{s1c} \end{cases} \tag{3.18}$$

The three phase inverter equations are:

$$\begin{cases} v_{s1a} + v_{no} = \frac{v_{dc}}{2}\left(2s_{ap} - 1\right) \\ v_{s1b} + v_{no} = \frac{v_{dc}}{2}\left(2s_{bp} - 1\right) \\ v_{s1b} + v_{no} = \frac{v_{dc}}{2}\left(2s_{cp} - 1\right) \end{cases} \tag{3.19}$$

Where:

where the parameters v_{s1abc}, i_{s1abc} and s_{abcp} are output phase voltages, phase currents and switching functions of the inverter system.

Using the transformation matrix in 2.3a, with $\xi = 0$, the model equation in the arbitrary

reference frame is:

$$\begin{cases} pi_{s1q} = \frac{1}{L_{l1}} \left(m_{q1}\frac{v_{dc}}{2} - v_{q_{pcc}} - R_{l1}i_{s1q} - L_{s1}\omega i_{s1d} \right) \\ pi_{s1d} = \frac{1}{L_{l1}} \left(m_{d1}\frac{v_{dc}}{2} - v_{d_{pcc}} - R_{l1}i_{s1d} + L_{s1}\omega i_{s1q} \right) \end{cases} \tag{3.20}$$

Where:

where i_{s1qd}, R_{sl} and L_{sl} are qd-axis current, resistance and inductance of the network line. m_{qd1} is the modulating indexes of the inverter. ω speed at common point of coupling. v_{qdcc}, is the $q-d$ voltage at the point of common coupling. v_{dc} is the dc-link voltage.

3.2.7   Load side model
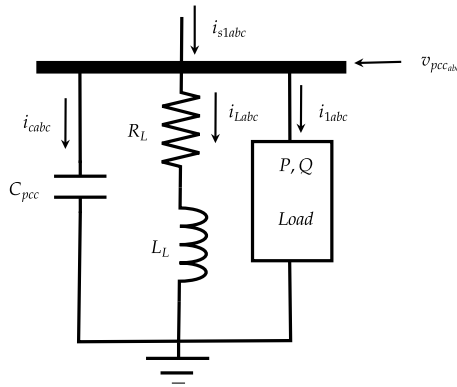
Figure 3.7: Hybrid Energy system load

The load model at the point of common coupling in the abc frame using KVL at load point:

- $R-L$ load side equation in $a-b-c$ frame

$$\begin{cases} v_{pcc_a} = R_L i_{L_a} + L_L pi_{L_a} \\ v_{pcc_b} = R_L i_{L_b} + L_L pi_{L_b} \\ v_{pcc_c} = R_L i_{L_c} + L_L pi_{L_c} \end{cases} \tag{3.21}$$

- Capacitor C load side equation in $a-b-c$ frame

The capacitor equation at the PCC in the abc reference frame ican be determined using

Chapter 3. Modeling of Studied system

KCL at the point of common coupling:

$$\begin{cases} C_{pcc}pv_{pcc_a} = i_{s1a} - i_{L_a} - i_{1a} \\ C_{pcc}pv_{pcc_b} = i_{s1b} - i_{L_b} - i_{1b} \\ C_{pcc}pv_{pcc_c} = i_{s1c} - i_{L_c} - i_{1c} \end{cases} \tag{3.22}$$

- Constant Power load side equation in the $a - b - c$ frame

$$\begin{cases} v_{pcc_a} = i_{1a}R_0 + L_0pi_{1a} \\ v_{pcc_b} = i_{1b}R_0 + L_0pi_{1b} \\ v_{pcc_c} = i_{1c}R_0 + L_0pi_{1c} \end{cases} \tag{3.23}$$

- Transformation of load side quantities to $q - d$ frame

Using the transformation matrix in 2.3a, with $\xi = 0$, the model equation (3.21)-(3.23) in the $q - d$ arbitrary reference frame is:

- $R - L$ load side equation in $q - d$ frame

$$\begin{cases} pi_{Lq} = \frac{1}{L_L}\left(v_{q_{pcc}} - R_Li_{Lq} - L_L\omega i_{Ld}\right) \\ pi_{Ld} = \frac{1}{L_L}\left(v_{d_{pcc}} - R_Li_{Ld} + L_L\omega i_{Lq}\right) \end{cases} \tag{3.24a}$$

- Capacitor C load side equation in $q - d$ frame

$$\begin{cases} pv_{q_{pcc}} = \frac{1}{C_{pcc}}\left(i_{s1q} - i_{Lq} - i_{1q} - C_{pcc}\omega v_{d_{pcc}}\right) \\ pv_{d_{pcc}} = \frac{1}{C_{pcc}}\left(i_{s1d} - i_{Ld} - i_{1d} + C_{pcc}\omega v_{q_{pcc}}\right) \end{cases} \tag{3.24b}$$

Where: $v_{qd_{pcc}}$ is the $q - d$ voltage of the point of common coupling. $i_{i_{Lqd}}$ is $q - d$ current through $R - L$ load. i_{1qd} is the current delivered to the constant power (i.e $P - Q$ load). C_{pcc} is the capacitance of parallel capacitor connected to the loads.

The constant $P - Q$ load model in $q - d$ frame.

Assume that, the constant power load is represented by the impedance, $Z_0 = R_0 + j\omega_0 L_0$.

Assuming, we represent the constant power load, $S_0 = P_0 + jQ_0 = \frac{3}{2}v_{qdpcc}i_{1qd}^*$.

$$Z_0 = \frac{v_{qdpcc}}{i_{1qd}} = \frac{v_{qpcc} + jv_{dpcc}}{i_{1q} + ji_{1d}} = \frac{v_{qpcc} + jv_{dpcc}}{i_{1q} + ji_{1d}} \times \frac{v_{qpcc} - jv_{dpcc}}{v_{qpcc} - jv_{dpcc}}. \tag{3.25a}$$

So, Z_0, could be represented as after the above expression as: $Z_0 = \frac{3}{2}\left(\frac{v_{qpcc}^2+v_{dpcc}^2}{S_0^*}\right)$.
Further modification of the Z_0 expression yield:

$$Z_0 = \frac{3}{2}\left(\frac{v_{qpcc}^2 + v_{dpcc}^2}{P_0 - jQ_0} \times \frac{P_0 + jQ_0}{P_0 + jQ_0}\right). \tag{3.25b}$$

Becauuse, $S_0^* = (P_0 - jQ_0)$

$$Z_0 = \frac{3}{2}\left(\frac{v_{qpcc}^2 + v_{dpcc}^2}{P_0^2 + Q_0^2}\right)(P_0 + jQ_0) \tag{3.25c}$$

Expanding (3.25g), and comparing with $Z_0 = R_0 + j\omega_0 L_0$ yield:

$$\begin{cases} R_0 = \frac{3}{2}\left(\frac{v_{qpcc}^2+v_{dpcc}^2}{P_0^2+Q_0^2}\right)P_0 \\ \omega L_0 = \frac{3}{2}\left(\frac{v_{qpcc}^2+v_{dpcc}^2}{P_0^2+Q_0^2}\right)Q_0 \end{cases} \tag{3.25d}$$

The current for the constant load is:

$$\begin{cases} i_{1q} = \frac{2}{3}\frac{P_0 v_{qpcc} + Q_0 v_{dpcc}}{v_{qpcc}^2 + v_{dpcc}^2} \\ i_{1d} = \frac{2}{3}\frac{P_0 v_{qpcc} - Q_0 v_{dpcc}}{v_{qpcc}^2 + v_{dpcc}^2} \end{cases} \tag{3.25e}$$

Transforming the constant load model of equation (3.23) into $q - d$ frame yield:

$$\begin{cases} v_{qpcc} = i_{1q}R_0 + L_0 p i_{1q} + \omega L_0 i_{1d} \\ v_{dpcc} = i_{1d}R_0 + L_0 p i_{1d} - \omega L_0 i_{1q} \end{cases} \tag{3.25f}$$

Subtituting equation (3.25d) and (3.25e) into equation (3.25f) yield the constant load model in $q - d$ frame as:

$$pi_{1q} = \frac{\omega}{Q_0}\left[-\frac{2}{3}\frac{P_0^2 + Q_0^2}{v_{qpcc}^2 + v_{dpcc}^2}v_{qpcc} + (P_0 i_{1q} - Q_0 i_{1d})\right]$$

$$pi_{1d} = \frac{\omega}{Q_0}\left[-\frac{2}{3}\frac{P_0^2 + Q_0^2}{v_{qcc}^2 + v_{dpcc}^2}v_{dpcc} + (P_0 i_{1d} + Q_0 i_{1q})\right] \tag{3.25g}$$

3.3 Steady State Analysis of Tri-three Phase Induction Machine

The model equation of the Tri-three phase derived so far is based on dynamic state equations of the machine. This section deals with the study of steady state analysis of the tri-three phase in detail. At steady state, the differential of variables of interest is zero. i.e $p(x) = 0$. where x are list of variable of interest. Here complex vector form approach will be utilize, because of the order of the multiphase induction machine describing equations. First we define the $q - d$ axis condensed vector form variables: $v_{qdsi} = v_{qsi} + jv_{dsi}, v_{qdr} = v_{qr} + jv_{dr}, \lambda_{qdsi} = \lambda_{qsi} + j\lambda_{dsi}, \lambda_{qdr} = \lambda_{qr} + j\lambda_{dr}, i_{qdsi} = i_{qsi} + ji_{dsi}, i_{qdr} = i_{qr} + ji_{dr}$. The 'j' operator in the preceding expression denote a $90°$ apart from the second variable. The dynamic model equation of tri-three phase induction machine in complex vector form at steady state, obtained from equation (3.1), $p(x) = 0$ is given by:

$$
\begin{cases}
V_{qds1} = r_{s1}i_{qds1} - j\omega_{e1}\lambda_{qds1} + \cancel{p\lambda_{qds1}}^0 \\
V_{qds2} = r_{s2}i_{qds2} - j\omega_{e2}\lambda_{qds2} + \cancel{p\lambda_{qds2}}^0 \\
V_{qds3} = r_{s3}i_{qds3} - j\omega_{e3}\lambda_{qds3} + \cancel{p\lambda_{qds3}}^0 \\
V_{qdr} = 0 = r_r i_{qdr} - j\omega_{sl}\lambda_{qdr} + \cancel{p\lambda_{qdr}}^0 \quad \text{where } \omega_{sl} \to slip
\end{cases}
\tag{3.26}
$$

In the context of equation (3.1), 'k' taking values of 1, 2, and 3, it represents the variables for the first, second, and third winding sets respectively. 'r_{sk}' denotes the stator resistance, 'r_r' signifies the rotor resistance, 'ω_{ek}' stands for electric speed, 'wsk' represents the slip, and 'ω_{rm}' corresponds to the rotor's mechanical speed. The slip for the three phase windings sets for different pole numbers can be mathematically expressed as: $\omega_{s1} = \omega_{e1} - \frac{P_1}{2}\omega_{rm}, \omega_{s2} = \omega_{e2} - \frac{P_2}{2}\omega_{rm}, \omega_{s3} = \omega_{e3} - \frac{P_3}{2}\omega_{rm}$. For the same pole numbers $P_1 = P_2 = P_3 = P$, the slips, $\omega_{s1}, \omega_{s2}, \omega_{s3}$ are equal. Figure 3.8 shows the equivalent circuit of a nine phase induction machine.

If we present the equation (3.2) for flux linkage in relation to currents in a matrix

format, it would appear as follows:

$$
\begin{bmatrix} \lambda_{qds1} \\ \lambda_{qds2} \\ \lambda_{qds3} \\ \lambda_{qdr} \end{bmatrix} = \begin{bmatrix} L_{1,1} & L_{lm}+L_m & L_{lm}+L_m & L_{lm}+L_m \\ L_{lm}+L_m & L_{2,2} & L_{lm}+L_m & L_{lm}+L_m \\ L_{lm}+L_m & L_{lm}+L_m & L_{3,3} & L_{lm}+L_m \\ L_m & L_m & L_m & L_{lr}+L_m \end{bmatrix} \times \begin{bmatrix} i_{qds1} \\ i_{qds2} \\ i_{qds3} \\ i_{qds3} \end{bmatrix}
\tag{3.27}
$$

Where:

$$L_{1,1} = L_{2,2} = L_{3,3} = L_{ls} + L_m + L_{lm}$$
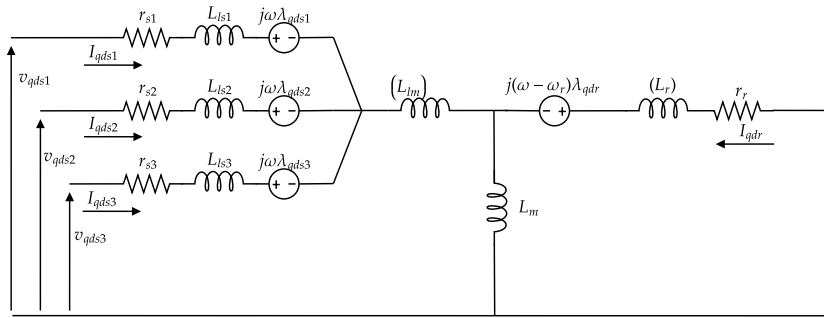
Figure 3.8: Nine Phase Induction Machine Equvalent Circuit

Solving for the current in complex compact form in terms of the flux linkage equations yield:

$$
\begin{cases}
i_{qdr} = \frac{a_1}{L_\sigma} \\[2mm]
i_{qds1} = \frac{a_2}{L_\sigma} \\[2mm]
i_{qds2} = \frac{a_3}{L_\sigma} \\[2mm]
i_{qds3} = \frac{a_4}{L_\sigma}
\end{cases}
\tag{3.28}
$$

Where:

$$L_{\sigma k} = \left(3L_{lm} + 3L_{lr} + L_{ls}\right) L_m + 3 \left(L_{lm} + \frac{L_{ls}}{3}\right) L_{lr}$$

Chapter 3. Modeling of Studied system

$$a_1 = (3\lambda_{qdr} - \lambda_{qds1} - \lambda_{qds2} - \lambda_{qds3})\, L_m + 3\lambda_{qdr}\left(L_{lm} + \tfrac{L_{ls}}{3}\right)$$

$$
\begin{aligned}
a_2 &= ((2\lambda_{qds1} - \lambda_{qds2} - \lambda_{qds3})\, L_{lr} + (2\lambda_{qds1} - \lambda_{qds2} - \lambda_{qds3})\, L_{lm} \\
&\quad - L_{ls}\,(\lambda_{qdr} - \lambda_{qds1})\, L_m + 2\left(\left(\lambda_{qds1} - \frac{\lambda_{qds2}}{2} - \frac{\lambda_{qds3}}{2}\right) L_{lm} + \frac{L_{ls}\lambda_{qds1}}{2}\right) L_{lr} \\
a_3 &= ((-\lambda_{qds1} + 2\lambda_{qds2} - \lambda_{qds3})\, L_{lr} + (-\lambda_{qdsI} + 2\lambda_{qds2} - \lambda_{qds3})\, L_{lm} \\
&\quad - L_{ls}\,(\lambda_{qdr} - \lambda_{qds2})\, L_m - L_{lr}\,((\lambda_{qdsI} - 2\lambda_{qds2} + \lambda_{qds3})\, L_{lm} - L_{ls}\lambda_{qds2}) \\
a_4 &= ((-\lambda_{qdsI} - \lambda_{qds2} + 2\lambda_{qds3})\, L_{lr} + (-\lambda_{qdsI} - \lambda_{qds2} + 2\lambda_{qds3})\, L_{lm} \\
&\quad - L_{ls}\,(\lambda_{qdr} - \lambda_{qds3})\, L_m - ((\lambda_{qdsI} + \lambda_{qds2} - 2\lambda_{qds3})\, L_{lm} - L_{ls}\lambda_{qds3})\, L_{lr}
\end{aligned}
$$

Eliminating the current values in equation(3.26), using equation (3.28), in addition, eliminating rotor flux linkage. Re-modifying the equations in terms of flux linkages equations, we have:

$$
\begin{cases}
V_{qds1} = (C_{s1} - j\omega_{e1})\,\lambda_{qds1} + B_{s1}\lambda_{qds2} + A_{s1}\lambda_{qds3} \\
V_{qds2} = A_{s2}\lambda_{qds1} + (C_{s2} - j\omega_{e2})\,\lambda_{qds2} + B_{s2}\lambda_{qds3} \\
V_{qds3} = B_{s3}\lambda_{qds1} + A_{s3}\lambda_{qds2} + (C_{s3} - j\omega_{e3})\,\lambda_{qds3}
\end{cases}
\tag{3.29}
$$

The parameters of equation(3.29) are defined in the appendix C.1:

Where, $A_{s1}, A_{s2}, A_{s3}, B_{s1}, B_{s2}, B_{s3}, C_{s1}, C_{s2}, C_{s3}$

Solving for the equations (3.29) at steady state, for $\lambda_{qds1}, \lambda_{qds2}, \lambda_{qds3}$, yield sets of long equations. This equations due to space constraint here has been transferred to appendix. A matlab script based on this obtained equations have been developed to illustrate the steady state plot of the nine phase induction machine using the concept of V/Hz applied to each three phase winding sets, of the nine phase induction machine. steady state plots for the nine phase induction machine are obtained and shown in plot of Figure (3.9)-(3.16).
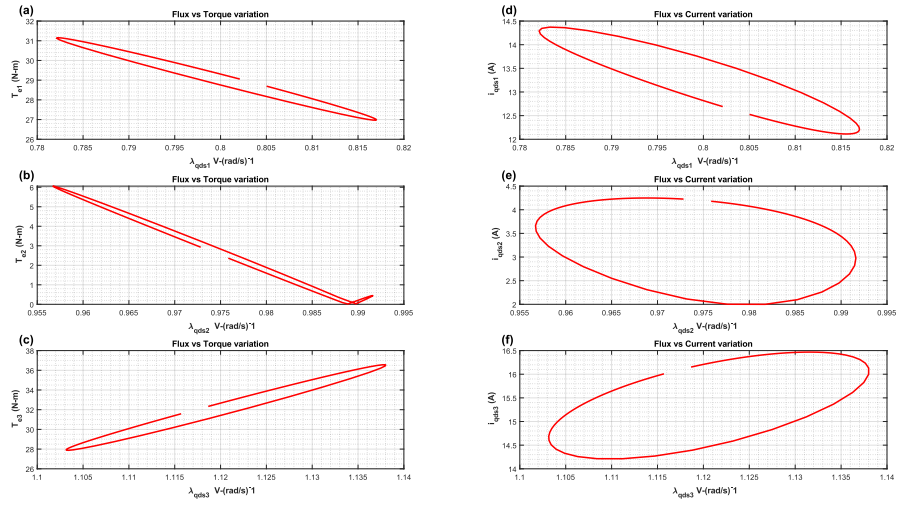
Figure 3.9: 2D-Plot of (a)–(c) Flux vs torque variations, (d)–(f) Flux vs current variations

Case I

Figure (3.9), (a)-(c), shows the variations of the flux of winding set 1,2 and 3 with respect to their respective torque, based on V/Hz operations. These curve which is obtained clearly from the steady state result of equation (3.30), using the parameter in table C.1, in appendix for frequency of each winding sets of the nine phase induction machine, sets for $f = 50Hz, 220V, P = 4$, taking into account the disposition between the winding sets when the analysis was carried out. The graph in Figure (3.9), (a)-(c) shows that the graph follow an elliptical path, with major axis of each curve shown stretching between turning points at the end of the curves. The steady state curve shows that for a nine phase induction machine, the torque are not equally shared between windings sets as the flux for each windings is varied. This assertion has been supported in the paper of [141], to keep the torque sharing balanced. Figure (3.9), (d)-(f), shows the variations of the flux of winding set 1,2 and 3 with current. The steady state current is obtained based on expanded equation of (3.27)–(3.28) solved in complex form. The plot also show the elliptical path of the current set variations for each windings.

The figure 3.10 shows the $3 - D$ plot of the torque, power factor, current of the studied nine phase induction machine expressed in terms of the current and torque of the nine phase induction machine.The graph shows the variations of each component studied

73

parameter of the multiple phase induction machine and how this affect other winding set of the induction machine. At higher torque levels, the efficiency of the nine machine increases. This is visibly shown in the plot of Figure 3.10
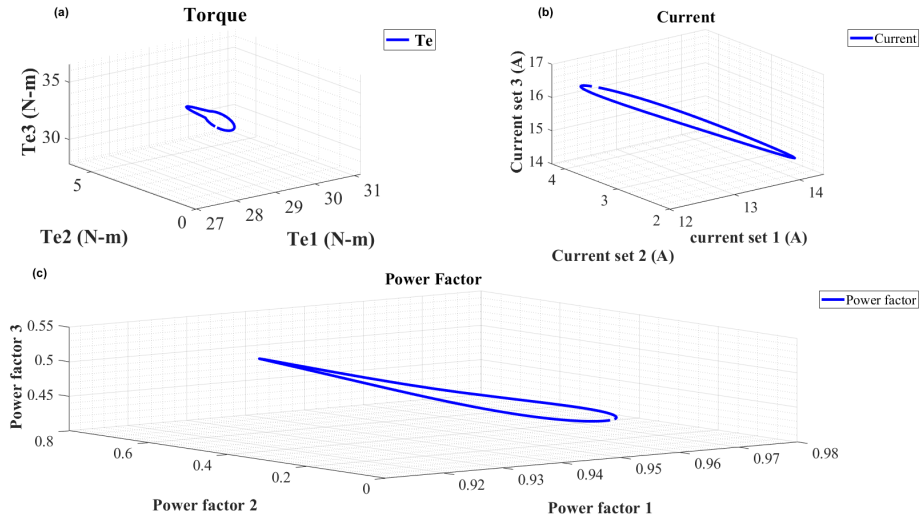
Figure 3.10: 3D-Plot of (a) torque, (b) current, (c) power factor

Again, having obtained the flux equation for the three set based on solving equation (3.29). We can find the current relations for the winding sets in terms of the stator flux linkage equation. Substituting the rotor flux equation (3.27) into equation(3.28), yield the stator current equation in terms of the stator flux linkages, Figure 3.11(d)-(f). Relation between torque and each respective winding power factor variation 3.11 (g)-(i).
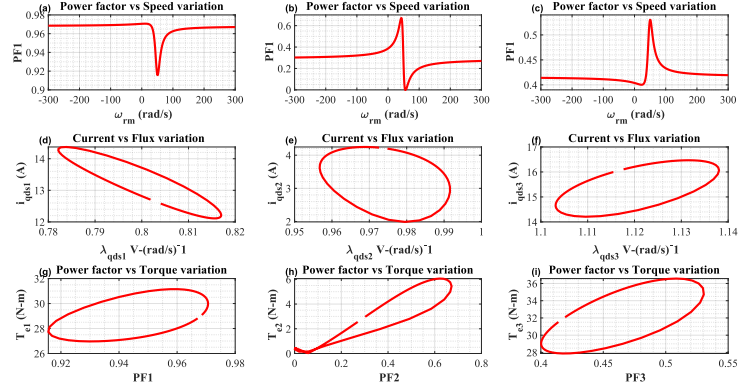
Figure 3.11: 2D-Plot of (a)–(c) Power factor vs speed(d)–(f) current vs flux variations (g)–(i) Torque vs power factor variations

The equation describing the electromagnetic torque for each stator winding set can be presented in a complex format as:

$$T_{ek} = \frac{3}{2} \frac{P_k}{2} \, \text{Im} \left(\lambda_{qdsk} i^*_{qdsk} \right) \tag{3.30}$$

The combined electromagnetic torque of the nine-phase stator winding induction machine arises from the summation of the torques produced by the two stator winding sets, and this can be represented as:

$$T_e = T_{e1} + T_{e2} + T_{e3} = \sum_{k=1}^{3} \frac{3}{2} \frac{P_k}{2} \, \text{Im} \left(\lambda_{qdsk} i^*_{qdsk} \right) \tag{3.31}$$

The gross slip, for the machine is expressed mathematically as:

$$s \underbrace{\sum_{1}^{3} \omega_{si}}_{gross\ slip} = \sum_{1}^{3} \omega_{si} - w_r \tag{3.32}$$

Assuming the machine parameters remain constant under any operational circumstance and applying a constant V/Hz control to the machine, the variables in equation (3.28)–(3.35) encompass the electromagnetic torque T_{ek}, rotor mechanical speed ω_{rm}, as well as the electric and electrical speeds of winding set 1, 2, and 3, denoted as $\omega_{e1}, \omega e2$ and

ω_{e3}, respectively.

The machine's equation for complex power is provided as follows:

$$S_k = \frac{3}{2} \left(V_{qdsk} i^*_{qdsk} \right) \tag{3.33}$$

Similarly the power factor relation is given by:

$$\text{Power Factor } (PF) = \frac{\text{Re} \left(S_k \right)}{Abs \left(S_k \right)} \tag{3.34}$$

In addition, the overall efficiency of the nine phase machine configuration is:

$$\eta = \frac{T_e \cdot \omega_{rm}}{\text{Re} \left(S_1 \right) + \text{Re} \left(S_2 \right) + \text{Re} \left(S_3 \right)} \tag{3.35}$$
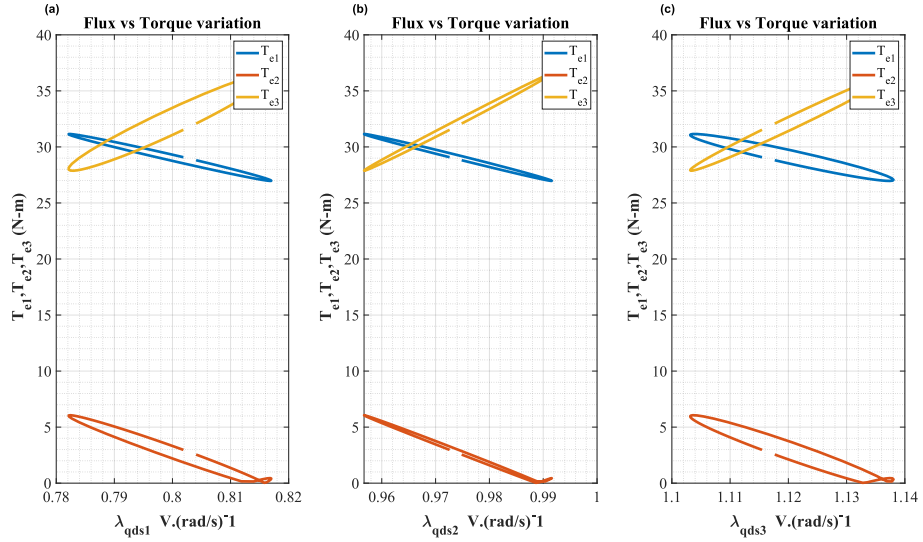
Figure 3.12: Torque variations (a)–(c) of each winding set in relation to specific winding linkage flux for winding set 1 frequency set at $f_1 = 50Hz$, winding set 2 frequency set at $f_2 = 50Hz$ and winding set 3 frequency set at $f_3 = 50Hz$

Figure 3.12 shows a plot of the various component torque variations for a nine phase induction machine in relation to flux variations of each respective windings. The philosophy behind this plot is to see how varying the flux of a specific windings affect the the torque of the connected specific windings and the torque of the unconnected specific windings. This variations is clearly illustrated in the plot that for torque of

76

winding set 3, the torque increases for all variations of the flux in all windings. However, for winding set 1 and 2, the torque decreases following an elliptical path as the flux levels in this windings are increased.

Case II

The steady state analysis of the nine phase induction machine was then carried out with slight changes to the frequency and voltage of the specific winding set of the induction machine, whilst keeping the frequency of a one winding set constant. The plot for the variation in the torque for various flux of each winding set, based on the different frequencies is shown in Figure 3.13 to Figure 3.16. From the Figure 3.13, it is observed that for a given flux variation from $1.14v(rad/s)^{-1}$ to $1.16v(rad/s)^{-1}$, there is an increase in the electromagnetic torque of winding set 1 and decrease in the contribution of torque from winding set 2 and winding set 3. This notable effect is expected since the frequency of winding set 3 is fixed at $50Hz$ and the frequency of other winding is varied to $20Hz$. A decrease in supply frequency with a fixed supply voltage results in an increase in the V/Hz ratio and flux. Increased flux enhances the motor's capacity to produce torque. However, Over fluxing can occur when a motor works at a greater V/Hz than its rated capacity, potentially leading to saturation of the stator and rotor magnetic core, which mush be avoided, during the design phase. From the graphs in Figure 3.13 (a),(b),(c), a conclusion can be drawn that as the flux levels in the winding sets are increased, the torque in the winding sets 1 increase and winding set 2 decrease. A noticeable effect is that the torque in winding set 3 decrease at first and then increases when the magnitude of the flux in the winding set 3 is increase further to keep the flux within defined steady state values for winding set 3.
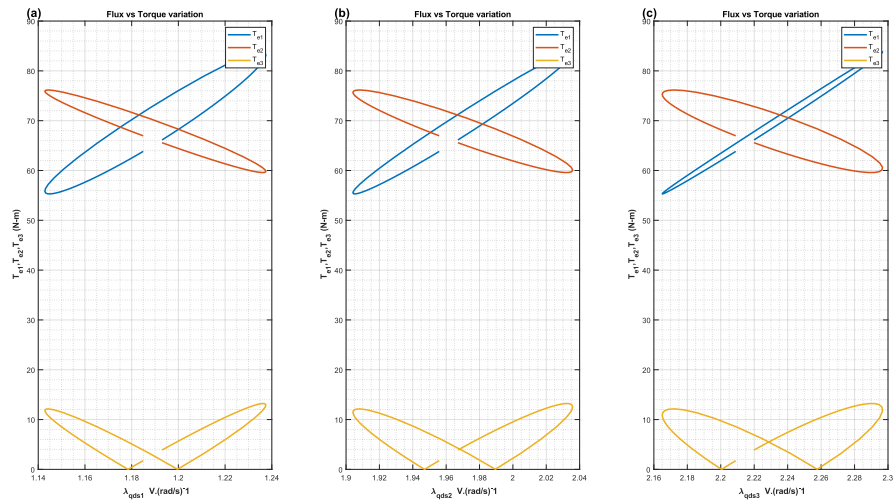
Figure 3.13: Torque variations (a)–(c) of each winding set in relation to specific winding linkage flux for winding set 1 frequency set at $f_1 = 20Hz$, winding set 2 frequency set at $f_2 = 20Hz$ and winding set 3 frequency set at $f_3 = 50Hz$

A different perspective is observed when the frequency of winding set 1 and winding set 2 is increased to $35Hz$ as shown in figure Figure 3.14. Here, it is observed that keeping the frequency of the winding set 3 constant , with frequency of the other winding set 1 and winding 2 varied, the electromagnetic torque in winding set 3 increases with increase in flux linkage, while the electromagnetic torque in winding set 1 and winding set 2 decreases with increase in flux linkage. At low flux linkage level, in Figure 3.14(a)-(c), the winding set 2 and 3 show the same torque contributions, and winding set 1 at $15Nm$. However, as the flux linkage in the winding set 1 increases, the torque contribution from winding set 2 and winding set 3 diverge with torque contribution from winding set 3 increasing and that of winding set 2 decreasing.
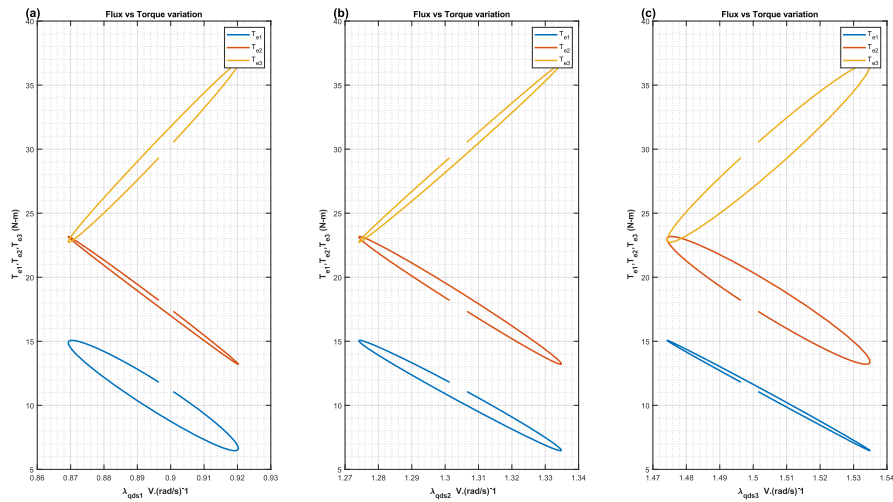
Figure 3.14: Torque variations (a)–(c) of each winding set in relation to specific winding linkage flux for winding set 1 frequency set at $f_1 = 35Hz$, winding set 2 frequency set at $f_2 = 35Hz$ and winding set 3 frequency set at $f_3 = 50Hz$

Some interesting perspectives regarding the variation of the torque and flux linkage is observed when the frequency of winding set 1 and winding set 2 is again increase further to $40Hz$, while keeping frequency of winding set 3 at $50Hz$, as shown in figure Figure 3.15. Here, as it is observed, unlike Figure 3.14, there was no point in the graph at which two of the winding sets contributed same torque. The Figure 3.15 shows that as the flux linkage is increased, that of winding set 3 increase proportionately which the torque from the other set sets (winding set 1 and winding set 2)decreases.
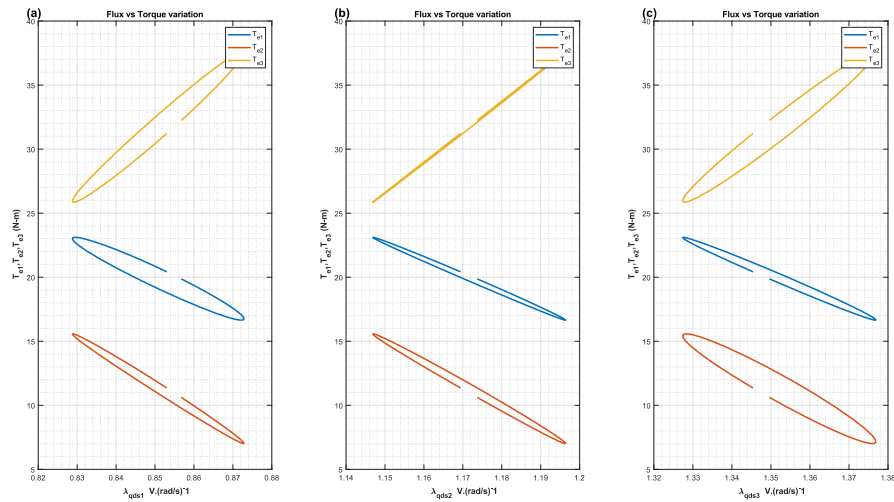
Figure 3.15: Torque variations (a)–(c) of each winding set in relation to specific winding linkage flux for winding set 1 frequency set at $f_1 = 40Hz$, winding set 2 frequency set at $f_2 = 40Hz$ and winding set 3 frequency set at $f_3 = 50Hz$

A change in the frequency of winding set 1 and winding set 2 to $45Hz$ is shown in Figure 3.16. It is clearly seen that at lower flux linkage values, winding set 1 and winding set 3, contributed the same amount of torque magnitude. However, this tend to change as the flux linkage is varied. Torque contribution from winding set 3 increases with increase in flux linkage, while the torque contribution from winding set 1 decreases. During this phase, the torque contribution from the winding set 2 decreases with increase with flux linkage. Conclusively, one can assert that there is a gain in torque improvement, when the frequency of at most two of the winding set is decreased while the frequency of the remaining winding set maintained at rated values. However, this must be done with good engineering judgement in order to ensure the multiple phase induction machine is not oversaturated.
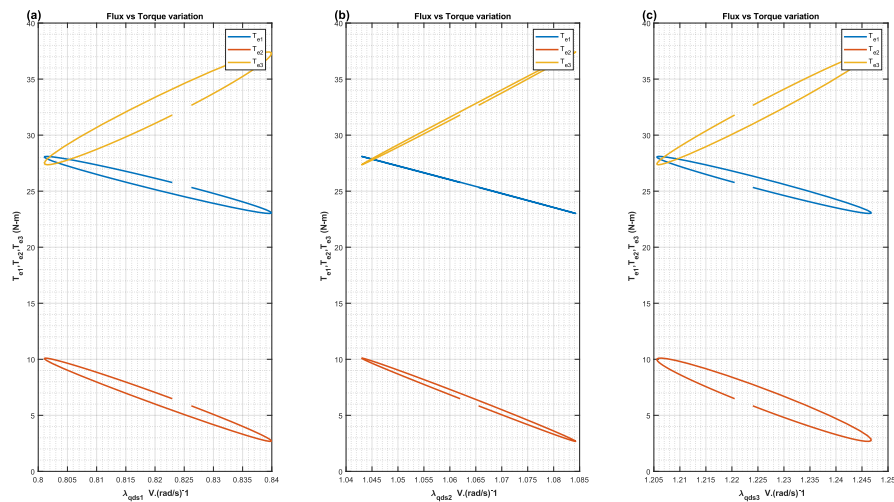
Figure 3.16: Torque variations (a)–(c) of each winding set in relation to specific winding linkage flux for winding set 1 frequency set at $f_1 = 45Hz$, winding set 2 frequency set at $f_2 = 45Hz$ and winding set 3 frequency set at $f_3 = 50Hz$

3.4 Power Flow Management and Rectifier converter Connection Dynamics

To understand how the boost converter connected to the output terminals of the multiple set induction machine operates, there is that need to understand the operation of the rectifier converter connected to a voltage source. This section will investigate the rectifier operation for series and parallel connection operation of this converters and hence, it becomes obvious from the analysis from this section the parallel connection topology offers the best connection approach for the multiple set induction machine approached in this thesis. The series and parallel rectifier connection topologies has been shown Figure 2.16, section 2.9 in chapter. Here, in these section, the analysis is carried out in expanded form.

3.4.1 Series Rectifier converter Connection topology and analysis

In power electronics, it's common to connect multiple series rectifier converters to a single load, which offers advantages like better performance, flexibility, and reliability. Each of these converters gets a part of the AC supply voltage and together they power

the load, enhancing control and increasing the DC voltage levels. This is particularly useful in applications requiring high-voltage DC, such as HVDC transmission lines.
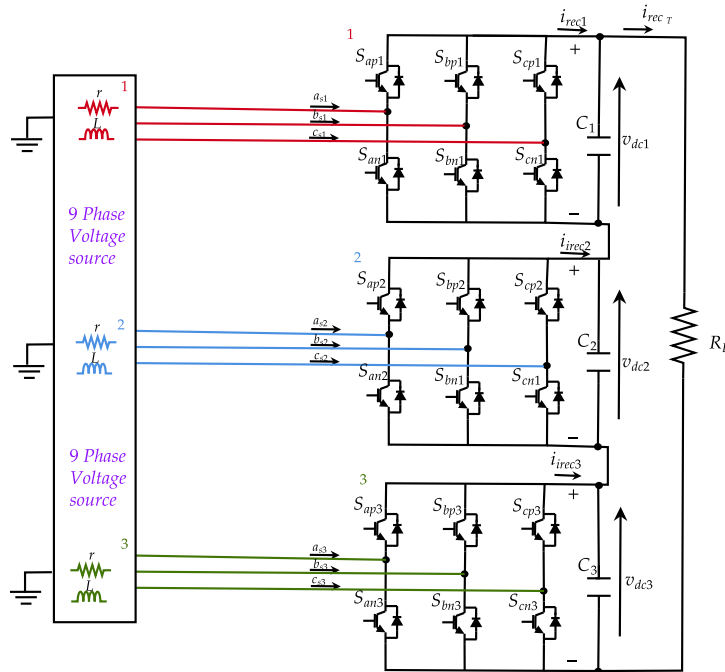
Figure 3.17: Series Converter rectifier topology

A couple of research work has been carried out to connect two or more cascaded converters namely: stacking of dc-dc converter based on the output voltage balancing [175], series connection of windfarm generator side converters in series [176]. All these configurations of converter connections have presented great benefits following different converter topologies.

Cascading these converters also improves system reliability. If one converter fails, the others can keep working, reducing downtime, which is crucial in data centers and vital infrastructure. Each converter can be controlled individually for precise adjustments, making it suitable for variable load requirements. To ensure efficiency, voltage balancing techniques, like adjusting semiconductor device firing angles, was also reported in the work of [177]. Figure 3.17 shows a series connection of a cascaded converter connected to a nine phase source. r, L is the source resistances and inductance of the connected

voltage source.

3.4.2   Model equation of series rectifier in the abc reference frame

Here, in the succeeding analysis, it is assumed that the sources to each converter are unconnected and neutral point of the sources are isolated from each other. The source resistance resistances and inductance are the same.

- **Source voltage rectifier voltage relation set 1**

$$\left.\begin{aligned}
V_{as1} &= ri_{as1} + Lpi_{as1} + V_{dc}\left[\tfrac{2}{3}S_{ap1} - \tfrac{1}{3}S_{bp1} - \tfrac{1}{3}S_{cp1}\right] \\
V_{bs1} &= ri_{bs1} + Lpi_{bs1} + V_{dc}\left[-\tfrac{1}{3}S_{ap1} + \tfrac{2}{3}S_{bp1} - \tfrac{1}{3}S_{cp1}\right] \\
V_{cs1} &= ri_{cs1} + Lpi_{cs1} + V_{dc}\left[-\tfrac{1}{3}S_{ap1} - \tfrac{1}{3}S_{bp1} + \tfrac{2}{3}S_{cp1}\right]
\end{aligned}\right\} \tag{3.36}$$

- **Source current rectifier current relation set 1**

$$i_{rec1} = S_{ap1}i_{as1} + S_{bp1}i_{bs1} + S_{cp1}i_{cs1} \tag{3.37}$$

- **Source voltage rectifier voltage relation set 2**

$$\left.\begin{aligned}
V_{as2} &= ri_{as2} + Lpi_{as2} + V_{dc}\left[\tfrac{2}{3}S_{ap2} - \tfrac{1}{3}S_{bp2} - \tfrac{1}{3}S_{cp2}\right] \\
V_{bs2} &= ri_{bs2} + Lpi_{bs2} + V_{dc}\left[-\tfrac{1}{3}S_{ap1} + \tfrac{2}{3}S_{bp1} - \tfrac{1}{3}S_{cp1}\right] \\
V_{cs2} &= ri_{cs2} + Lpi_{cs2} + V_{dc}\left[-\tfrac{1}{3}S_{ap2} - \tfrac{1}{3}S_{bp2} + \tfrac{2}{3}S_{cp2}\right]
\end{aligned}\right\} \tag{3.38}$$

- **Source current rectifier current relation set 2**

$$i_{rec2} = S_{ap2}i_{as2} + S_{bp2}i_{bs2} + S_{cp2}i_{cs2} \tag{3.39}$$

- **Source voltage rectifier voltage relation set 3**

$$\left.\begin{aligned}
V_{as3} &= ri_{as3} + Lpi_{as3} + V_{dc}\left[\tfrac{2}{3}S_{ap3} - \tfrac{1}{3}S_{bp3} - \tfrac{1}{3}S_{cp3}\right] \\
V_{bs3} &= ri_{bs3} + Lpi_{bs3} + V_{dc}\left[-\tfrac{1}{3}S_{ap3} + \tfrac{2}{3}S_{bp3} - \tfrac{1}{3}S_{cp3}\right] \\
V_{cs3} &= ri_{cs3} + Lpi_{cs3} + V_{dc}\left[-\tfrac{1}{3}S_{ap3} - \tfrac{1}{3}S_{bp3} + \tfrac{2}{3}S_{cp3}\right]
\end{aligned}\right\} \tag{3.40}$$

- **Source current rectifier current relation set 3**

$$i_{rec3} = S_{ap3}i_{as3} + S_{bp3}i_{bs3} + S_{cp3}i_{cs3} \tag{3.41}$$

Chapter 3. Modeling of Studied system

The equation (3.36)–(3.41) is the model equation of rectifier set 1,2 and 3.

The capacitor voltage equations:

$$\left.\begin{aligned} CpV_{dc1} &= i_{rec1} - \frac{V_{dc}}{3R_L} \\ CpV_{dc2} &= i_{rec2} - \frac{V_{dc}}{3R_L} \\ CpV_{dc3} &= i_{rec3} - \frac{V_{dc}}{3R_L} \end{aligned}\right\} \tag{3.42}$$

Where:

$C_1 = C_2 = C_3 = C$, $V_{dc1}, V_{dc2}, V_{dc3}$ are the voltages for converter capacitor sett 1, set 2 and set 3.

Since the capacitors are connected in series, the output voltage is the sum of individual output voltages across each converters. expressed mathematically as:

$$V_{dc} = \sum_{i=1}^{3} V_{dci} \tag{3.43}$$

Where: $V_{dc1} = V_{dc2} = V_{dc3} = \frac{V_{dc}}{3}$

Next, to carry out steady state analysis on the derive model equations for the rectifier, equation (3.36)–(3.41) is transformed to synchronous reference frame, using the transformation matrix equation(2.3a) and equation(2.3a) . These transformation matrix is repeated here, taking into account the disposition angle between sources.

• Stator transformation

$$T_s\left(\xi\right) = \frac{2}{3} \begin{bmatrix} \cos(\theta - \xi) & \cos(\theta - \xi - \beta) & \cos(\theta - \xi + \beta) \\ \sin\left(\theta - \xi\right) & \sin\left(\theta - \xi - \beta\right) & \sin\left(\theta - \xi + \beta\right) \\ \frac{1}{2} & \frac{1}{2} & \frac{1}{2} \end{bmatrix}, \; \forall, \; \xi = 0, \frac{\pi}{9}, \frac{2\pi}{9} \text{ and } \beta = \frac{2\pi}{3}$$

$$\tag{3.44a}$$

• The inverse Clarke transform Matrix is given by:

$$T_s^{-1}\left(\xi\right) = \begin{bmatrix} \cos(\theta - \xi) & \sin\left(\theta - \xi\right) & 1 \\ \cos(\theta - \xi - \beta) & \sin\left(\theta - \xi - \beta\right) & 1 \\ \cos(\theta - \xi + \beta) & \sin\left(\theta - \xi + \beta\right) & 1 \end{bmatrix}, \; \forall, \; \xi = 0, \frac{\pi}{9}, \frac{2\pi}{9} \text{ and } \beta = \frac{2\pi}{3} \tag{3.44b}$$

If it is assumed the system is balanced, neglecting zero sequence current as it does not flow. We then apply a set of transformation matrix equation to equation (3.36)–(3.41).

Chapter 3. Modeling of Studied system

The $q-d$ model equation of rectifier converter system in the synchronous reference frame is given by:

$$
\left.
\begin{aligned}
V_{qs1} &= rI_{qs1} + LpI_{qs1} + \omega_{e1}LI_{ds1} + \tfrac{M_{qs1}V_{dc}}{6} \\
V_{ds1} &= rI_{ds1} + LpI_{ds1} - \omega_{e1}LI_{qs1} + \tfrac{M_{ds1}V_{dc}}{6} \\
V_{qs2} &= rI_{qs2} + LpI_{qs2} + \omega_{e2}LI_{ds2} + \tfrac{M_{qs2}V_{dc}}{6} \\
V_{ds2} &= rI_{ds2} + LpI_{ds2} - \omega_{e2}LI_{qs2} + \tfrac{M_{ds2}V_{dc}}{6} \\
V_{qs3} &= rI_{qs3} + LpI_{qs3} + \omega_{e3}LI_{ds3} + \tfrac{M_{qs3}V_{dc}}{6} \\
V_{ds3} &= rI_{ds3} + LpI_{ds3} - \omega_{e3}LI_{qs3} + \tfrac{M_{ds3}V_{dc}}{6} \\
CpV_{dc1} &= \tfrac{3}{2}\left(M_{qs1}I_{qs1} + M_{ds1}I_{ds1}\right) - \tfrac{V_{dc}}{3R_L} \\
CpV_{dc2} &= \tfrac{3}{2}\left(M_{qs2}I_{qs2} + M_{ds2}I_{ds2}\right) - \tfrac{V_{dc}}{3R_L} \\
CpV_{dc3} &= \tfrac{3}{2}\left(M_{qs3}I_{qs3} + M_{ds3}I_{ds3}\right) - \tfrac{V_{dc}}{3R_L}
\end{aligned}
\right\}
\tag{3.45}
$$

The equation(3.45), depicts the dynamic state equations of the series rectifier converter systems. Parameters in the equation(3.45) are thus defined: $V_{qs1}, V_{qs2}, V_{qs3}, V_{ds1}, V_{ds2}, V_{ds3}$, are the $q-$ and $d-$ axis voltages of the rectifier systems. $I_{qs1}, I_{qs2}, I_{qs3}, I_{ds1}, I_{ds2}, I_{ds3}$ are the $q-$ and $d-$ axis current of the rectifier systems. $M_{qs1}, M_{qs2}, M_{qs3}, M_{ds1}, M_{ds2}, M_{ds3}$ are the $q-$ and $d-$ axis modulation signals for the rectifier systems. Here, the source speed expression $\omega_{e1} = \omega_{e2} = \omega_{e3} = \omega$ is the same if the frequency of the sources are the same. However for different sources, this ω will differ, and have to be accounted for in the equation.

3.4.2.1 Steady State Analysis of Series Rectifier

The state variables of the converter rectifier system is thus defined by the set of variables: $x = \{I_{qs1}, I_{ds1}, I_{qs2}, I_{ds2}, I_{qs3}, I_{ds3}, V_{dc1}, V_{dc2}, V_{dc3}\}$. At steady state, $p(x) = 0$. Equation

(3.45) is further reduced to equation (3.46).

$$\left.\begin{array}{l} V_{qs1} = rI_{qs1} + \omega_{e1}LI_{ds1} + \frac{M_{qs1}V_{dc}}{6} \\[4pt] V_{ds1} = rI_{ds1} - \omega_{e1}LI_{qs1} + \frac{M_{ds1}V_{dc}}{6} \\[4pt] V_{qs2} = rI_{qs2} + \omega_{e2}LI_{ds2} + \frac{M_{qs2}V_{dc}}{6} \\[4pt] V_{ds2} = rI_{ds2} - \omega_{e2}LI_{qs2} + \frac{M_{ds2}V_{dc}}{6} \\[4pt] V_{qs3} = rI_{qs3} + \omega_{e3}LI_{ds3} + \frac{M_{qs3}V_{dc}}{6} \\[4pt] V_{ds3} = rI_{ds3} - \omega_{e3}LI_{qs3} + \frac{M_{ds3}V_{dc}}{6} \\[4pt] 0 = \frac{3}{2}\left(M_{qs1}I_{qs1} + M_{ds1}I_{ds1}\right) - \frac{V_{dc}}{3R_L} \\[4pt] 0 = \frac{3}{2}\left(M_{qs2}I_{qs2} + M_{ds2}I_{ds2}\right) - \frac{V_{dc}}{3R_L} \\[4pt] 0 = \frac{3}{2}\left(M_{qs3}I_{qs3} + M_{ds3}I_{ds3}\right) - \frac{V_{dc}}{3R_L} \end{array}\right\} \quad (3.46)$$

To simplify equation (3.46), if it is assumed that the rectifier operates at unity power factor conditions, i.e for unity power factor, the $d-$ axis current and $d-$axis voltage is set to zero ($i_{dsi} = 0, V_{dsi} = 0, \forall\ i\ =\ 1,2,3$). The equation is further simplified to equation (3.47).

$$\left.\begin{array}{l} V_{qs1} = rI_{qs1} + \frac{M_{qs1}V_{dc}}{6} \\[4pt] 0 = 0 - \omega_{e1}LI_{qs1} + \frac{M_{ds1}V_{dc}}{6} \\[4pt] V_{qs2} = rI_{qs2} + \frac{M_{qs2}V_{dc}}{6} \\[4pt] 0 = 0 - \omega_{e2}LI_{qs2} + \frac{M_{ds2}V_{dc}}{6} \\[4pt] V_{qs3} = rI_{qs3} + \frac{M_{qs3}V_{dc}}{6} \\[4pt] 0 = 0 - \omega_{e3}LI_{qs3} + \frac{M_{ds3}V_{dc}}{6} \\[4pt] 0 = \frac{3}{2}\left(M_{qs1}I_{qs1}\right) - \frac{V_{dc}}{3R_L} \\[4pt] 0 = \frac{3}{2}\left(M_{qs2}I_{qs2}\right) - \frac{V_{dc}}{3R_L} \\[4pt] 0 = \frac{3}{2}\left(M_{qs3}I_{qs3}\right) - \frac{V_{dc}}{3R_L} \end{array}\right\} \quad (3.47)$$

There are nine sets of equations given in equation(3.47). For a particular operating point and given output voltage, the modulation indexes for the rectifier converters have to be determined. This can be found by solving the set of the given nine sets of equation for nine unknown i.e $I_{qs1}, I_{qs2}, I_{qs3}, M_{q1}, M_{q2}, M_{q3}, M_{d1}, M_{d2}, M_{d3}$. The steady state solutions resulting from the reduce equation of (3.47), $i_{qs1} = \frac{M_{ds1}V_{dc}}{6\omega_{e1}L}$, and $V_{qs1} = \frac{rM_{ds1}V_{dc}}{6\omega_{e1}L} + \frac{M_{qs1}V_{dc}}{6}$. The steady state results solutions obtained are plotted and shown in Figure (3.18)–(3.22).

Parameters used for the simulation is shown in appendix for the three set of converters.
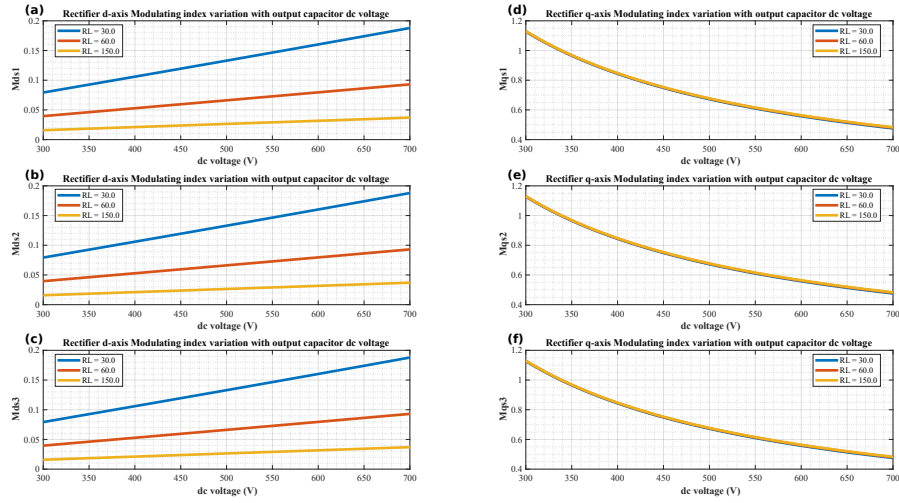
Figure 3.18: Modulating Index vs dc voltage variations for different load resistance

The provided diagram illustrates the fluctuations in the direct current (dc) load voltage and the q-d modulating indexes in a nine-phase source-powered series-connected cascaded rectifier converter configuration, as seen in Figure 3.17. These variations are observed across various load resistances. The plots were derived using the steady state equations (3.47) by eliminating the variables of interest, resulting in reduced form steady state equations for the specific plots. The plots illustrate the impact of varied loads connected to the output of the rectifier converter system on the modulation indexes along the $d-$axis. Nevertheless, the impact of load resistance on the modulation index of the $q-$axis has minimal influence across various loads when considering the variation in output dc voltage.

Figure 3.19 illustrates a plot depicting the variances in modulation indexes among the relevant converters, with varied load resistances foe a dc voltage of $440V$. The plot of converter converter 1, as depicted in Figure 3.19(a), exhibits intriguing characteristics.
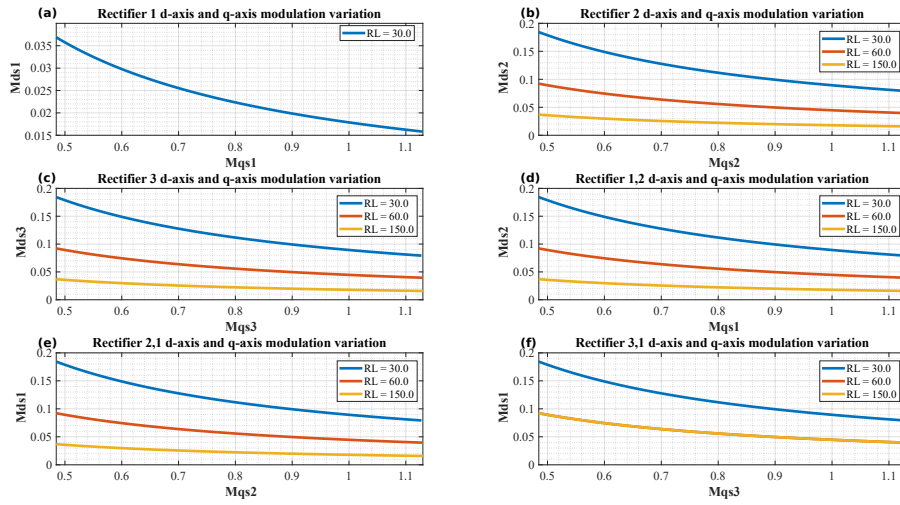
Figure 3.19: Modulating Indexes for different rectifier converter

Notably, the observed variations in modulation indexes alone impact the load resistance of 30 ohms. A similar phenomenon, but from a different perspective, is depicted in Figure 3.19(f), where the modulation indexes exclusively impact the load resistances of 30 ohms and 60 ohms, respectively. The observed pattern of the two curves can be attributed to the fact that the resistances of the load under investigation for these modulation changes go beyond the scope of the steady state analysis conducted in the numerical evaluation. The curve depicted in Figure 3.19(c)–(d) illustrates the variations observed in the modulation indices when the load resistances are incremented. A further increase in the load to the value of 160 ohms for the purpose of steady state study reveals that the modulation index on the load's $d-$ axis has no notable effect. The figure depicted in Figure 3.21 illustrates the variations in modulation indexes of the converters and $q - d$ currents of each converter in relation to various load resistances. The illustrated figures, namely Figure 3.20 (a), (c), and (e), demonstrate a comparable feature in terms of the variations of the source currents along the $d-$ axis with modulation indexes. However, the plot depicted in Figure 3.20(b),(d),(f) exhibits a distinct change upon observation. The plot pattern seen in Figure 3.20 was also found to be similar in Figure 3.21, where the modulation indexes were plotted against variations in power. Both plots illustrate the relationship between current increases and

different load resistances. Additionally, it can be shown that a load resistance of 50 ohms provides a broad range for adjusting the modulating indices along the $d-$ axis. The modulating indexes of Figure 3.20 (b),(d),(f) decrease as the current and power consumption of the load grow.
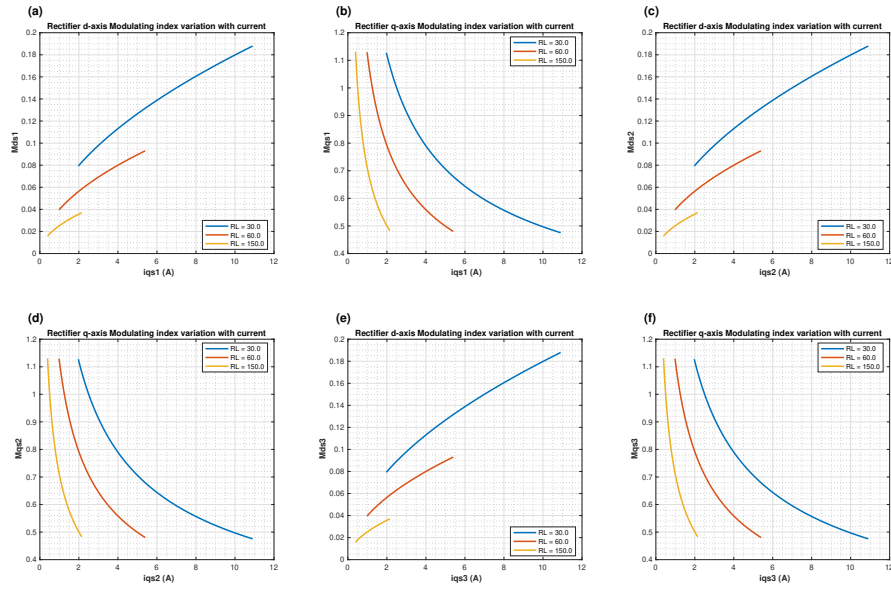
Figure 3.20: Series converter rectifier topology modulating indexes vs source current for the nine phase source
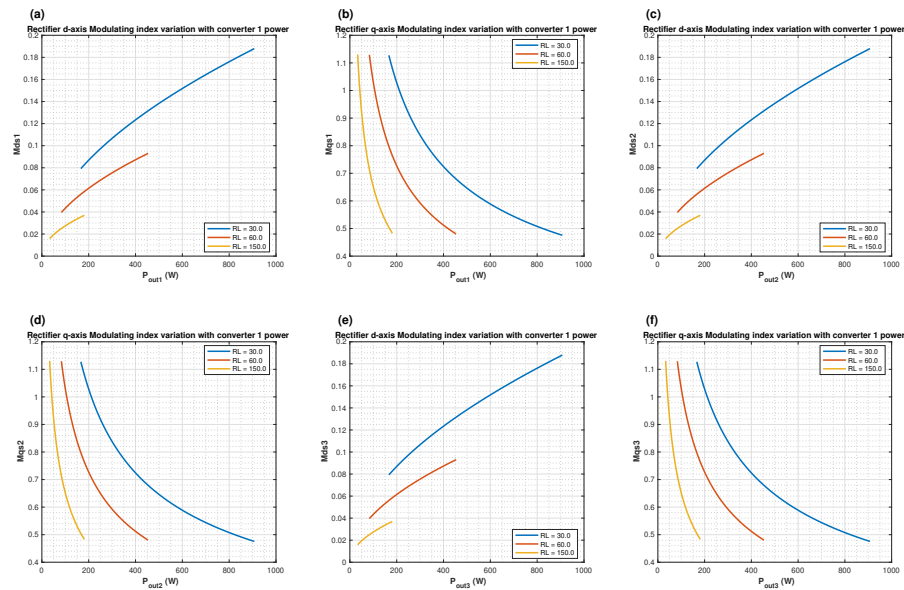
Figure 3.21: Series converter rectifier topology modulating indexes vs power delivered by a nine phase source to load resistances

3.4.3 Parallel Rectifier converter Connection topology and analysis

The figure depicted in Figure 3.22 illustrates the topological connection configuration of stacked parallel rectifier converters. Cascaded parallel rectifier converters are widely utilised in the field of power electronics due to its advantageous characteristics, such as enhanced reliability, scalability, and load distribution [177, 178]. The aforementioned converters effectively allocate the load among numerous interconnected units in parallel, so guaranteeing that the load is supplied with the required current. The ability to proportionally vary their output in response to changes in load enables effective power distribution. The enhancement of system dependability is achieved by the use of numerous converters in a cascade configuration, which enables the system to continue functioning and distribute the workload in the event of a breakdown. According to [179], the presence of redundancy has the potential to reduce downtime and enhance the overall availability of the power system.
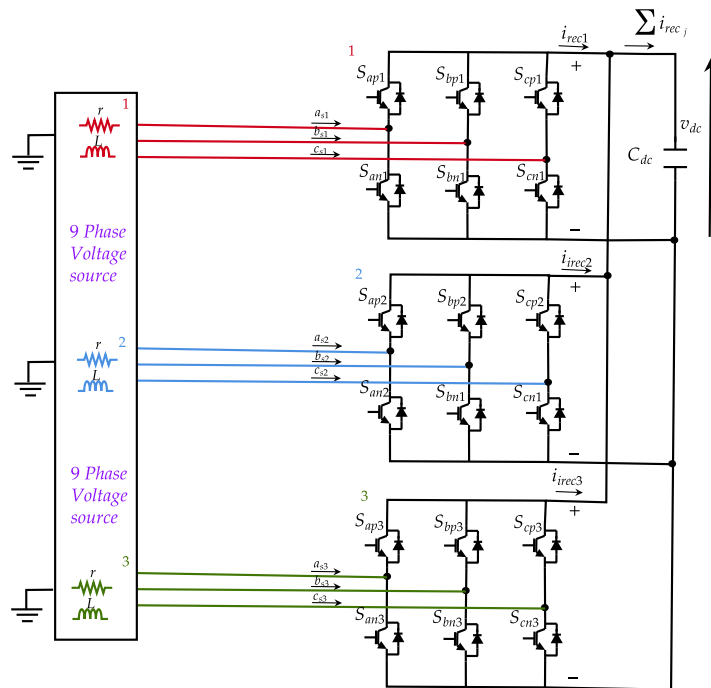
Figure 3.22: Parallel converter rectifier topology

Accurate control and modulation of each converter in the cascade allows for accurate adjustment of output voltage and current, allowing for greater response to changing conditions. To ensure steady operation, the converters' current balance must be maintained [180]. Cascaded converters are used in various industries, including motor drive applications, critical power backup systems, renewable energy systems, and electric car charging systems. Power electronics and electrical engineers and designers must understand the fundamentals and practical uses of cascaded parallel rectifier converters.

3.4.4 Model equation of Parallel rectifier in the abc reference frame

Here, in the succeeding analysis, it is assumed that the sources to each converter are unconnected and neutral point of the sources are isolated from each other. The source resistance resistances and inductance are the same. The output of the rectifier converter system are connected together as shown in Figure 3.18. The rectifier converter expression is the same as was derived for series rectifier topology. So it is repeated here, except

that the output current from the rectifiers to the output capacitor is the sum of all current contributions from the rectifiers. This have been noted and accounted for in the succeeding equations.

- **Source voltage rectifier voltage relation set 1**

$$\left.\begin{aligned}
V_{as1} &= ri_{as1} + Lpi_{as1} + V_{dc}\left[\tfrac{2}{3}S_{ap1} - \tfrac{1}{3}S_{bp1} - \tfrac{1}{3}S_{cp1}\right] \\
V_{bs1} &= ri_{bs1} + Lpi_{bs1} + V_{dc}\left[-\tfrac{1}{3}S_{ap1} + \tfrac{2}{3}S_{bp1} - \tfrac{1}{3}S_{cp1}\right] \\
V_{cs1} &= ri_{cs1} + Lpi_{cs1} + V_{dc}\left[-\tfrac{1}{3}S_{ap1} - \tfrac{1}{3}S_{bp1} + \tfrac{2}{3}S_{cp1}\right]
\end{aligned}\right\} \tag{3.48}$$

- **Source current rectifier current relation set 1**

$$i_{rec1} = S_{ap1}i_{as1} + S_{bp1}i_{bs1} + S_{cp1}i_{cs1} \tag{3.49}$$

- **Source voltage rectifier voltage relation set 2**

$$\left.\begin{aligned}
V_{as2} &= ri_{as2} + Lpi_{as2} + V_{dc}\left[\tfrac{2}{3}S_{ap2} - \tfrac{1}{3}S_{bp2} - \tfrac{1}{3}S_{cp2}\right] \\
V_{bs2} &= ri_{bs2} + Lpi_{bs2} + V_{dc}\left[-\tfrac{1}{3}S_{ap1} + \tfrac{2}{3}S_{bp1} - \tfrac{1}{3}S_{cp1}\right] \\
V_{cs2} &= ri_{cs2} + Lpi_{cs2} + V_{dc}\left[-\tfrac{1}{3}S_{ap2} - \tfrac{1}{3}S_{bp2} + \tfrac{2}{3}S_{cp2}\right]
\end{aligned}\right\} \tag{3.50}$$

- **Source current rectifier current relation set 2**

$$i_{rec2} = S_{ap2}i_{as2} + S_{bp2}i_{bs2} + S_{cp2}i_{cs2} \tag{3.51}$$

- **Source voltage rectifier voltage relation set 3**

$$\left.\begin{aligned}
V_{as3} &= ri_{as3} + Lpi_{as3} + V_{dc}\left[\tfrac{2}{3}S_{ap3} - \tfrac{1}{3}S_{bp3} - \tfrac{1}{3}S_{cp3}\right] \\
V_{bs3} &= ri_{bs3} + Lpi_{bs3} + V_{dc}\left[-\tfrac{1}{3}S_{ap3} + \tfrac{2}{3}S_{bp3} - \tfrac{1}{3}S_{cp3}\right] \\
V_{cs3} &= ri_{cs3} + Lpi_{cs3} + V_{dc}\left[-\tfrac{1}{3}S_{ap3} - \tfrac{1}{3}S_{bp3} + \tfrac{2}{3}S_{cp3}\right]
\end{aligned}\right\} \tag{3.52}$$

- **Source current rectifier current relation set 3**

$$i_{rec3} = S_{ap3}i_{as3} + S_{bp3}i_{bs3} + S_{cp3}i_{cs3} \tag{3.53}$$

The equation (3.48)–(3.58) is the model equation of rectifier set 1,2 and 3. The capacitor voltage equations:

$$CpV_{dc} = i_{rec1} + i_{rec2} + i_{rec3} - \frac{V_{dc}}{R_L} \tag{3.54}$$

Chapter 3. Modeling of Studied system

Where:

C, $V_{dc1}, V_{dc2}, V_{dc3}$ is the capacitance and voltages for converter capacitor set 1, set 2 and set 3 respectively.

Since the capacitors are connected in parallel, the output voltage is the same and equal across each converters. expressed mathematically as:

$$V_{dc} = V_{dc1} = V_{dc2} = V_{dc3} \qquad (3.55)$$

Next, to carry out steady state analysis on the derive model equations for the rectifier, equation (3.48)–(3.54) is transformed to synchronous reference frame, using the transformation matrix equation(3.44a) and equation(3.44b) . These transformation matrix is repeated here, taking into account the disposition angle between sources.

If it is assumed the system is balanced, neglecting zero sequence current as it does not flow. We then apply a set of transformation matrix equation to equation (3.48)–(3.54). The $q - d$ model equation of rectifier converter system in the synchronous reference frame is given by:

$$\left.\begin{aligned}
V_{qs1} &= rI_{qs1} + LpI_{qs1} + \omega_{e1}LI_{ds1} + \frac{M_{qs1}V_{dc}}{2} \\
V_{ds1} &= rI_{ds1} + LpI_{ds1} - \omega_{e1}LI_{qs1} + \frac{M_{ds1}V_{dc}}{2} \\
V_{qs2} &= rI_{qs2} + LpI_{qs2} + \omega_{e2}LI_{ds2} + \frac{M_{qs}V_{dc}}{2} \\
V_{ds2} &= rI_{ds2} + LpI_{ds2} - \omega_{e2}LI_{qs2} + \frac{M_{ds2}V_{dc}}{2} \\
V_{qs3} &= rI_{qs3} + LpI_{qs3} + \omega_{e3}LI_{ds3} + \frac{M_{qs3}V_{dc}}{2} \\
V_{ds3} &= rI_{ds3} + LpI_{ds3} - \omega_{e3}LI_{qs3} + \frac{M_{ds3}V_{dc}}{2} \\
CpV_{dc} &= \tfrac{3}{2}\sum_{i=1}^{3}\left(M_{qsi}I_{qsi} + M_{dsi}I_{dsi}\right) - \frac{V_{dc}}{R_L}
\end{aligned}\right\} \qquad (3.56)$$

The equation(3.56), depicts the dynamic state equations of the series rectifier converter systems. Parameters in the equation(3.56) are thus defined: $V_{qs1}, V_{qs2}, V_{qs3}, V_{ds1}, V_{ds2}, V_{ds3},$ are the $q-$ and $d-$ axis voltages of the rectifier systems. $I_{qs1}, I_{qs2}, I_{qs3}, I_{ds1}, I_{ds2}, I_{ds3}$ are the $q-$ and $d-$ axis current of the rectifier systems. $M_{qs1}, M_{qs2}, M_{qs3}, M_{ds1}, M_{ds2}, M_{ds3}$ are the $q-$ and $d-$ axis modulation signals for the rectifier systems. Here, the source speed expression $\omega_{e1} = \omega_{e2} = \omega_{e3} = \omega$ is the same if the frequency of the sources are

93

Chapter 3. Modeling of Studied system

the same. However for different sources, this ω will differ, and have to be accounted for in the equation.

3.4.4.1   Steady State Analysis of Parallel Rectifier

The state variables of the converter rectifier system is thus defined by the set of variables: $x = \{I_{qs1}, I_{ds1}, I_{qs2}, I_{ds2}, I_{qs3}, I_{ds3}, V_{dc1}, V_{dc2}, V_{dc3}\}$. At steady state, $p(x) = 0$. Equation (3.56) is further reduced to equation (3.57).

$$\left.\begin{aligned}
V_{qs1} &= rI_{qs1} + \omega_{e1}LI_{ds1} + \tfrac{M_{qs1}V_{dc}}{2} \\
V_{ds1} &= rI_{ds1} - \omega_{e1}LI_{qs1} + \tfrac{M_{ds1}V_{dc}}{2} \\
V_{qs2} &= rI_{qs2} + \omega_{e2}LI_{ds2} + \tfrac{M_{qs2}V_{dc}}{2} \\
V_{ds2} &= rI_{ds2} - \omega_{e2}LI_{qs2} + \tfrac{M_{ds2}V_{dc}}{2} \\
V_{qs3} &= rI_{qs3} + \omega_{e3}LI_{ds3} + \tfrac{M_{qs3}V_{dc}}{2} \\
V_{ds3} &= rI_{ds3} - \omega_{e3}LI_{qs3} + \tfrac{M_{ds3}V_{dc}}{2} \\
0 &= \tfrac{3}{2}\sum_{i=1}^{3}\left(M_{qsi}I_{qsi} + M_{dsi}I_{dsi}\right) - \tfrac{V_{dc}}{R_L}
\end{aligned}\right\} \tag{3.57}$$

To simplify equation (3.57), if it is assumed that the rectifier operates at unity power factor conditions, i.e for unity power factor, the $d-$ axis current and $d-$axis voltage is set to zero ($i_{dsi} = 0, V_{dsi} = 0, \forall\ i\ =\ 1, 2, 3$). The equation is further simplified to equation (3.58).

$$\left.\begin{aligned}
V_{qs1} &= rI_{qs1} + \tfrac{M_{qs1}V_{dc}}{2} \\
0 &= -\omega_{e1}LI_{qs1} + \tfrac{M_{ds1}V_{dc}}{2} \\
V_{qs2} &= rI_{qs2} + \tfrac{M_{qs2}V_{dc}}{2} \\
0 &= -\omega_{e2}LI_{qs2} + \tfrac{M_{ds2}V_{dc}}{2} \\
V_{qs3} &= rI_{qs3} + \tfrac{M_{qs3}V_{dc}}{2} \\
0 &= -\omega_{e3}LI_{qs3} + \tfrac{M_{ds3}V_{dc}}{2} \\
0 &= \tfrac{3}{2}\sum_{i=1}^{3}\left(M_{qsi}I_{qsi}\right) - \tfrac{V_{dc}}{R_L}
\end{aligned}\right\} \tag{3.58}$$

There are seven sets of equations given in equation(3.57). For a particular operating point and given output voltage, the modulation indexes for the rectifier converters have to be determined. This can be found by solving the seven sets of equation, however there

are nine unknown i.e $I_{qs1}, I_{qs2}, I_{qs3}, M_{q1}, M_{q2}, M_{q3}, M_{d1}, M_{d2}, M_{d3}$. This present a challenge, as the number of unknown variables exceeds the number of steady state equation to solve for. To solve for this, we have to incorporate additional constraint equations to make the equation solvable. This is done from the power relations from each source: Let's assume the total power of each converter system is defined as:

$$\left.\begin{aligned} P_1 &= \tfrac{3}{2}\left(V_{qs1}I_{qs1} + V_{ds1}I_{ds1}\right) \\ P_2 &= \tfrac{3}{2}\left(V_{qs2}I_{qs2} + V_{ds2}I_{ds2}\right) \\ P_3 &= \tfrac{3}{2}\left(V_{qs3}I_{qs3} + V_{ds3}I_{ds3}\right) \end{aligned}\right\} \tag{3.59}$$

At unity power factor, $V_{ds1} = V_{ds2} = V_{ds3} = 0$, The expression reduce to:

$$\left.\begin{aligned} P_1 &= \tfrac{3}{2}\left(V_{qs1}I_{qs1}\right) \\ P_2 &= \tfrac{3}{2}\left(V_{qs2}I_{qs2}\right) \\ P_3 &= \tfrac{3}{2}\left(V_{qs3}I_{qs3}\right) \end{aligned}\right\} \tag{3.60}$$

If P_T is the total power of the three rectifier converters, and k_1, k_2, k_3 is chosen to denote the fraction of the total power. The worth of each power relation based on this sharing ratios of the rectifier converters is $\frac{P_T}{k_1+k_2+k_3}$, The power sharing relation resulting from this is given by:

$$\left.\begin{aligned} P_1 &= \tfrac{k_1}{k_1+k_2+k_3} \times P_T = \tfrac{3}{2}\left(V_{qs1}I_{qs1}\right) \\ P_2 &= \tfrac{k_2}{k_1+k_2+k_3} \times P_T = \tfrac{3}{2}\left(V_{qs2}I_{qs2}\right) \\ P_3 &= \tfrac{k_3}{k_1+k_2+k_3} \times P_T = \tfrac{3}{2}\left(V_{qs3}I_{qs3}\right) \end{aligned}\right\} \tag{3.61}$$

At all point in time in the foregoing analysis, $k_1 + k_2 + k_3 = 1$. Using the equation 3.61, clearly three constraint equations can be established from the relation. Two out of these relations are combined with the equation (3.58) to find the steady equations required to solve the steady state equation.The full order steady state equations for

Chapter 3.   Modeling of Studied system

nine equations and nine unknowns is given by equation (3.62).

$$\left.\begin{aligned}
V_{qs1} &= rI_{qs1} + \tfrac{M_{q1}V_{dc}}{2} \\
0 &= -\omega_{e1}LI_{qs1} + \tfrac{M_{d1}V_{dc}}{2} \\
V_{qs2} &= rI_{qs2} + \tfrac{M_{q2}V_{dc}}{2} \\
0 &= -\omega_{e2}LI_{qs2} + \tfrac{M_{d2}V_{dc}}{2} \\
V_{qs3} &= rI_{qs3} + \tfrac{M_{q3}V_{dc}}{2} \\
0 &= -\omega_{e3}LI_{qs3} + \tfrac{M_{d3}V_{dc}}{2} \\
0 &= \tfrac{3}{2}\sum_{i=1}^{3}\left(M_{qsi}I_{qsi}\right) - \tfrac{V_{dc}}{R_L} \\
0 &= k_1 V_{qs2}I_{qs2} - k_2 V_{qs1}I_{qs1} \\
0 &= k_2 V_{qs3}I_{qs3} - k_3 V_{qs2}I_{qs2}
\end{aligned}\right\} \tag{3.62}$$

The steady state results solutions for the parallel converter configuration obtained are plotted and shown in Figure 3.23–(3.24). Parameters used for the simulation is shown in appendix for the three set of converters.

The figure depicted in Figure 3.23 illustrates the variations in modulation indexes of the converters and $q-d$ currents of each converter in relation to various load resistances. The illustrated figures, namely Figure 3.23 (a),(c), and (e), demonstrate a comparable feature in terms of the variations of the source currents along the $d-$ axis with modulation indexes. However, the plot depicted in Figure 3.24(b),(d),(f) exhibits a distinct change upon observation. The plot pattern seen in Figure 3.24. Both plots illustrate the relationship between current increases and different load resistances. Additionally, it can be shown that a load resistance of 50 ohms provides a broad range for adjusting the modulating indices along the $d-$ axis.
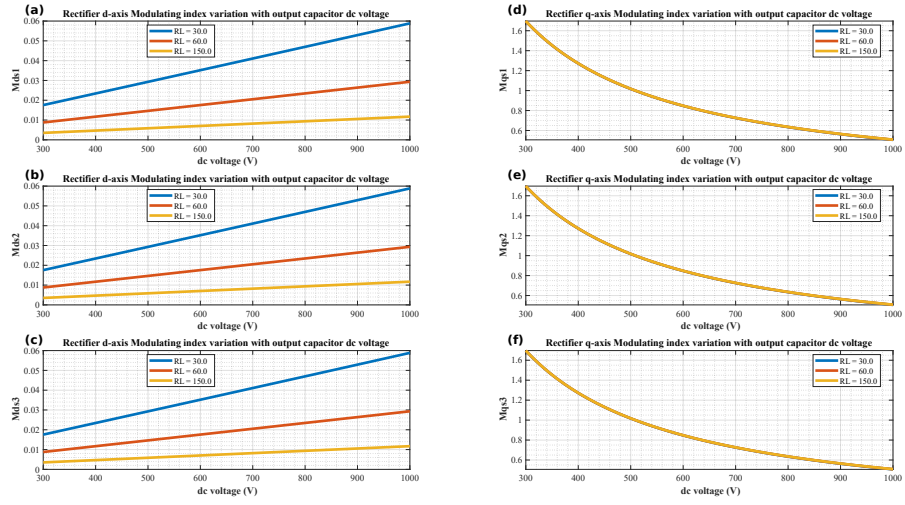
Figure 3.23: Modulating Index vs dc voltage variations for different load resistance, for $k_1 = k_2 = k_3 = \frac{1}{3}$
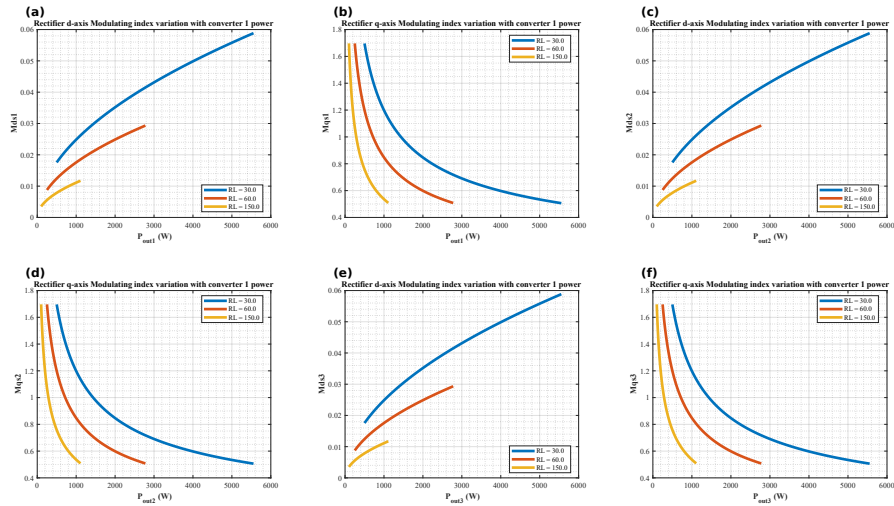
Figure 3.24: Parallel converter rectifier topology for $k_1 = k_2 = k_3 = 33.33\%$

The investigation focuses on the power variations with regard to the $d-$ and $q-$ axes of each modulating index for each converter. This analysis is conducted for different scenarios, taking into account the sharing ratio for the parallel converter: (I) In the given scenario, converters two and three are fully deactivated, whereas converter one remains operational with($k_1 = 100\%$), and converters two and three ($k_2 = k_3 = 0\%$),

97

see Figure 3.25(a)–(d). (II) Converter one and converter two are both operational. Converter one exports 60% of the total power from the power source, while converter two handles a 40% of the total. The power ratio k_3 for converter three is set at 0%, Figure3.26(a)–(d). (III) Converter one has a power efficiency of 60%, whereas converter two and three each have a power efficiency of 20% see Figure 3.27(a)–(d). The various circumstances described above has been clearly described in Figure 3.25–(3.27).
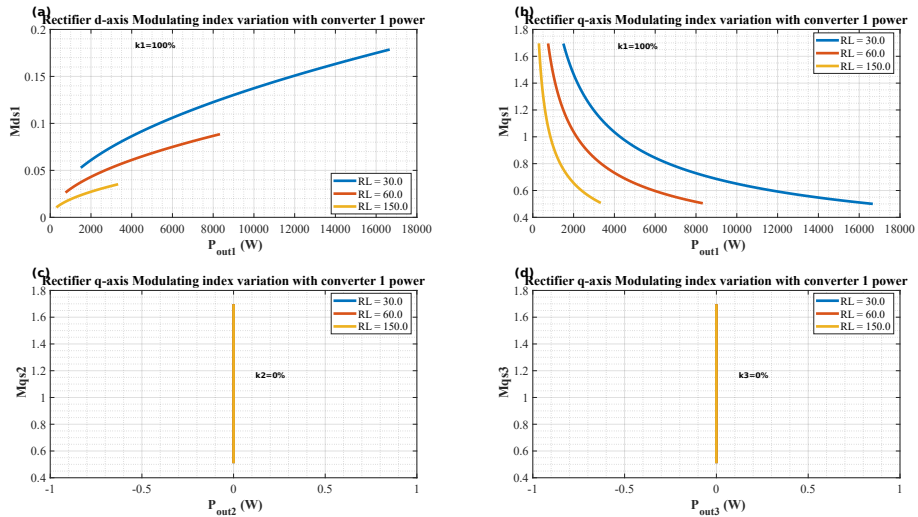
Figure 3.25: Parallel converter rectifier topology for $k_1 = 100\%, k_2 = k_3 = 0\%$
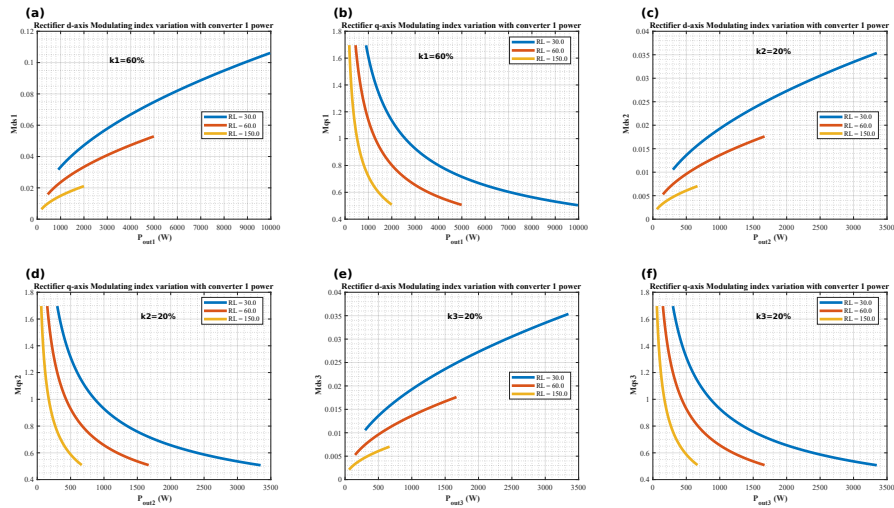
Figure 3.26: Parallel converter rectifier topology for $k_1 = 60\%, k_2 = 20\%, k_3 = 20\%$
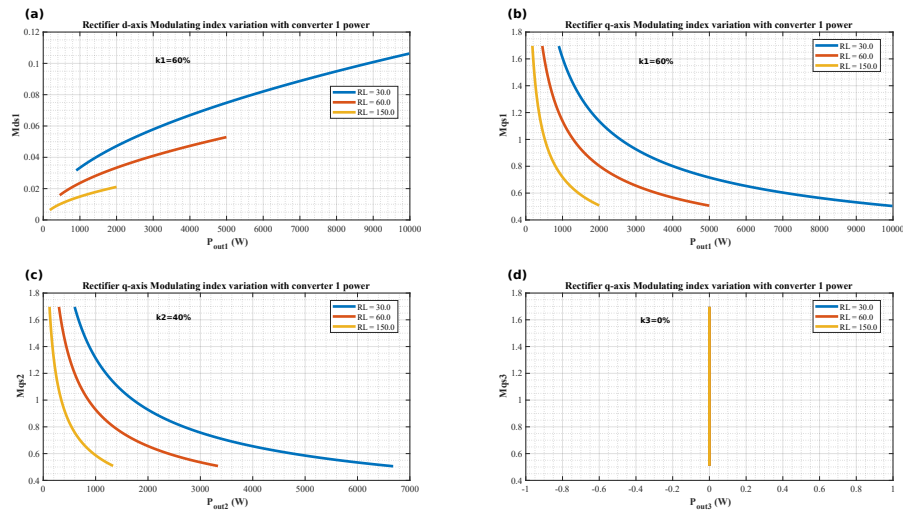
Figure 3.27: Parallel converter rectifier topology for $k_1 = 60\%, k_2 = 40\%, k_3 = 0\%$

3.4.5   Wind Speed–Power Profile

Every studied wind turbine system has a defined power profile, which describe varying attainable wind speeds and and power corresponding for each region in their profile. Figure 3.28 shows a typical winding profile of a wind turbine system. Based on this figure, four regions are identified: **Region 1**, **Region 2**, **Region3**, **Region4**.
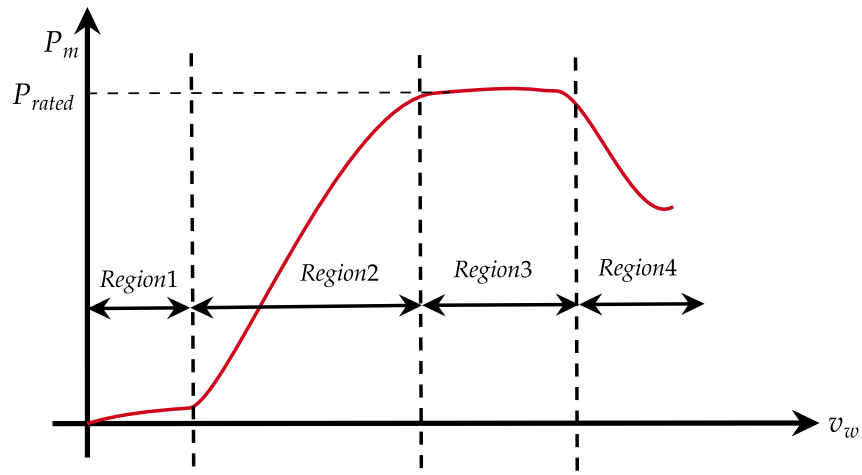
Figure 3.28: Wind Turbine Power Profile

The Cut-In Speed, represented as area 1 in the graph, is the threshold wind speed

at which a wind turbine may begin generating power with optimal efficiency. Small domestic turbines often operate within a velocity range of 3–5 m/s. At speeds below this threshold, the turbine's power generation is negligible due to the insufficient force exerted by the wind to rotate the turbine blades. In the graphical representation, Region 2 denotes the moment at which the turbine begins power generation, albeit in an uncontrolled manner. Region 3 is the optimal wind speed range within which a wind turbine functions with utmost efficiency, hence generating its maximum rated power output. Wind turbines are engineered to achieve their maximum efficiency at a certain velocity. The rated wind speed for the majority of commercial turbines typically falls within the range of 12–15 m/s. Region 4 denotes the threshold wind velocity at which a wind turbine ceases operation due to the activation of its control system, which either initiates a shutdown or modifies the blade configuration to diminish power generation. The normal range of cut-out speeds for commercial wind turbines is between 25–30 m/s. The purpose of this measure is to mitigate the operation of the turbine under severe wind conditions, hence minimising the potential for mechanical strain or harm. The comprehension and effective administration of these velocity parameters are essential to guarantee the safety and efficacy of wind turbine systems. The operating envelope of a turbine is efficiently and safely defined by the range between its cut-in and cut-out speeds, during which power generation occurs.

3.4.6 Wind Turbine and Pitch Controller

The turbine serves as the primary mechanism in a wind energy conversion system (WECS), facilitating the transformation of wind's kinetic energy (E_w) into mechanical power (P_m), which is then converted into electricity [181].

The power relations from a wind turbine system can be derived from first principles using the kinetic energy of a moving mass of air.

$$
\begin{cases}
\text{Kinetic Energy } (E_w) \;=\; \frac{1}{2}\rho \times Vol_{air} \times V_w^2 \\[2mm]
\text{Volume of air } Vol_{air} = A_{air} \times V_w \\[2mm]
\text{Area of } (A_{air}) \text{ swept} = \pi R^2 \\[2mm]
\text{Turbine Mech. Power } \;=\; \frac{\partial E_w}{\partial t}
\end{cases}
\tag{3.63}
$$

The extracted power(Mech. Power) from the turbine is obtained by multiplying the turbine mech. power by C_p, which depends on the turbine pitch β and tip speed ratio λ

$$
\begin{cases}
P_m = \frac{\partial E_w}{\partial t} C_p = \frac{1}{2}\rho A V_w^3 C_p \\[2mm]
C_p(\lambda, \beta) = 0.5176 \left(\frac{116}{\lambda_i} - 0.4\beta - 5 \right) e^{-21/\lambda_i} + 0.0068\lambda
\end{cases}
\tag{3.64}
$$

The variable V_w represents the wind speed at the centre of the rotor, measured in metres per second. The symbol ρ denotes the air density, expressed in kg/m^3. $A = \pi R^2$ represents the frontal area of the wind turbine, measured in square metres, while R represents the rotor radius. The performance coefficient, denoted as C_p, is influenced by the turbine parameters, namely the blade pitch angle β and the tip speed ratio λ. These factors play a crucial role in the energy conversion process by contributing to the losses incurred.

$$
\begin{cases}
\lambda = \frac{\omega_t R}{V_w} \\[2mm]
\frac{1}{\lambda_i} = \frac{1}{\lambda + 0.08\beta} - \frac{0.035}{\beta^3 + 1}
\end{cases}
\tag{3.65}
$$

where w_t is the turbine speed and R is the wind turbine blade radius. Figure 3.29 depicts the plot of C_p vs λ for various values of β. When the wind speed exceeds the rated amount, the electromagnetic torque is insufficient to regulate the rotor speed, causing an overload on the generator and the converter. To avoid excessive rotor speed, the extracted power from incoming wind must be regulated. This may be accomplished by lowering the turbine's coefficient of performance (the C_p value). The pitch angle can be used to change the C_p value, see Figure 3.29. Changing the pitch angle involves moving the turbine blades along the axis significantly. Figure 3.31 depicts the pitch controller model.
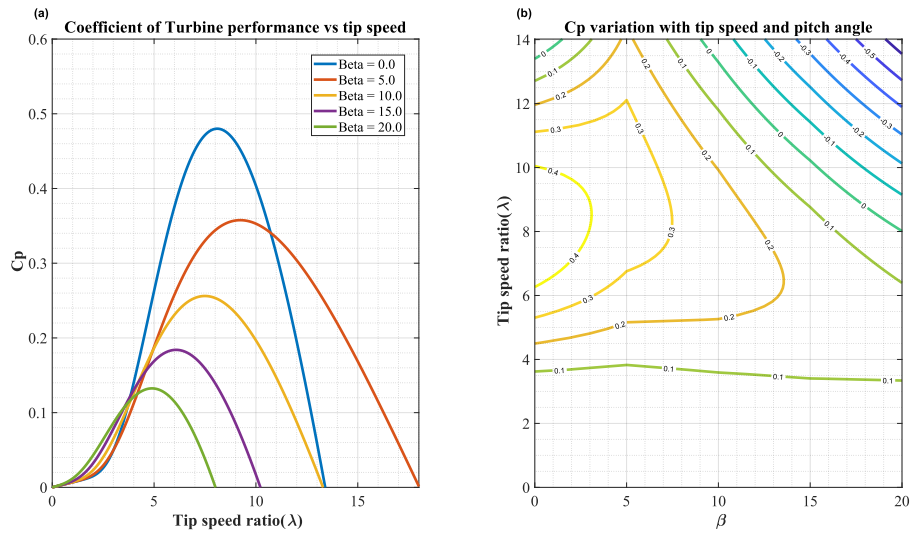
Figure 3.29: (a) Variation of c_P vs Tip ratio (b) C_p variation with tip ratio speed λ and pitch angle β
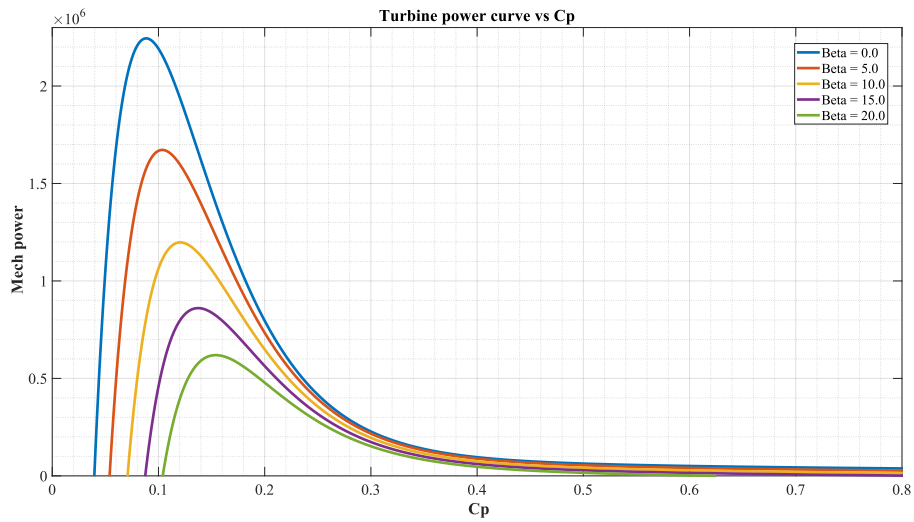
Figure 3.30: Mechanical power Variations vs C_p

The turbine speed regulator is represented in the lower section of the pitch controller in Figure 3.31, while the upper part is an aerodynamic power limitation. The full control may be realised with the help of a PI controller.
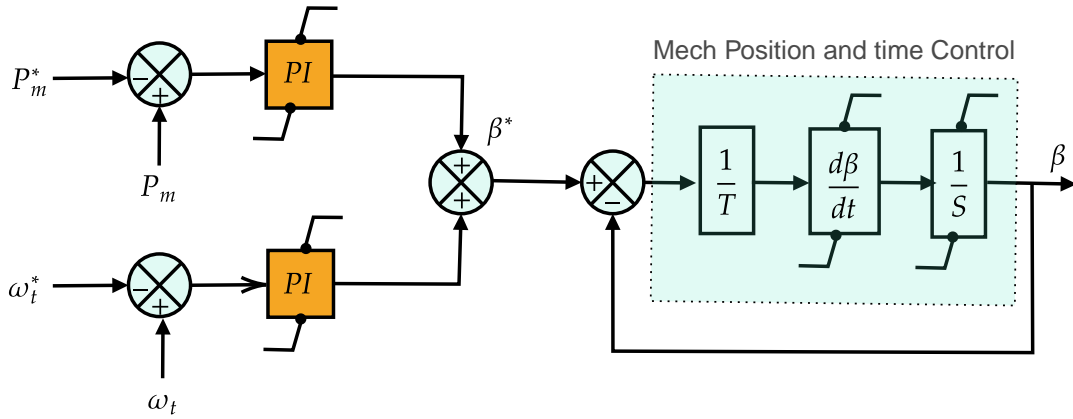
Figure 3.31: Pitch angle Control with PI controller

3.4.7 Wind Turbine Speed Systems

Wind turbine system can be operated in two speed modes: (I) Fixed speed mode and (II) Variable speed mode. Most commercial wind turbine systems operates in the variable speed mode due to the stochastic nature of the wind gust for the region where the wind turbine system is installed. This section elaborates more on the feasible variable speed operating regions and expressions of the close form energy production of a wind turbine system [181]. Let's denote the output power from a wind turbine system to be P_e and assume this power varies between cut in and rated wind speed.. Therefore, a close form expression for the energy production is established.

$$\begin{cases} P_e = 0, & \forall \, (V_w \leq V_c) \\ P_e = a + bV_w^k, & \forall \, (V_c \leq V_w \leq V_r) \\ P_e = P_r, & \forall \, (V_w \geq V_r) \end{cases} \tag{3.66}$$

The rated electrical power, denoted as P_r, is a key component in the examined system. The Weibull shape parameter, k, is determined to be 2. Additionally, the coefficients a and b are provided as part of the system's specifications. $a = \frac{P_r V_c^k}{V_c^k - V_r^k}$ and $b = \frac{P_r}{V_r^k - V_c^k}$. The variable speed wind energy conversion system (WECS) has the capability to operate in two modes: maximum power point tracking (MPPT) mode and blade pitch control mode (also known as constant power mode). The selection of the mode depends on the

Chapter 3. Modeling of Studied system

wind velocity, with the objective of extracting the maximum power from the wind and regulating the power output of the wind turbine.

Three operating modes are identified from equation (3.66): (i) Maximum power point tracking (ii) Pitch Control (Rated Power Operation) (c) Power regulation mode.

- Maximum power point

Operating the wind turbine in the maximum power point tracking, is about locating and finding the the C_p values for different wind speed that makes the wind energy conversion system to operate at maximum power point for low to medium wind speed.

$$\begin{cases} T_m = \frac{P_m}{\omega_t} \\ T_m = \frac{1}{2\omega_t}\rho A V_w^3 C_p = \frac{R}{2\lambda}\rho A V_w^2 C_p \\ P_m = K V_w^3 \\ @ \text{ mppt, } C_p = C_{p_{max}} \end{cases} \tag{3.67}$$

- Pitch angle Control Operations

In this mode, the generator and converter overload when the wind speed exceeds the rated threshold because the electromagnetic torque is no longer enough to control the rotor speed. Pitch angle can be adjusted to reduce the turbine's coefficient of performance, C_p, and hence limit power extraction. This method uses mathematical formulas to establish the precise pitch angle, ensuring that the turbine operates at its rated speed and power output.

- Power Regulation Mode

Given the escalating amount of wind power integration within a power system, it becomes impractical to exclusively run wind turbines in either maximum power point tracking (MPPT) mode or constant power mode. In order to ensure the consistent regulation of frequency and voltage within the power system, it is imperative that the generated power matches the required power. Therefore, in such circumstances, it is recommended to run the variable-speed variable-pitch wind turbine in power regulation

mode. In the event of load reduction, it is necessary to correspondingly lower the power output from the turbine to align with the reduced demand. In instances where the wind speed falls below the designated threshold, the pitch angle β is consistently maintained at zero degrees. However, the value of the parameter λ is adjusted, and subsequently the corresponding value of C_p is computed. This process is undertaken to achieve the desired power output from the wind turbine. The wind speed is determined by calculating the needed power output (P) as specified in equation (3.68).

$$\begin{cases} V_w = \left(\frac{P}{\frac{1}{2}A\rho C_p} \right)^{\frac{1}{3}} \\ \omega_r = \frac{\lambda V_w}{R} \times G \end{cases} \tag{3.68}$$

Where:

G is the gear ratio of the turbine to generator syatem

3.5   System Complete Full Model Equations

The complete dynamic state equation in condensed form for the studied multiple phase induction machine and the connected system system of Figure 3.1 is:

- **Generator–Rectifier System Section**

$$\begin{cases} p\lambda_{qdsk} = -r_s i_{qdsk} + j\omega\lambda_{qdsk} + \frac{M_{qdsk} \cdot v_{dc}}{2} \quad \forall \; k = 1, 2, 3 \\ p\lambda_{qdr} = -r_r i_{qdr} + j(\omega - \omega_r)\lambda_{qdr} \\ p\omega_r = \frac{1}{J}\left(T_e - T_j\right), \quad \forall \begin{cases} j = m \quad \text{generator convention} \\ j = L \quad \text{motor convention} \end{cases} \end{cases} \tag{3.69}$$

Where the electromagnetic torque of the nine phase induction machine, is mathematically represented $T_e = \frac{3}{2}\left(\frac{P}{2}\right)\left(\frac{L_m}{L_r}\right)\left[\lambda_{dr}\sum\limits_{k=1}^{3}(i_{qsk}) - \lambda_{qr}\sum\limits_{k=1}^{3}(i_{dsk})\right]$. For a squirrel cage rotor, note:, $v_{qr} = v_{dr} = 0$.

$$\begin{cases} \lambda_{qdsk} = L_{ls}i_{qdsk} + L_{lm}\sum\limits_{j=1}^{3}i_{qdsj} + L_m\sum\limits_{j=1}^{3}(i_{qdsj} + i_{qdr}) \quad \forall, k = 1, 2, 3 \\ \lambda_{qdr} = L_{lr}i_{qdr} + L_m\sum\limits_{j=1}^{3}(i_{qdsj} + i_{qdr}) \end{cases} \tag{3.70}$$

- **dc-link battery System Section**

$$
\begin{cases}
pv_{dc} = \frac{1}{C_{dc}} \left(\frac{3}{4} \sum_{k=1}^{3} (M_{qsk}i_{qs1} + M_{dsk}i_{dsk}) - i_{inv} - i_{dc} \right) \\[2mm]
pi_{Lo} = \frac{1}{L_o}(d_1 v_{dc} - v_b) , \quad i_{dc} = d_1 i_{Lo} \\[2mm]
pv_b = \frac{1}{C_b} \left(i_{Lo} - \frac{v_b}{R_s} + \frac{v_c}{R_s} + \frac{V_{oc}}{R_s} \right) \\[2mm]
pv_c = \frac{1}{C} \left(\frac{v_b}{R_s} - \left(\frac{1}{R_s} + \frac{1}{R_p} \right) v_c + \frac{1}{R_s}V_{oc} \right) \\[2mm]
pSoC = \frac{1}{q_{max}} \left(v_b - \frac{v_c}{R_s} - \frac{V_{oc}}{R_s} \right) \\[2mm]
i_{inv} = \frac{3}{4} \left(M_{q1}i_{s1q} + M_{d1}i_{s1d} \right)
\end{cases}
\tag{3.71a}
$$

The battery resistances and open circuit voltage are dependent on the battery state of charge, given by equation (3.71b)

$$
\begin{cases}
v_b = v_c + i_b R_s(\text{SoC}) + V_{oc}(\text{SoC}) \\[2mm]
V_{oc}(\text{SoC}) = A_1 e^{-B_1 SoC} + C_1 + DSoC + ESoC^2 + FSoC^3 \\[2mm]
R_s(\text{SoC}) = A_2 e^{-B_2 SoC} + C_2 \\[2mm]
R_p(\text{SoC}) = A_3 e^{-B_3 SoC} + C_3
\end{cases}
\tag{3.71b}
$$

- **dc-link inverter System Section**

$$
\begin{cases}
pi_{s1q} = \frac{1}{L_{l1}} \left(\frac{M_{q1}v_{dc}}{2} - v_{qpcc} - R_{l1}i_{s1q} - L_{s1}\omega i_{s1d} \right) \\[2mm]
pi_{s1d} = \frac{1}{L_{l1}} \left(\frac{M_{d1}v_{dc}}{2} - v_{dpcc} - R_{l1}i_{s1d} + L_{s1}\omega i_{s1q} \right)
\end{cases}
\tag{3.72}
$$

- **Load side Model**

$$
\begin{cases}
pi_{Lq} = \frac{1}{L_l} \left(v_{qpcc} - R_L i_{Lq} - L_l \omega i_{Ld} \right) \\[2mm]
pi_{Ld} = \frac{1}{L_l} \left(v_{dpcc} - R_L i_{Ld} - L_l \omega i_{Lq} \right) \\[2mm]
pi_{1q} = \frac{\omega}{Q_0} \left(-\frac{2}{3} \frac{P_0^2 + Q_0^2}{v_{qpcc}^2 + v_{dpcc}^2} v_{qpcc} + (P_0 i_{1q} - Q_0 i_{1d}) \right) \\[2mm]
pi_{1d} = \frac{\omega}{Q_0} \left(-\frac{2}{3} \frac{P_0^2 + Q_0^2}{v_{qcc}^2 + v_{dpcc}^2} v_{dpcc} + (P_0 i_{1d} + Q_0 i_{1q}) \right) \\[2mm]
pv_{qcc} = \frac{1}{C_{pcc}} \left(i_{s1q} - i_{Lq} - \frac{2}{3} \frac{P_0 v_{qpcc} + Q_0 v_{dpcc}}{v_{qpcc}^2 + v_{dpcc}^2} - C_{pcc}\omega v_{dpcc} \right) \\[2mm]
pv_{dcc} = \frac{1}{C_{pcc}} \left(i_{s1d} - i_{Ld} - \frac{2}{3} \frac{P_0 v_{qpcc} - Q_0 v_{dpcc}}{v_{qpcc}^2 + v_{dpcc}^2} + C_{pcc}\omega v_{dpcc} \right)
\end{cases}
\tag{3.73}
$$

Assuming a power balance between the nine phase induction machine and the battery and load, The power balance flow expression.

$$\sum P_{9\phi} = \alpha \sum P_{batt} + (1 - \alpha) \sum P_{inv} \qquad (3.74)$$

Where:

$P_{9\phi}$ is the total power from the nice phase induction machine, P_{batt} power delivered to the battery, P_{inv}, power delivered to the load via the inverter model, α is the power allocation factor, which varies between [0,1].

3.6 Conclusion

This chapter presents the derivation of the dynamic state model for the researched system, which encompasses many subcomponent models. The investigation has focused on analysing the model equations pertaining to each component assembly. The relationships between individual equations within a system have been well demonstrated. Upon examining the model and analysing the effects of different factors, several significant conclusions may be drawn for this particular chapter. The study focuses on analysing based on multiple $d - q$ approach the dynamic and steady state equations of a nine-phase induction machine. The investigation is based on a predetermined volt/hertz relationship, which has been arbitrarily selected to examine the steady state relationships of the variables under examination. This study examines the diverse plot interactions between torque and flux, torque and current, as well as the fluctuation of flux within one set of windings and its impact on the torque of other winding sets. Furthermore, in the succeeding portions of this chapter, an analysis was conducted on a model of a wind turbine system. The correlation between turbine mechanical power and the coefficient of tip speed ratio, as well as the power coefficient, was effectively demonstrated. Additionally, a comprehensive analysis was conducted on the configuration of a rectifier converter coupled to a voltage source, examining both series and parallel connections. The parallel rectifier connection configuration is a submodel configuration that has been researched in this thesis. The examination of this converter revealed that the

distribution of power in a series rectifier configuration differs from that of a parallel configuration, specifically in the context of a nine-phase linked voltage source applied to a cascaded rectifier converter. The rationale for this lies in the fact that the steady state model equation, when applied to a series linked rectifier operating at unity power factor, yields a set of model equations that are well-defined. However, in the case of a parallel rectifier setup, the equations derived for steady state and unity power factor provide a model that is ill conditioned. In order to render these equations amenable to solution, constraint equations were developed from the rectifier system, taking into account the power sharing ratio of the rectifier converters in the parallel connection arrangement.

Chapter 4

Steady State Stability Investigation of Nine Phase Induction Machine

4.1 Introduction

The primary challenge associated with the integration of multiple phase induction machine into established power networks pertains to their capacity to deliver the necessary power while maintaining a certain level of stability. The steady-state stability of wind producing systems is influenced by several parameters, such as wind speed interconnected assembly systems and the interchange of actual and reactive electricity with the grid or its operations in the autonomous mode. The complexity of the problem is further heightened with wind generating systems that have variable-speed and variable-pitch capabilities.

The primary goal in variable-speed, variable-pitch wind turbines is to optimise power extraction at wind speeds that range from low to medium. This is achieved by adhering to the power coefficient's maximum profile. Figure 3.29 has shown that however that, when wind speeds are elevated but still below the turbine cut-out speed, the typical approach is to employ blade pitch angle control. This method serves to sustain a specific rated shaft speed and effectively dissipate aerodynamic power, hence ensuring the safe

functioning of the turbine [182, 183]. The management of pitch angle poses significant challenges because of the presence of highly nonlinear features, hence contributing to the intricacy of the control architecture for wind production.

A significant milestone is reached in this dissertation with the introduction of an all-encompassing analytical expression that characterises the steady-state stability of a multiple-phase induction generator. The expression relies on parameters including maximum power tracking (MPT), among others. Power regulation modes and rated capacity are disregarded. The derivation incorporates the effects of wind speed, rotor speed, and blade pitch angle variation. This study deviates from the traditional methodology by exclusively examining the intrinsic factors that contribute to the instability of the system, while disregarding external controls and other connections. This decision was inspired by a previous reference [184]. The subsequent segment of this chapter explores unexplored domains by analysing the stability of multiphase induction devices. This study specifically investigates the stability limits of a three-phase induction machine in comparison to a multiple-phase induction generator when the latter is employed as a generator. The dissertation employs pertinent contour graphs in order to visually represent the comparative analysis.

4.2 Steady State Stability Criterion

The behaviour of the rotor shaft is the primary determinant of the dynamics of any interaction inside a wind turbine system. When examining a simplified model that treats the system as a single mass and neglects the effects of frictional losses, the equation regulating the dynamics of the shaft may be expressed as follows:

$$p\omega_r = \frac{P}{2J}(T_e - T_m) = f(\omega_r, V_w, \beta) \tag{4.1}$$

In this context, the symbol "J" denotes the aggregate inertia of the turbine-generator system, "T_m" signifies the mechanical torque created by the turbine, and "T_e" represents the electromagnetic torque produced by the generator. The variables denoted as "ω_r," "V_w," and "β" represent the shaft speed, wind speed, and blade pitch angle, respectively.

The symbol $"f(.)"$ is used to denote "a function of."

If we take the operating point of equation (4.1) to be $(\omega_{ro}, V_{wo}, \beta_o)$, and use Taylor expansion on equation (4.1), and then linearize it around this operating, neglecting higher order terms results in:

$$p\Delta\omega_r = \left.\frac{\partial f}{\partial \omega_r}\right|_{op} \Delta\omega_r + \left.\frac{\partial f}{\partial u}\right|_{op} \Delta V_w + \left.\frac{\partial f}{\partial \beta}\right|_{op} \Delta\beta \tag{4.2}$$

$$p\Delta\omega_r = \frac{P}{2J}\left[\left.\frac{\partial T_e}{\partial \omega_r}\right|_{op} \Delta\omega_r - \left.\frac{\partial T_m}{\partial \omega_r}\right|_{op} \Delta\omega_r - \left.\frac{\partial T_m}{\partial u}\right|_{op} \Delta V_w - \left.\frac{\partial T_m}{\partial \beta}\right|_{op} \Delta\beta\right] \tag{4.3}$$

$$\left(p - \frac{P}{2J}\left.\frac{\partial T_e}{\partial \omega_r}\right|_{op} + \frac{P}{2J}\left.\frac{\partial T_m}{\partial \omega_r}\right|_{op}\right)\Delta\omega_r = -\frac{P}{2J}\left(\left.\frac{\partial T_m}{\partial u}\right|_{op} \Delta V_w + \left.\frac{\partial T_m}{\partial \beta}\right|_{op} \Delta\beta\right) \tag{4.4}$$

The transfer function can be extracted from the relations equations (4.4) thus:

Transfer function between turbine mechanical speed and wind speed.

$$\left.\frac{\Delta\omega_r}{\Delta V_w}\right|_{\Delta\beta=0} = \frac{-\frac{P}{2J}\left.\frac{\partial T_m}{\partial u}\right|_{op} \Delta V_w}{\left(p - \frac{P}{2J}\left.\frac{\partial T_e}{\partial \omega_r}\right|_{op} + \frac{P}{2J}\left.\frac{\partial T_m}{\partial \omega_r}\right|_{op}\right)} \tag{4.5}$$

Transfer function between turbine mechanical speed and pitch angle.

$$\left.\frac{\Delta\omega_r}{\Delta\beta}\right|_{\Delta V_w=0} = \frac{-\frac{P}{2J}\left.\frac{\partial T_m}{\partial u}\right|_{op} \Delta V_w}{\left(p - \frac{P}{2J}\left.\frac{\partial T_e}{\partial \omega_r}\right|_{op} + \frac{P}{2J}\left.\frac{\partial T_m}{\partial \omega_r}\right|_{op}\right)} \tag{4.6}$$

Based on this two equations (4.5)–(4.6), we can establish the stability of the multiple phase induction machine wind turbine system by examing the pole of the characteristic equation of the transfer function. The system is stable if all the poles lies on the left hand plane of the $S-$ plane as given in section 2.8 opening synopsis, Figure 2.17(a). Based on this assertion, the wind turbine system is stable when:

$$\left(p - \frac{P}{2J}\left.\frac{\partial T_e}{\partial \omega_r}\right|_{op} + \frac{P}{2J}\left.\frac{\partial T_m}{\partial \omega_r}\right|_{op}\right) = 0 \tag{4.7}$$

i.e,

$$p = \frac{P}{2J}\frac{\partial T_e}{\partial \omega_r}\bigg|_{op} + \frac{P}{2J}\frac{\partial T_m}{\partial \omega_r}\bigg|_{op} \qquad (4.8)$$

p here denotes pole of the characteristic equation. For stability, the term:

$$\frac{P}{2J}\frac{\partial T_e}{\partial \omega_r}\bigg|_{op} + \frac{P}{2J}\frac{\partial T_m}{\partial \omega_r}\bigg|_{op} < 0 \qquad (4.9)$$

Taking the partial derivative of equation (3.64),(3.65) and (3.67) here, we can find the differentials as it relates to the equation (4.3)

$$\frac{\partial T_m}{\partial \omega_r} = \frac{\rho \pi R^2}{2\omega_r}V_w^2\left(-C_p\frac{V_w}{\omega_r} + R\frac{\partial C_p}{\partial \lambda}\right)$$

$$\frac{\partial T_m}{\partial V_w} = \frac{\rho \pi R^2}{2}V_w\left(3C_p\frac{V_w}{\omega_r} - R\frac{\partial C_p}{\partial \lambda}\right) \qquad (4.10)$$

$$\frac{\partial T_m}{\partial \beta} = \frac{\rho \pi R^2}{2\omega_r}V_w^3\frac{\partial C_p}{\partial \beta}$$

In order to establish the stability of multiphase induction machine wind turbine studied in this thesis, there is need to find the partial differential of the torque with respect to speed ω_r. A look at second component of equation (4.9), it is easy to find the relation from equation (3.67), which is repeated in equation (4.10). Next, is to find the partial derivative $\frac{\partial T_e}{\partial \omega_r}$. That will be explicitly derived in the next section, from there the stability boundary is determined using contour plots.

4.3 Stability Boundary

Here we derive the expression for electromagnetic torque relations in terms of the speed, using equation (3.1)–(3.2) as a starting point. If we ignore the zero sequence component and assume a balancing scenario, there are eight $q - d$ voltage equations for the nine-phase induction machine that is the subject of this thesis. This equations when re-written in complex number formation, result in four equations easy to be handled.

Writing this equation in complex form result in:

$$
\begin{cases}
v_{qdsk} = r_{sk}i_{qdsk} + p\lambda_{qdsk} - j\omega\lambda_{qdsk} \\
v_{qdr} = r_r i_{qdr} + p\lambda_{qdr} - j(\omega - \omega_r)\lambda_{qdr} = 0
\end{cases}
\qquad for \; k = 1, 2, 3 \qquad (4.11)
$$

For a squirrel cage rotor, note:, $v_{qr} = v_{dr} = 0$.

$$
\begin{cases}
\lambda_{qdsk} = L_{ls}i_{qdsk} + L_{lm}\sum_{k=1}^{3} i_{qdsk} + L_m \sum_{k=1}^{3} (i_{qdsk} + i_{qdr}) \\
\lambda_{qdr} = L_{lr}i_{qdr} + L_m \sum_{k=1}^{3} (i_{qdsk} + i_{qdr})
\end{cases}
\qquad (4.12)
$$

At steady state, differential of the variables of interest equal zero. i.e $p(x) = 0$. Decomposing equation (4.11)–(4.12) for $k = 1, 2, 3$. Next substituting the values for equation (4.12), into steady state voltage equation result in.

$$
\begin{bmatrix} V_{qds1} \\ V_{qds2} \\ V_{qds3} \\ V_{qdr} \end{bmatrix}
=
\begin{bmatrix}
Z_{11} & -j\omega_e L_a & -j\omega_e L_a & -j\omega_e L_m \\
-j\omega_e L_a & Z_{22} & -j\omega_e L_a & -j\omega_e L_m \\
-j\omega_e L_a & -j\omega_e L_a & Z_{33} & -j\omega_e L_m \\
Z_{r1}(\omega_r) & Z_{r2}(\omega_r) & Z_{r3}(\omega_r) & Z_{44}(\omega_r)
\end{bmatrix}
\times
\begin{bmatrix} I_{qds1} \\ I_{qds2} \\ I_{qds3} \\ I_{qdr} \end{bmatrix}
\qquad (4.13)
$$

Where:

$\omega_{e1} = \omega_{e2} = \omega_{e3} = \omega_e$

$Z_{11} = Z_{22} = Z_{33} = r_{si} - j\omega_{ei}(L_{ls} + L_{lm} + L_m) \; \forall i = 1, 2, 3$

$Z_{44} = r_{rr} - j(\omega_{ei} - \omega_r)(L_{lr} + L_m)$

$L_a = L_{lm} + L_m$

$Z_{r1}(\omega_r) = Z_{r2}(\omega_r) = Z_{r3}(\omega_r) = -j(\omega_{ei} - \omega_r)L_m$

note $Z_{ri} = f(\omega_r)$

Unlike the DFIG, for a singly excited system like the squirrel cage rotor used in this thesis makes $V_{qdr} = 0$

The electromagnetic torque of the nine phase induction machine is

$$
T_e = k\Im \left(L_m I_{qdr} I_{qds1}^* + L_m I_{qdr} I_{qds2}^* + L_m I_{qdr} I_{qds3}^* \right) \qquad (4.14)
$$

Where:

$k = \frac{3}{4}P$, P is the number of poles of the machine windings. The imaginary complex symbol, here it is use as $\Im(.)$ of the expression in the bracket.

Solving for the current from expression of equation (4.13), yield:

$$\begin{cases} I_{qdr} = \frac{a_1 a_2}{z_1 z_2} \\[2mm] I_{qds1} = \frac{a_3 + a_4}{z_3 z_2} \\[2mm] I_{qds2} = \frac{a_5 + a_6}{z_3 z_2} \\[2mm] I_{qds3} = \frac{a_7 + a_8}{z_3 z_2} \end{cases} \tag{4.15}$$

Where:

$a_1 = V_{qds1} + V_{qds2} + V_{qds3}$

$a_2 = \left(jL_a^2\omega_{e1}^2 - jZ_{11}^2 + 2L_a Z_{11}\omega_{e1} \right) Z_{r1}$

$a_3 = j\left(Z_{44}\left(V_{qds1} - V_{qds2} - V_{qds3}\right) L_a - 2L_m \left(V_{qds1} - \frac{V_{qds2}}{2} - \frac{V_{qds3}}{2}\right) Z_{r1} \right) L_a\omega_e^2$

$a_4 = \left(Z_{44}\left(V_{qds2} + V_{qds3}\right) L_a + 2L_m \left(V_{qds1} - \frac{V_{qds2}}{2} - \frac{V_{qds3}}{2}\right) Z_{r1} \right) Z_{11}\omega_{e1} + jV_{qds1}Z_{11}^2 Z_{44}$

$a_5 = -jL_a \left(Z_{44}\left(V_{qds1} - V_{qds2} + V_{qds3}\right) L_a - L_m Z_{r1}\left(V_{qds1} - 2V_{qds2} + V_{qds3}\right) \right) \omega_e^2$

$a_6 = -Z_{11}\left(Z_{44}\left(V_{qds1} + V_{qds3}\right) L_a - L_m Z_{r1}\left(V_{qds1} - 2V_{qds2} + V_{qds3}\right) \right) \omega_e + jV_{qds2}Z_{11}^2 Z_{44}$

$a_7 = -j\left(Z_{44}\left(V_{qds1} + V_{qds2} - V_{qds3}\right) L_a - L_m Z_{r1}\left(V_{qds1} + V_{qds2} - 2V_{qds3}\right) \right) L_a\omega_e^2$

$a_8 = -Z_{11}\left(Z_{44}\left(V_{qds1} + V_{qds2}\right) L_a - L_m Z_{r1}\left(V_{qds1} + V_{qds2} - 2V_{qds3}\right) \right) \omega_{e1} + jV_{qds3}Z_{11}^2 Z_{44}$

$z_1 = \left(-3L_m Z_{11}Z_{rl}\omega_e + 2jL_a^2 Z_{44}\omega_e^2 - 3jL_a L_m Z_{r1}\omega_e^2 + jZ_{11}^2 Z_{44} + L_a Z_{11} Z_{44}\omega_e \right)$

$z_2 = jL_a\omega_e + Z_{11}$

$z_3 = 2\left(j\left(L_a Z_{44} - \frac{3L_m Z_{r1}}{2}\right) L_a\omega_e^2 + \frac{Z_{11}\omega_e(L_a Z_{44} - 3L_m Z_{r1})}{2} + \frac{jZ_{11}^2 Z_{44}}{2} \right)$

Now, After solving for the current from equation (4.15), they are substituted into equation (4.14) to get the electromagnetic torque expression, which is a function of rotor speed. The differential torque with respect to the speed $\frac{\partial T_e}{\partial \omega_r}$ is obtained by differentiating the expression obtained from the substitution.

Figure 4.1–4.3, shows the contour plot based on maximum power tracking obtained based on the parameters of a multi-phase induction machine used for this thesis shown in appendix and also listed is the parameter of a three phase induction, doubly fed induction machine too. Both of which is use to compare the two curves.

Stability boundary for nine phase induction machine
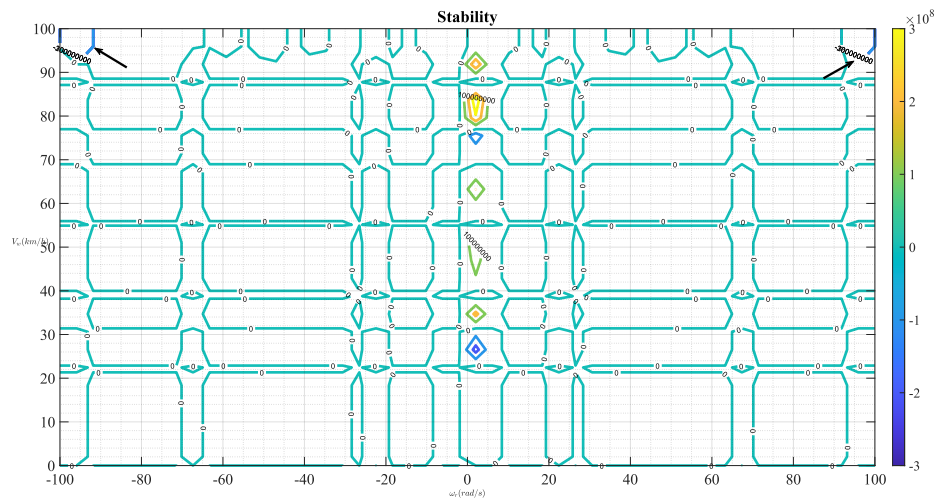
Figure 4.1: Stability boundary for nine phase induction machine as generator

As illustrated in Figure 4.1, the stability boundary of a nine-phase induction generator is presented. This thesis investigates the stability of the nine-phase induction machine system, revealing stability within specific segments (i.e with arrows) on the contour graph and instability in other defined portions. The graph results from the analysis of equations (4.13)–(4.15) and equations (4.5)–(4.9), assessing the stability of the wind turbine system featuring a nine-phase induction machine. A MATLAB script, was developed based on the equations and turbine system parameters. The contour plot, generated using MATLAB's built-in Gaussian function, facilitates the evaluation of wind turbine system stability. Figure 4.2 provides an enlarged perspective of the stability region, delineating areas of both stability and instability in the context of a nine-phase wind turbine system.
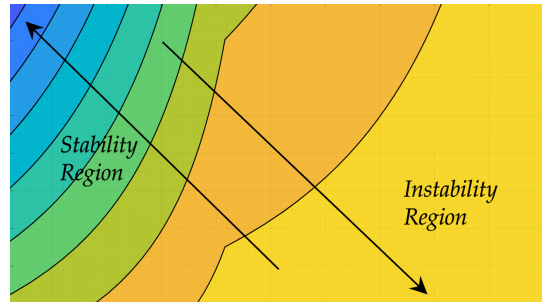
Figure 4.2: Stability boundary of nine phase induction machine as generator, expanded view

Stability boundary for three phase induction machine

To assess the stability of a conventional three-phase induction generator system, a similar approach was adopted as in the analysis of the nine-phase induction generator wind turbine system. The stability of a typical induction generator system, with parameters provided in the appendix, was examined. Employing the same analytical methodology as applied to the nine-phase induction machine, the results indicate that the three-phase induction machine, particularly at higher machine speeds, exhibits stability when compared to a nine-phase induction machine system. This suggests that a gear system booster for rotor speed may not be necessary in the case of the three-phase induction generator. These findings are visually represented in Figure 4.3. The figure depict contour plots generated by a MATLAB script utilizing a Gaussian distribution function, providing insights into the stability region.
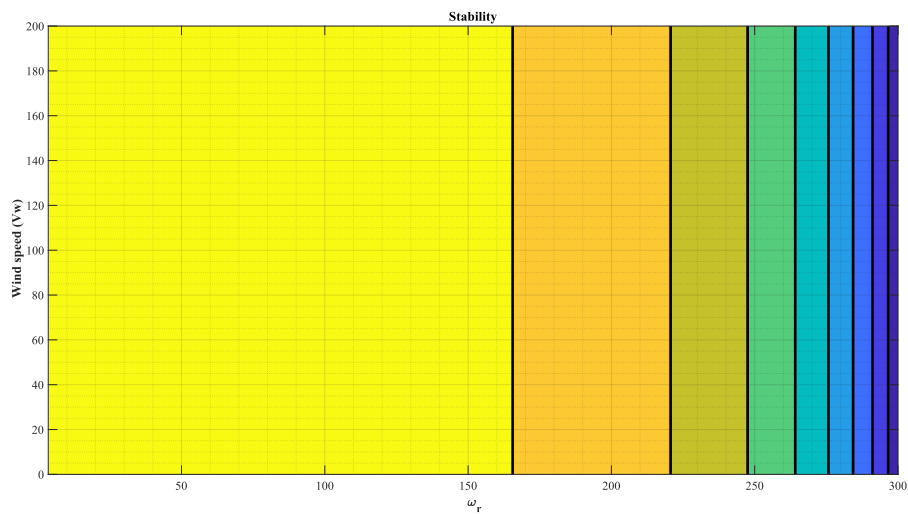
Figure 4.3: Stability boundary of three phase induction machine as generator

Stability boundary for three phase Doubly Fed induction machine as a generator

In the case of a Doubly Fed Induction Generator (DFIG), Figure 4.4, utilizing the same analytical approach, the stability condition $\frac{\partial T_e}{\partial \omega_r} - \frac{\partial T_m}{\partial \omega_r} < 0$ was assessed concerning changes in rotor voltage angle and machine mechanical speed. The results indicate that the DFIG exhibits stability within a speed range of approximately 10 rad/sec to 30 rad/sec. This suggests that the DFIG possesses a limited speed stability region when contrasted with a three-phase induction generator.

117
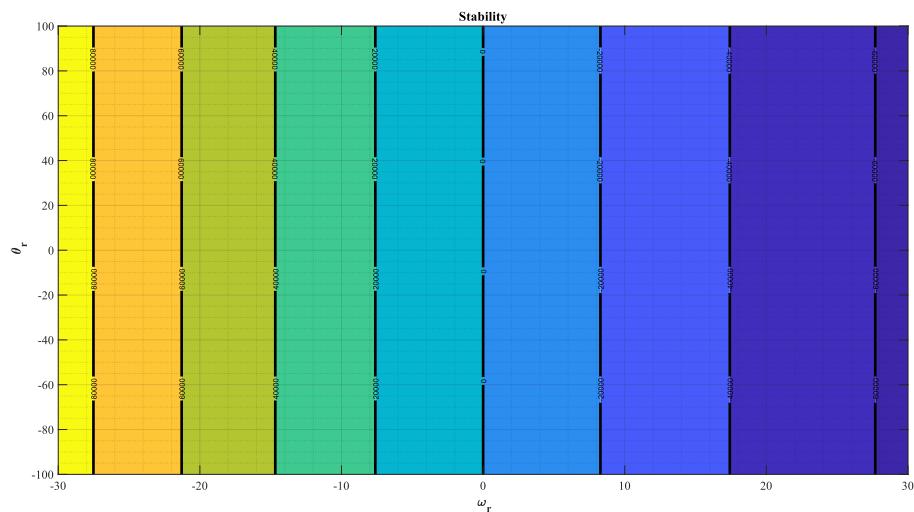
Figure 4.4: Stability boundary for DFIG

4.4 Natural Variable Model

The state variables in the models presented in Section 2.4.1 are vector quantities, implying that they are dependent on the reference frames used, or, more broadly, on the coordinate system in which they are oriented. Because the angular reference frequency, which defines the angle of transformation, is intrinsic in such models, these state variables are not the same in all reference frames of transformation. However, following inverse translation back to the $a - b - c$ reference frame, these state variables are invariant. To describe the nine phase induction machine analytically, a scalar variable model is devised. The state variables in such a model are independent of coordinate system orientation, which indicates that they are the same in all reference frames of transformation. The natural variables of the nine phase induction machine system are provided as state variables. The electromagnetic torque (T_e), reactive torque (T_r), magnitude of stator flux linkage (λ_s), active power P, reactive power Q and rotor speed (ω_r) are the natural variables.

4.5 Mathematical analysis based on vector space decomposition

The complete mathematical model of the studied nine phase induction machine, based on multiple $q - d$ approach brought forward here in a compact form is represented as in equation (4.16), therefore making the application of natural variable technique quite involving.

$$
p \begin{bmatrix} \lambda_{qdsk} \\ \lambda_{qdr} \\ \omega_r \\ v_{dc} \\ i_{Lo} \\ v_b \\ v_c \\ SoC \\ i_{s1q} \\ i_{s1d} \\ i_{Lq} \\ i_{Ld} \\ i_{1q} \\ i_{1d} \\ v_{qcc} \\ v_{dcc} \end{bmatrix} = \begin{bmatrix} -r_s i_{qdsk} + j\omega\lambda_{qdsk} + \frac{M_{qdsk}.v_{dc}}{2} \ , \ k = 1,2,3 \\ -r_r i_{qdr} + j(\omega - \omega_r)\lambda_{qdr} \\ \frac{1}{J}(T_e - T_j), \ \ \forall \begin{cases} j = m \quad \text{generator convention} \\ \\ j = L \quad \text{motor convention} \end{cases} \\ \frac{1}{C_{dc}} \left(\frac{3}{4} \sum_1^3 (M_{qsk}i_{qs1} + M_{dsk}i_{dsk}) - i_{inv} - i_{dc} \right) \\ \frac{1}{L_o}[d_1 v_{dc} - v_b], \ \forall \ d_1\varepsilon[0,1] \\ \frac{1}{C_b}\left(i_{Lo} - \frac{v_b}{R_s} + \frac{v_c}{R_s} + \frac{V_{oc}}{R_s}\right) \\ \frac{1}{C}\left(\frac{v_b}{R_s} - \left(\frac{1}{R_s} + \frac{1}{R_p}\right)v_c + \frac{1}{R_s}V_{oc}\right) \\ \frac{1}{q_{max}}\left(v_b - \frac{v_c}{R_s} - \frac{V_{oc}}{R_s}\right) \\ \frac{1}{L_{l1}}\left(\frac{M_{q1}v_{dc}}{2} - v_{qpcc} - R_{l1}i_{s1q} - L_{s1}\omega i_{s1d}\right) \\ \frac{1}{L_{l1}}\left(\frac{M_{d1}v_{dc}}{2} - v_{dpcc} - R_{l1}i_{s1d} + L_{s1}\omega i_{s1q}\right) \\ \frac{1}{L_l}\left(v_{qpcc} - R_L i_{Lq} - L_l\omega i_{Ld}\right) \\ \frac{1}{L_l}\left(v_{dpcc} - R_L i_{Ld} - L_l\omega i_{Lq}\right) \\ \frac{\omega}{Q_0}\left(-\frac{2}{3}\frac{P_0^2+Q_0^2}{v_{qpcc}^2+v_{dpcc}^2}v_{qpcc} + P_0 i_{1q} - Q_0 i_{1d}\right) \\ \frac{\omega}{Q_0}\left(-\frac{2}{3}\frac{P_0^2+Q_0^2}{v_{qcc}^2+v_{dpcc}^2}v_{dpcc} + P_0 i_{1d} + Q_0 i_{1q}\right) \\ \frac{1}{C_{pcc}}\left(i_{s1q} - i_{Lq} - \frac{2}{3}\frac{P_0 v_{qpcc}+Q_0 v_{dpcc}}{v_{qpcc}^2+v_{dpcc}^2} - C_{pcc}\omega v_{dpcc}\right) \\ \frac{1}{C_{pcc}}\left(i_{s1d} - i_{Ld} - \frac{2}{3}\frac{P_0 v_{qpcc}-Q_0 v_{dpcc}}{v_{qpcc}^2+v_{dpcc}^2} + C_{pcc}\omega v_{dpcc}\right) \end{bmatrix} \tag{4.16}
$$

A first observation at the nine phase induction machine equation in the condensed form of equation (4.16), present some obvious formidable challenge. The equations using the multiple $q - d$ approach is highly coupled. In order to minimise this coupling to some

lesser extent, the coupled equations of a higher phase order multiple phase induction machine, are decoupled using a decoupling transformation matrix [53, 74].

In the method of vector space decomposition (VSD) [52], to address higher phase order machine, The first criteria are to transform these equations to multiple 2D subspaces using a decoupling transformation matrix. The first of this subspace $(\alpha - \beta)$ is responsible for the electromechanical energy conversion. The intermediate subspace $(x - y)$ is not useful, as it not responsible for torque production. The last subspace (0^+0^-) is the zero-sequence subspace, and the current in this subspace, does not flow, if the neutral point of the winding sets is isolated.

The choice of VSD in this thesis is crucial in deriving the steady state equation of machine–rectifier–inverter–battery and load relations. Certainly, any available decoupling transformation matrix may be exploited, but there seems to be no way available at present to make our analysis simpler for the steady state studies, except the VSD technique. Selecting a transformation matrix remains somewhat on author's intuition, experience and nature the problem to address. So, therefore, the question of choice method to arriving at solution which address the problem at hand warrant thorough investigation. The outcome equations from the VSD can be used for several other studies and modeling outcomes: *arbitrary power sharing*, *fault tolerant control* and *battery charging* for HEV etc. The work of [185] uses multiple $q - d$ approach to solve their own problem, while other authors [131], emphasized that modeling difficulty can be avoided if the model for higher order machine are exploited using VSD. A full order model of the system based on multiple $q - d$ model is shown in appendix and the complexity of these equation is evident from the compact model.

In the next section, we establish a full order steady state model of the complete system. However, before that, there is need to illustrate mathematical trajectory to arriving at the $d - q$ equation of the nine phase induction machine, established using VSD. The mathematical expression to transform the sets of phase variable equations into the $\alpha - \beta$ frame is given as:

$$\left[f_{\alpha\beta, x_1y_1, \ldots 0_+0_-}\right]_{n \times 1} = [T_{9asy3}]_{n \times n} \left[f_{1,2,\ldots n}\right]_{n \times 1} \tag{4.17}$$

where the expressions $[f_{1,2,\dots n}]_{n\times 1}$ represent the original phase variable model. The expression $\left[f_{\alpha\beta,x_1 y_1,\dots 0_+ 0_-}\right]_{n\times 1}$ represent the new fictitious variable model using the transformation matrix $[T_{9asy3}]_{n\times n}$ given in appendix A1.1. The variable f could represent any variable: *voltage*, *current* or *flux linkage* for the rotor or stator.

- Stator side VSD model

$$
\begin{cases}
v_{\alpha s} = r_s i_{\alpha s} + (L_{ls} + L_m)\frac{\mathrm{d}i_{\alpha s}}{\mathrm{d}t} + L_m \frac{\mathrm{d}}{\mathrm{d}t}\left(i_{\alpha r}\cos\theta_e - i_{\beta r}\sin\theta_e\right)\\[2mm]
v_{\beta s} = r_s i_{\beta s} + (L_{ls} + L_m)\frac{\mathrm{d}i_{\beta s}}{\mathrm{d}t} + L_m \frac{\mathrm{d}}{\mathrm{d}t}\left(i_{\alpha r}\sin\theta_e + i_{\beta r}\cos\theta_e\right)\\[2mm]
v_{x_k s} = r_s i_{x_k s} + L_{ls}\frac{\mathrm{d}i_{x_k s}}{\mathrm{d}t}\\[2mm]
v_{y_k s} = r_s i_{y_k s} + L_{ls}\frac{\mathrm{d}i_{y_k s}}{\mathrm{d}t}\\[2mm]
v_{0s} = r_s i_{0s} + L_{ls}\frac{\mathrm{d}i_{0s}}{\mathrm{d}t}
\end{cases}
\tag{4.18}
$$

- Rotor side VSD model

$$
\begin{cases}
v_{\alpha r} = r_r i_{\alpha r} + (L_{lr} + L_m)\frac{\mathrm{d}i_{\alpha r}}{\mathrm{d}t} + L_m \frac{\mathrm{d}}{\mathrm{d}t}\left(i_{\alpha s}\cos\theta_e + i_{\beta s}\sin\theta_e\right)\\[2mm]
v_{\beta r} = r_r i_{\beta r} + (L_{lr} + L_m)\frac{\mathrm{d}i_{\beta r}}{\mathrm{d}t} + L_m \frac{\mathrm{d}}{\mathrm{d}t}\left(i_{\alpha s}\sin\theta_e - i_{\beta s}\cos\theta_e\right)\\[2mm]
v_{x_k r} = r_r i_{x_k r} + L_{lr}\frac{\mathrm{d}i_{x_k r}}{\mathrm{d}t}\\[2mm]
v_{y_k r} = r_r i_{y_k r} + L_{lr}\frac{\mathrm{d}i_{y_k r}}{\mathrm{d}t}\\[2mm]
v_{0r} = r_r i_{0r} + L_{lr}\frac{\mathrm{d}i_{0r}}{\mathrm{d}t}
\end{cases}
\tag{4.19}
$$

- The electromagnetic torque VSD model

$$
T_e = PL_m\left(\cos\theta_e\left(i_{\alpha r}i_{\beta s} - i_{\beta r}i_{\alpha s}\right) - \sin\theta_e\left(i_{\alpha r}i_{\alpha s} + i_{\beta r}i_{\beta s}\right)\right)
\tag{4.20}
$$

So, only the part coupled to the rotor that is transform to $q-d$ reference frame. Applying a transformation matrix of equation (2.9), yield:

$$
\begin{cases}
v_{ds} = R_s i_{ds} + \frac{\mathrm{d}\lambda_{ds}}{\mathrm{d}t} - \omega\lambda_{qs}\\[2mm]
v_{qs} = R_s i_{qs} + \frac{\mathrm{d}\lambda_{qs}}{\mathrm{d}t} + \omega\lambda_{ds}\\[2mm]
v_{dr} = R_r i_{dr} + \frac{\mathrm{d}\lambda_{dr}}{\mathrm{d}t} - \left(\omega - \omega_r\right)\lambda_{qr}\\[2mm]
v_{qr} = R_r i_{qr} + \frac{\mathrm{d}\lambda_{qr}}{\mathrm{d}t} + \left(\omega - \omega_r\right)\lambda_{dr}
\end{cases}
\tag{4.21}
$$

where:

$$
\begin{cases}
\lambda_{ds} = (L_{ls} + L_m)\, i_{ds} + L_m i_{dr} \\[6pt]
\lambda_{qs} = (L_{ls} + L_m)\, i_{ds} + L_m i_{dr} \\[6pt]
\lambda_{dr} = (L_{lr} + L_m)\, i_{dr} + L_m i_{ds} \\[6pt]
\lambda_{qr} = (L_{lr} + L_m)\, i_{qr} + L_m i_{qs}
\end{cases}
\tag{4.22}
$$

The electromagnetic torque after applying the rotational transformation matrix to the equation (A2.15) yield, the set of any choice of expression for electromagnetic torque given as:

$$
\begin{cases}
T_e = P L_m \left(i_{dr} i_{qs} - i_{ds} i_{qr} \right) \\[6pt]
T_e = P \left(\lambda_{ds} i_{qs} - \lambda_{qs} i_{ds} \right) \\[6pt]
T_e = P \frac{L_m}{L_r} \left(\lambda_{dr} i_{qs} - \lambda_{qr} i_{ds} \right)
\end{cases}
\tag{4.23}
$$

The equation(4.18)–(4.23), obtained for the vector space decomposition here for the nine phase induction machine results in the familiar expression for the voltage equation and torque equations for a conventional three phase induction machine, operated as a motor or generator. These equation, although similar to the three phase induction machine model has the information regarding the individual windings current of the three phase set concealed. This is one drawback of the VSD approach to the multiple $q-d$ approach. However, its been proven that VSD present a simplistic approach to modeling of induction machines of higher phase order.

4.6 Full Order Model Equation and Steady State Solutions

Following the conceptual framework on vector space decomposition technique given in chapter two, the VSD model equations will be repeated here and consequently modified, to encapsulate the natural variable technique proposed to be adopted for the steady state equations analysis. Here, only the $d-q$ equations of the nine phase induction machines induction machine is repeated here. Since using the nine phase transformation matrix given in appendix A1.1, decouples the phase variable equations

given in equations(2.1)-(2.2a,2.2b) in to sets of 2D orthogonal subspace. Only the fundamental subspace will be considered in our foregoing analysis, as other subspace component equations are neglected. The reason for this is that only the first subspace, i.e fundamental component subspace of the decoupled nine phase model that is coupled to the rotor. Whence is the reason for this choice in our subsequent analysis. It is in this subspace that electro-mechanical energy conversion takes place.

- Natural Variable Model

Our focus here is to obtain the natural variable model of the nine phase induction machine, comprising multiple sets of three phase windings co-sharing the same stator compartment. The natural variable model of the nine phase induction machine constitute: the *torque ,*(T_e, T_r)*, square of the magnitude of the stator flux,*(λ_s^2)*, rotor speed,* (ω_r) and *power quantities,*(P, Q). These natural quantities remains the same in all frame of reference and do not change. They will be use as state variables for the nine phase induction machine model equation derived using VSD.

A question which arise, is that why chose natural variable technique for the model equation of the nine phase induction machine? This question will be answered in subsequent analysis that follows in the following section.

In the natural variable model, the electromagnetic, reactive torque and the square of stator flux magnitude is expressed as:

$$
\begin{cases}
T_e = k(\lambda_{ds} i_{qs} - \lambda_{qs} i_{ds}) \\
T_r = -k(\lambda_{ds} i_{qs} + \lambda_{qs} i_{ds}) \\
\lambda_{ss} = \lambda_{qs}^2 + \lambda_{ds}^2
\end{cases}
\tag{4.24}
$$

Now expressing the voltage equation (4.21) in terms of current using equation equation (4.22), then differentiating equation (4.24), substituting appropriate variables and eliminating some variables and leaving some variables of interest, result in an equation obtained in the natural variable form, with stator current, torques stator square of flux magnitude and rotor speed as state variables :

$$\frac{\mathrm{d}}{\mathrm{d}t}i_{qs} = \frac{L_m V_{qr}}{L_m^2 - L_r L_s} - \frac{r_r \lambda_{qs}}{L_m^2 - L_r L_s} + \frac{(L_r r_s + L_s r_r)\,i_{qs}}{L_m^2 - L_r L_s} - \frac{L_r V_{qs}}{L_m^2 - L_r L_s}$$
$$+ \frac{L_r \omega_r \lambda_{ds}}{L_m^2 - L_r L_s} + i_{ds}\,(-\omega + \omega_r) \quad (4.25)$$

$$\frac{\mathrm{d}}{\mathrm{d}t}i_{ds} = \frac{L_m V_{dr}}{L_m^2 - L_r L_s} - \frac{r_r \lambda_{ds}}{L_m^2 - L_r L_s} - \frac{(-L_r r_s - L_s r_r)\,i_{ds}}{L_m^2 - L_r L_s} - \frac{L_r V_{ds}}{L_m^2 - L_r L_s}$$
$$- \frac{L_r \omega_r \lambda_{qs}}{L_m^2 - L_r L_s} - i_{qs}\,(-\omega + \omega_r) \quad (4.26)$$

$$L_\sigma \frac{\mathrm{d}}{\mathrm{d}t}T_e = -\left(L_\sigma i_{ds} + \lambda_{ds}\frac{L_r}{L_m}\right) k_t V_{qs} + \left(L_\sigma i_{qs} + \lambda_{qs}\frac{L_r}{L_m}\right) k_t V_{ds} + \frac{(L_r r_s + L_s r_r)T_e}{L_m^2 - L_r L_s}$$
$$- \omega_r T_r + \frac{k_t L_r \omega_r \lambda_{ss}}{L_m^2 - L_r L_s} + \frac{k_t \lambda_{ds} L_m V_{qr}}{L_m^2 - L_r L_s} - \frac{k_t \lambda_{qs} L_m V_{dr}}{L_m^2 - L_r L_s}$$
$$(4.27)$$

$$\frac{\mathrm{d}}{\mathrm{d}t}T_r = -\frac{k_t\left(\left(L_m^2 - L_r L_s\right) i_{qs} - \lambda_{qs} L_r\right) V_{qs}}{L_m^2 - L_r L_s} - \frac{k_t\left(\left(L_m^2 - L_r L_s\right) i_{d_s} - \lambda_{ds} L_r\right) V_{ds}}{L_m^2 - L_r L_s}$$
$$+ \frac{k_t r_r \lambda_{ss}}{L_m^2 - L_r L_s} + \frac{\left(T_r^2 + T_e^2\right) r_s}{k_t \lambda_{ss}} + \frac{(L_r r_s + L_s r_r)\,T_r}{L_m^2 - L_r L_s} + \omega_r k_t T_e - \frac{k_t \lambda_{qs} L_m V_{qr}}{L_m^2 - L_r L_s}$$
$$- \frac{k_t \lambda_{ds} L_m V_{dr}}{L_m^2 - L_r L_s}$$
$$(4.28)$$

$$\frac{\mathrm{d}}{\mathrm{d}t}\lambda_{ss} = 2\lambda_{qs} V_{qs} + 2\lambda_{ds} V_{ds} + \frac{2 r_s T_r}{k_t} \quad (4.29)$$

$$\frac{d}{dt}\omega_r = \frac{P}{2J}(T_e - T_j) \quad (4.30)$$

Equation(4.25)–(4.30) is the *natural variable model* equation for the nine phase induction machine based on VSD model considering the first subspace, where electromagnetic interactions with the rotor takes place. The state variables of the derived nine phase model are $x = [i_{qs}, i_{ds}, T_e, T_r, \lambda_{ss}, \omega_r]$. If this equation is simplified using place holder, in

order to make it more compact and fit into the general system model equation, we have:

$$L_\sigma \frac{\mathrm{d}}{\mathrm{d}t} i_{qs} = V_{qr} - \frac{r_r \lambda_{qs}}{L_m} + \frac{(L_r r_s + L_s r_r) i_{qs}}{L_m} - \frac{L_r V_{qs}}{L_m} + \frac{L_r \omega_r \lambda_{ds}}{L_m} + i_{ds} L_\sigma (-\omega + \omega_r)$$

(4.31)

$$L_\sigma \frac{\mathrm{d}}{\mathrm{d}t} i_{ds} = V_{dr} - \frac{r_r \lambda_{ds}}{L_m} - \frac{(-L_r r_s - L_s r_r) i_{ds}}{L_m} - \frac{L_r V_{ds}}{L_m} - \frac{L_r \omega_r \lambda_{qs}}{L_m} - i_{qs} L_\sigma (-\omega + \omega_r)$$

(4.32)

$$L_\sigma \frac{\mathrm{d}}{\mathrm{d}t} T_e = - \left(L_\sigma i_{ds} + \lambda_{ds} \frac{L_r}{L_m} \right) k_t V_{qs} + \left(L_\sigma i_{qs} + \lambda_{qs} \frac{L_r}{L_m} \right) k_t V_{ds} + \frac{(L_r r_s + L_s r_r) T_e}{L_m}$$
$$- L_\sigma \omega_r T_r + \frac{k_t L_r \omega_r \lambda_{ss}}{L_m} + k_t \lambda_{ds} V_{qr} - k_t \lambda_{qs} V_{dr}$$

(4.33)

$$\frac{\mathrm{d}}{\mathrm{d}t} T_r = -k_t \left(L_\sigma i_{qs} - \lambda_{qs} \frac{L_r}{L_m} \right) V_{qs} - k_t \left(L_\sigma i_{ds} - \lambda_{ds} \frac{L_r}{L_m} \right) V_{ds} k_t \frac{r_r}{L_m} \lambda_{ss}$$
$$+ \frac{(T_r^2 + T_e^2) L_\sigma r_s}{k_t \lambda_{ss}} + \frac{(L_r r_s + L_s r_r)}{L_m} T_r + \omega_r k_t L_\sigma T_e \quad - k_t \lambda_{qs} V_{qr} - k_t \lambda_{ds} V_{dr}$$

(4.34)

$$\frac{\mathrm{d}}{\mathrm{d}t} \lambda_{ss} = 2\lambda_{qs} V_{qs} + 2\lambda_{ds} V_{ds} + \frac{2 r_s T_r}{k_t}$$

(4.35)

$$\frac{d}{dt} \omega_r = \frac{P}{2J} (T_e - T_j)$$

(4.36)

Where:

$L_\sigma = \frac{L_m^2 - L_r L_s}{L_m}$

Fusing this equation (4.31)–(4.36) in a compact form of the complete system model equation(4.37)–(4.38). we have:

$$p \begin{bmatrix} i_{qs} \\ i_{ds} \\ T_e \\ T_r \\ \lambda_{ss} \\ \omega_r \\ v_{dc} \\ i_{Lo} \\ v_b \\ v_c \\ SoC \\ \vdots \\ \vdots \end{bmatrix} = \begin{bmatrix} \frac{1}{L_\sigma} \begin{pmatrix} V_{qr} - \frac{r_r \lambda_{qs}}{L_m} + \frac{(L_r r_s + L_s r_r) i_{qs}}{L_m} - \frac{L_r V_{qs}}{L_m} + \frac{L_r \omega_r \lambda_{ds}}{L_m} \\ + i_{ds} L_\sigma \left(-\omega + \omega_r \right) \end{pmatrix} \\ \frac{1}{L_\sigma} \begin{pmatrix} V_{dr} - \frac{r_r \lambda_{ds}}{L_m} - \frac{(-L_r r_s - L_s r_r) i_{ds}}{L_m} - \frac{L_r V_{ds}}{L_m} - \frac{L_r \omega_r \lambda_{qs}}{L_m} \\ - i_{qs} L_\sigma \left(-\omega + \omega_r \right) \end{pmatrix} \\ \frac{1}{L_\sigma} \begin{pmatrix} - \left(L_\sigma i_{ds} + \lambda_{ds} \frac{L_r}{L_m} \right) k_t V_{qs} + \left(L_\sigma i_{qs} + \lambda_{qs} \frac{L_r}{L_m} \right) k_t V_{ds} \\ + \frac{(L_r r_s + L_s r_r) T_e}{L_m} - L_\sigma \omega_r T_r + \frac{k_t L_r \omega_r \lambda_{ss}}{L_m} + k_t \lambda_{ds} V_{qr} \\ - k_t \lambda_{qs} V_{dr} \end{pmatrix} \\ \frac{1}{L_\sigma} \begin{pmatrix} -k_t \left(L_\sigma i_{qs} - \lambda_{qs} \frac{L_r}{L_m} \right) V_{qs} - k_t \left(L_\sigma i_{ds} - \lambda_{ds} \frac{L_r}{L_m} \right) V_{ds} + k_t \frac{r_r}{L_m} \lambda_{ss} \\ + \frac{(T_r^2 + T_e^2) L_\sigma r_s}{k_t \lambda_{ss}} + \frac{(L_r r_s + L_s r_r)}{L_m} T_r + \omega_r k_t L_\sigma T_e \quad - k_t \lambda_{qs} V_{qr} \\ - k_t \lambda_{ds} V_{dr} \end{pmatrix} \\ \left(2\lambda_{qs} V_{qs} + 2\lambda_{ds} V_{ds} + \frac{2r_s T_r}{k_t} \right) \\ \frac{P}{2J} \left(T_e - T_j \right), \forall \ j = \begin{cases} m & \text{Gen} \\ L & \text{motor} \end{cases} \\ \frac{1}{C_{dc}} \left(\frac{3}{4} \left(M_{qs} i_{qs} + M_{ds} i_{ds} \right) - \frac{3}{4} \left(M_{q1} i_{s1q} + M_{d1} i_{s1d} \right) - d_1 i_{Lo} \right) \\ \frac{1}{L_o} \left[d_1 v_{dc} - v_b \right], \ \forall \ d_1 \varepsilon [0,1] \\ \frac{1}{C_b} \left(i_{Lo} - \frac{v_b}{R_s} + \frac{v_c}{R_s} + \frac{V_{oc}}{R_s} \right) \\ \frac{1}{C} \left(\frac{v_b}{R_s} - \left(\frac{1}{R_s} + \frac{1}{R_p} \right) v_c + \frac{1}{R_s} V_{oc} \right) \\ \frac{1}{q_{max}} \left(v_b - \frac{v_c}{R_s} - \frac{V_{oc}}{R_s} \right) \\ \vdots \\ \vdots \end{bmatrix}$$

$$(4.37)$$

The second split is:

$$
p \begin{vmatrix} \vdots \\ i_{s1q} \\ i_{s1d} \\ i_{Lq} \\ i_{Ld} \\ i_{1q} \\ i_{1d} \\ v_{qcc} \\ v_{dcc} \end{vmatrix} = \begin{vmatrix} \vdots \\ \frac{1}{L_{l1}}\left(\frac{M_{q1}v_{dc}}{2} - v_{qpcc} - R_{l1}i_{s1q} - L_{s1}\omega i_{s1d}\right) \\ \frac{1}{L_{l1}}\left(\frac{M_{d1}v_{dc}}{2} - v_{dpcc} - R_{l1}i_{s1d} + L_{s1}\omega i_{s1q}\right) \\ \frac{1}{L_l}\left(v_{qpcc} - R_L i_{Lq} - L_l\omega i_{Ld}\right) \\ \frac{1}{L_l}\left(v_{dpcc} - R_L i_{Ld} + L_l\omega i_{Lq}\right) \\ \frac{\omega}{Q_0}\left(-\frac{2}{3}\frac{P_0^2+Q_0^2}{v_{qpcc}^2+v_{dpcc}^2}v_{qpcc} + P_0 i_{1q} - Q_0 i_{1d}\right) \\ \frac{\omega}{Q_0}\left(-\frac{2}{3}\frac{P_0^2+Q_0^2}{v_{qpcc}^2+v_{dpcc}^2}v_{dpcc} + P_0 i_{1d} + Q_0 i_{1q}\right) \\ \frac{1}{C_{pcc}}\left(i_{s1q} - i_{Lq} - \frac{2}{3}\frac{P_0 v_{qpcc}+Q_0 v_{dpcc}}{v_{qpcc}^2+v_{dpcc}^2} - C_{pcc}\omega v_{dpcc}\right) \\ \frac{1}{C_{pcc}}\left(i_{s1d} - i_{Ld} - \frac{2}{3}\frac{P_0 v_{qpcc}-Q_0 v_{dpcc}}{v_{qpcc}^2+v_{dpcc}^2} + C_{pcc}\omega v_{dpcc}\right) \end{vmatrix} \tag{4.38}
$$

The above equations gives the dynamic state equations of the studied system in compact form, with the following nineteen state variables.

$x = \{i_{qs}, i_{ds}, T_e, T_r, \lambda_{ss}, \omega_r, v_{dc}, i_{Lo}, v_b, v_c, SoC, i_{s1q}, i_{s1d}, i_{Lq}, i_{Ld}, i_{1q}, i_{1d}, v_{qpcc}, v_{dpcc}\}$

Which are respectively defined as: $q-d$ current of the nine phase induction machine winding ,$(i_{qs}, i_{ds},)$ winding set 1,winding set 2, and winding set 3, encapsulated. Nine phase induction machine rotor speed ω_r, dc-link voltage v_{dc}, Battery input current from boost converter system i_{Lo}, battery input voltage v_b, voltage across the internal battery RC network v_c, battery state of charge SoC, inverter output current i_{s1q}, i_{s1d}, constant load current $(i_{1q}, i_{1d},)$ current through the $R-L$ load $(i_{Lq}, i_{Ld},)$ output capacitor voltage at point of common coupling (v_{qcc}, v_{dcc}) and $p = \frac{d}{dt}$.

For a singly excited induction machine, $V_{qr} = V_{dr} = 0$. Moreso, If the $q-$ axis flux component of each windings set of the nine phase induction machine is synchronously aligned to the stator flux, i.e $\lambda_{qs} = \lambda_s$, their $d-$ axis respective components is equals zero i.e $\lambda_{ds} = 0$. With the load voltage aligned to the $q-$ axis reference voltage for the load voltage, the $d-$ axis component is zero. So, eliminating these variables from

equation (4.37)–(4.38) yield:

$$
p \begin{bmatrix} i_{qs} \\ i_{ds} \\ T_e \\ T_r \\ \lambda_{ss} \\ \omega_r \\ v_{dc} \\ i_{Lo} \\ v_b \\ v_c \\ SoC \\ \vdots \\ \vdots \end{bmatrix} = \begin{bmatrix} \frac{1}{L_\sigma}\left(-\frac{r_r\lambda_{qs}}{L_m} + \frac{(L_r r_s + L_s r_r)i_{qs}}{L_m} - \frac{L_r V_{qs}}{L_m} + i_{ds}L_\sigma\left(-\omega+\omega_r\right) \right) \\ \frac{1}{L_\sigma}\left(-\frac{(-L_r r_s - L_s r_r)i_{ds}}{L_m} - \frac{L_r V_{ds}}{L_m} - \frac{L_r\omega_r\lambda_{qs}}{L_m} - i_{qs}L_\sigma\left(-\omega+\omega_r\right) \right) \\ \frac{1}{L_\sigma}\left(\begin{array}{c} -\left(L_\sigma i_{ds}\right)k_t V_{qs} + \left(L_\sigma i_{qs} + \lambda_{qs}\frac{L_r}{L_m}\right)k_t V_{ds} + \frac{(L_r r_s + L_s r_r)T_e}{L_m} \\ -L_\sigma\omega_r T_r + \frac{k_t L_r\omega_r\lambda_{ss}}{L_m} \end{array} \right) \\ \frac{1}{L_\sigma}\left(\begin{array}{c} -k_t\left(L_\sigma i_{qs} - \lambda_{qs}\frac{L_r}{L_m}\right)V_{qs} - k_t\left(L_\sigma i_{ds}\right)V_{ds}k_t\frac{r_r}{L_m}\lambda_{ss} + \frac{\left(T_r^2 + T_e^2\right)L_\sigma r_s}{k_t\lambda_{ss}} \\ + \frac{(L_r r_s + L_s r_r)}{L_m}T_r + \omega_r k_t L_\sigma T_e \end{array} \right) \\ \left(2\lambda_{qs}V_{qs} + \frac{2r_s T_r}{k_t} \right) \\ \frac{P}{2J}\left(T_e - T_j\right), \forall\ j = \begin{cases} m & \text{Gen} \\ L & \text{motor} \end{cases} \\ \frac{1}{C_{dc}}\left(\frac{3}{4}\left(M_{qs}i_{qs} + M_{ds}i_{ds}\right) - \frac{3}{4}\left(M_{q1}i_{s1q} + M_{d1}i_{s1d}\right) - d_1 i_{Lo} \right) \\ \frac{1}{Lo}\left[d_1 v_{dc} - v_b \right],\ \forall\ d_1\varepsilon[0,1] \\ \frac{1}{C_b}\left(i_{Lo} - \frac{v_b}{R_s} + \frac{v_c}{R_s} + \frac{V_{oc}}{R_s} \right) \\ \frac{1}{C}\left(\frac{v_b}{R_s} - \left(\frac{1}{R_s} + \frac{1}{R_p}\right)v_c + \frac{1}{R_s}V_{oc} \right) \\ \frac{1}{q_{max}}\left(v_b - \frac{v_c}{R_s} - \frac{V_{oc}}{R_s} \right) \\ \vdots \\ \vdots \end{bmatrix}
$$

$$(4.39)$$

$$
p \begin{bmatrix} \vdots \\ i_{s1q} \\ i_{s1d} \\ i_{Lq} \\ i_{Ld} \\ i_{1q} \\ i_{1d} \\ v_{qcc} \\ v_{dcc} \end{bmatrix} = \begin{bmatrix} \vdots \\ \frac{1}{L_{l1}}\left(\frac{M_{q1}v_{dc}}{2} - v_{qpcc} - R_{l1}i_{s1q} - L_{s1}\omega i_{s1d} \right) \\ \frac{1}{L_{l1}}\left(\frac{M_{d1}v_{dc}}{2} - R_{l1}i_{s1d} + L_{s1}\omega i_{s1q} \right) \\ \frac{1}{L_l}\left(v_{qpcc} - R_L i_{Lq} - L_l\omega i_{Ld} \right) \\ \frac{1}{L_l}\left(-R_L i_{Ld} + L_l\omega i_{Lq} \right) \\ \frac{\omega}{Q_0}\left(-\frac{2}{3}\frac{P_0^2 + Q_0^2}{v_{qpcc}^2}v_{qpcc} + P_0 i_{1q} - Q_0 i_{1d} \right) \\ \frac{\omega}{Q_0}\left(P_0 i_{1d} + Q_0 i_{1q} \right) \\ \frac{1}{C_{pcc}}\left(i_{s1q} - i_{Lq} - \frac{2}{3}\frac{P_0 v_{qpcc}}{v_{qpcc}^2} \right) \\ \frac{1}{C_{pcc}}\left(i_{s1d} - i_{Ld} - \frac{2}{3}\frac{P_0 v_{qpcc}}{v_{qpcc}^2} \right) \end{bmatrix}
$$

$$(4.40)$$

- Steady State Model

128

Chapter 4. Steady State Stability Investigation of Nine Phase Induction Machine

The term "steady state" refers to the condition of a system where all transients and disturbances have been resolved. In this state, the differential equations governing the system transform into algebraic equations, simplifying the handling process. Consequently, at steady state, the solution involves simultaneously solving algebraic equations instead of engaging in the more intricate task of solving multiple differential equations. So, at steady state, the left hand side of the model equation (4.39)–(4.40), i.e the differential part is set equal to zero $p = \frac{d}{dt} = 0$. The equation reduce to algebraic equations, which can be solved for variables of interest. Equation (4.41) and (4.42) gives the full order model of studied system and it steady state equations.

$$
p \begin{bmatrix} i_{qs} \\ i_{ds} \\ T_e \\ T_r \\ \lambda_{ss} \\ \omega_r \\ v_{dc} \\ i_{Lo} \\ v_b \\ v_c \\ SoC \\ i_{s1q} \\ i_{s1d} \\ i_{Lq} \\ i_{Ld} \\ i_{1q} \\ i_{1d} \\ v_{qcc} \\ v_{dcc} \end{bmatrix} = \begin{bmatrix}
\frac{1}{L_\sigma}\left(-\frac{r_r\lambda_{qs}}{L_m} + \frac{(L_r r_s + L_s r_r)i_{qs}}{L_m} - \frac{L_r V_{qs}}{L_m} + i_{ds}L_\sigma\left(-\omega + \omega_r\right)\right) \\
\frac{1}{L_\sigma}\left(-\frac{(-L_r r_s - L_s r_r)i_{ds}}{L_m} - \frac{L_r V_{ds}}{L_m} - \frac{L_r \omega_r \lambda_{qs}}{L_m} - i_{qs}L_\sigma\left(-\omega + \omega_r\right)\right) \\
\frac{1}{L_\sigma}\left(\begin{array}{c} -\left(L_\sigma i_{ds}\right)k_t V_{qs} + \left(L_\sigma i_{qs} + \lambda_{qs}\frac{L_r}{L_m}\right)k_t V_{ds} + \frac{(L_r r_s + L_s r_r)T_e}{L_m} \\ -L_\sigma \omega_r T_r + \frac{k_t L_r \omega_r \lambda_{ss}}{L_m} \end{array}\right) \\
\frac{1}{L_\sigma}\left(\begin{array}{c} -k_t\left(L_\sigma i_{qs} - \lambda_{qs}\frac{L_r}{L_m}\right)V_{qs} - k_t\left(L_\sigma i_{ds}\right)V_{ds}k_t\frac{r_r}{L_m}\lambda_{ss} + \frac{(T_r^2 + T_e^2)L_\sigma r_s}{k_t \lambda_{ss}} \\ + \frac{(L_r r_s + L_s r_r)}{L_m}T_r + \omega_r k_t L_\sigma T_e \end{array}\right) \\
\left(2\lambda_{qs}V_{qs} + \frac{2r_s T_r}{k_t}\right) \\
\frac{P}{2J}\left(T_e - T_j\right), \forall\, j = \begin{cases} m & \text{Gen} \\ \\ L & \text{motor} \end{cases} \\
\frac{1}{C_{dc}}\left(\frac{3}{4}\left(M_{qs}i_{qs} + M_{ds}i_{ds}\right) - \frac{3}{4}\left(M_{q1}i_{s1q} + M_{d1}i_{s1d}\right) - d_1 i_{Lo}\right) \\
\frac{1}{L_o}\left[d_1 v_{dc} - v_b\right], \forall\, d_1 \varepsilon [0,1] \\
\frac{1}{C_b}\left(i_{Lo} - \frac{v_b}{R_s} + \frac{v_c}{R_s} + \frac{V_{oc}}{R_s}\right) \\
\frac{1}{C}\left(\frac{v_b}{R_s} - \left(\frac{1}{R_s} + \frac{1}{R_p}\right)v_c + \frac{1}{R_s}V_{oc}\right) \\
\frac{1}{q_{max}}\left(v_b - \frac{v_c}{R_s} - \frac{V_{oc}}{R_s}\right) \\
\frac{1}{L_{l1}}\left(\frac{M_{q1}v_{dc}}{2} - v_{qpcc} - R_{l1}i_{s1q} - L_{s1}\omega i_{s1d}\right) \\
\frac{1}{L_{l1}}\left(\frac{M_{d1}v_{dc}}{2} - R_{l1}i_{s1d} + L_{s1}\omega i_{s1q}\right) \\
\frac{1}{L_l}\left(v_{qpcc} - R_L i_{Lq} - L_l\omega i_{Ld}\right) \\
\frac{1}{L_l}\left(-R_L i_{Ld} + L_l\omega i_{Lq}\right) \\
\frac{\omega}{Q_0}\left(-\frac{2}{3}\frac{P_0^2 + Q_0^2}{v_{qpcc}^2}v_{qpcc} + P_0 i_{1q} - Q_0 i_{1d}\right) \\
\frac{\omega}{Q_0}\left(P_0 i_{1d} + Q_0 i_{1q}\right) \\
\frac{1}{C_{pcc}}\left(i_{s1q} - i_{Lq} - \frac{2}{3}\frac{P_0 v_{qpcc}}{v_{qpcc}^2}\right) \\
\frac{1}{C_{pcc}}\left(i_{s1d} - i_{Ld} - \frac{2}{3}\frac{P_0 v_{qpcc}}{v_{qpcc}^2}\right)
\end{bmatrix}
$$

(4.41)

- **Steady state equations**

$$
\begin{bmatrix} 0 \\ 0 \\ 0 \\ 0 \\ 0 \\ 0 \\ 0 \\ 0 \\ 0 \\ 0 \\ 0 \\ 0 \\ 0 \\ 0 \\ 0 \\ 0 \\ 0 \\ 0 \\ 0 \\ 0 \\ 0 \\ 0 \end{bmatrix}
=
\begin{bmatrix}
\frac{1}{L_\sigma}\left(-\frac{r_r\lambda_{qs}}{L_m} + \frac{(L_r r_s + L_s r_r)i_{qs}}{L_m} - \frac{L_r V_{qs}}{L_m} + i_{ds}L_\sigma(-\omega + \omega_r)\right) \\[4pt]
\frac{1}{L_\sigma}\left(-\frac{(-L_r r_s - L_s r_r)i_{ds}}{L_m} - \frac{L_r V_{ds}}{L_m} - \frac{L_r \omega_r \lambda_{qs}}{L_m} - i_{qs}L_\sigma(-\omega + \omega_r)\right) \\[4pt]
\frac{1}{L_\sigma}\left(\begin{array}{c} -(L_\sigma i_{ds})k_t V_{qs} + \left(L_\sigma i_{qs} + \lambda_{qs}\frac{L_r}{Lm}\right)k_t V_{ds} + \frac{(L_r r_s + L_s r_r)T_e}{L_m} \\ -L_\sigma \omega_r T_r + \frac{k_t L_r \omega_r \lambda_{ss}}{L_m}\end{array}\right) \\[4pt]
\frac{1}{L_\sigma}\left(\begin{array}{c} -k_t\left(L_\sigma i_{qs} - \lambda_{qs}\frac{L_r}{Lm}\right)V_{qs} - k_t(L_\sigma i_{ds})V_{ds}k_t + k_t\frac{r_r}{Lm}\lambda_{ss} + \frac{(T_r^2 + T_e^2)L_\sigma r_s}{k_t \lambda_{ss}} \\ +\frac{(L_r r_s + L_s r_r)}{L_m}T_r + \omega_r k_t L_\sigma T_e\end{array}\right) \\[4pt]
\left(2\lambda_{qs}V_{qs} + \frac{2r_s T_r}{k_t}\right) \\[4pt]
\frac{P}{2J}\left(T_e - T_j\right), \forall\, j = \begin{cases} m & \text{Gen} \\ L & \text{motor} \end{cases} \\[4pt]
\frac{1}{C_{dc}}\left(\frac{3}{4}(M_{qs}i_{qs} + M_{ds}i_{ds}) - \frac{3}{4}(M_{q1}i_{s1q} + M_{d1}i_{s1d}) - d_1 i_{Lo}\right) \\[4pt]
\frac{1}{L_o}\left[d_1 v_{dc} - v_b\right], \forall\, d_1 \varepsilon[0,1] \\[4pt]
\frac{1}{C_b}\left(i_{Lo} - \frac{v_b}{R_s} + \frac{v_c}{R_s} + \frac{V_{oc}}{R_s}\right) \\[4pt]
\frac{1}{C}\left(\frac{v_b}{R_s} - \left(\frac{1}{R_s} + \frac{1}{R_p}\right)v_c + \frac{1}{R_s}V_{oc}\right) \\[4pt]
\frac{1}{q_{max}}\left(v_b - \frac{v_c}{R_s} - \frac{V_{oc}}{R_s}\right) \\[4pt]
\frac{1}{L_{l1}}\left(\frac{M_{q1}v_{dc}}{2} - v_{qpcc} - R_{l1}i_{s1q} - L_{s1}\omega i_{s1d}\right) \\[4pt]
\frac{1}{L_{l1}}\left(\frac{M_{d1}v_{dc}}{2} - R_{l1}i_{s1d} + L_{s1}\omega i_{s1q}\right) \\[4pt]
\frac{1}{L_l}\left(v_{qpcc} - R_L i_{Lq} - L_l \omega i_{Ld}\right) \\[4pt]
\frac{1}{L_l}\left(-R_L i_{Ld} + L_l \omega i_{Lq}\right) \\[4pt]
\frac{\omega}{Q_0}\left(-\frac{2}{3}\frac{P_0^2 + Q_0^2}{v_{qpcc}^2}v_{qpcc} + P_0 i_{1q} - Q_0 i_{1d}\right) \\[4pt]
\frac{\omega}{Q_0}\left(P_0 i_{1d} + Q_0 i_{1q}\right) \\[4pt]
\frac{1}{C_{pcc}}\left(i_{s1q} - i_{Lq} - \frac{2}{3}\frac{P_0 v_{qpcc}}{v_{qpcc}^2}\right) \\[4pt]
\frac{1}{C_{pcc}}\left(i_{s1d} - i_{Ld} - \frac{2}{3}\frac{P_0 v_{qpcc}}{v_{qpcc}^2}\right)
\end{bmatrix}
$$

$$(4.42)$$

Expressions for variables of interest in equation (4.42) are solved for, through simultaneous elimination and connection of variables from one model system to another. The idea is to find the steady state equations which describe the system variables of interest at steady state. The steady state equations are so lengthy, so only a few will be shown, the remaining and full solving of the steady state equation are shown in appendix. Figure 4.5 to Figure 4.10 shows various steady state plot obtained from solving equation

131

(4.42) for different variables of interest. Figure 4.5 shows increase in battery open circuit voltage as the state of charge of the battery increases. Between battery state of charge of zero and 0.2 the battery voltage function is non linear. However, as the state of charge (SoC) increases beyond 0.2, the battery open circuit voltage and the SoC can be approximate as a linear function. At SoC of 100%, the battery open circuit volage is $162V$.
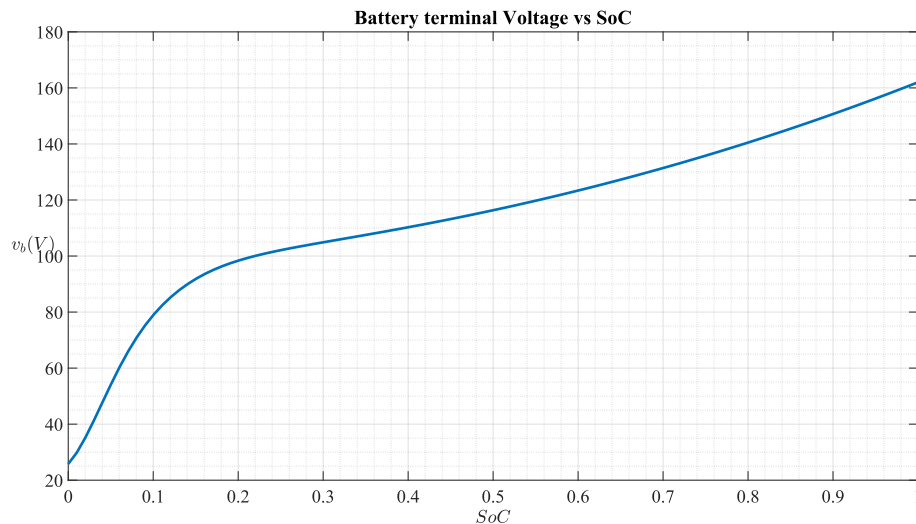
Figure 4.5: Battery open circuit voltage vs battery state of charge

Figure 4.6 shows the power absorbed and released by the battery during the charging and discharging process. The negative sign mean the battery is absorbing power and the positive sign convention means the battery is discharging power in the event of deficit power to the load. The graph gracious illustrate this variations between the battery input current, battery voltage and input power. Figure 4.7 shows the variation of the battery input current and the battery state of charge.
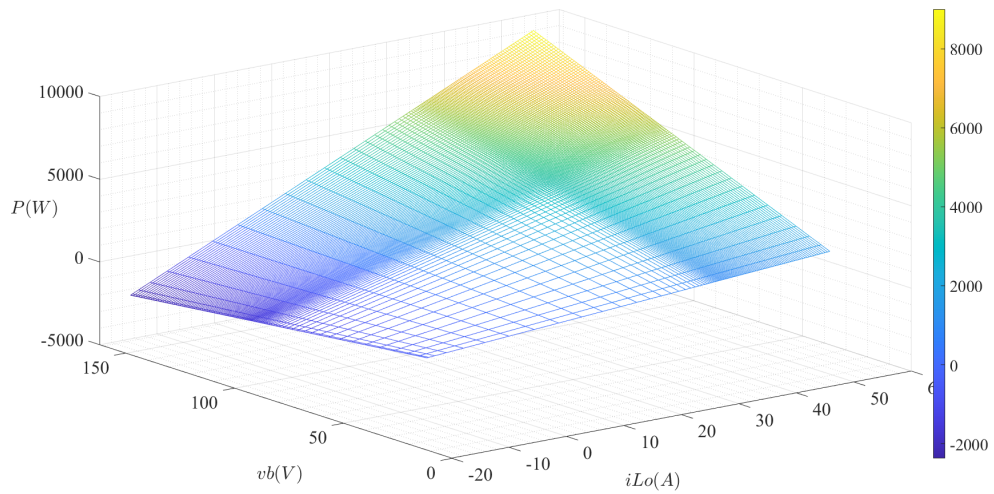
Figure 4.6: Input Power variation with battery voltage and input battery current as
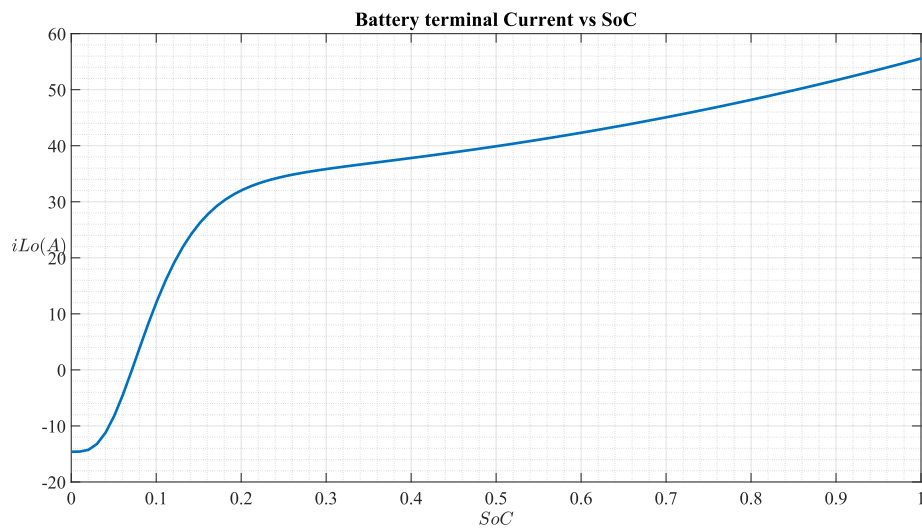
Figure 4.7: Battery current vs battery state of charge

Figure 4.8 illustrate the graph of various modulation indexes as a function of the dc link voltage and input power to the converter system. The graph shows that to push in extra power to connected system or load, the dc link voltage should be increase in order the meet the demand of higher load. Moreso, Figure 4.8 illustrate the graph of different modulation indexes as a function of the dc link voltage. and input power to the converter system. The graph shows that to push in extra power to connected system

or load, the dc link voltage should be increase in order the meet the demand of higher load.
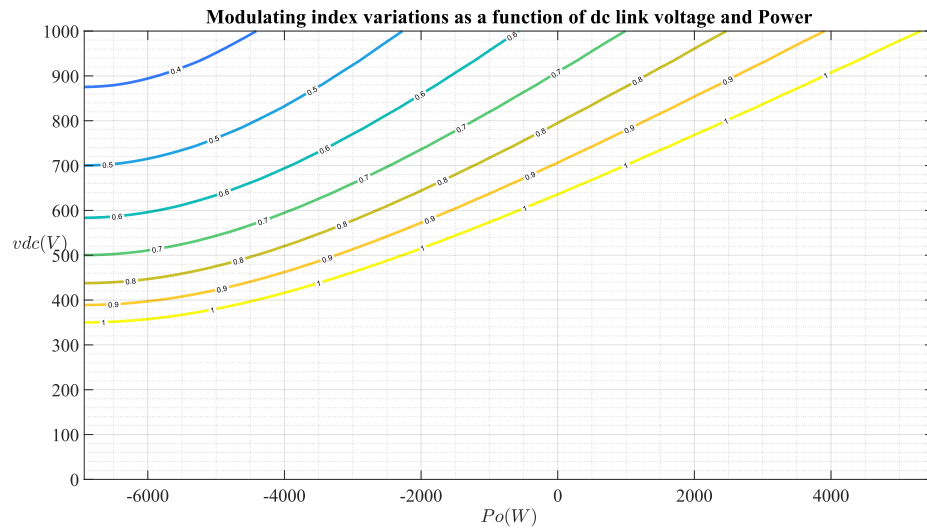
Figure 4.8: Inverter modulation index as a function of dc link voltage and power
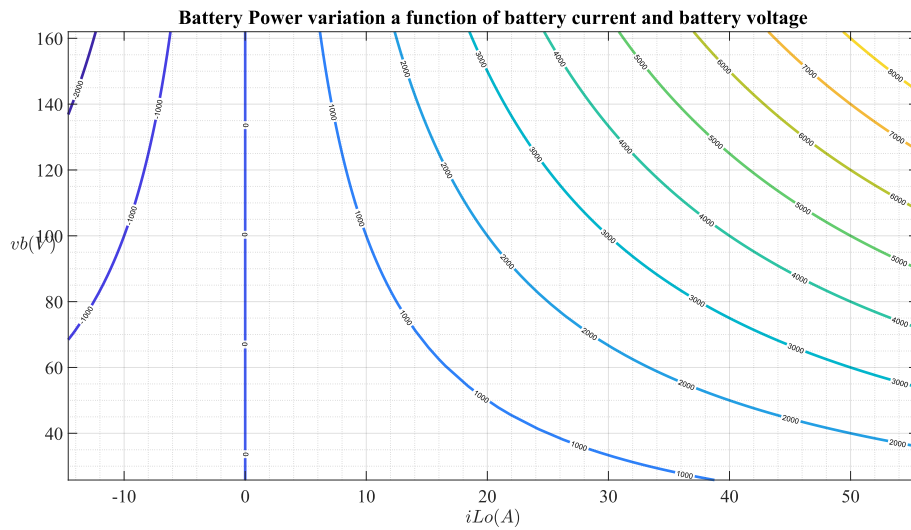
Figure 4.9: Contour plot of input Power variation with battery voltage and input battery current

Figure 4.9 shows various contour plots of the battery power variations as a function of the battery voltage and battery current. As will be observed from the graph at zero power, The battery draws no current (Input power) from the nine phase induction generator system. This plot agrees with the steady state equations derived and affirm
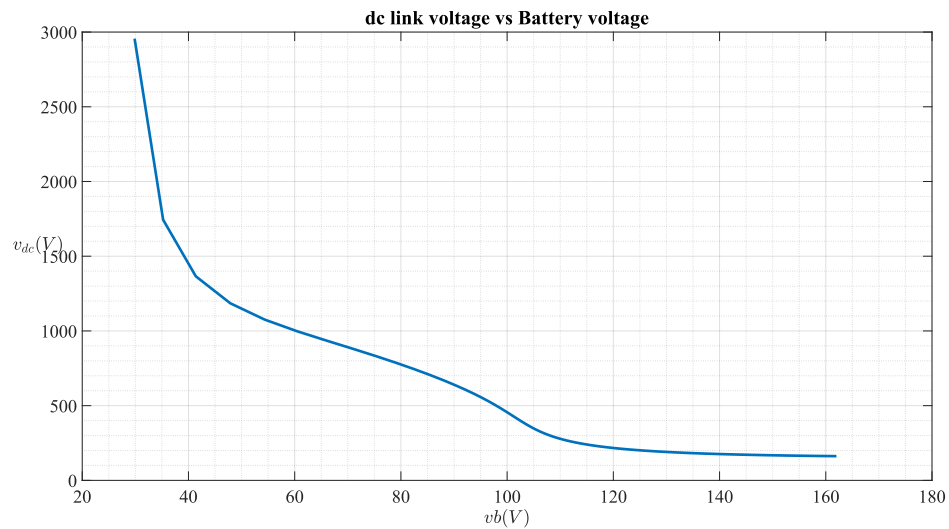
Figure 4.10: Battery dc link voltage variation with battery voltage

that in the event the battery is fully charged (i.e SoC = 100%), the battery needs no current from the input source. As such the control unit around the battery model should activate to deactivate the charging process of the battery. However, as the load demand power from the source, the battery discharges to meet the load power demand. This load demand is shown by the various contour plot to the right of reference power zero for the battery. This plot shows different power demand and different discharging current and battery voltage levels. On the graph, the left hand side of the reference zero denote the battery energy system absorbing energy. Figure 4.10 shows the steady state variation of the battery voltage and the dc link voltage.

4.7   Conclusions

An investigation of the stability of a nine-phase induction machine wind turbine system opens the chapter. Using the equation connecting the wind turbine system and machine terminal voltages, the study looks at the dynamics of the systems. The notion of stability analysis presented in chapter two, section 2.8 served as the foundation for the establishment of the steady state stability criteria. That if all of the characteristic equations' roots are located in the left-hand plane, the system is stable. In order to

compare the stability boundaries of these machines, the study in this chapter was performed on three phase, nine phase, and doubly fed induction machines that were functioning as generators. The equation for each variable linking the wind turbine system and the electrical quantity of each machine was then subjected to a partial differential function. There were reported contour maps illustrating the stability boundary of each individual machine. The obtained result demonstrates that, in comparison to three- and nine-phase induction machines, the DFIG has a broader range stability boundary. The depiction of the derived system equations from chapter three in the creation of natural variables was covered in another section of this chapter. From the dynamic state equations, a steady state equation was subsequently derived and variations of steady state variables of interest was shown.

Chapter 5

Field Analysis of Tri-three phase Induction machine

5.1   Introduction

This chapter introduces an analysis of the tri-three phase induction machine magnetic field analysis. Just as describe in the opening synopsis of this thesis, the squirrel cage, tri-three phase induction machine winding sets, consist of three set of three phase winding with isolated neutrals, segmented and asymmetrically distributed in slots of the stator of a reconfigured three phase windings. The three set of three phase windings are wound here for the same number of poles and uniformly distributed. A premeditated assumptions and idea from coupled circuit approach, relates closely wound windings and windings with other circuit in close proximity to be coupled. This chapter unfolds the field distribution of nine phase windings distribution that are coupled, the interaction of the field contributions from one winding sets to the other winding sets. As a first attempt here using magnetic field analysis, a gross understanding of the tri-three phase induction machine distributed winding field analysis is revealed. The justification of using this analytical approach is that all the field distribution of a winding set and their interactions with other circuits in close proximity as was not reported in the work of [103, 186], becomes evident using the approach as would be presented in this chapter. Also, obtained detailed analysis, from this field distribution can be used to calculate(not

shown here) each machine set torque components and subsequently the aggregate torque of the tri-three phase machine. it can present an advantages of studying the conditions of the stator frequencies of each winding sets and the rotor speeds of each respective torque component of each winding sets.

5.2 Field Analysis Development
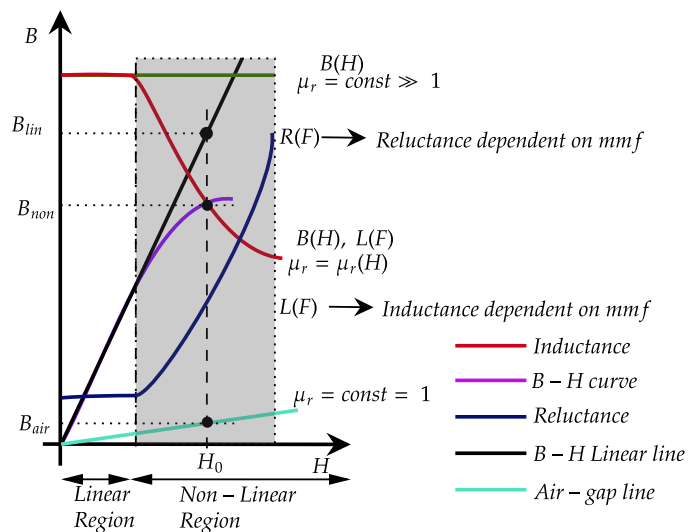
Figure 5.1: B-H curve of magnetic material

Magnetic saturation of induction machine for generator operations is an inevitable characteristic the machine must undergo to generate electricity. From the control angle according to [187, 188], pushing the limit of the magnetic material well into saturation has an increase influence on torque output, efficiency, and other performance gains. However, main or magnetising reactance, a crucial parameter in the classical equivalent circuit of the induction machine, was not readily calculable. This parameter's value varies greatly for inverter-fed motors, depending on the saturation degree of the magnetic circuit, which can alter across a large range for different magnitudes and frequencies of voltage supply. Figure 5.1, illustrate the B-H characteristics curve of a ferromagnetic

material related to the discussion of the phenomena just outlined.

5.3 MMF Distribution of Nine Phase Induction Machine

The mathematical analysis of the MMF distribution in the airgap of a balance winding three phase induction machine, with MMF contributions from the phase currents yield a constant amplitude sinusoidal field distribution [189, 190] For a tri-three phase induction machine, a similar approach analysis as in three phase system can be applied, by exciting each subspace comprising the model of the induction machine. Figure 5.2 (a) shows the magnetic axis spatial projections of tri-three phase, induction machine. Figure 5.2(b) also show the MMF's distribution for each winding sets of three phase windings. Only the MMF fundamental waveform of phase a_1 with dotted line is shown in the figure.
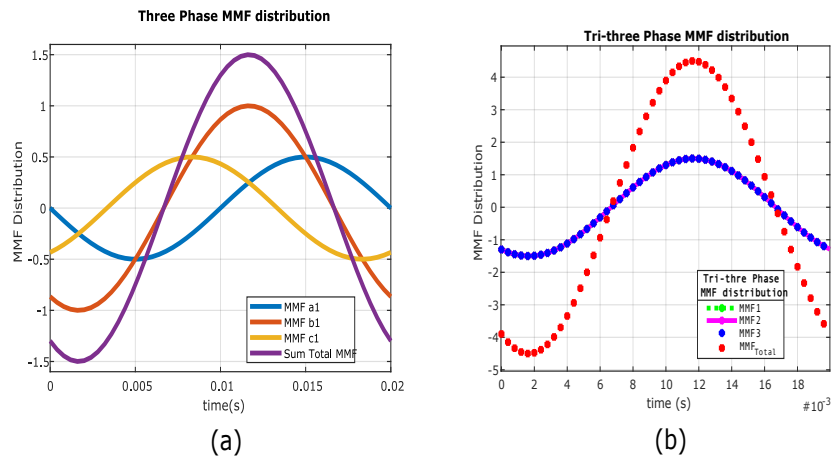
Figure 5.2: Tri-three phase Induction Machine MMF distribution(a) MMF distribution for each three phase Machine.(b) Combine MMF distribution of each stator windings.

In the tri-three phase induction machine, the stator core is co-shared by the three sets of three phase windings, which means there will be three MMFs' distribution in the frame airgap, one for each, produce by each winding set. Each winding sets MMF distribution is determined, and the result added to find the combine MMF distribution of the tri-three phase induction machine. The phases of the set $a_1b_1c_1, a_2b_2c_2$ and $a_3b_3c_3$ are spatially separated from each other by the usual 120° apart respectively. The shift angle '20°', which is the angle between phase a_1 of set 1 and phase a_2 of set

Chapter 5. Field Analysis of Tri-three phase Induction machine

2. Each individual stator pair windings generate the requisite magnetomotive force (MMF) reaction to to each stator pair excitation current. The MMF distribution for each winding sets will be derived analytically, for for each:

It is useful to make some assumptions in order to simplify further the equations.

- **For winding set 1**

$$
\begin{cases}
MMF_{a1}(\omega t, \theta) = F_m \sin(\omega t) \cos(h\theta) \\
MMF_{b1}(\omega t, \theta) = F_m \sin(\omega t - \frac{2\pi}{3}) \cos(h\theta - \frac{2\pi}{3}) \\
MMF_{c1}(\omega t, \theta) = F_m \sin(\omega t - \frac{4\pi}{3}) \cos(h\theta - \frac{4\pi}{3})
\end{cases}
\tag{5.1}
$$

Decomposing the right hand side of the MMF's equation(5.1) into a forward and backward rotating MMF, we have the equation equal to:

$$
\begin{cases}
MMF_{a1}(\omega t, \theta) = \frac{1}{2} F_m \sin(\omega t - h\theta) + \frac{1}{2} F_m \sin(\omega t + h\theta) \\
MMF_{b1}(\omega t, \theta) = \frac{1}{2} F_m \sin(\omega t - h\theta) + \frac{1}{2} F_m \sin(\omega t + h\theta - \frac{4\pi}{3}) \\
MMF_{c1}(\omega t, \theta) = \frac{1}{2} F_m \sin(\omega t - h\theta) + \frac{1}{2} F_m \sin(\omega t + h\theta - \frac{2\pi}{3})
\end{cases}
\tag{5.2}
$$

- **For winding set 2**

$$
\begin{cases}
MMF_{a2}(\omega t, \theta, \xi) = F_m \sin(\omega t - h\xi) \cos(h\theta - h\xi) \\
MMF_{b2}(\omega t, \theta, \xi) = F_m \sin(\omega t - h\xi - \frac{2\pi}{3}) \cos(h\theta - h\xi - \frac{2\pi}{3}) \\
MMF_{c2}(\omega t, \theta, \xi) = F_m \sin(\omega t - h\xi - \frac{4\pi}{3}) \cos(h\theta - h\xi - \frac{4\pi}{3})
\end{cases}
\tag{5.3}
$$

Decomposing the right hand side of the MMF's equation(5.3) into a forward and backward rotating MMF, we have the equation equal to:

$$
\begin{cases}
MMF_{a2}(\omega t, \theta, \xi) = \frac{1}{2} F_m \sin(\omega t - h\theta) + \frac{1}{2} F_m \sin(\omega t + h\theta - 2h\xi) \\
MMF_{b2}(\omega t, \theta, \xi) = \frac{1}{2} F_m \sin(\omega t - h\theta) + \frac{1}{2} F_m \sin(\omega t + h\theta - 2h\xi - \frac{4\pi}{3}) \\
MMF_{c2}(\omega t, \theta, \xi) = \frac{1}{2} F_m \sin(\omega t - h\theta) + \frac{1}{2} F_m \sin(\omega t + h\theta - 2h\xi - \frac{2\pi}{3})
\end{cases}
\tag{5.4}
$$

140

• **For winding set 3**

$$
\begin{cases}
MMF_{a3}(\omega t, \theta, \xi) = F_m \sin(\omega t - 2h\xi) \cos(h\theta - 2h\xi) \\
MMF_{b3}(\omega t, \theta, \xi) = F_m \sin(\omega t - 2h\xi - \frac{2\pi}{3}) \cos(h\theta - 2h\xi - \frac{2\pi}{3}) \\
MMF_{c3}(\omega t, \theta, \xi) = F_m \sin(\omega t - 2h\xi - \frac{4\pi}{3}) \cos(h\theta - 2h\xi - \frac{4\pi}{3})
\end{cases}
\tag{5.5}
$$

Decomposing the right hand side of the MMF's equation(5.5) into a forward and backward rotating MMF, we have the equation equal to:

$$
\begin{cases}
MMF_{a3}(\omega t, \theta, \xi) = \frac{1}{2}F_m \sin(\omega t - h\theta) + \frac{1}{2}F_m \sin(\omega t + \theta - 4h\xi) \\
MMF_{b3}(\omega t, \theta, \xi) = \frac{1}{2}F_m \sin(\omega t - h\theta) + \frac{1}{2}F_m \sin(\omega t + \theta - 4h\xi - \frac{4\pi}{3}) \\
MMF_{c3}(\omega t, \theta, \xi) = \frac{1}{2}F_m \sin(\omega t - h\theta) + \frac{1}{2}F_m \sin(\omega t + \theta - 4h\xi - \frac{2\pi}{3})
\end{cases}
\tag{5.6}
$$

If the MMF's for each winding sets of equation (5.2), equation (5.4), and equation (5.6) are are added together, All the backward travelling MMF's sum up to zero. Now, Assuming the same number of poles for all winding, same number of turns, which will mean same winding factor, and same current, the total sum of the MMF for the three set of three phase winding will be:

$$
F_{total} = \frac{9}{2}F_m \sin(\omega t - h\theta)
\tag{5.7}
$$

where $F_m = \frac{2\sqrt{2}}{\pi} \frac{N_t K_{wh}}{hP} I$.

The MMF space phasor for each three phase winding set of the tri-three phase system for any harmonic component $h = 1, -5, 7, ...$ fed from a balance three set of three phase current for each winding set, considering the spatial disposition between each winding sets and also in their respective currents, it is thus given by equation (5.3)-(5.6). Where k_{wh} is the 'h' harmonic winding factor (note the sign of the harmonic order indicates direction of rotation of corresponding flux components), N_t is the number of turns per phase, P is the number of poles, I_m is the phase current amplitude, θ is the stator spatial peripheral angle, a coordinate along which moves the coil with

inductance of the winding, ξ is the disposition angle between the three winding sets, ω is the frequency of the supply. The three set of three phase stator windings have a 20° spatial shift in the winding layout. The total sum of the MMF distributions in the airgap of the tri-three phase induction machine expressed in exponential form is obtained by summing all the three MMFs' contributions in the airgap of the stator compartment.

It becomes clear from equation(5.7), that the total MMF distribution is higher in space magnitude and varies in time, as well as the harmonic angle.

5.4   Nine Phase Air gap flux density Analysis

Tri-three phase induction machines, stator, wound with three independent symmetrical/asymmetrical three-phase windings, are the subject of this study. The machine considered here share same number of poles 'P' in contrast to the dual stator induction machine reported in [191]. It is therefore, vital to study the magnetic field distribution of this multiple set winding induction machine from the magnetic field of the stator perspective. One of the challenges in designing this type of machine is ensuring that the teeth and core do not become oversaturated under normal operating conditions. Maximising output power within a fixed motor size is another difficult problem to solve. Assessing the effective air-gap flux density for the machine with multiple stator windings and selecting the flux density produced by each pair of stator windings are the solutions to these problems. Several articles have discussed this vital component of design [192, 193]. The arrangement of the winding can have a notable impact on the operation and effectiveness of the machine. It is therefore important to study the magnetic field interactions in the airgap of this machines. Total air gap flux density from stator winding sets is defined equation (5.8). The flux density value is influenced by the phase angle between the two flux density components, the stator circumferential angle, and the length of time. As oppose to dual stator machine considered in the work of [194], here we consider for a nine phase induction machine, the same number of poles for all the winding sets considered. In [194], a pole ratio of 3, for the two winding set

was selected as the numeric value which minimizes the peak value of the effectivee air gap flux density and value which justifies the full utillization of the magnetic material of a dual stator induction machine.

$$B_{mT}(t, \theta, \xi) = B_1 \cos(\omega t - P_1 \theta) + B_2 \cos(\omega t - P_2 \theta + \xi) + B_3 \cos(\omega t - P_3 \theta + 2\xi) \quad (5.8)$$

Here, B_{mT}, is total instantaneous flux density of the nine phase induction machine. B_1, B_2, B_3, are the maximum flux density of winding set 1,2 and 3. P_1, P_2, P_3 denote the number of poles for each winding. ω denote the electrical speed and ξ is the disposition angle between the winding sets. For our case the number of poles has been chosen to be the same $P_1 = P_2 = P_3 = P$. Therefore, equation (5.8) is rewritten as:

$$B_{mT}(t, \theta, \xi) = B_1 \cos(\omega t - P\theta) + B_2 \cos(\omega t - P\theta + \xi) + B_3 \cos(\omega t - P\theta + 2\xi) \quad (5.9)$$

Maximum overall flux density does not vary with time. This leads us to an expression for the total air gap flux density, which will be used in the subsequent analysis:

$$B_{mT} = B_1 \cos(P\theta) + B_2 \cos(P\theta + \xi) + B_3 \cos(P\theta + 2\xi) \quad (5.10)$$

Dropping the bracketed parameters in equation (5.10) RHS, without loss of brevity and expressing in per-unit, we modify the relation in equation(5.10). All other expression as define before.

$$\frac{B_{mT}}{B_1} = \cos(P\theta) + \hat{B}_2 \cos(P\theta + \xi) + \hat{B}_3 \cos(P\theta + 2\xi) \quad (5.11)$$

Where:
$\hat{B}_2$ and $\hat{B}_3$ are the relative flux density of peak flux densities of B_2 and B_3. In order to prevent deep saturation of the magnetic part, the flux density of the respective winding sets must be apportion a certain flux value. If say, the peak air gap flux density is given, the air gap flux densities of the respective stator winding sets can be found. Figure 5.3(a), shows peak flux density in the airgap of a nine phase induction machine for different variation of airgap flux density of winding set 2 and winding set 3. The

figure 5.3(a),(b) drawn to scale in per-unit, shows comparison of the flux variations map, of winding set 2 and winding set 3, for symmetrical and asymmetrical nine phase induction machine. This figure shows that if both machines is to be subjected to the same operations, their performance and choices of flux for each winding sets for a given airgap flux density differ.
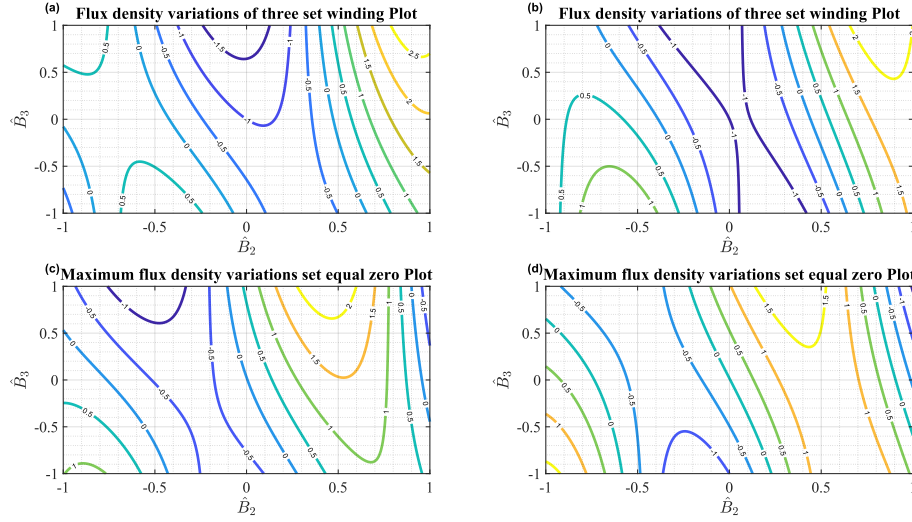
Figure 5.3: Air gap flux density plot.(a) peak flux density variation for asymmetrical induction machine (b) peak flux density variation for symmetrical induction machine

From Figure 5.3(a), the asymmetrical case, it can be seen the peak flux density variations paths for various peak flux densities. As well as the relationship between the relative flux densities $\hat{B}_2$ of winding set 2,and $\hat{B}_3$ of winding set 3. For each map of peak flux densities, the relative peak flux density in per-unit is varied from $-1 \leq \hat{B}_2 \leq 1$, $-1 \leq \hat{B}_3 \leq 1$. Three notable points to attain zero peak flux density (i.e $B_{pk} = 0$) in the air gap is shown. This lines correspond to the equilibrium points and relates on apportion choices of $\hat{B}_2$ and $\hat{B}_3$ to maintain airgap zero flux in the airgap. The negative values of the peak airgap flux densities denotes the nine phase induction machine capability operation as a generator. So, for positive peak air gap flux densities, the nine phase induction machine operates as a motor. For example, for a peak flux density of -1.0 T, the flux level of winding 3 should be varied from $-0.05 \leq \hat{B}_3 \leq 1$, while the flux level for winding set 2 should be maintained between the flux window level

$-0.15 \leq \hat{B}_3 \leq 0.22$ per unit to maintain a peak air gap flux of -1.0 T in the airgap of the nine phase induction machine, configured in the asymmetrical configuration. At peak flux level of -1.5 T, the flux window level $-0.25 \leq \hat{B}_2 \leq 0.25$ should be maintained for winding set 2, while the flux window level $0.65 \leq \hat{B}_3 \leq 1.0$ be maintained for winding set 3. For higher airgap peak flux level, related to motoring operations, winding set 2 and winding set 3 should be maintained at peak airgap flux level close to 1.0 per unit. An airgap flux density map for a symmetrical nine phase induction machine is given in Figure 5.3(b), peak airgap flux level for generator operations for winding set 2, should be maintained at $-0.4 \leq \hat{B}_2 \leq 0.4$ per unit. Outside this flux band, the nine phase induction machine can be drafted for motoring operations. Figure 5.3(c) and 5.3(d) various maximum peak airgap flux density variations for asymmetrical and symmetrical nine phase induction machine. The plot was obtained, by setting equation(5.11) to zero (i.e $\frac{d\left(\frac{B_m T}{B_1}\right)}{d\theta} = 0$) for various machine types(i.e asymmetrical and symmetrical induction machine) The plot shows the maximum peak airgap flux densities at various instance of flux levels for winding set 2 and 3 to obtain the various choices of air gap flux level.

$$\theta_p = -\frac{\tan^{-1}\left(\frac{(\hat{B}_3 - 1)\sin\xi}{\hat{B}_3\cos\xi + \cos\xi + \hat{B}_2}\right) + \xi}{P} \tag{5.12}$$

Figure 5.4 illustrate the plot for various angles variations for asymmetrical (Figure 5.4(a)), nine phase induction machine and symmetrical (Figure 5.4(b)), nine phase induction machine. The both figures Figure 5.4(a),(b), have been plotted using the equation (5.12). It can be easily seen that, for asymmetrical nine phase machine case, the stator angle corresponding to peak angle increases from $0°$ to 30^0 as the per-unit flux levels of both winding set 2 and 3 are reduce, which satisfies motoring operations within this band of stator peak angle. However, beyond $30°$ the stator angle begin to decrease, with a noticeable crowding of negative stator flux angle around $\hat{B}_2 < 1$ and $\hat{B}_3 < 1$. The reason for this is that the asymmetrical nine phase induction machine is experiencing birfurcation. A phenomenon related to voltage collaspe, as a result of the maximum airgap flux falling to zero value. This is easily corroborate in the maximum flux density variations of Figure 5.3(c). From Figure 5.4(b), one can see
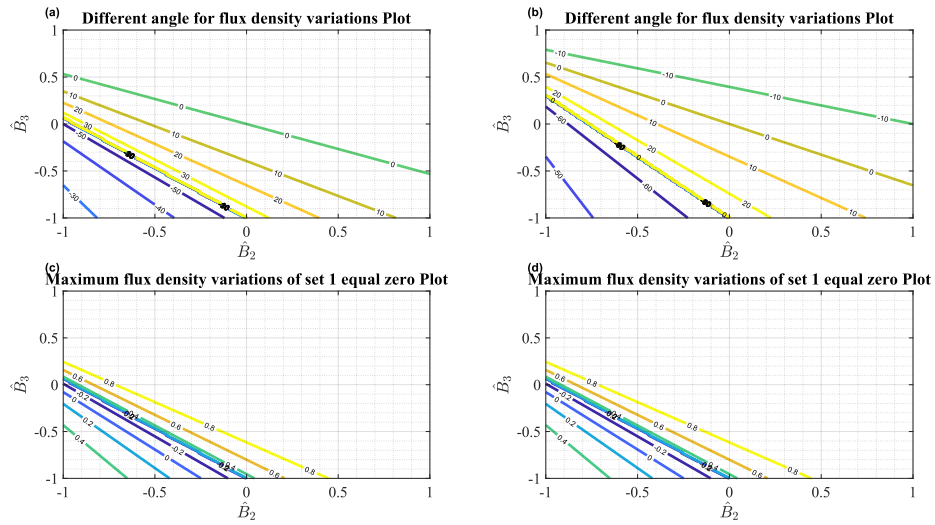
Figure 5.4: (a),(b) different peak angles variation for variety of airgap flux density magnitude for winding set 1 and 2, for asymmetrical and symmetrical induction machine. (c),(d) Peak airgap flux density contribution on account of winding set 1, for asymmetrical and symmetrical induction machine

a change of stator angle for symmetrical case for variety of stator angles. At stator angle of $-10°$ and $0°$, shown on the graph of Figure 5.4(b) the nine phase symmetrical induction can operate from motoring to generating mode, owing to the maximum peak airgap flux density shown in Figure 5.4(d). However, as the peak airgap flux levels $\hat{B}_2$ and $\hat{B}_3$ are reduce further, The mechanism of voltage collapse phenomena experience in asymmetrical configuration as the per unit flux $\hat{B}_2$ and $\hat{B}_2$ is reduce further of the nine phase induction machine is observed. From the Figures 5.4(c)(d), a linear relationship for both machine configuration, (i.e asymmetrical and symmetrical) induction machine coexist for the maximum air gap flux density of winding set 1, as the per unit flux value of $\hat{B}_2$ and $\hat{B}_3$ are varied. The two graphs are similar for both configurations. The reason for this similarity is that, the two graph will exhibit similar maximum flux density variations as they each correspond to the first winding set of a nine phase induction machine, and therefore, will exhibit similar electrical characteristics.

Figure 5.5 illustrate the different variety of maximum airgap flux densities for asymmetrical and symmetrical induction machine. It is worth observing that there exist

146

on both curve a line at which the maximum airgap flux is zero. Both perspective views and contour plots of the two types of machine configurations have been plotted for the maximum peak flux density in the airgap for winding set 2 of the nine phase induction machine.
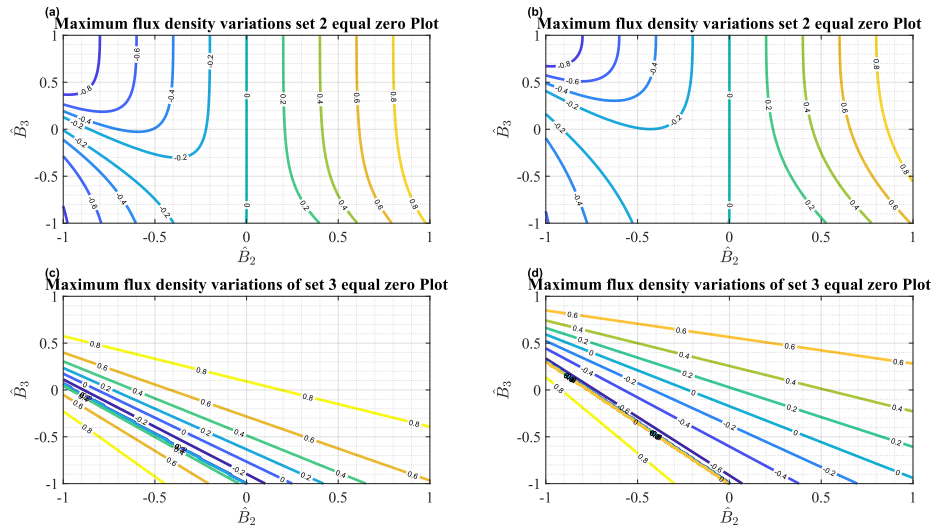
Figure 5.5: Peak maximum airgap flux density contribution on account of winding set 2 and 3, for asymmetrical (a,c) and symmetrical (b,d) induction machine .

Far to the right of the curve, the winding set 2 can assume motoring responsibilities. Far to the left hand side the winding set 2 can assume generating responsibilities. The corresponding perspective view for both machine peak flux density plot corresponding to $\hat{B}_2 = 0$ is of similar type where it is adjudge the winding set 2 is completely switched off. This corresponding situation can be related to fault tolerant operation as reported in [195].

5.5 Conclusions

In this section, an un-discussed area in many papers is the appropriate allocation of the peak airgap flux density in the control architecture to each respective windings of multiple phase induction machine. A concise analytical determination of a nine phase MMF distribution is studied. Various flux density map for nine phase induction machine is studied. Based on this study, we draft out the contribution of this chapter.

Figure 5.6: Total Flux density plot for all winding set. (a) Asymmetrical winding induction machine (b) Symmetrical winding induction machine

a) Results from this map can be used to investigate the operation of the nine phase induction machine for generating or motoring mode of operations. b) The result from this work can serve as a map for various control settings of flux levels for multiple phase induction machine for both asymmetrical and symmetrical induction machine. c)This work shows that a nine phase induction machine is similar in terms of phase number for asymmetrical and symmetrical induction machine, however, their operations as regard allocation of peak flux for efficient control to meet performance objective differ. This is key to the control engineer to ensure efficient control operations. d) The analysis presented here , although, obtained for a nine phase induction machine, but it can be subsequently modified to account for any number of phase. e) It is easy to seee region of birfucation (voltage collapse) using the approach presented here. As the best choice of airgap flux level to present voltage collapse is evident. f) A concept for arbitrary power sharing was discuss in [60], with using assume current sharing coefficient to apportion active and reactive power between winding sets in a nine phase induction machine, with no graphical or analytical calculation of the precise flux level which should be allotted to each winding set for the objective of power sharing between windings to be met. A leap in our contribution in this chapter over the presented work [60] is that, our

analysis and graphic plot gives range of optimize flux contributions from each winding sets in per-unit, to obtained the optimize peak flux density to ensure the arbitrary power sharing.

Chapter 6

Nine Phase Inductance Determination

In section 2.1, we explored the profound implications of structural winding arrangements and the number of neutral points in the classification of multiphase induction machines. These arrangements, characterized as either symmetrical or asymmetrical, encompass the stator slots, dictating the machine's behavior. Single neutral point multiphase induction machines exhibit symmetrical properties, with a spatial separation between phases denoted by $\frac{2\pi}{n}$. These machines typically have an odd number of phases, such as $n = 5, 7, 9...$ and so on. Conversely, multiple neutral point induction machines can manifest both symmetrical and asymmetrical attributes, featuring phase sets of three (3), five (5), or seven (7) interconnected in groups of 2, 3, 4, and beyond. The neutral points within these machines are uniformly distributed within the stator slot compartment of electric machines, either collectively or individually.

The winding topologies of multiple-phase induction machines replicate those observed in single or three-phase induction machines. However, due to the inclusion of additional windings and the arrangement of $k-$ winding groups, the coupling inductance between phases and other winding sets within the stator slot intensifies. This coupling inductance encompasses both self-inductance and leakage inductance, factors of utmost importance that demand careful consideration.

In recent years, the design and development of multiphase machines have undergone

a rapid pace of advancement. Consequently, it is crucial to effectively evaluate the inductances between phases and other windings within the multiphase induction machine to facilitate efficient dynamic and steady-state simulation studies. To accomplish this goal, a comprehensive analysis of an $n-$ phase machine is indispensable, encompassing meticulous assessments of the machine's geometry and winding layouts.

This section delves into the analytical determination of winding inductances in multiple set induction machines, employing the turn function and winding function approach. Moreover, it sheds light on the often-neglected matter of leakage inductances that emerge between distinct winding sets in symmetrical and asymmetrical configurations of a nine-phase induction machine. Through this analysis, we gain profound insights into the calculations and derivations of leakage inductance. Additionally, this section presents a comparative study, scrutinizing the two leakage inductances resulting from the aforementioned structural winding arrangements, thereby unveiling compelling findings.

6.1   Turn Function and Winding Function

The section introduces a coupled circuit approach model for a nine-phase stator winding induction machine equipped with a squirrel-cage rotor. The inductances of both the stator windings and rotor bars are computed using the winding function methodology, which relies on the spatial distribution of the windings as depicted in the figure appendix A1.2. In the figure, the winding spread round the stator slot for each set have been clearly distinguished. The turn and winding function theory is founded on the arrangement of windings within the stator slots of an induction machine [196]. By utilizing a piecewise linear function, the turn function (TF) and winding function (WF) are defined for both the stator and rotor loops, capturing their values along the stator and rotor periphery. Plotting the TF and WF involves varying the circumferential angle around the stator slots. The turn and winding function methodology greatly facilitates the determination of machine inductances, air-gap flux densities, and the harmonics of the magnetomotive force (MMF).

The WF approach assumes the absence of symmetry in the arrangement of motor

windings across the entire slot structure. Figure 6.1 visually illustrates the turn function and winding function of a typical two-pole stator winding featuring a $30°$ geometric shift between slots, a phase belt of $60°$, and a slot per pole per phase value of $q = 3$.
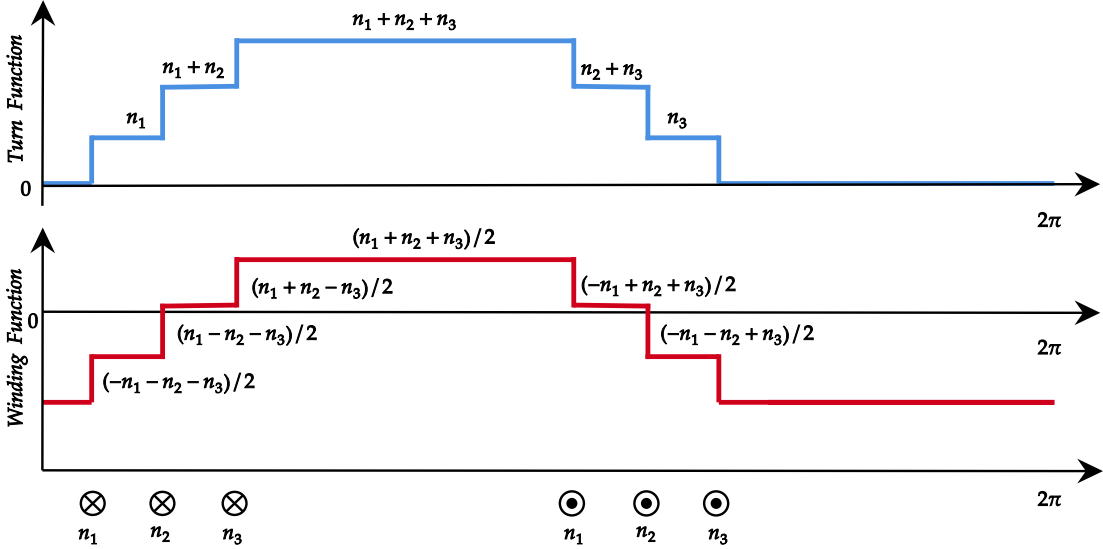
Figure 6.1: Turn function and Winding function background

6.2   Self and Mutual Inductance Between Windings of Multiple Sets

Figure 6.2 shows a schematic visualization of the nine phase induction machine system. The magnetic coupling that exist between one stator winding and the other and also between the rotor winding is shown. The rotor considered here is a squirrel cage rotor.

6.2.1   Stator-Stator Inductance

Equation (6.1) represents the inductances that exist between the phases within a set of windings. On the other hand, equation (6.2) provides a matrix representation of the mutual inductance between different sets of stator windings in a tri-three phase inductance machine.
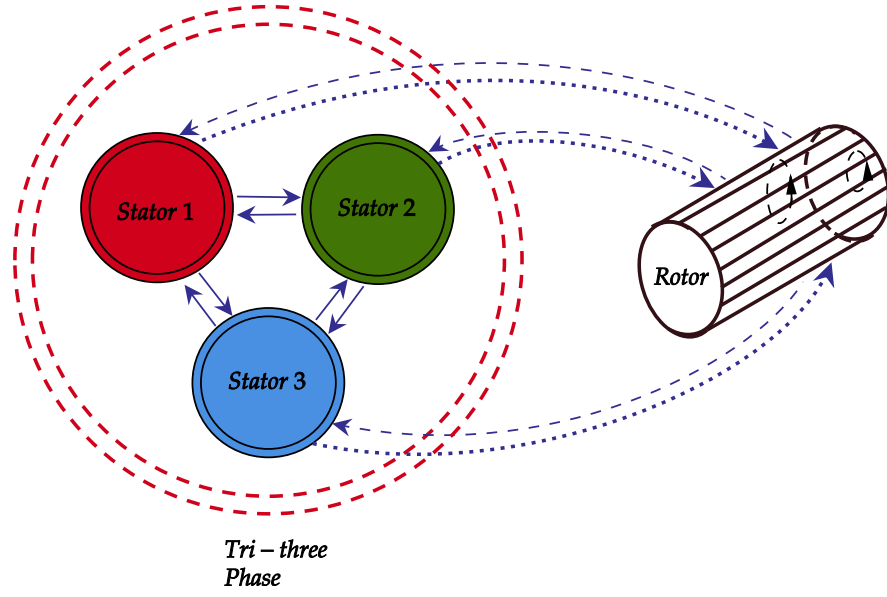
Figure 6.2: Tri-three phase Induction Machine Magnetic Coupling.

$$L_{ii} = \begin{bmatrix} L_{asiasi} & L_{asibsi} & L_{asicsi} \\ L_{bsiasi} & L_{bsibsi} & L_{bsicsi} \\ L_{csiasi} & L_{csibsi} & L_{csicsi} \end{bmatrix}, \forall\, i \; = \; 1,2,3 \tag{6.1}$$

$$M_{ij} = \begin{bmatrix} L_{asiasj} & L_{asibsj} & L_{asicsj} \\ L_{bsiasj} & L_{bsibsj} & L_{bsicsj} \\ L_{csiasj} & L_{csibsj} & L_{csicsj} \end{bmatrix}, \forall\, i\,j \; = \; 1,2,3 \tag{6.2}$$

The off-diagonal mutual inductance matrices can be calculated using equation (6.2) by following the same procedure for each sub-winding matrix. Matrices M_{12} and M_{13} are obtained for all $i = 1$ and $j = 2,3$. Similarly, matrices M_{21} and M_{23} are obtained for all $i = 2$ and $j = 1,3$, and matrices M_{31} and M_{23} are obtained for all $i = 3$ and $j = 1,2$. The mutual inductance between the three sets of stator windings and the rotor winding can be calculated in a similar manner using equation (6.3).

$$L_{sri} = \begin{bmatrix} L_{asir1} & L_{asir2} & \cdots & L_{asirn} \\ L_{bsir1} & L_{bsir2} & \cdots & L_{bsirn} \\ L_{csir1} & L_{csir2} & \cdots & L_{csir2} \end{bmatrix} \forall,\; i = 1,2,3 \tag{6.3}$$

The individual elements of the inductance matrices in equations (6.1) and (6.2) are calculated using equation (6.4). By applying equation (6.4), a matrix can be constructed to represent the self-inductance and mutual inductance between different sets of windings.

$$L_{ij} = L_{ji} = L_{ms} \cos \left(|i - j| \frac{2\pi}{m} + b\xi \right) \forall, \ b = 0, 1, 2 \tag{6.4}$$

The variables i and j correspond to the indices that denote the rows and columns of the inductance matrices in equations (6.1) and (6.2). In this context, m represents the number of phase sets, which is equal to 3 for the nine-phase induction machine. The parameter ξ refers to the angular shift between the sets of windings, and in the case of asymmetrical winding with isolated neutral, it is given by $\xi = \pi/9$ radians. The quantity L_{ms} denotes the peak value of the magnetizing inductance.

6.2.2 Rotor-Rotor Inductance

This section focuses on the determination of rotor inductances for a squirrel cage rotor. The turn function and winding function are represented by a piecewise linear function, as outlined in equations (6.5) and (6.6). The inductances of a non-skewed rotor are calculated using the piecewise function along with equation (6.19), resulting in the inductance values given by equations (6.8) to (6.9).

$$n_i(\theta) = \begin{cases} 0 & 0 \leq \theta \leq \theta_i \\ 1 & \theta_i \leq \theta \leq \theta_i + \alpha_r \\ 0 & \theta_i + \alpha_r \leq \theta \leq 2\pi \end{cases} \tag{6.5}$$

$$N_i(\theta) = \begin{cases} \frac{-\alpha_r}{2\pi} & 0 < \theta < \theta_i \\ 1 - \frac{\alpha_r}{2\pi} & \theta_i < \theta < \theta_{i+1} \\ \frac{-\alpha_r}{2\pi} & \theta_{i+1} < \theta < 2\pi \end{cases} \tag{6.6}$$

Equation (6.7) represents the rotor inductance matrix. Each element of the rotor

inductances is defined as follows:

$$
L_r = \begin{bmatrix}
L_{kk} + L_0 & L_{ki} - L_b & L_{ki} & \cdots & L_{ki} - L_b \\
L_{ki} - L_b & L_{kk} + L_0 & L_{ki} - L_b & \cdots & L_{ki} \\
L_{ki} & L_{ki} - L_b & L_{kk} + L_0 & \cdots & L_{ki} \\
\vdots & \vdots & \vdots & \ddots & \vdots \\
L_{ki} - L_b & L_{ki} & \cdots & \cdots & L_{kk} + L_0
\end{bmatrix}
\tag{6.7}
$$

$$
\text{where } L_0 = 2\left(L_b + L_e\right)
$$

The self-inductance matrix of the rotor is determined by the inductance of the rotor bar (L_b) and the end ring (L_e). It can be expressed as:

$$
L_{kk} = \frac{\mu_0 r l \alpha_r}{g}\left(1 - \frac{\alpha_r}{2\pi}\right)
\tag{6.8}
$$

Where:

The parameters α_r is the angle between rotor bars or phases, r is the radius of the rotor member, l is the axial length of the rotor frame, g is the average air gap length, μ_0 is the relative permittivity of the air gap.

The mutual inductance of the rotor with other rotor bars can be defined as:

$$
L_{ki} = -\frac{\mu_0 r l}{g}\left(\frac{\alpha_r^2}{2\pi}\right)
\tag{6.9}
$$

6.2.3 Stator-Rotor Mutual Inductance

The elements of the inductance matrices in equation equation (6.3) are calculated using equation (6.10). These matrices represent the stator-rotor inductance matrices, which account for the mutual inductances between the stator and rotor windings of each set, considering the angular displacement between the winding sets.

$$
L_{srj}(\theta_r) = L_m \cos\left(P'\left(\theta_{r\delta} + \frac{\alpha_r}{2} + b\xi\right) \mp k\frac{2\pi}{m}\right)
\tag{6.10}
$$

$$
\forall,\ j = 1, 2, 3
$$

$$L_m = \frac{16}{\pi} \frac{\sin\left(P'\frac{\alpha_r}{2}\right)}{(2P')^2 \, N_{si}} L_{msi} \tag{6.11}$$

$$L_{msi} = \frac{\mu_0 \pi l r}{g} \left(\frac{N_{si}}{2P'}\right)^2 \tag{6.12}$$

The matrices L_{sr1}, L_{sr2}, and L_{sr3}, which are dependent on the rotor angle θ_r, are formed using equation (6.10). These matrices represent the mutual inductances between the stator and rotor windings. The elements of the first three rows of L_{sr1} are calculated using equation (6.10) for $b = 0$, where the loop k runs from 0 to 2. The same procedure is repeated for $b = 1, 2$, with the loop k running from 0 to 2, to populate the matrices L_{sr2} and L_{sr3} as shown in equation (6.13). In these expressions, n represents the total number of rotor bars, $\alpha_r = \frac{2\pi}{n}$, and $\theta_{r\delta} = \theta_r + (i-1)\alpha_r$. The index i represents the rotor bar number, ranging from 1 to n.

Expressing the inductance matrix in a concise and compact notation:

$$L = \begin{bmatrix} [L_{11}] & [M_{12}] & [M_{13}] & [L_{sr1}] \\ [M_{21}] & [L_{22}] & [M_{23}] & [L_{sr2}] \\ [M_{31}] & [M_{32}] & [L_{33}] & [L_{sr3}] \\ [L_{sr1}]^T & [L_{sr2}]^T & [L_{sr3}]^T & [L_r] \end{bmatrix} \tag{6.13}$$

In this context, the matrices L_{11}, L_{22}, L_{33}, M_{12}, M_{13}, M_{21}, M_{23}, M_{31}, and M_{32} are all 3×3 matrices. The matrices L_{sr1}, L_{sr2}, and L_{sr3} have dimensions of $3 \times n$, while L_r is an $n \times n$ matrix. The matrices L_{11}, L_{22}, and L_{33} are equal and can be determined using equation (6.1).

$$L_{ii} = \begin{bmatrix} L_{ls1} + L_{ms1} & L_{ms1}\cos\left(\frac{2\pi}{3}\right) & L_{ms1}\cos\left(\frac{4\pi}{3}\right) \\ L_{ms1}\cos\left(\frac{4\pi}{3}\right) & L_{ls1} + L_{ms1} & L_{ms1}\cos\left(\frac{2\pi}{3}\right) \\ L_{ms1}\cos\left(\frac{2\pi}{3}\right) & L_{ms1}\cos\left(\frac{4\pi}{3}\right) & L_{ls1} + L_{ms1} \end{bmatrix} \tag{6.14}$$

The matrices M_{ij} represent the mutual inductance between one set of windings and another set of windings.

$$M_{ij} = L_{ms1} \begin{bmatrix} \cos{(k\xi)} & \cos{\left(\frac{2\pi}{3} \pm k\xi\right)} & \cos{\left(\frac{4\pi}{3} \pm k\xi\right)} \\ \cos{\left(\frac{4\pi}{3} \pm k\xi\right)} & \cos{(k\xi)} & \cos{\left(\frac{2\pi}{3} \pm k\xi\right)} \\ \cos{\left(\frac{2\pi}{3} \pm k\xi\right)} & \cos{\left(\frac{4\pi}{3} \pm k\xi\right)} & \cos{(k\xi)} \end{bmatrix} \tag{6.15}$$

$$ij = ji, \ \forall \ i,j \ = 1,2 \text{ and } i,j \ = 2,3 \text{ where, } k = 1$$

$$ij = ji, \ \forall \ i,j = 1,3 \text{ where, } k = 2$$

The stator-to-rotor inductance matrices are calculated using equations (6.10)–(6.12), taking into account the shift angle ξ between the three sets of windings. To visualize the turn function and winding function of the chorded nine-phase machine, a script code is implemented based on the schematic shown in Figure A1.2. The resulting plot of the turn function and winding function as a function of the spatial angle is presented in the results section.

6.3 Nine Phase Stator Inductances Calculations

Accurate estimation of machine parameters is of utmost importance as it directly influences the modeling, performance, and control of the machine. Various comprehensive techniques for parameter estimation in electric machines have been extensively reviewed and documented in the research conducted by [197]. In the case of multiphase machines, which consist of multiple windings in the stator, it is crucial to accurately determine the mutual inductance between different winding layers. This knowledge contributes to improving the modeling, performance, and control strategies employed for these machines. However, extracting all the necessary stator and rotor leakage inductances solely from standard tests presents a challenging task.

The calculation of winding inductances involves utilizing the turn function and winding function of the windings. The winding function associated with the ith winding can be represented as $N_i(\theta)$, where θ denotes the angular position around the stator. The magnetic field and magnetic field intensity around the stator can be mathematically

described as indicated by [198].

$$
\begin{cases}
H_i(\theta) = \frac{N_i(\theta)}{g(\theta,\theta_{rm})} i_i \\
B_i(\theta) = \mu_0 \frac{N_i(\theta)}{g(\theta,\theta_{rm})} i_i
\end{cases}
\tag{6.16}
$$

The air gap function $g(\theta, \theta_{rm})$ represents the variation of the air gap length, and i denotes the current flowing through the i-th winding. In the case of a squirrel cage rotor, the air gap function is constant, and we can replace $g(\theta, \theta_{rm})$ with the parameter 'g_0', representing the gap length.

Suppose we wish to determine the mutual inductance between the i-th and j-th coils, with the turn function of the j-th winding denoted as $n_j(\theta)$. We can formulate an expression for the flux coupling induced in the j-th winding by the current i_i in the i-th winding as:

$$
\lambda_{ji} = \mu_0 r l \cdot i_i \cdot \int_0^{2\pi} \frac{1}{g(\theta, \theta_{rm})} \cdot n_j(\theta) \cdot N_i(\theta) \cdot d\theta
\tag{6.17}
$$

Here, r represents the average radius of the air gap middle line, and l denotes the effective length of the stator core.

The mutual inductance between the j-th and i-th windings, denoted as L_{ji}, can be expressed as:

$$
L_{ji} = \mu_0 r l \cdot \int_0^{2\pi} \frac{1}{g(\theta, \theta_{rm})} \cdot n_j(\theta) \cdot N_i(\theta) \cdot d\theta
\tag{6.18}
$$

Equation (6.3) can be utilized to determine the self and mutual inductances between stator windings, as well as between different stator winding sets. Moving forward, we can calculate the self and mutual inductances of the nine-phase stator winding sets, namely a_1, b_1, c_1, a_2, b_2, c_2, and a_3, b_3, c_3. Moreover, equation (6.3) can also be employed to determine the self inductance of the rotor bar and the mutual inductances between the stator and rotor bar.

6.3.1   Self Inductances of $a_i b_i c_i$ Winding set

By utilizing equation (6.3), we can derive the expression for the self-inductance of the i-th winding as follows:

$$L_{ii} = \mu_0 r l \cdot \int_0^{2\pi} \frac{1}{g_0} \cdot n_i(\theta) \cdot N_i(\theta) \cdot d\theta \tag{6.19}$$

Here, $n_i(\theta)$ and $N_i(\theta)$ have the same definitions as before, and we replace $j = i$ in equation (6.3).

The expression for the self-inductance of phase a_i can be simplified as:

$$L_{a_i a_i} = \frac{\mu_0 r l}{g_0} \int_0^{2\pi} n_{a_i}(\theta) \cdot [n_{a_i}(\theta) - \langle n_{a_i}(\theta) \rangle] \cdot d\theta \tag{6.20}$$

Similarly, we can derive the expressions for phases b_i and c_i:

$$L_{b_i b_i} = \frac{\mu_0 r l}{g_0} \int_0^{2\pi} n_{b_i}(\theta) \cdot [n_{b_i}(\theta) - \langle n_{b_i}(\theta) \rangle] \cdot d\theta \tag{6.21}$$

$$L_{c_i c_i} = \frac{\mu_0 r l}{g_0} \int_0^{2\pi} n_{c_i}(\theta) \cdot [n_{c_i}(\theta) - \langle n_{c_i}(\theta) \rangle] \cdot d\theta \tag{6.22}$$

In the above equations, $\langle n_{a_i}(\theta) \rangle$, $\langle n_{b_i}(\theta) \rangle$, and $\langle n_{c_i}(\theta) \rangle$ represent the average values of phase a_i, b_i, and c_i, respectively, for all $i = 1, 2, 3$.

6.3.2   Mutual Inductances of the $a_i b_i c_i$ winding Set and other phases winding set $a_j b_j c_j$

The mutual inductance between windings can be expressed in a similar manner to equation (6.3):

$$L_{ij} = \mu_0 r l \cdot \int_0^{2\pi} \frac{1}{g_0} \cdot n_i(\theta) \cdot N_j(\theta) \cdot d\theta \tag{6.23}$$

In this equation, $n_i(\theta)$ and $N_j(\theta)$ retain their previous definitions, and it is important to note that $i \neq j$.

The expression for the mutual inductance between phase a_i and other winding sets,

such as a_j, b_j, and c_j, can be simplified as follows:

$$L_{a_i a_j} = \frac{\mu_0 r l}{g_0} \int_0^{2\pi} n_{a_i}(\theta) \cdot \left[n_{a_j}(\theta) - \left\langle n_{a_j}(\theta) \right\rangle \right] \cdot d\theta \tag{6.24}$$

Similarly, we can derive the expressions for phases b_i and c_i:

$$L_{b_i b_j} = \frac{\mu_0 r l}{g_0} \int_0^{2\pi} n_{b_i}(\theta) \cdot \left[n_{b_j}(\theta) - \left\langle n_{b_j}(\theta) \right\rangle \right] \cdot d\theta \tag{6.25}$$

$$L_{c_i c_j} = \frac{\mu_0 r l}{g_0} \int_0^{2\pi} n_{c_i}(\theta) \cdot \left[n_{c_j}(\theta) - \left\langle n_{c_j}(\theta) \right\rangle \right] \cdot d\theta \tag{6.26}$$

In these equations, n_{a_1}, n_{b_1}, and n_{c_1} represent the turn function of the i-th winding for phases a_i, b_i, and c_i, respectively. $\left\langle n_{a_j}(\theta) \right\rangle$, $\left\langle n_{b_j}(\theta) \right\rangle$, and $\left\langle n_{c_j}(\theta) \right\rangle$ are the average values of the turn function for the j-th winding of phases a_j, b_j, and c_j, respectively. It is worth noting that during the integration process to determine the inductance, we consider $i \neq j$.
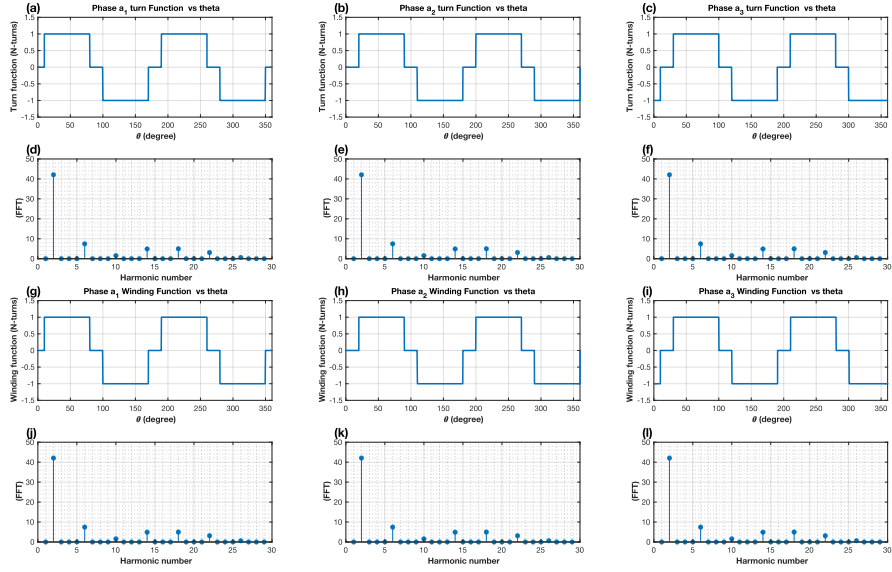
Figure 6.3: (a),(b),(c):-Turn function **and** (g),(h),(i):-winding function between phase $a_{s1} - a_{s1}$, $a_{s2} - a_{s2}$, $a_{s3} - a_{s3}$ winding set phases as a function of spatial angle. (d),(e),(f)(j),(k),(l) fast fourier transform of the turn Fuunction and winding function waveform

The significance of turn and winding functions is paramount in the electromagnetic

design of electrical equipment. Turn and winding functions facilitate the analysis of air gap flux density, parameter estimation, and the resulting MMF harmonics. But in order to accomplish this, we must first start with the clock diagram. i.e see figure B.1 appendix. Here, the windings are arranged in the stator slots according to different phase sequences and pole numbers. Figure 6.3–Figure 6.5 shows the turn function and winding function variation with respect to stator circumferential angle. Below each turn function and winding function is the fast Fourier transform for each winding sets and between phases. Figure 6.3 shows the winding function and Fourier transform of winding of same phase $a_{s1} - a_{s1}$, $a_{s2} - a_{s2}$, $a_{s3} - a_{s3}$. Observe the turn function and winding function presented, show the same graphical shape over the stator circumferential angle and consequently the fast Fourier transform waveform.
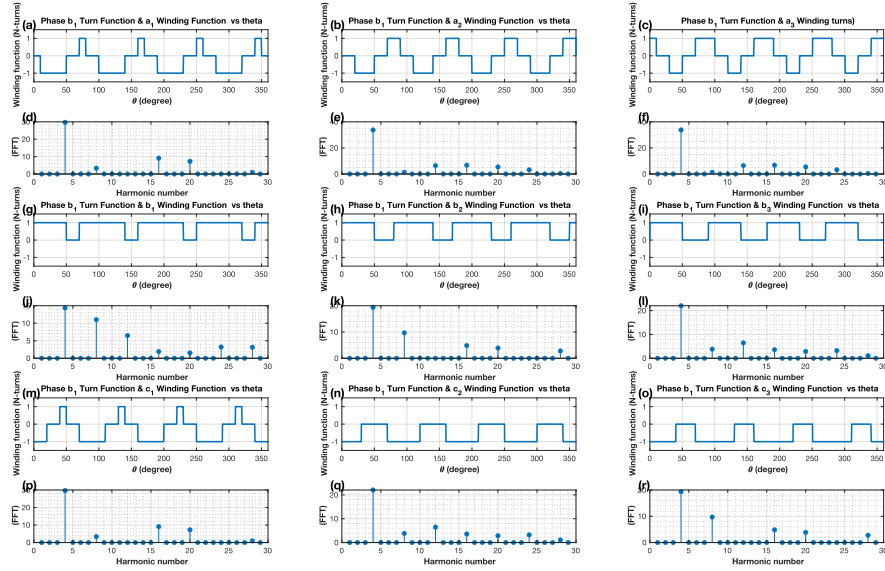
Figure 6.4: Turn function and winding function combination of winding set phases, and other winding group as a function of spatial angle, alongside their respective FFT

Figure 6.4, 6.5, 6.6, shows the turn function and winding function between two different phases in the studied nine phase induction machine. The graph also shows the respective fast Fourier transform corresponding to each turn and winding function waveform. Each plots, shows the variation of the turn function and the winding function as we move from one stator slot angle to another within the stator circumferential

geometry. The plot also shown different fast Fourier transform developed for each waveform does differ. The reason for this difference is due to different frequency component this waveform present. It is easy to visualize a frequency components or a collection of frequency component that makes up the waveform.
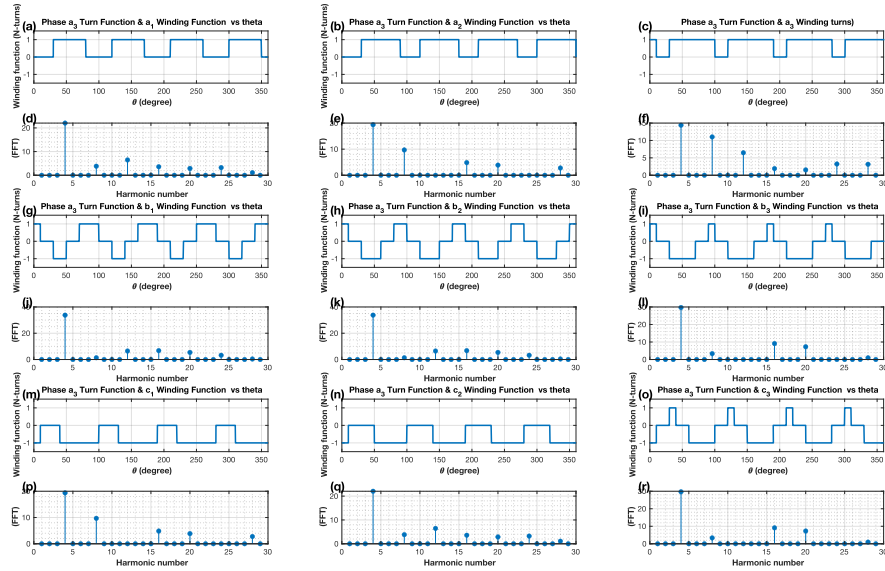
Figure 6.5: Turn function and winding function combination of winding set phases, and other winding group as a function of spatial angle, alongside their respective FFT
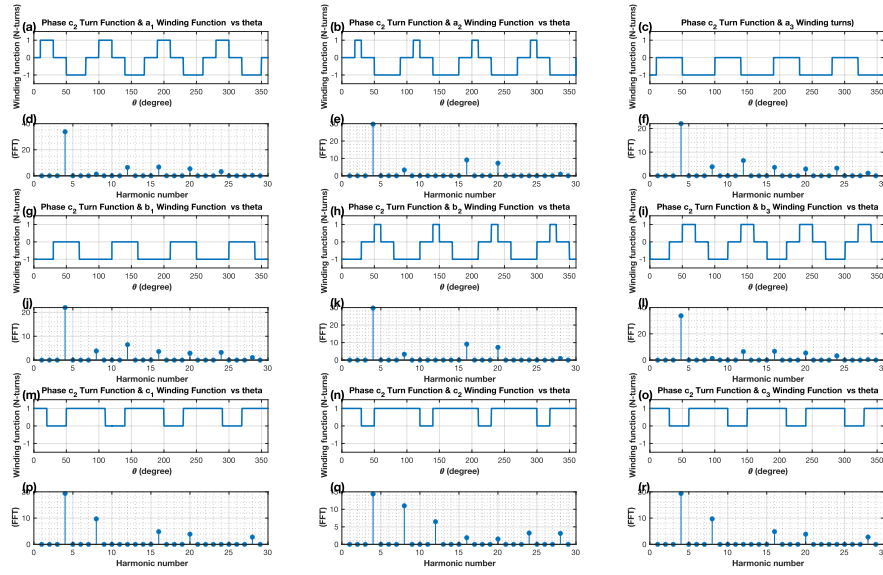
Figure 6.6: Turn function and winding function combination of winding set phases, and other winding group as a function of spatial angle, alongside their respective FFT

There remains a task here to observing the combine effect of the winding function for each set of three phase windings of a nine phase induction machine. The interest is to see if the combination of the winding function for each respective three phase winding contribution minimize or suppress, some harmonic number for an asymmetrical nine phase induction machine topology, taking a second look at the fast fourier transform of the combination. The plot in Figure 6.7 shows these cumulative sum of the winding function plot and it respective fast Fourier transform. This plot have be obtained based on an algorithm written in matlab based on $\sum_{i=1}^{3} n_{ji} \left[N_{ji}(\theta) - \langle N_{ji}(\theta) \rangle \right], \ \forall \ j = \ a_i, b_i, c_i$. There is a slight departure from the Figure 6.7(b) winding function when compared to the Figure 6.3(d), observe that the frequency bin number of the FFT for Figure6.7(b) had been suppress compared to the some identify frequency bin component in Figure 6.3(d). The reason for this is that asymmetrical winding for multi-phase induction machine present less ripple compare to symmetrical winding induction machine. This assertion has been corroborated in the work of [199].

Figure 6.7: (a) Winding function combinations of the three winding set phase $a_{s1} - a_{s2} - a_{s3}$ as a function of spatial angle (b) Fast Fourier transform of waveform (a)

6.4 Numerical Evaluation of the Nine Phase Induction Machine

Having knowledge of the machine parameters is crucial for achieving efficiency in a motor control system. However, determining the inductance of a multiple phase induction machine can be a time-consuming process. Typically, there are two approaches: conducting experimental work or employing the computationally intensive finite element method. Both methods require significant time and effort. Unfortunately, many applications lack a comprehensive discussion or procedure for finding the inductances of multiple phase machines.

To address this issue, a developed algorithm is presented in this section, outlining a clear procedure for obtaining the inductances. The algorithm utilizes a clock diagram

shown in Fig.B.2. It evaluates the inductances of a nine-phase induction machine by
combining the turn function and winding function waveforms derived from the piecewise
linear function of three sets of three-phase windings around the stator slots. The
piecewise linear function takes into account the usual three-phase angular shift ($\pm 120°$)
between phases within a set and the geometric shift angle ($\xi = \pm\frac{\pi}{9}°$) between one set of
three-phase windings and another set while developing the function.

Equation (6.23) is used to evaluate the inductances between phases. A Matlab
script is developed to plot the turn function and winding function for the respective
inductances within a winding set. The script incorporates the "trapz" function to
calculate the area under the curve of the winding function. Numerical evaluations of the
area are performed using discrete steps throughout the full range of the rotor angle θ_r for
one cycle. By following the described procedure and considering the machine's geometric
parameters, the inductance values are numerically determined from the graph. These
results provide the inductances for the nine-phase induction machine with multiple sets
of windings. They can be used for quick simulation studies on multiple stator winding
sets, allowing the examination of transient and dynamic characteristics of the nine-phase
induction machine.

A conference paper related to this section has been presented at a conference [200].

Table 6.1 presents the algorithm developed to obtain the inductance of the asym-
metrical nine-phase induction machine. The numerical results obtained from the output
of the algorithm are displayed in equations (6.27)–(6.30). The highlighted matrices
in equation (6.13) and their respective elements are numerically obtained using the
algorithm described in Table 6.1. The matrices L_r are straightforward to obtain. The
stator-rotor matrices, which depend on the rotor angle, are also shown in equations
(6.31)–(6.33).

Table 6.1: Algorithm to obtain Nine phase Inductances

Algorithm for Nine Phase Inductance Matrix Calculation

1: Define all machine geometric parameters
2: Choose a reference magnetic axis
3: Obtain the geometric angle between windings
4: Define the Turn Function(TF) and Winding Function(WF) expressions
5: **for** $i = 1, 2....36$ slots, **do** Turn function (TF) of each phase windings
6: solve for the mean value of the TF $\langle n_i(\phi, \theta) \rangle$
7: Evaluate the winding numerically : $N_i(\phi, \theta) = n_i(\phi, \theta) - \langle n_i(\phi, \theta) \rangle$
8: Obtain plots for the TF and WF based on machine geometry
9: **for** $k = 1, 2....9$, **do** inductance for each phase
10: Numerically evaluate the WF using **'Trapz'** function in Matlab
11: Return all results of phase inductances in matrix form
12: **end**
13: **end**
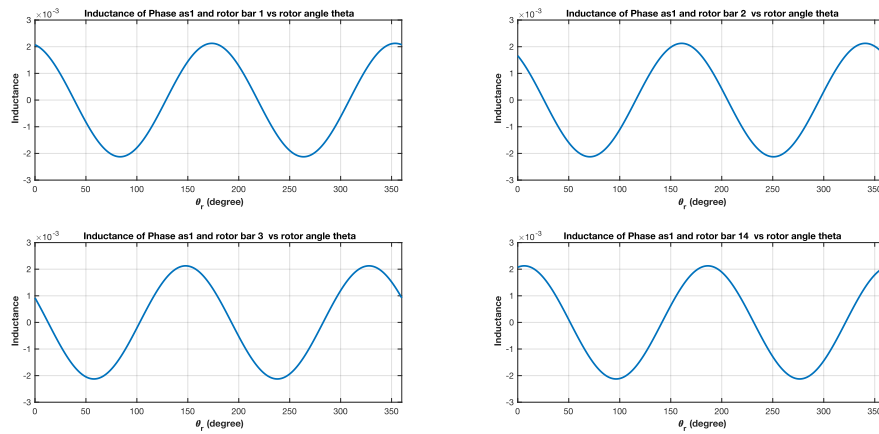
Figure 6.8: Inductance between phase a_{s1} and rotor bar $1, 2, 3, 14$
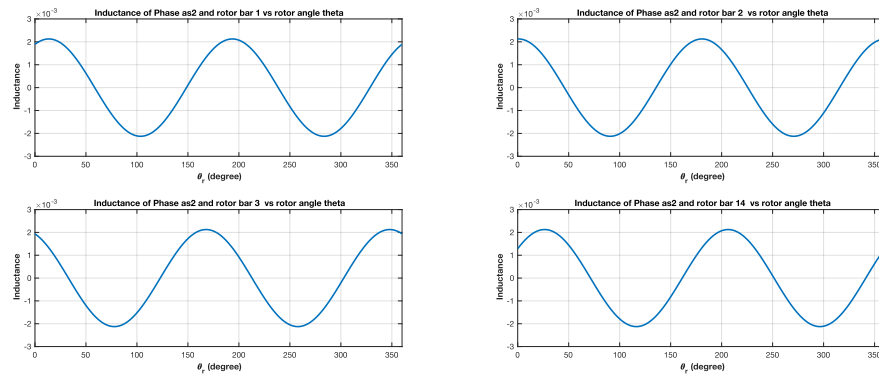
Figure 6.9: Inductance between phase a_{s2} and rotor bar $1, 2, 3, 14$
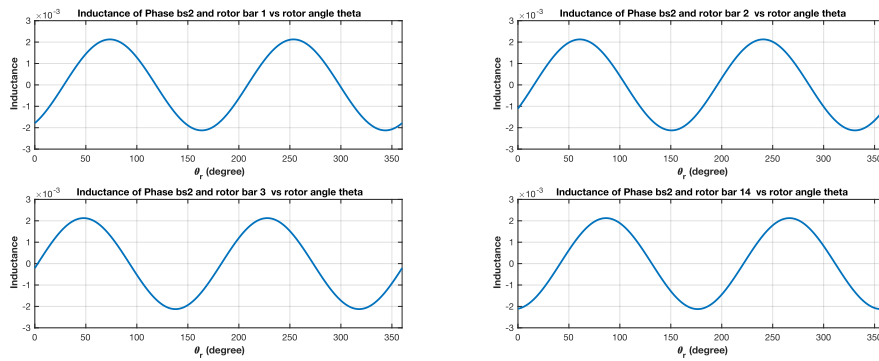
Figure 6.10: Inductance between phase b_{s2} and rotor bar $1, 2, 3, 14$
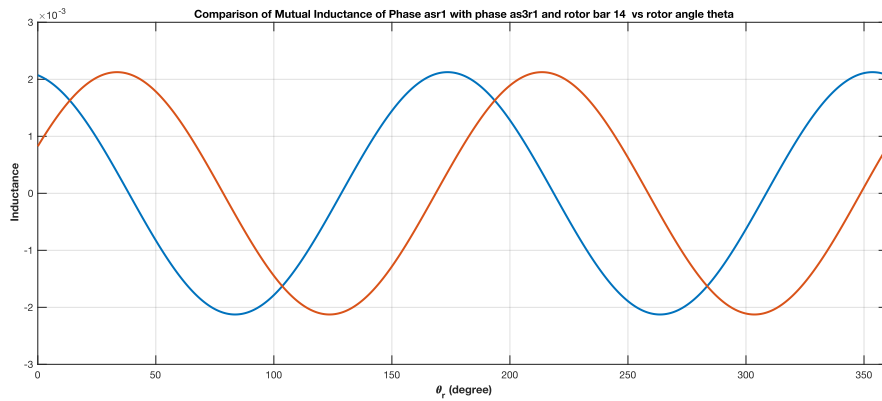
Figure 6.11: Comparison of Mutual Inductance between phase a_{s1r1}, a_{s3r1} and rotor bar 14

$$L_{11} = L_{22} = L_{33} = 1.0 \times 10^{-3} * \begin{bmatrix} 0.8789 & -0.2511 & -0.2511 \\ -0.2510 & 0.8788 & -0.2511 \\ -0.2510 & -0.2511 & 0.8788 \end{bmatrix} \tag{6.27}$$

$$M_{12} = M_{21} = M_{23} = M_{32} = 1.0 \times 10^{-3} * \begin{bmatrix} 0.3138 & -0.2511 & -0.2511 \\ -0.2510 & 0.3138 & -0.2511 \\ -0.2510 & -0.2511 & 0.3138 \end{bmatrix} \tag{6.28}$$

$$M_{13} = 1.0 \times 10^{-3} * \begin{bmatrix} -0.2511 & 0.3139 & -0.2511 \\ -0.2511 & -0.2511 & 0.3138 \\ 0.3138 & -0.2511 & -0.2511 \end{bmatrix} \tag{6.29}$$

$$M_{31} = 1.0 \times 10^{-3} * \begin{bmatrix} -0.2510 & -0.2511 & 0.3138 \\ 0.3140 & -0.2511 & -0.2511 \\ -0.2510 & 0.3138 & -0.2511 \end{bmatrix} \tag{6.30}$$

$$L_{sr1} = 4.1604 \times 10^{-6} * \begin{bmatrix} \cos\left(2\theta_r + (2n-1)\alpha_r\right) \\ \cos\left(2\theta_r + (2n-1)\alpha_r - \frac{2\pi}{3}\right) \\ \cos\left(2\theta_r + (2n-1)\alpha_r + \frac{2\pi}{3}\right) \end{bmatrix} \forall\ n = 1, 2, 3... \tag{6.31}$$

$$L_{sr2} = 4.1604 \times 10^{-6} * \begin{bmatrix} \cos\left(2\theta_r + (2n-1)\alpha_r + \frac{2\pi}{9}\right) \\ \cos\left(2\theta_r + (2n-1)\alpha_r - \frac{4\pi}{9}\right) \\ \cos\left(2\theta_r + (2n-1)\alpha_r + \frac{8\pi}{9}\right) \end{bmatrix} \forall\ n = 1, 2, 3... \tag{6.32}$$

$$L_{sr3} = 4.1604 \times 10^{-6} * \begin{bmatrix} \cos\left(2\theta_r + (2n-1)\alpha_r + \frac{4\pi}{9}\right) \\ \cos\left(2\theta_r + (2n-1)\alpha_r - \frac{2\pi}{9}\right) \\ \cos\left(2\theta_r + (2n-1)\alpha_r + \frac{10\pi}{9}\right) \end{bmatrix} \forall\ n = 1, 2, 3... \tag{6.33}$$

6.5 Novel Effect of Leakage Inductance in the Multiple $\alpha - \beta$ frame extended to Nine Phase machine

The leakage inductance of multiple set induction machine, has been presented in recent literature, owing to its importance in applications and different values between multiple set induction machine sub-spaces. A complete treatment of the subspace leakage inductance is less common. In this section, we present an approach to investigate the relationship between leakage inductance and mutual inductances of multiphase induction machine. The objective is to determine whether there is any coupling of the mutual inductances to other winding sets. Based on the findings of Hang et al. in their study on a six-phase induction machine [162], it was concluded that there is no coupling of the zero sequence mutual inductance to the other winding set. This is advantageous because the leakage coupling field energy is solely concentrated in the $\alpha\beta$ subspace and does not affect the zero sequence subspace.

The interest here, usually centres on whether or not there exist a difference or similarity between the two studied configurations: symmetrical and asymmetrical. such solutions, if there, afford the designer the best winding configurations that best minimize the leakage energy.

In the upcoming analysis, the focus will be on the leakage inductance of winding set one (a_1, b_1, c_1). The analysis assumes a *uniform air gap* and *uniform winding distribution*. The results obtained for the leakage inductance of this winding set will be applicable to the other sets as well. The compact form of the leakage flux for the nine-phase induction machine will be derived.

$$
\begin{bmatrix} [\lambda_{ls1}] \\ [\lambda_{ls2}] \\ [\lambda_{ls3}] \end{bmatrix} = \begin{bmatrix} [L_{ls} + M_{lss11}] & [M_{lss12}] & [M_{lss13}] \\ [M_{lss21}] & [L_{ls} + M_{lss22}] & [M_{lss23}] \\ [M_{lss31}] & [M_{lss32}] & [L_{ls} + M_{lss33}] \end{bmatrix} \times \begin{bmatrix} [i_{s1}] \\ [i_{s2}] \\ [i_{s3}] \end{bmatrix} \quad (6.34)
$$

6.5.1 Nine Phase Asymmetrical Induction Machine Case

The power invariant transformation matrix specific to an asymmetrical induction machine for each winding set is as follows:

$$[T_{3-i}] = \sqrt{\tfrac{2}{3}} \begin{bmatrix} \cos(\theta) & \cos(\theta + 120) & \cos(\theta - 120) \\ \sin(\theta) & \sin(\theta + 120) & \sin(\theta - 120) \\ \frac{1}{\sqrt{2}} & \frac{1}{\sqrt{2}} & \frac{1}{\sqrt{2}} \end{bmatrix} \forall \ i = 1, 2, 3 \qquad (6.35)$$

$$[\theta = 0°, 20°, 40°]$$

The leakage flux equation for winding set 1 in the $\alpha\beta$ subspace is:

$$[\lambda_{ls1}] = [L_{ls}][i_{s1}] + [M_{lss11}][i_{s1}] + [M_{lss12}][i_{s2}] + [M_{lss13}][i_{s3}] \qquad (6.36)$$

Applying the transformation matrix of equation (6.35) $\forall, i = 1, 2, 3$ from phase variable form to the equation (6.36) in the $\alpha\beta0$ form. The angle θ in the equation (6.35)is substituted $\theta = 0, \frac{\pi}{9}, \frac{2\pi}{9}, \forall, i = 1, 2, 3$ The equation transform to:

$$[T_{3-1}]^{-1}[\lambda_{ls\alpha\beta01}] = [L_{ls}][T_{3-1}]^{-1}[i_{s\alpha\beta1}] + [M_{lss11}][T_{3-1}]^{-1}[i_{s\alpha\beta1}]$$
$$+ [M_{lss12}][T_{3-2}]^{-1}[i_{s\alpha\beta2}] + [M_{lss13}][T_{3-3}]^{-1}[i_{s\alpha\beta3}] \quad (6.37)$$

Multiply equation (6.37) by $[T_{3-1}]$, and noting that $[T_{3-1}] \cdot [T_{3-1}]^{-1} = I$, where I is a 3×3 identity matrix, result in:

$$[\lambda_{ls\alpha\beta1}] = [L_{ls}][i_{s\alpha\beta1}] + [M_{lss11}][i_{s\alpha\beta1}] + [T_{3-1}][M_{lss12}][T_{3-2}]^{-1}[i_{s\alpha\beta2}]$$
$$+ [T_{3-1}][M_{lss13}][T_{3-3}]^{-1}[i_{s\alpha\beta3}] \quad (6.38)$$

In subsequent development of equation (6.36), the matrices are decomposed into equations (6.37) to (6.38), using the transformation matrices for each respective currents. Within the matrix equation (6.39) to (6.40), the parameters k_1, k_2, and k_3 represent pitch factors. Specifically, k_1 and k_2 denote the pitch factor for the first winding set, while k_3 corresponds to the pitch factor associated with the mutual inductance between winding

set 1 and the other sets. Additionally, M_{tb} represents the mutual inductance between the top and bottom conductors within a slot of a double-layer winding configuration.

$$[M_{lss12}] = 2M_{tb} \begin{bmatrix} k_3 & -k_3 & -k_3 \\ -k_3 & k_3 & -k_3 \\ -k_3 & -k_3 & k_3 \end{bmatrix}, [M_{lssii}] = 2M_{tb} \begin{bmatrix} k_1 & k_2 & k_2 \\ k_2 & k_1 & k_2 \\ k_2 & k_2 & k_1 \end{bmatrix}, \forall\, i = 1, 2, 3$$

$$(6.39)$$

$$[M_{lss13}] = 2M_{tb} \begin{bmatrix} k_3 & -k_3 & k_3 \\ k_3 & k_3 & -k_3 \\ -k_3 & k_3 & k_3 \end{bmatrix}, \quad \begin{cases} [i_{s\alpha\beta 01}] = [i_{s\alpha 1} i_{s\beta 1}\ i_{s01}]^T \\ [i_{s\alpha\beta 02}] = [i_{s\alpha 2}\ i_{s\beta 2}\ i_{s02}]^T \\ [i_{s\alpha\beta 03}] = [i_{s\alpha 3}\ i_{s\beta 3}\ i_{s03}]^T \end{cases} \qquad (6.40)$$

By substituting equation (6.35) for the appropriate shift angle in the case of asymmetrical induction machines, along with equations (6.39) to (6.40), into equation (6.37), the flux leakage equation corresponding to the respective leakage terms in the $\alpha - \beta - 0$ frame, as shown in equation (6.41), can be derived. Equation (6.41) considers only the leakage inductance for the first winding set (winding set 1), but the same result can be obtained for winding set 2 and winding set 3.

$$\begin{bmatrix} \lambda_{l\alpha 1} \\ \lambda_{l\beta 1} \\ \lambda_{l01} \end{bmatrix} = \begin{bmatrix} C_{1,1} & 0 & 0 & C_{1,4} & C_{1,5} & 0 & C_{1,7} & C_{1,8} & 0 \\ 0 & C_{2,2} & 0 & C_{2,4} & C_{2,5} & 0 & C_{2,7} & C_{2,8} & 0 \\ 0 & 0 & C_{3,3} & 0 & 0 & C_{3,6} & 0 & 0 & C_{3,9} \end{bmatrix} \times \begin{bmatrix} [i_{s\alpha\beta 01}] \\ [i_{s\alpha\beta 02}] \\ [i_{s\alpha\beta 03}] \end{bmatrix}$$

$$(6.41)$$

Where:

$C_{1,1} = C_{2,2} = ((2k_1 - 2k_2)\, M_{tb} + L_t + L_b),$

$C_{1,4} = C_{1,7} = C_{2,5} = C_{2,8} = 4\cos\left(\frac{\pi}{9}\right) M_{tb} k_3,$

$C_{1,5} = \left(-4 M_{tb} k_3 \sqrt{3} \cos\left(\frac{\pi}{9}\right) + 8 k_3 M_{tb} \sin\left(\frac{4\pi}{9}\right)\right),$

$C_{2,7} = \left(4 M_{tb} k_3 \sqrt{3} \cos\left(\frac{\pi}{9}\right) + 8 k_3 M_{tb} \sin\left(\frac{4\pi}{9}\right)\right)$

$C_{1,8} = C_{2,4} = \left(4 M_{tb} k_3 \sqrt{3} \cos\left(\frac{\pi}{9}\right) - 8 k_3 M_{tb} \sin\left(\frac{4\pi}{9}\right)\right),$

$C_{3,3} = ((2k_1 + 4k_2)\, M_{tb} + L_t + L_b),$

$C_{3,6} = -2 M_{tb} k_3,$

$C_{3,9} = 2 M_{tb} k_3,$
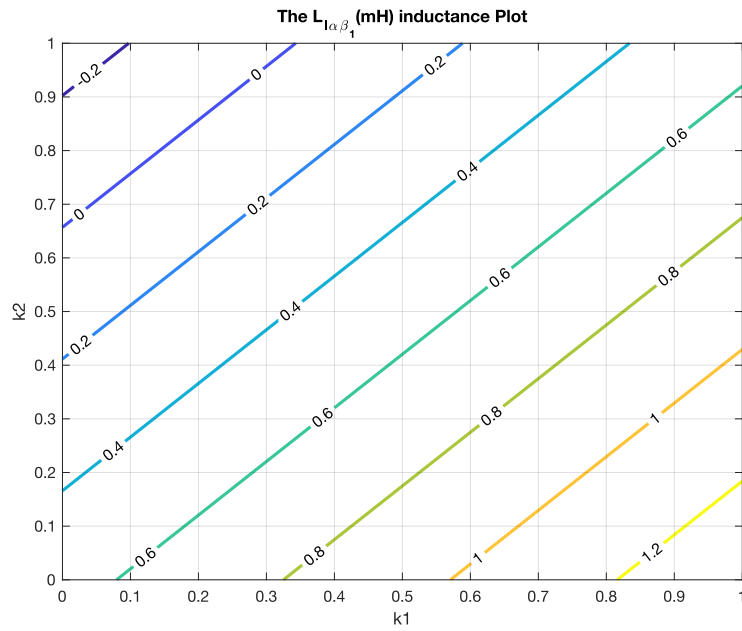
Figure 6.12: Fundamental component of the leakage inductance based on multiple $d - q$

There remain here only task of choosing $k1$ and $k2$ that is of interest in the developed equation to finding the optimize pitch factors that will optimize the flux. The developed flux equation are sufficient to determine uniquely the relationship between pitch factors k_1, k_2, k_3, and the top L_t, bottom L_b and mutual inductance M_{tb}.
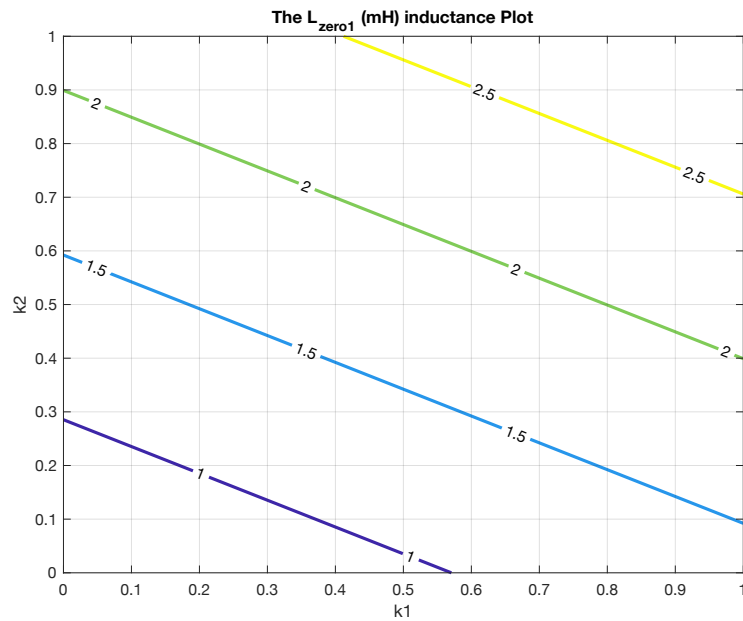
Figure 6.13: Zero sequence leakage inductance based on multiple $d - q$

The problem of choosing an appropriate diverse pitch factors for obtaining the least flux for symmetrical windings still remains. Some insight are gained by considering the connecting variables for the different subspace α and β and their corresponding $x - y$ sequence components. The $L_{\alpha\beta 1}$, are for the electromechanical related component, while the non electromechanical related leakage inductance term has been lumped to the L_{zero1} component term. It may be noted that in the $\alpha\beta$ graphs in Figure 6.13, the leakage inductance in the $\alpha\beta$ plane increases with increase in pitch factor k_1 and a reduction in pitch factor k_2. On the other hand, as could be seen in Figure 6.13 at higher pitch factor of k_1 the zero sequence inductance increases with increase in k_2 pitch factor. So to minimize the current flow in this plane, the pitch factors k_1, k_2 should be increase.

6.5.2 Nine Phase Symmetrical Induction Machine Case

The same procedure described in section 6.5.1 is repeated. The equation derivations remain the same, with the exception that a modification is made to the matrix equation to

accommodate the pitch and mutual inductance between the top and bottom conductors in the symmetrical case. This modification is denoted by an asterisk ($*$) to differentiate it from the earlier mutual inductance equation used for the asymmetrical case.

$$[M^*_{lss12}] = [M^*_{lss13}] = 2M_{tb} \begin{bmatrix} k_3 & -k_3 & k_3 \\ k_3 & k_3 & -k_3 \\ -k_3 & k_3 & k_3 \end{bmatrix} \tag{6.42}$$

The same procedure as described in equations (6.37) to (6.38) is repeated, but not shown here. By substituting equation (6.35) for the respective shift angles $[\theta = 0°, 40°, 80°]$ in the symmetrical case, along with $[M_{lssii}]$ from equations (6.39) and (6.40), into equation (6.37), the flux leakage equation corresponding to the respective leakage terms in the $\alpha - \beta - 0$ frame can be obtained. Equation (6.43) represents the flux leakage equation for the first winding set (winding set 1) in the symmetrical case. The same result can be derived for winding set 2 and winding set 3.

$$\begin{bmatrix} \lambda_{l\alpha1} \\ \lambda_{l\beta1} \\ \lambda_{l01} \end{bmatrix} = \begin{bmatrix} D_{1,1} & 0 & 0 & D_{1,4} & D_{1,5} & 0 & D_{1,7} & D_{1,8} & 0 \\ 0 & D_{2,2} & 0 & D_{2,4} & D_{2,5} & 0 & D_{2,7} & D_{2,8} & 0 \\ 0 & 0 & D_{3,3} & 0 & 0 & D_{3,6} & 0 & 0 & D_{3,9} \end{bmatrix} \times \begin{bmatrix} [i_{s\alpha\beta01}] \\ [i_{s\alpha\beta02}] \\ [i_{s\alpha\beta03}] \end{bmatrix} \tag{6.43}$$

Where:

$D_{1,1} = D_{2,2} = ((2k_1 - 2k_2) M_{tb} + L_t + L_b)$,

$D_{1,4} = D_{1,7} = D_{2,5} = D_{2,8} = 4\cos\left(\frac{\pi}{9}\right) M_{tb}k_3$,

$D_{1,5} = D_{2,7} = \left(4M_{tb}k_3\sqrt{3}\cos\left(\frac{\pi}{9}\right) - 8k_3 M_{tb}\sin\left(\frac{4\pi}{9}\right)\right)$,

$D_{1,8} = D_{2,4} = \left(-4M_{tb}k_3\sqrt{3}\cos\left(\frac{\pi}{9}\right) + 8k_3 M_{tb}\sin\left(\frac{4\pi}{9}\right)\right)$,

$D_{3,3} = ((2k_1 + 4k_2) M_{tb} + L_t + L_b)$,

$D_{3,6} = 2M_{tb}k_3$,

$D_{3,9} = 2M_{tb}k_3$,
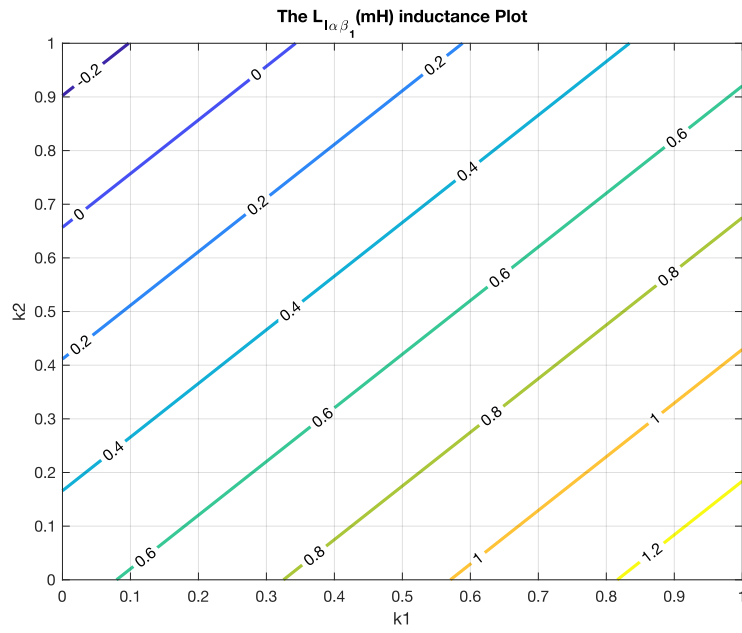
Figure 6.14: Fundamental component of the leakage inductance based on multiple $d - q$
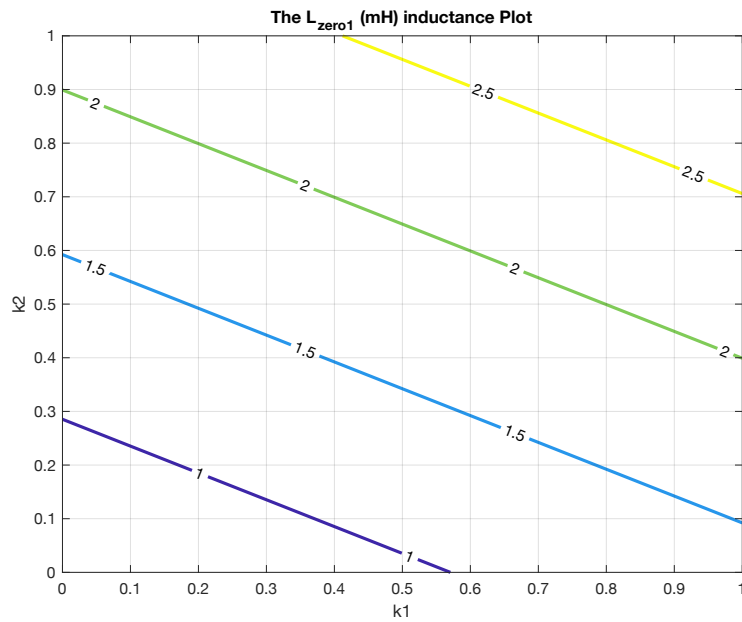
Figure 6.15: Zero sequence leakage inductance based on multiple $d - q$

Similar results for symmetrical case for the multiple $d - q$ model was obtained. This is presented in Figure 6.14 and Figure 6.15. These plots are obtained purely from

175

Table 6.2: Table of Leakage Inductance Comparison for Asymmetrical and Symmetrical nine phase induction machine showing self and mutual leakage inductance coupling to other winding topology based on multiple $d - q$ approach

		set 1			set 2			set 3	
1	α_1	β_1	0_1	α_2	β_2	0_2	α_3	β_3	0_3
Asym									
α_1	C_{11}	0	0	C_{14}	C_{15}	0	C_{17}	C_{18}	0
β_1	0	C_{22}	0	C_{24}	C_{25}	0	C_{27}	C_{28}	0
0_1	0	0	C_{33}	0	0	C_{36}	0	0	C_{39}
Sym									
α_1	D_{11}	0	0	C_{14}	$-C_{15}$	0	D_{17}	$-C_{18}$	0
β_1	0	D_{22}	0	$-C_{24}$	C_{25}	0	D_{27}	C_{28}	0
0_1	0	0	D_{33}	0	0	$-C_{36}$	0	0	D_{39}

the developed equations approach as in the nine phase induction machine asymmetrical case. The Figure 6.14 and Figure 6.15 shows clearly the dependence of the pitch factors on each subspace leakage inductance. Of particular interest here, is the contour plot for each showing similar characteristics for multiple $d - q$ approach. However, a difference exist, from the mutual leakage coupling inductance to other winding sets as shown in Table 6.2.

A relationship for these posit here with k_3 for the nine phase, asymmetrical and symmetrical case in this thesis. Note a very remarkable effect of the the pitch factors on the leakage inductance terms. This mutual inductance values become large at higher value of pitch factor k_3, and lower for some value of pitch factor k_3 . A more vivid representation of the effect of this pitch factors is given in Table 6.2. for the connecting pitch factors: self leakage inductance and mutual coupling inductance. Some interesting phenomena come to light in the both graph for asymmetrical and symmetrical case, if the pitch factors are large the magnitude of the leakage inductance increases. so there is more of the leakage inductance, at the given excitation for the plane, hence reduce in current for that subspace. To cause a reduce current flow,for the subspace the pitch factor should be selected across the leakage inductance barrier. Which is be based on winding topology and chording.

6.5.3 Nine Phase Asymmetrical Induction Machine Case With VSD

In this context, we are examining the leakage inductance expression for the symmetrical case of an Induction machine. The analysis employs the vector space decomposition technique, which, when subjected to identical current excitation across different winding sets, effectively restricts the leakage flux in the machine. The leakage flux expression can be described using the **vector space decomposition** approach.

$$[\lambda_{ls}] = [L_{ls}][i_s] + [Ml_{9assy}][i_s] \tag{6.44}$$

Where:

$\lambda_{ls} = [\lambda_{sla1}, \lambda_{slb1}, \lambda_{slc1}, \lambda_{sla2}, \cdots\cdots, \lambda_{slb3}, \lambda_{slc3}]^T$, is the leakage flux in phase variable form. $i_s = [i_{a1}, i_{b1}, i_{c1}, i_{a2}, i_{b2}, i_{c2}, i_{a3}, i_{b3}, i_{c3}]^T$ is the current in the phase variable form. $[Ml_{9assy}]$ is the matrix expression with all entry element relating to the product of the pitch factor and the mutual inductance of the nine phase windings. $[L_{ls}] = $ diag $[L_t + L_b]_{9\times9}$ is the diagonal matrix expression relating to the sum and bottom inductance in a double layer slot.

If the equation (6.44), is multiplied by the transformation matrix in (A1.3), result in

$$[T_{9asy3}]^{-1}[\lambda_{\alpha\beta x_i y_i o_i}] = [L_{ls}][T_{9asy3}]^{-1}[i_{\alpha\beta x_i y_i o_i}] + [Ml_{9assy}][T_{9asy3}]^{-1}[i_{\alpha\beta x_i y_i o_i}] \tag{6.45}$$

Multiply equation (6.45) by $[T_{9asy}]$ yield:

$$\left[\lambda_{\alpha\beta x_i y_i o_j}\right]_{9\times1} = \text{diag}\,[L_{ls}]\left[i_{\alpha\beta x_i y_i o_j}\right]_{9\times1} + [T_{9asy3}][Ml_{9assy}][T_{9asy3}]^{-1}\left[i_{\alpha\beta x_i y_i o_j}\right]_{9\times1}$$
$$[\forall,\ i = 1, 2\ ,\ j = 1, 2, 3]$$
$$\tag{6.46}$$

where:

diag $[L_{ls}] = $ diag $[L_t + L_b]_{9\times9}$, is the leakage inductance corresponding to the top and bottom inductor in a double layer slots. $[Ml_{9assy}] = 2M_{tb}*f(k_1, k_2, k_3)$ is a 9×9 matrix expression of the pitch factor and mutual inductance between slots. The expression is the mutual leakage inductance between winding set 1 and with other winding sets in a group of $n-$ phase induction machine. k_1, k_2, k_3 are the respective pitch factors for the windings.

$\left[i_{\alpha\beta x_i y_i o_j}\right]^T_{9\times 1} = [i_\alpha, i_\beta, i_{xi}, i_{yi}, \cdots, i_{o1}, i_{o2}, i_{o3}]^T_{9\times 1}$ $\forall$ $i = 1, 2.$ $j = 1, 2, 3.$ The flux expression $\left[\lambda_{\alpha\beta x_i y_i o_j}\right]^T_{9\times 1} = [\lambda_\alpha, \lambda_\beta, \lambda_{xi}, \lambda_{yi}, \cdots, \lambda_{o1}, \lambda_{o2}, \lambda_{o3}]^T_{9\times 1}$ $\forall$ $i = 1, 2.$ $j = 1, 2, 3$ The 'T' denote transpose of the matrices. The mutual leakage inductance $[Ml_{9assy}]$ is expressed in equation (6.47):

$$[Ml_{9assy}] = \begin{bmatrix} [M_{lssii}] & [M_{lss12}] & [M_{lss13}] \\ [M_{lss12}]^T & [M_{lssii}] & [M_{lss12}] \\ [M_{lss13}]^T & [M_{lss12}]^T & [M_{lssii}] \end{bmatrix} \tag{6.47}$$

Where:

$M_{lssii}, M_{lss12}, M_{lss13}$, is as defined in equation (6.39)–(6.40) respectively. Using the transformation matrix in (A1.3), applied to equation(6.44). The leakage inductance expressed in terms of the top and bottom conductor is given by equation (6.48):

$$[L_{\alpha\beta xiyioj}]^T_{9\times 1} = [L_\alpha, L_\beta, L_{xi}, L_{yi}, \cdots, L_{o1}, L_{o2}, L_{o3}]^T_{9\times 1}, \quad \forall\, i = 1, 2., \quad j = 1, 2, 3. \tag{6.48}$$

The mutual leakage flux expression in terms of pitch factor, for a giving excitation current is given by equation (6.49)is:

$$[Ml_{9assy}] = M_{tb} * f(k_1, k_2, k_3) \tag{6.49}$$

Where: k_1, k_2, k_3 is pitch factors relating to the winding arrangement between phases in the stator slots and with other winding sets of a nine phase induction machine.

$$
\begin{bmatrix}
\lambda_{l\alpha} \\
\lambda_{l\beta} \\
\lambda_{lx1} \\
\lambda_{ly1} \\
\lambda_{lx2} \\
\lambda_{ly2} \\
\lambda_{lo1} \\
\lambda_{lo2} \\
\lambda_{lo3}
\end{bmatrix}
=
\begin{bmatrix}
E_{1,1} & 0 & 0 & 0 & 0 & 0 & 0 & 0 & 0 \\
0 & E_{2,2} & 0 & 0 & 0 & 0 & 0 & 0 & 0 \\
0 & 0 & E_{3,3} & 0 & 0 & 0 & 0 & 0 & 0 \\
0 & 0 & 0 & E_{4,4} & 0 & 0 & 0 & 0 & 0 \\
0 & 0 & 0 & 0 & E_{5,5} & 0 & 0 & 0 & 0 \\
0 & 0 & 0 & 0 & 0 & E_{6,6} & 0 & 0 & 0 \\
0 & 0 & 0 & 0 & 0 & 0 & E_{7,7} & E_{7,8} & E_{7,9} \\
0 & 0 & 0 & 0 & 0 & 0 & E_{8,7} & E_{8,8} & E_{8,9} \\
0 & 0 & 0 & 0 & 0 & 0 & E_{9,7} & E_{9,8} & E_{9,9}
\end{bmatrix}
\begin{bmatrix}
i_{\alpha} \\
i_{\beta} \\
i_{x1} \\
i_{y1} \\
i_{x2} \\
i_{y2} \\
i_{o1} \\
i_{o2} \\
i_{o3}
\end{bmatrix}
\tag{6.50}
$$

Where:

$E_{1,1} = (L_t + L_b) + 2M_{tb}\left(4\cos\left(\frac{\pi}{9}\right)k_3 + k_1 - k_2\right),$

$E_{2,2} = (L_t + L_b) + 2M_{tb}\left(4\cos\left(\frac{\pi}{9}\right)k_3 + k_1 - k_2\right)$

$E_{3,3} = \left(L_t + L_b - 2M_{tb}\left(-k_1 + k_2 + 4\cos\left(\frac{\pi}{9}\right)k_3 - 4k_3\cos\left(\frac{2\pi}{9}\right)\right)\right),$

$E_{4,4} = \left(L_t + L_b - 2M_{tb}\left(-4\sqrt{3}\sin\left(\frac{4\pi}{9}\right)k_3 + 8\cos\left(\frac{\pi}{9}\right)k_3 - k_1 + k_2\right)\right),$

$E_{5,5} = \left(L_t + L_b - 2M_{tb}\left(4k_3\cos\left(\frac{2\pi}{9}\right) - k_1 + k_2\right)\right),$

$E_{6,6} = \left(L_t + L_b + 2M_{tb}\left(-4\sqrt{3}\sin\left(\frac{4\pi}{9}\right)k_3 + 4\cos\left(\frac{\pi}{9}\right)k_3 + k_1 - k_2\right)\right),$

$E_{7,7} = \left(L_t + L_b + 2M_{tb}\left(k_1 + 2k_2\right)\right),\ E_{7,8} = -2M_{tb}k_3,\ E_{7,9} = 2M_{tb}k_3$

$E_{8,7} = -2M_{tb}k_3,\ E_{8,8} = \left(L_t + L_b + 2M_{tb}\left(k_1 + 2k_2\right)\right),\ E_{8,9} = -2M_{tb}k_3$

$E_{9,7} = 2M_{tb}k_3,\ E_{9,8} = -2M_{tb}k_3,\ E_{9,9} = \left(L_t + L_b + 2M_{tb}\left(k_1 + 2k_2\right)\right),$
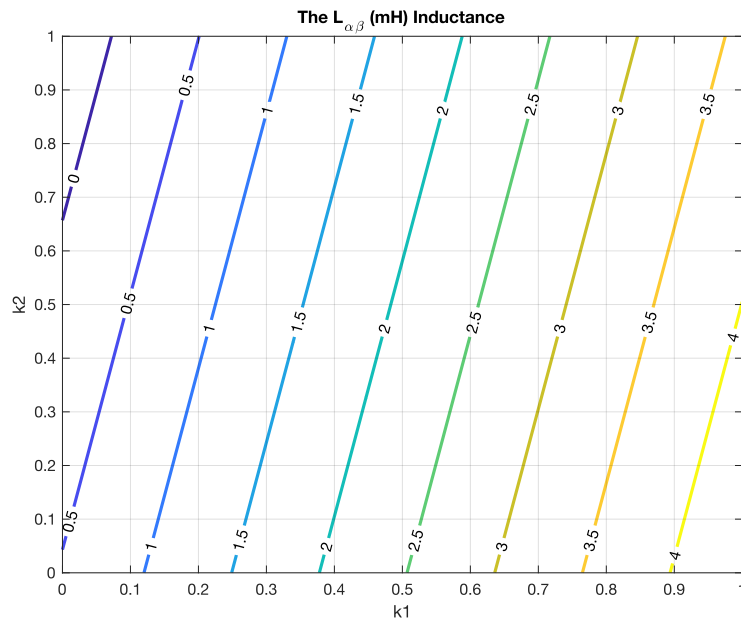
Figure 6.16: Fundamental component leakage inductance based on Vector Space decomposition model

A comparison of the $C_{1,1}$ and $D_{1,1}$ obtained previously mapped to multiple $d - q$ compared to that obtained to the VSD model in this section differ by the expression $4\cos\left(\frac{\pi}{9}\right)k_3$. If $k_3 = 0$, the two $\alpha - \beta$ fundamental subspaces are equal for multiple $d - q$ and VSD model. With this in mind, we can establish here that the VSD subspace offers a higher leakage inductance subspace compare to multiple $d - q$ analyse in this chapter. Clearly points on the plot, increase in all pitch factors k_1, k_2, k_3 increase the leakage inductance for that subspace. Here, different leakage inductance plots are shown in Figure 6.16 and Figure 6.18. While, Figure 6.16 and Figure 6.18, that of The leakage inductance for 6.17 shows a decrease in leakage inductance of this subspace as the pitch factor k_1, k_2 is increased.
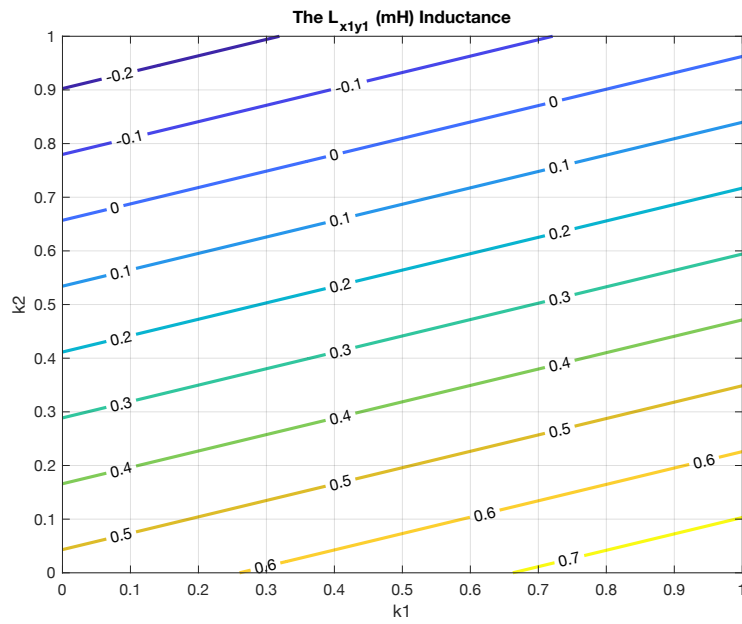
Figure 6.17: Higher subspace component leakage inductance based on VSD Asymmetrical Induction Machine model model $x_1 - y_1$ Plane
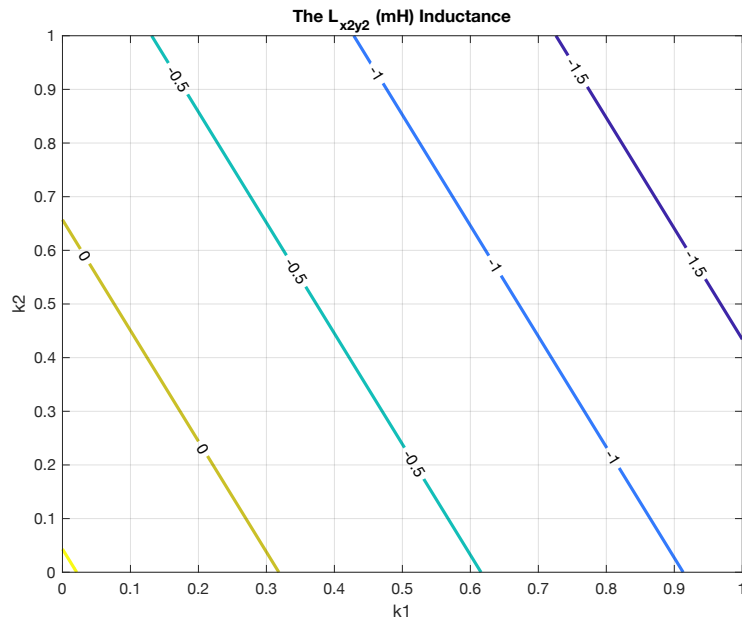
Figure 6.18: Higher subspace component leakage inductance based on VSD Asymmetrical Induction Machine model model $x_2 - y_2$ Plane

6.5.4 Nine Phase Symmetrical Induction Machine Case With VSD

The analysis here refers to the the leakage inductance expression for the symmetrical case of Induction machine, using the vector space decomposition technique, which under the same current excitation for the diverse winding sets will limit the leakage flux in the machine. The leakage flux expression in the **vector space decomposition**:

$$[\lambda_{ls}] = [L_{ls}][i_s] + [Ml_{9ssy}][i_s] \tag{6.51}$$

Where:

$\lambda_{ls} = [\lambda_{sla1}, \lambda_{slb1}, \lambda_{slc1}, \lambda_{sla2}, \cdots\cdots, \lambda_{slb3}, \lambda_{slc3}]^T$, is the leakage flux in phase variable form. $i_s = [i_{a1}, i_{b1}, i_{c1}, i_{a2}, i_{b2}, i_{c2}, i_{a3}, i_{b3}, i_{c3}]^T$ is the current in the phase variable form. $[Ml_{9ssy}]$ is the matrix expression with all entry element relating to the product of the pitch factor and the mutual inductance of the nine phase windings. $[L_{ls}] = \mathrm{diag}\,[L_t + L_b]_{9\times9}$ is the diagonal matrix expression relating to the sum and bottom inductance in a double layer slot.

If the equation (6.51), is multiplied by the transformation matrix in (A1.1), result in

$$[T_{9sy1}]^{-1}[\lambda_{\alpha\beta x_i y_i o_i}] = [L_{ls}][T_{9sy1}]^{-1}[i_{\alpha\beta x_i y_i o_i}] + [Ml_{9ssy}][T_{9sy1}]^{-1}[i_{\alpha\beta x_i y_i o_i}] \tag{6.52}$$

Multiply equation (6.52) by $[T_{9sy1}]$ yield:

$$\left[\lambda_{\alpha\beta x_i y_i o_j}\right]_{9\times1} = \mathrm{diag}\,[L_{ls}]\left[i_{\alpha\beta x_i y_i o_j}\right]_{9\times1} + [T_{9sy1}][Ml_{9ssy}][T_{9sy1}]^{-1}\left[i_{\alpha\beta x_i y_i o_j}\right]_{9\times1}$$
$$[\forall,\ i = 1,2,3\ ,\ j = 1] \tag{6.53}$$

where:

$\mathrm{diag}\,[L_{ls}] = \mathrm{diag}\,[L_t + L_b]_{9\times9}$, is the leakage inductance corresponding to the top and bottom inductor in a double layer slots. $[Ml_{9ssy}] = 2M_{tb} * f(k_1, k_2, k_3)$ is a 9×9 matrix expression of the pitch factor and mutual inductance between slots. The expression is the mutual leakage inductance between winding set 1 and with other winding sets in a group of $n-$ phase induction machine. k_1, k_2, k_3 are the respective pitch factors for the windings. $\left[i_{\alpha\beta x_i y_i o_j}\right]_{9\times1}^T = [i_\alpha, i_\beta, i_{xi}, i_{yi}, \cdots, i_{o1}, i_{o2}, i_{o3}]_{9\times1}^T \ \forall\ i = 1,2,3.\ \ j = 1.$ The

flux expression $\left[\lambda_{\alpha\beta x_i y_i o_j}\right]^T_{9\times1} = [\lambda_\alpha, \lambda_\beta, \lambda_{xi}, \lambda_{yi}, \cdots, \lambda_{o1}, \lambda_{o2}, \lambda_{o3}]^T_{9\times1}$ $\forall$ $i = 1, 2, 3$ $j = 1$

The 'T' denote transpose of the matrices. The mutual leakage inductance $[Ml_{9ssy}]$ is expressed in equation (6.54): leakage flux due to top and bottom conductor is given by:

$$[Ml_{9ssy}] = \begin{bmatrix} [M_{lssii}] & [M^*_{lss12}] & [M^*_{lss13}] \\ [M^*_{lss12}]^T & [M_{lssii}] & [M^*_{lss12}] \\ [M^*_{lss13}]^T & [M^*_{lss12}]^T & [M_{lssii}] \end{bmatrix} \tag{6.54}$$

Where:

M_{lssii} is defined by the second matrix of equation (6.39), M^*_{lss12}, M^*_{lss13}, is as defined in equation (6.54) respectively. Using the transformation matrix in (A1.1), applied to equation(6.51). The leakage inductance expressed in terms of the top and bottom conductor is given by equation (6.55):

$$[L_{\alpha\beta xiyioj}]^T_{9\times1} = [L_\alpha, L_\beta, L_{xi}, L_{yi}, \cdots, L_{o1}, L_{o2}, L_{o3}]^T_{9\times1}, \quad \forall\, i = 1, 2., \quad j = 1, 2, 3. \tag{6.55}$$

The mutual leakage flux expression in the same form as equation(6.49) is repeated here for equation (6.56):

$$[Ml_{9ssy}] = M_{tb} * f(k_1, k_2, k_3) \tag{6.56}$$

Where: k_1, k_2, k_3 is pitch factors relating to the winding arrangement between phases in

the stator slots and with other winding sets of a nine phase induction machine.

$$
\begin{bmatrix} \lambda_{l\alpha} \\ \lambda_{l\beta} \\ \lambda_{lx1} \\ \lambda_{ly1} \\ \lambda_{lx2} \\ \lambda_{ly2} \\ \lambda_{lo1} \\ \lambda_{lo2} \\ \lambda_{lo3} \end{bmatrix} = \begin{bmatrix} F_{1,1} & F_{1,2} & F_{1,3} & 0 & F_{1,5} & F_{1,6} & 0 & 0 & 0 \\ F_{2,1} & F_{2,2} & 0 & F_{2,4} & F_{2,5} & F_{2,6} & 0 & 0 & 0 \\ F_{3,1} & F_{3,2} & F_{3,3} & F_{3,4} & F_{3,5} & 0 & 0 & 0 & 0 \\ F_{4,1} & F_{4,2} & F_{4,3} & F_{4,4} & 0 & F_{4,6} & 0 & 0 & 0 \\ F_{5,1} & 0 & F_{5,3} & F_{5,4} & F_{5,5} & F_{5,6} & 0 & 0 & 0 \\ 0 & F_{6,2} & F_{6,3} & F_{6,4} & F_{6,5} & F_{6,6} & 0 & 0 & 0 \\ 0 & 0 & 0 & 0 & 0 & 0 & F_{7,7} & F_{7,8} & F_{7,9} \\ 0 & 0 & 0 & 0 & 0 & 0 & F_{8,7} & F_{8,8} & F_{8,9} \\ 0 & 0 & 0 & 0 & 0 & 0 & F_{9,7} & F_{9,8} & F_{9,9} \end{bmatrix} \begin{bmatrix} i_{\alpha} \\ i_{\beta} \\ i_{x1} \\ i_{y1} \\ i_{x2} \\ i_{y2} \\ i_{o1} \\ i_{o2} \\ i_{o3} \end{bmatrix} \tag{6.57}
$$

Where:

$F_{1,1} = \left(L_t + L_b - 4\left(-\frac{\sqrt{3}k_3 \sin\left(\frac{4\pi}{9}\right)}{3} - \frac{k_1}{2} + \frac{k_2}{2} \right) M_{tb} \right); \ F_{1,2} = -4 \sin\left(\frac{4\pi}{9}\right) M_{tb}k_3$

$F_{1,3} = -\frac{8\sqrt{3} \sin\left(\frac{4\pi}{9}\right) M_{tb}k_3}{3}; \ F_{1,5} = -4\left(-\frac{\sqrt{3}k_3 \sin\left(\frac{4\pi}{9}\right)}{3} + \cos\left(\frac{\pi}{9}\right) k_3 \right) M_{tb}$

$F_{1,6} = -4\left(\cos\left(\frac{\pi}{9}\right) \sqrt{3}k_3 - k_3 \sin\left(\frac{4\pi}{9}\right) \right) M_{tb}$

$F_{2,1} = 4 \sin\left(\frac{4\pi}{9}\right) M_{tb}k_3; \ F_{2,2} = \left(L_t + L_b + 4\left(\frac{\sqrt{3}k_3 \sin\left(\frac{4\pi}{9}\right)}{3} + \frac{k_1}{2} - \frac{k_2}{2} \right) M_{tb} \right)$

$F_{2,4} = \frac{8\sqrt{3} \sin\left(\frac{4\pi}{9}\right) M_{tb}k_3}{3}; \ F_{2,5} = \frac{4M_{tb}\left(3 \cos\left(\frac{\pi}{9}\right)\sqrt{3}k_3 - 3k_3 \sin\left(\frac{4\pi}{9}\right) \right)}{3}$

$F_{2,6} = \frac{4M_{tb}\left(3 \sin\left(\frac{\pi}{9}\right)\sqrt{3}k_3 - 3k_3 \cos\left(\frac{4\pi}{9}\right) \right)}{3}$

$F_{3,1} = \frac{4\sqrt{3} \sin\left(\frac{4\pi}{9}\right) M_{tb}k_3}{3}; \ F_{3,2} = 4 \sin\left(\frac{4\pi}{9}\right) M_{tb}k_3$

$F_{3,3} = \left(L_t + L_b + 4M_{tb}\left(-\frac{2\sqrt{3}k_3 \sin\left(\frac{4\pi}{9}\right)}{3} + \cos\left(\frac{\pi}{9}\right) k_3 + \frac{k_1}{2} - \frac{k_2}{2} \right) \right)$

$F_{3,4} = 4M_{tb}\left(\cos\left(\frac{\pi}{9}\right) \sqrt{3}k_3 - 2k_3 \sin\left(\frac{4\pi}{9}\right) \right); \ F_{3,5} = 4M_{tb}\left(\frac{4\sqrt{3}k_3 \sin\left(\frac{4\pi}{9}\right)}{3} - 2 \cos\left(\frac{\pi}{9}\right) k_3 \right)$

$F_{4,1} = 4k_3 \sin\left(\frac{4\pi}{9}\right) M_{tb}; \ F_{4,2} = -\frac{4\sqrt{3} \sin\left(\frac{4\pi}{9}\right) M_{tb}k_3}{3}; \ F_{4,3} = -\frac{4\left(3 \cos\left(\frac{\pi}{9}\right)\sqrt{3}k_3 - 6k_3 \sin\left(\frac{4\pi}{9}\right) \right) M_{tb}}{3}$

$F_{4,4} = \left(L_t + L_b - \frac{4\left(2\sqrt{3}k_3 \sin\left(\frac{4\pi}{9}\right) - 3 \cos\left(\frac{\pi}{9}\right) k_3 - \frac{3k_1}{2} + \frac{3k_2}{2} \right) M_{tb}}{3} \right),$

$F_{4,6} = -\frac{4\left(4\sqrt{3}k_3 \sin\left(\frac{4\pi}{9}\right) - 6 \cos\left(\frac{\pi}{9}\right) k_3 \right) M_{tb}}{3}$

$F_{5,1} = -\frac{8M_{tb}\left(\sqrt{3}k_3 \sin\left(\frac{4\pi}{9}\right) - 3 \cos\left(\frac{\pi}{9}\right) k_3 \right)}{3}; \ F_{5,3} = -\frac{8M_{tb}\left(-\frac{3 \cos\left(\frac{\pi}{9}\right) k_3}{2} + \sqrt{3}k_3 \sin\left(\frac{4\pi}{9}\right) \right)}{3}$

$F_{5,4} = -\frac{8M_{tb}\left(\frac{3 \cos\left(\frac{\pi}{9}\right)\sqrt{3}k_3}{2} - 3k_3 \sin\left(\frac{4\pi}{9}\right) \right)}{3}$

$$F_{5,5} = \left(L_t + L_b - \frac{8 M_{tb}\left(\frac{3\cos\left(\frac{\pi}{9}\right)k_3}{2} - \frac{\sqrt{3}k_3 \sin\left(\frac{4\pi}{9}\right)}{2} - \frac{3k_1}{4} + \frac{3k_2}{4} \right)}{3} \right)$$

$$F_{5,6} = -\frac{8 M_{tb}\left(-\frac{3\cos\left(\frac{\pi}{9}\right)\sqrt{3}k_3}{2} + \frac{3k_3 \sin\left(\frac{4\pi}{9}\right)}{2} \right)}{3}$$

$$F_{6,2} = -\frac{8 M_{tb}\left(\sqrt{3}k_3 \sin\left(\frac{4\pi}{9}\right) - 3\cos\left(\frac{\pi}{9}\right)k_3 \right)}{3}; \ F_{6,3} = -\frac{8 M_{tb}\left(\frac{3\cos\left(\frac{\pi}{9}\right)\sqrt{3}k_3}{2} - 3k_3 \sin\left(\frac{4\pi}{9}\right) \right)}{3}$$

$$F_{6,4} = -\frac{8 M_{tb}\left(\frac{3\cos\left(\frac{\pi}{9}\right)k_3}{2} - \sqrt{3}k_3 \sin\left(\frac{4\pi}{9}\right) \right)}{3}; \ F_{6,5} = -\frac{8 M_{tb}\left(\frac{3\cos\left(\frac{\pi}{9}\right)\sqrt{3}k_3}{2} - \frac{3k_3 \sin\left(\frac{4\pi}{9}\right)}{2} \right)}{3}$$

$$F_{6,6} = \left(L_t + L_b - \frac{8 M_{tb}\left(\frac{3\cos\left(\frac{\pi}{9}\right)k_3}{2} - \frac{\sqrt{3}k_3 \sin\left(\frac{4\pi}{9}\right)}{2} - \frac{3k_1}{4} + \frac{3k_2}{4} \right)}{3} \right)$$

$$F_{7,7} = (L_t + L_b + 2 M_{tb} (k_1 + 2k_2)); \ F_{7,8} = F_{7,9} = 2 M_{tb} k_3$$

$$F_{8,8} = (L_t + L_b + 2 M_{tb} (k_1 + 2k_2)); \ F_{8,7} = F_{8,9} = 2 M_{tb} k_3$$

$$F_{9,9} = (L_t + L_b + 2 M_{tb} (k_1 + 2k_2)); \ F_{9,7} = F_{9,8} = 2 M_{tb} k_3$$
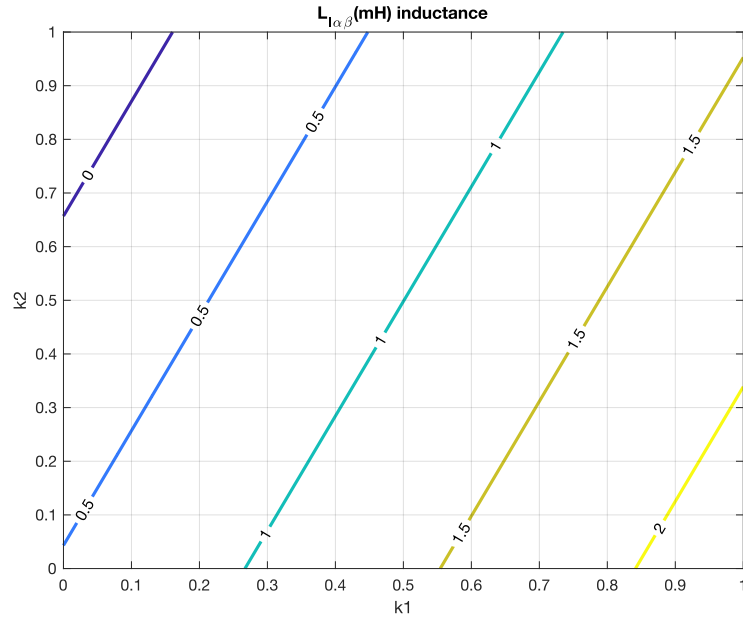
Figure 6.19: Fundamental component leakage inductance based on VSD model:Symmetrical Induction Machine model
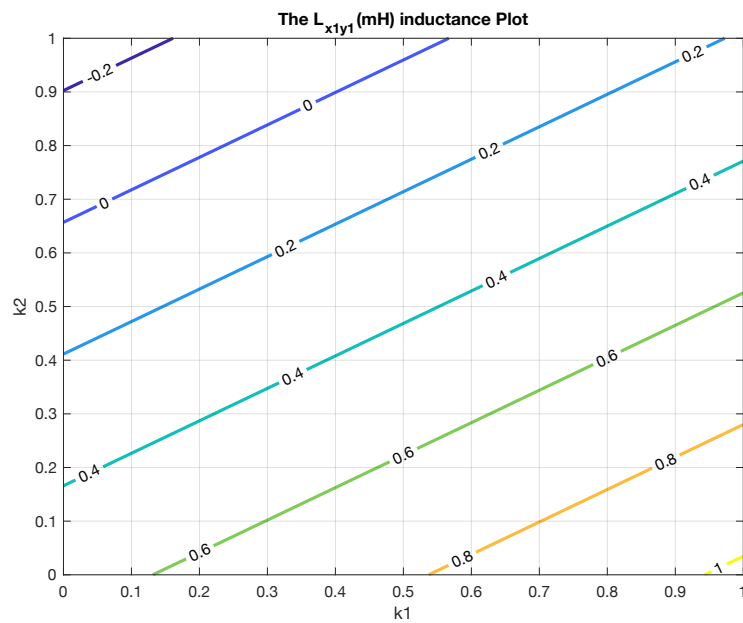
Figure 6.20: Higher subspace component leakage inductance based on VSD Symmetrical Induction Machine model $x_1 - y_1$ Plane
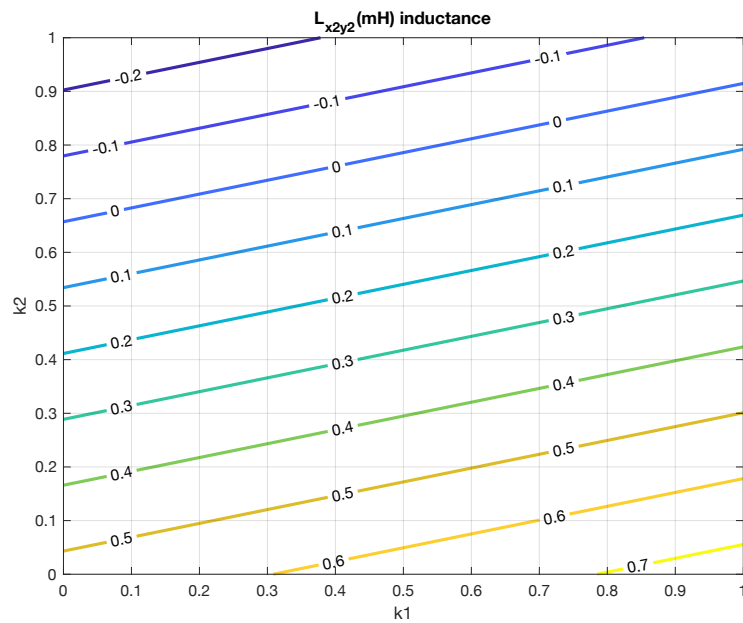
Figure 6.21: Higher subspace component leakage inductance based on VSD Symmetrical Induction Machine model model $x_2 - y_2$ Plane

More typical plots for different leakage inductance for symmetrical case for varying pitch factors are shown Figure 6.19 –Figure 6.21. The following observations may be made regarding the obtained leakage inductance for this case: The fundamental leakage inductance for symmetrical case is less compare to asymmetrical case. The $x_i - y_i$ leakage inductance plot shows the variations in pitch factor. Conclusively the asymmetrical nine phase induction machine appears to minimize subspace current magnitude for varying pitch factors.

6.6   Conclusion

The following are the contributions of this chapter:

a) The winding function approach gives a better way to determine machine self and mutual inductance between phase windings and other sets of windings co-sharing the same stator frame can be used for quick simulation studies. The inductance are obtained in a single step without expensive and elaborate experimental layout to determine machine inductance.

b) Determination of the inductance of the multiphase induction machine for electromagnetic studies comes with great simplicity as long as the information regarding the machine geometry is known and its associate winding pattern.

c) The analytical approach to determine machine inductance can be quickly configured into a matlab programe script to calculate the inductance in readiness for simulation studies.

d) In order to access the relative importance of various terms in the leakage inductance terms, numerical analysis and plot of the leakage inductance is obtained. The plot obtained shows various leakage inductance term variations as the pitch factors are varied.

The results for that of six phase induction machine are known in literature, and the analysis presented for nine phase induction machine here is a substantial modification of the approach of Hang *et al*(2016). However, the approach presented in this thesis has been applied to symmetrical and asymmetrical induction machine. Moreover, this approach when compared to various approaches requires less computational effort and

been very efficient for analysing $n-$ phase induction machine for symmetrical and asymmetrical machines.

It can be seen that the choice of asymmetrical winding induction machine from the inductance matrix equation helps to keep the leakage distribution balance in contrast with the inductance of symmetrical windings, due to the natural decoupled nature of the elements of the leakage inductance, in comparison to the sparsely distributed elements of the leakage inductance symmetrical matrix. By this, we can conclude that asymmetrical induction machine winding offers the best.

Chapter 7

Conclusion and Recommendation for Future Work

7.1 Conlusions

In this research work, the model of a nine phase induction machine have been studied simultaneously with the stability of the wind turbine system, flux density distribution metric in the air gap for symmetrical and asymmetrical winding configurations of the nine phase induction machine, and the leakage inductance influence on circulating current of the multiple phase induction machine on account of two modeling approach: multiple $d - q$ and vector space decomposition approach.

In the first instance, an in-depth mathematical analysis relating two converter configurations: series and parallel configurations have been analyzed. A power allocation strategy was then used to analyse both converter connection configurations. The study have enabled the steady state behaviour of the induction machine under a define operating scenario to be investigated.

Findings on this first instance, portray the relationship and interaction between torque, flux and current as it relates with same three phase winding and torque relations with other winding sets in a nine phase induction machine. In addition, findings established that, power shared in a nine phase series converter system configuration differ from the parallel converter system configurations.

Chapter 7. Conclusion and Recommendation for Future Work

In order to study the stability boundary of multiple phase induction machine in comparison with other variant induction machine. The stability of multiple-phase induction machine, three phase induction machine and a doubly fed induction machine wind turbine system was investigated compared and analyzed. The doubly fed induction machine have a wider stability boundary compared to three phase and multiple-phase induction machine system. Model equation of the studied system in the natural variable form was also derived developing model equations for each sub system assembly. A comprehensive model equation suitable for steady state study was then obtained in compact form.

Air gap peak field flux density has been misconstrued phenomenon for symmetrical and asymmetrical winding configuration of multiple set induction machine. A clear distinction of the air gap flux density for motoring and generating operation of multiphase induction machine based on the symmetrical and asymmetrical winding configuration is illustrated.

Multiple-phase induction machine biggest challenge is the flow of exceptional high current in the higher order plane of the multiphase induction machine model. This research work proposed the best choice of modeling approach that helps to minimise this circulating current and enhance the economic span of the multiple phase induction machine.

This research modeling of a nine phase induction machine for hybrid generation has been modeled and investigated meeting the earlier stated objectives, and these are the conclusion extract.

- A systematic step by step model development of the nine phase induction machine system, rectifiers, and other associated component systems has been carried out.

- Multiple $d - q$ modeling approach has been deployed in analysing two converter configurations: series and parallel configurations. It is was shown that power shared by the parallel converter configurations differ from the series converter configurations.

- Steady state equation relations showing the interrelations of the nine phase induction machine torque, flux and current is shown.

- A stability boundary comparison between variant induction machine was developed and shown with DFIG having an extended stability boundary compared to other kind of machines.

- An field analysis carried out on symmetrical and asymmetrical multiphase induction machine shows their peak flux density variations to meet control objective differ.

- An algorithm which efficiently obtained the turn and winding function inductance of multiple set induction machine and inductance between multiple set windings is analyzed.

- A comprehensive novel modeling approach based on multiple dq and VSD approach to minimize circulating current peculiar to multiple phase induction machine was developed.

- Finding shows that modeling approach based on vector space decomposition for asymmetrical configurations, offers the best approach to suppressing circulating current due to the decoupled nature of the leakage inductance matrix analysis compared to multiple $d - q$ and symmetrical nine phase induction machine.

7.2   Recommendation for Future work

- There is potential for future exploration of the gains and approaches presented in this thesis for future work. The effect of winding asymmetries on account of vector space decomposition to study this system model will suffice in future. In this thesis, we have assumed balanced winding sets with no asymmetries. So we neglected higher frequency components and only consider the fundamental components. Since this is the part coupled to the rotor. It would be an improvement in the current effort if future work considers asymmetries so that full scale analysis of the system including the higher other components can be integrated into the model

to study system interactions.

- In the converter analysis, we looked at unity power factor. However, future work can carry out investigation to study the effect of non unity power factor case.

- Further research work on other types of multiple phase electric machine i.e permanent magnet machines can be investigated, following the same configurations to compare and contrast it performance with other variant multiple phase electric machines.

- Further research work to corroborate the results of the leakage inductance for symmetrical and asymmetrical induction machine can be corroborated with FEM results.

- Further research work on controller development and design can be carry out to develop close loop control design for the system.

Appendix A1

Nine Phase Induction Machine Transformation Matrices

A1.1 Nine Phase Machine Transformation

For a **jointed neutral** points of the nine phase machine, the nine phase transformation matrix is given by (A1.1) and the elements constituting the matrix are obtained using the expression in (A1.2).

$$
[T_{9sy1}] = \sqrt{\frac{2}{9}} \cdot
\begin{matrix}
\alpha \\
\beta \\
x_1 \\
y_1 \\
x_2 \\
y_2 \\
x_3 \\
y_3 \\
0
\end{matrix}
\begin{bmatrix}
T_{1,1} & T_{1,2} & T_{1,3} & T_{1,4} & T_{1,5} & T_{1,6} & T_{1,7} & T_{1,8} & T_{1,9} \\
T_{2,1} & T_{2,2} & T_{2,3} & T_{2,4} & T_{2,5} & T_{2,6} & T_{2,7} & T_{2,8} & T_{2,9} \\
T_{3,1} & T_{3,2} & T_{3,3} & T_{3,4} & T_{3,5} & T_{3,6} & T_{3,7} & T_{3,8} & T_{3,9} \\
T_{4,1} & T_{4,2} & T_{4,3} & T_{4,4} & T_{4,5} & T_{4,6} & T_{4,7} & T_{4,8} & T_{4,9} \\
T_{5,1} & T_{5,2} & T_{5,3} & T_{5,4} & T_{5,5} & T_{5,6} & T_{5,7} & T_{5,8} & T_{5,9} \\
T_{6,1} & T_{6,2} & T_{6,3} & T_{6,4} & T_{6,5} & T_{6,6} & T_{6,7} & T_{6,8} & T_{6,9} \\
T_{7,1} & T_{7,2} & T_{7,3} & T_{7,4} & T_{7,5} & T_{7,6} & T_{7,7} & T_{7,8} & T_{7,9} \\
T_{8,1} & T_{8,2} & T_{8,3} & T_{8,4} & T_{8,5} & T_{8,6} & T_{8,7} & T_{8,8} & T_{8,9} \\
T_{9,1} & T_{9,2} & T_{9,3} & T_{9,4} & T_{9,5} & T_{9,6} & T_{9,7} & T_{9,8} & T_{9,9}
\end{bmatrix}
\tag{A1.1}
$$

Appendix A1.   Nine Phase Induction Machine Transformation Matrices

$$
\begin{cases}
T_{i,1\ldots j,n} = \cos[0 \ \alpha \ 2\alpha \ 6\alpha \ 7\alpha \ 8\alpha \ 12\alpha \ 13\alpha \ 14\alpha] \quad \forall \ i = 1, \ j, n = 1..9 \\[4pt]
T_{i,1\ldots j,n} = \sin[0 \ \alpha \ 2\alpha \ 6\alpha \ 7\alpha \ 8\alpha \ 12\alpha \ 13\alpha \ 14\alpha], \ \forall \ i = 2, \ j, n = 1..9 \\[4pt]
T_{i,1\ldots j,n} = \cos[0 \ 3\alpha \ 6\alpha \ 0 \ 3\alpha \ 6\alpha \ 0 \ 3\alpha \ 6\alpha], \ \forall \ i = 3, \ j, n = 1..9 \\[4pt]
T_{i,1\ldots j,n} = \sin[0 \ 3\alpha \ 6\alpha \ 0 \ 3\alpha \ 6\alpha \ 0 \ 3\alpha \ 6\alpha], \ \forall \ i = 4, \ j, n = 1..9 \\[4pt]
T_{i,1\ldots j,n} = \cos[0 \ 5\alpha \ 10\alpha \ 12\alpha \ 17\alpha \ 4\alpha \ 6\alpha \ 11\alpha \ 16\alpha], \ \forall \ i = 5, \ j, n = 1..9 \\[4pt]
T_{i,1\ldots j,n} = \sin[0 \ 5\alpha \ 10\alpha \ 12\alpha \ 17\alpha \ 4\alpha \ 6\alpha \ 11\alpha \ 16\alpha], \ \forall \ i = 6, \ j, n = 1..9 \\[4pt]
T_{i,1\ldots j,n} = \cos[0 \ 7\alpha \ 14\alpha \ 6\alpha \ 13\alpha \ 2\alpha \ 12\alpha \ \alpha \ 8\alpha], \ \forall \ i = 7, \ j, n = 1..9 \\[4pt]
T_{i,1\ldots j,n} = \sin[0 \ 7\alpha \ 14\alpha \ 6\alpha \ 13\alpha \ 2\alpha \ 12\alpha \ \alpha \ 8\alpha], \ \forall \ i = 8, \ j, n = 1..9 \\[4pt]
T_{i,1\ldots j,n} = \left[\frac{1}{\sqrt{2}} \ \frac{-1}{\sqrt{2}} \ \frac{1}{\sqrt{2}} \ \frac{1}{\sqrt{2}} \ \frac{-1}{\sqrt{2}} \ \frac{1}{\sqrt{2}} \ \frac{1}{\sqrt{2}} \ \frac{-1}{\sqrt{2}} \ \frac{1}{\sqrt{2}}\right] \ \forall \ i = 9, \ j, n = 1..9
\end{cases} \tag{A1.2}
$$

For **isolated neutral**, of the nine phase machine, the nine phase transformation matrix is given by (A1.3). The elements of the transformation matrix are obtained using (A1.4).

$$
[T_{9asy3}] = \sqrt{\frac{2}{9}} \cdot
\begin{array}{c}
\alpha \\ \beta \\ x_1 \\ y_1 \\ x_2 \\ y_2 \\ 0_1 \\ 0_2 \\ 0_3
\end{array}
\begin{bmatrix}
T_{1,1} & T_{1,2} & T_{1,3} & T_{1,4} & T_{1,5} & T_{1,6} & T_{1,7} & T_{1,8} & T_{1,9} \\
T_{2,1} & T_{2,2} & T_{2,3} & T_{2,4} & T_{2,5} & T_{2,6} & T_{2,7} & T_{2,8} & T_{2,9} \\
T_{3,1} & T_{3,2} & T_{3,3} & T_{3,4} & T_{3,5} & T_{3,6} & T_{3,7} & T_{3,8} & T_{3,9} \\
T_{4,1} & T_{4,2} & T_{4,3} & T_{4,4} & T_{4,5} & T_{4,6} & T_{4,7} & T_{4,8} & T_{4,9} \\
T_{5,1} & T_{5,2} & T_{5,3} & T_{5,4} & T_{5,5} & T_{5,6} & T_{5,7} & T_{5,8} & T_{5,9} \\
T_{6,1} & T_{6,2} & T_{6,3} & T_{6,4} & T_{6,5} & T_{6,6} & T_{6,7} & T_{6,8} & T_{6,9} \\
T_{7,1} & T_{7,2} & T_{7,3} & T_{7,4} & T_{7,5} & T_{7,6} & T_{7,7} & T_{7,8} & T_{7,9} \\
T_{8,1} & T_{8,2} & T_{8,3} & T_{8,4} & T_{8,5} & T_{8,6} & T_{8,7} & T_{8,8} & T_{8,9} \\
T_{9,1} & T_{9,2} & T_{9,3} & T_{9,4} & T_{9,5} & T_{9,6} & T_{9,7} & T_{9,8} & T_{9,9}
\end{bmatrix} \tag{A1.3}
$$

Appendix A1.   Nine Phase Induction Machine Transformation Matrices

$$
\begin{cases}
T_{i,1\ldots j,n} = \cos[0\ \alpha\ 2\alpha\ 6\alpha\ 7\alpha\ 8\alpha\ 12\alpha\ 13\alpha\ 14\alpha] \quad \forall\ i=1,\ j,n=1..9 \\[2mm]
T_{i,1\ldots j,n} = \sin[0\ \alpha\ 2\alpha\ 6\alpha\ 7\alpha\ 8\alpha\ 12\alpha\ 13\alpha\ 14\alpha],\ \forall\ i=2,\ j,n=1..9 \\[2mm]
T_{i,1\ldots j,n} = \cos[0\ 5\alpha\ 10\alpha\ 12\alpha\ 17\alpha\ 4\alpha\ 6\alpha\ 11\alpha\ 16\alpha],\ \forall\ i=3,\ j,n=1..9 \\[2mm]
T_{i,1\ldots j,n} = \sin[0\ 5\alpha\ 10\alpha\ 12\alpha\ 17\alpha\ 4\alpha\ 6\alpha\ 11\alpha\ 16\alpha],\ \forall\ i=4,\ j,n=1..9 \\[2mm]
T_{i,1\ldots j,n} = \cos[0\ 7\alpha\ 14\alpha\ 6\alpha\ 13\alpha\ 2\alpha\ 12\alpha\ \alpha\ 8\alpha],\ \forall\ i=5,\ j,n=1..9 \\[2mm]
T_{i,1\ldots j,n} = \sin[0\ 7\alpha\ 14\alpha\ 6\alpha\ 13\alpha\ 2\alpha\ 12\alpha\ \alpha\ 8\alpha16\alpha],\ \forall\ i=6,\ j,n=1..9 \\[2mm]
T_{i,1\ldots j,n} = \left[\sqrt{\tfrac{3}{2}}\ 0\ 0\ \sqrt{\tfrac{3}{2}}\ 0\ 0\ \sqrt{\tfrac{3}{2}}\ 0\ 0\right],\ \forall\ i=7,\ j,n=1..9 \\[2mm]
T_{i,1\ldots j,n} = \left[0\sqrt{\tfrac{3}{2}}\ 0\ 0\ \sqrt{\tfrac{3}{2}}\ 0\ 0\ \sqrt{\tfrac{3}{2}}\ 0\right],\ \forall\ i=8,\ j,n=1..9 \\[2mm]
T_{i,1\ldots j,n} = \left[0\ 0\sqrt{\tfrac{3}{2}}\ 0\ 0\ \sqrt{\tfrac{3}{2}}\ 0\ 0\ \sqrt{\tfrac{3}{2}}\right]\ \forall\ i=9,\ j,n=1..9
\end{cases}
\tag{A1.4}
$$

Appendix A2

Nine Phase induction machine differential flux modification to current differential

A2.1 Nine Phase Machine Analysis

The nine phase induction machine in the $d - q$ condense model is given by:

$$\begin{cases} v_{qdsk} = r_{sk}i_{qdsk} + p\lambda_{qdsk} - j\omega\lambda_{qdsk} \\ v_{qdr} = r_r i_{qdr} + p\lambda_{qdr} - j(\omega - \omega_r)\lambda_{qdr} = 0 \end{cases} \quad for \ k = 1, 2, 3 \quad \text{(A2.1)}$$

For a squirrel cage rotor, note:, $v_{qr} = v_{dr} = 0$.

$$\begin{cases} \lambda_{qdsk} = L_{ls}i_{qdsk} + L_{lm}\sum_{j=1}^{3} i_{qdsj} + L_m \sum_{j=1}^{3}\left(i_{qdsj} + i_{qdr}\right) \quad \forall \ k \ = 1, 2, 3 \\ \lambda_{qdr} = L_{lr}i_{qdr} + L_m \sum_{j=1}^{3}\left(i_{qdsj} + i_{qdr}\right) \end{cases} \quad \text{(A2.2)}$$

Appendix A2. Nine Phase induction machine differential flux modification to current differential

Decomposing the condensed voltage equation, we have

$$
\begin{cases}
v_{qds1} = r_{s1}i_{qds1} + p\lambda_{qds1} - j\omega\lambda_{qds1} \\[2mm]
v_{qds2} = r_{s2}i_{qds2} + p\lambda_{qds2} - j\omega\lambda_{qds2} \\[2mm]
v_{qds3} = r_{s3}i_{qds3} + p\lambda_{qds3} - j\omega\lambda_{qds3} \\[2mm]
v_{qdr} = r_r i_{qdr} + p\lambda_{qdr} - j(\omega - \omega_r)\lambda_{qdr} = 0
\end{cases}
\tag{A2.3}
$$

Decomposing the condensed flux equation, we have

$$
\begin{cases}
\lambda_{qds1} = L_{ls}i_{qds1} + (L_{lm} + L_m)\,(i_{qds1} + i_{qds2} + i_{qds3}) + L_m i_{qdr} \\[2mm]
\lambda_{qds2} = L_{ls}i_{qds2} + (L_{lm} + L_m)\,(i_{qds1} + i_{qds2} + i_{qds3}) + L_m i_{qdr} \\[2mm]
\lambda_{qds3} = L_{ls}i_{qds3} + (L_{lm} + L_m)\,(i_{qds1} + i_{qds2} + i_{qds3}) + L_m i_{qdr} \\[2mm]
\lambda_{qdr} = L_{lr}i_{qdr} + L_m\,(i_{qds1} + i_{qds2} + i_{qds3} + i_{qdr})
\end{cases}
\tag{A2.4}
$$

Eliminating the rotor flux and rotor current from Equation A2.4, we solve for the following variables: $\lambda_{qdr}, i_{qdr}, i_{qds1}, i_{qds2}$. In the decomposed form, the variables solved for is :

$$
\begin{cases}
i_{qr} = \dfrac{w_1 + w_2}{L_m L_{ls}} \\[3mm]
i_{dr} = \dfrac{w_3 + w_4}{L_m L_{ls}} \\[3mm]
i_{qs1} = \dfrac{L_{ls}i_{qs3} + \lambda_{qs1} - \lambda_{qs3}}{L_{ls}} \\[3mm]
i_{ds1} = \dfrac{L_{ls}i_{ds3} + \lambda_{ds1} - \lambda_{ds3}}{L_{ls}} \\[3mm]
i_{qs2} = \dfrac{L_{ls}i_{qs3} + \lambda_{qs2} - \lambda_{qs3}}{L_{ls}} \\[3mm]
i_{ds2} = \dfrac{L_{ls}i_{ds3} + \lambda_{ds2} - \lambda_{ds3}}{L_{ls}} \\[3mm]
\lambda_{qr} = \dfrac{w_5 + w_5' + w_6}{L_m L_{ls}} \\[3mm]
\lambda_{dr} = \dfrac{w_7 + w_7' + w_8}{L_m L_{ls}}
\end{cases}
\tag{A2.5}
$$

Where:

$w_1 = (2L_m + 2L_{lm} + L_{ls})\,\lambda_{qs3} - 3L_{ls}\left(L_m + L_{lm} + \frac{L_{ls}}{3}\right)i_{qs3}$

$w_4 = (2L_m + 2L_{lm} + L_{ls})\,\lambda_{ds3} - 3L_{ls}\left(L_m + L_{lm} + \frac{L_{ls}}{3}\right)i_{ds3}$

Appendix A2. Nine Phase induction machine differential flux modification to current differential

$$w_2 = -\left(\lambda_{qs1} + \lambda_{qs2}\right)\left(L_m + L_{lm}\right)$$

$$w_3 = -\left(\lambda_{ds1} + \lambda_{ds2}\right)\left(L_m + L_{lm}\right)$$

$$w_5 = \left(\left(2L_{lm} + 2L_{lr} + L_{ls}\right)L_m + 2L_{lr}\left(L_{lm} + \frac{L_{ls}}{2}\right)\right)\lambda_{qs3}$$

$$w_5' = -3L_{ls}\left(\left(L_{lm} + L_{lr} + \frac{L_{ls}}{3}\right)L_m \; L_{lr}\left(L_{lm} + \frac{L_{ls}}{3}\right)\right)i_{qs3}$$

$$w_6 = -\left(\left(L_{lm} + L_{lr}\right)L_m + L_{lm}L_{lr}\right)\left(\lambda_{qs1} + \lambda_{qs2}\right)$$

$$w_7 = \left(\left(2L_{lm} + 2L_{lr} + L_{ls}\right)L_m + 2L_{lr}\left(L_{lm} + \frac{L_{ls}}{2}\right)\right)\lambda_{ds3}$$

$$w_7' = -3L_{ls}\left(\left(L_{lm} + L_{lr} + \frac{L_{ls}}{3}\right)L_m \; L_{lr}\left(L_{lm} + \frac{L_{ls}}{3}\right)\right)i_{ds3}$$

$$w_8 = -\left(\left(L_{lm} + L_{lr}\right)L_m + L_{lm}L_{lr}\right)\left(\lambda_{ds1} + \lambda_{ds2}\right)$$

Substituting this obtained variables of equation (A2.5) into the voltage equations (A2.3) and deploying elimination of variables while retaining variables of interest, result in first order equations for the current equation for the nine phase induction machine, yield:

$$L_\sigma p i_{qs1} = c_2 \frac{M_{qs1}V_{dc}}{2} + c_1 \frac{M_{qs2}V_{dc}}{2} + c_1 \frac{M_{qs3}V_{dc}}{2} + L_\sigma(\omega_r - \omega)i_{ds3} + c_5\lambda_{ds1}\omega_r + c_5\lambda_{ds2}\omega_r$$
$$+ c_6\lambda_{ds3}\omega_r + c_9 i_{qs1} + c_3 i_{qs2} + c_{10} i_{qs3} + c_{11}\omega\lambda_{ds1} + c_{12}\omega\lambda_{ds3} + c_7\lambda_{qds1} + c_7\lambda_{qds2} + c_8\lambda_{qds3}$$

$$\text{(A2.6)}$$

$$L_\sigma p i_{ds1} = c_2 \frac{M_{ds1}V_{dc}}{2} + c_1 \frac{M_{ds2}V_{dc}}{2} + c_1 \frac{M_{ds3}V_{dc}}{2} + L_\sigma(\omega - \omega_r)i_{qs3} + c_1\omega_r\lambda_{qs1} + c_1\omega_r\lambda_{qs2}$$
$$- c_6\omega_r\lambda_{qs3} + c_9 i_{ds1} + c_3 i_{ds2} + c_{10} i_{ds3} + c_7\lambda_{ds1} + c_7\lambda_{ds2} + c_8\lambda_{ds3} - c_{11}\omega\lambda_{qds1} - c_{12}\omega\lambda_{qds3}$$

$$\text{(A2.7)}$$

$$L_\sigma p i_{qs2} = c_1 \frac{M_{qs1}V_{dc}}{2} + c_2 \frac{M_{qs2}V_{dc}}{2} + c_1 \frac{M_{qs3}V_{dc}}{2} + L_\sigma(\omega_r - \omega)i_{ds3} + c_5\lambda_{ds1} + c_5\lambda_{ds2} + c_6\lambda_{ds3}$$
$$+ c_3 i_{qs1} + c_9 i_{qs2} + c_{10} i_{qs3} + c_{11}\omega\lambda_{ds2} + c_{12}\omega\lambda_{ds3} + c_7\lambda_{qds1} + c_7\lambda_{qds2} + c_8\lambda_{qds3} \quad \text{(A2.8)}$$

Appendix A2.   Nine Phase induction machine differential flux modification to current differential

$$L_\sigma p i_{ds2} = c_1 \frac{M_{ds1} V_{dc}}{2} + c_2 \frac{M_{ds2} V_{dc}}{2} + c_1 \frac{M_{ds3} V_{dc}}{2} + L_\sigma (\omega - \omega_r) i_{qs3} + c_1 \omega_r \lambda_{qs1} + c_1 \omega_r \lambda_{qs2}$$
$$- c_6 \omega_r \lambda_{qs3} + c_3 i_{ds1} + c_9 i_{ds2} + c_{10} i_{ds3} + c_7 \lambda_{ds1} + c_7 \lambda_{ds2} + c_8 \lambda_{ds3} + c_{12} \omega \lambda_{qds2} - c_{11} \omega \lambda_{qds3}$$

$$(A2.9)$$

$$L_\sigma p i_{qs3} = c_1 \frac{M_{qs1} V_{dc}}{2} + c_1 \frac{M_{qs2} V_{dc}}{2} + c_2 \frac{M_{qs3} V_{dc}}{2} + L_\sigma (\omega_r - \omega) i_{ds3} + c_3 i_{qs1} + c_3 i_{qs2}$$
$$+ c_4 i_{qs3} + c_5 \lambda_{ds1} \omega_r + c_5 \lambda_{ds2} \omega_r + c_6 \lambda_{ds3} \omega_r + c_7 \lambda_{qs1} + c_7 \lambda_{qs2} + c_8 \lambda_{qs3} \quad (A2.10)$$

$$L_\sigma p i_{ds3} = c_1 \frac{M_{ds1} V_{dc}}{2} + c_1 \frac{M_{ds2} V_{dc}}{2} + c_2 \frac{M_{ds3} V_{dc}}{2} - L_\sigma (\omega_r - \omega) i_{qs3} + c_3 i_{ds1} + c_3 i_{ds2}$$
$$+ c_4 i_{ds3} + c_7 \lambda_{ds1} + c_7 \lambda_{ds2} + c_8 \lambda_{ds3} - c_5 \lambda_{qs1} \omega_r - c_5 \lambda_{qs2} \omega_r - c_6 \lambda_{qs3} \omega_r \quad (A2.11)$$

Where:

$L_\sigma = 3 \left(\left(L_{lm} + L_{lr} + \frac{L_{ls}}{3} \right) L_m + L_{lr} \left(L_{lm} + \frac{L_{ls}}{3} \right) \right) L_{ls}$

$c_1 = (-L_{lm} - L_{lr}) L_m - L_{lm} L_{lr}$

$c_2 = (2L_{lm} - 2L_{lr} + L_{ls}) L_m - L_{lr}(-2L_{lm} - L_{ls})$

$c_3 = r_s((L_{lm} + L_{lr}) L_m + L_{lm} L_{lr})$

$c_4 = \left(-2 r_s L_{lr} - 2 r_s L_{lm} - 3 L_{ls} \left(r_r + \frac{r_s}{3} \right) \right) L_m - 2 \left(L_{lm} + \frac{L_{ls}}{2} \right) r_s L_{lr} - 3 \left(L_{lm} + \frac{L_{ls}}{3} \right) r_r L_{ls}$

$c_5 = (L_{lm} + L_{lr}) L_m + L_{lm} L_{lr}$

$c_6 = -2 \left(\left(L_{lm} + L_{lr} + \frac{L_{ls}}{2} \right) L_m + L_{lr} \left(L_{lm} + \frac{L_{ls}}{2} \right) \right)$

$c_7 = r_r (L_m + L_{lm})$

$c_8 = 2 r_r (L_m + L_{lm} + \frac{L_{ls}}{2})$

$c_9 = -2 r_s \left(\left(L_{lm} + L_{lr} + \frac{L_{ls}}{2} \right) L_m + L_{lr} \left(L_{lm} + \frac{L_{ls}}{2} \right) \right)$

$c_{10} = (r_s L_{lm} + r_s L_{lr} - 3 L_{ls} r_r) L_m + r_s L_{lr} L_{lm} - 3 \left(L_{lm} + \frac{L_{ls}}{3} \right) r_r L_{ls}$

$c_{11} = (-3 L_{lm} - 3 L_{lr} - L_{ls}) L_m + (-3 L_{lm} - L_{ls}) L_{lr}$

$c_{12} = (3 L_{lm} + 3 L_{lr} + L_{ls}) L_m - 2 \left(-\frac{3 L_{lm}}{2} - \frac{L_{ls}}{2} \right) L_{lr}$

Appendix A2. Nine Phase induction machine differential flux modification to current differential

Appendix A2. Nine Phase induction machine differential flux modification to current differential

A2.2 Full Model system equation based on multiple $q - d$

The full order model dynamic state of the model system is given here. The equations been long is broken down to two: The first split is

$$
p \begin{bmatrix} i_{qs1} \\ i_{ds1} \\ i_{qs2} \\ i_{ds2} \\ i_{qs3} \\ i_{ds3} \\ \omega_r \\ v_{dc} \\ i_{Lo} \\ v_b \\ v_c \\ SoC \\ \vdots \\ \vdots \end{bmatrix} = \begin{bmatrix} \frac{1}{L_\sigma} \begin{pmatrix} c_9 i_{qs1} + c_3 i_{qs2} + c_{10} i_{qs3} + L_\sigma(\omega_r - \omega)i_{ds3} + c_5 \lambda_{ds1}\omega_r + c_5 \lambda_{ds2}\omega_r \\ + c_6 \lambda_{ds3}\omega_r + c_{11}\omega\lambda_{ds1} + c_{12}\omega\lambda_{ds3} + c_7\lambda_{qs1} + c_7\lambda_{qs2} + c_8\lambda_{qs3} \\ + c_2 \frac{M_{qs1}V_{dc}}{2} + c_1 \frac{M_{qs2}V_{dc}}{2} + c_1 \frac{M_{qs3}V_{dc}}{2} \end{pmatrix} \\ \frac{1}{L_\sigma} \begin{pmatrix} c_9 i_{ds1} + c_3 i_{ds2} + c_{10} i_{ds3} + L_\sigma(\omega - \omega_r)i_{qs3} + c_1\omega_r\lambda_{qs1} + c_1\omega_r\lambda_{qs2} \\ - c_6\omega_r\lambda_{qs3} - c_{11}\omega\lambda_{qs1} - c_{12}\omega\lambda_{qs3} + c_7\lambda_{ds1} + c_7\lambda_{ds2} + c_8\lambda_{ds3} \\ + c_2 \frac{M_{ds1}V_{dc}}{2} + c_1 \frac{M_{ds2}V_{dc}}{2} + c_1 \frac{M_{ds3}V_{dc}}{2} + \end{pmatrix} \\ \frac{1}{L_\sigma} \begin{pmatrix} c_3 i_{qs1} + c_9 i_{qs2} + c_{10} i_{qs3} + L_\sigma(\omega_r - \omega)i_{ds3} + c_5\omega_r\lambda_{ds1} + c_5\omega_r\lambda_{ds2} \\ + c_6\omega_r\lambda_{ds3} + c_{11}\omega\lambda_{ds2} + c_{12}\omega\lambda_{ds3} + c_7\lambda_{qs1} + c_7\lambda_{qs2} + c_8\lambda_{qs3} \\ + c_1 \frac{M_{qs1}V_{dc}}{2} + c_2 \frac{M_{qs2}V_{dc}}{2} + c_1 \frac{M_{qs3}V_{dc}}{2} \end{pmatrix} \\ \frac{1}{L_\sigma} \begin{pmatrix} c_3 i_{ds1} + c_9 i_{ds2} + c_{10} i_{ds3} + L_\sigma(\omega - \omega_r)i_{qs3} + c_1\omega_r\lambda_{qs1} + c_1\omega_r\lambda_{qs2} \\ - c_6\omega_r\lambda_{qs3} + c_{12}\omega\lambda_{qs2} - c_{11}\omega\lambda_{qs3} + c_7\lambda_{ds1} + c_7\lambda_{ds2} + c_8\lambda_{ds3} \\ c_1 \frac{M_{ds1}V_{dc}}{2} + c_2 \frac{M_{ds2}V_{dc}}{2} + c_1 \frac{M_{ds3}V_{dc}}{2} \end{pmatrix} \\ \frac{1}{L_\sigma} \begin{pmatrix} c_3 i_{qs1} + c_3 i_{qs2} + c_4 i_{qs3} + L_\sigma(\omega_r - \omega)i_{ds3} + c_5\lambda_{ds1}\omega_r + c_5\lambda_{ds2}\omega_r \\ + c_6\lambda_{ds3}\omega_r + c_7\lambda_{qs1} + c_7\lambda_{qs2} + c_8\lambda_{qs3} \\ + c_1 \frac{M_{qs1}V_{dc}}{2} + c_1 \frac{M_{qs2}V_{dc}}{2} + c_2 \frac{M_{qs3}V_{dc}}{2} \end{pmatrix} \\ \frac{1}{L_\sigma} \begin{pmatrix} c_3 i_{ds1} + c_3 i_{ds2} + c_4 i_{ds3} - L_\sigma(\omega_r - \omega)i_{qs3} - c_5\lambda_{qs1}\omega_r - c_5\lambda_{qs2}\omega_r \\ - c_6\lambda_{qs3}\omega_r + c_7\lambda_{ds1} + c_7\lambda_{ds2} + c_8\lambda_{ds3} \\ + c_1 \frac{M_{ds1}V_{dc}}{2} + c_1 \frac{M_{ds2}V_{dc}}{2} + c_2 \frac{M_{ds3}V_{dc}}{2} \end{pmatrix} \\ \frac{3P}{4J} \begin{pmatrix} \lambda_{ds1}i_{qs1} + \lambda_{ds2}i_{qs2} + \lambda_{ds3}i_{qs3} \\ -\lambda_{qs1}i_{ds1} - \lambda_{qs2}i_{ds2} - \lambda_{qs3}i_{ds3} - T_j \end{pmatrix}, \forall \, j = \begin{cases} m & \text{Gen} \\ L & \text{motor} \end{cases} \\ \frac{1}{C_{dc}} \left(\frac{3}{4} \sum_{k=1}^{3} (M_{qsk}i_{qs1} + M_{dsk}i_{dsk}) - \frac{3}{4}(M_{q1}i_{s1q} + M_{d1}i_{s1d}) - d_1 i_{Lo} \right) \\ \frac{1}{L_o}[d_1 v_{dc} - v_b], \; \forall \, d_1 \varepsilon[0,1] \\ \frac{1}{C_b} \left(i_{Lo} - \frac{v_b}{R_s} + \frac{v_c}{R_s} + \frac{V_{oc}}{R_s} \right) \\ \frac{1}{C} \left(\frac{v_b}{R_s} - \left(\frac{1}{R_s} + \frac{1}{R_p} \right) v_c + \frac{1}{R_s} V_{oc} \right) \\ \frac{1}{q_{max}} \left(v_b - \frac{v_c}{R_s} - \frac{V_{oc}}{R_s} \right) \\ \vdots \\ 201 \quad \vdots \end{bmatrix}
$$

(A2.12)

Appendix A2. Nine Phase induction machine differential flux modification to current differential

The second split is:

$$
p \begin{bmatrix} \vdots \\ i_{s1q} \\ i_{s1d} \\ i_{Lq} \\ i_{Ld} \\ i_{1q} \\ i_{1d} \\ v_{qcc} \\ v_{dcc} \end{bmatrix} = \begin{bmatrix} \vdots \\ \frac{1}{L_{l1}}\left(\frac{M_{q1}v_{dc}}{2} - v_{qpcc} - R_{l1}i_{s1q} - L_{s1}\omega i_{s1d}\right) \\ \frac{1}{L_{l1}}\left(\frac{M_{d1}v_{dc}}{2} - v_{dpcc} - R_{l1}i_{s1d} + L_{s1}\omega i_{s1q}\right) \\ \frac{1}{L_l}\left(v_{qpcc} - R_L i_{Lq} - L_l \omega i_{Ld}\right) \\ \frac{1}{L_l}\left(v_{dpcc} - R_L i_{Ld} + L_l \omega i_{Lq}\right) \\ \frac{\omega}{Q_0}\left(-\frac{2}{3}\frac{P_0^2+Q_0^2}{v_{qpcc}^2+v_{dpcc}^2}v_{qpcc} + P_0 i_{1q} - Q_0 i_{1d}\right) \\ \frac{\omega}{Q_0}\left(-\frac{2}{3}\frac{P_0^2+Q_0^2}{v_{qpcc}^2+v_{dpcc}^2}v_{dpcc} + P_0 i_{1d} + Q_0 i_{1q}\right) \\ \frac{1}{C_{pcc}}\left(i_{s1q} - i_{Lq} - \frac{2}{3}\frac{P_0 v_{qpcc}+Q_0 v_{dpcc}}{v_{qpcc}^2+v_{dpcc}^2} - C_{pcc}\omega v_{dpcc}\right) \\ \frac{1}{C_{pcc}}\left(i_{s1d} - i_{Ld} - \frac{2}{3}\frac{P_0 v_{qpcc}-Q_0 v_{dpcc}}{v_{qpcc}^2+v_{dpcc}^2} + C_{pcc}\omega v_{dpcc}\right) \end{bmatrix} \tag{A2.13}
$$

The above equations gives the dynamic state equations of the studied system in compact form, with the following twenty state variables.

$x = \{i_{qs1}, i_{ds1}, i_{qs2}, i_{ds2}, i_{qs3}, i_{ds3}, \omega_r, v_{dc}, i_{Lo}, v_b, v_c, SoC, i_{s1q}, i_{s1d}, i_{Lq}, i_{Ld}, i_{1q}, i_{1d}, v_{qpcc}, v_{dpcc}\}$

Which are respectively defined as: $q - d$ current of the nine phase induction machine winding set 1,$(i_{qs1}, i_{ds1},)$ winding set 2, $(i_{qs2}, i_{ds2,})$ winding set 3, $(i_{qs3}, i_{ds3,})$ nine phase induction machine rotor speed ω_r, dc-link voltage $v_{dc,}$ Battery input current from boost converter system $i_{Lo,}$ battery input voltage $v_{b,}$ voltage across the internal battery RC network $v_{c,}$ battery state of charge SoC, inverter output current i_{s1q}, i_{s1d}, constant load current $(i_{1q}, i_{1d,})$ current through the $R - L$ load $(i_{Lq}, i_{Ld,})$ output capacitor voltage at point of common coupling (v_{qcc}, v_{dcc}) and $p = \frac{d}{dt}$.

- Natural Variable Model

If the $q-$ axis flux component of each windings set of the nine phase induction machine is synchronously aligned to the stator flux, i.e $\lambda_{qs1}\lambda_{qs2} = \lambda_{qs3} = \lambda_{qs}$, their $d-$ axis respective components is equals zero i.e $\lambda_{ds1} = \lambda_{ds2} = \lambda_{ds3} = 0$. For obtaining the natural variable model, the $q-$axis of the respective voltage component of respective winding set are synchronously aligned to the maximum $d-$ axis voltage of the supplied voltage V_m for motor or generator operation, the $q-$ axis is set to zero. Then the active

Appendix A2. Nine Phase induction machine differential flux modification to current differential

power and reactive power relations associated with each winding set given by:

$$
\begin{cases}
P_k = \frac{3}{2}v_{qsk}i_{qsk} + \frac{3}{2}v_{dsk}i_{dsk} \\
Q_k = -\frac{3}{2}v_{dsk}i_{qsk} + \frac{3}{2}v_{qsk}i_{dsk}
\end{cases}
\quad \forall\ k = 1, 2, 3
\tag{A2.14}
$$

Now, reduce to:

$$
\begin{cases}
P_k = \frac{3}{2}v_{dsk}i_{dsk} \\
Q_k = -\frac{3}{2}v_{dsk}i_{qsk}
\end{cases}
\quad \forall\ k = 1, 2, 3
\tag{A2.15}
$$

If this value is substituted into equation (4.17)–(4.18). The natural variable model

Appendix A2. Nine Phase induction machine differential flux modification to current differential

equation for the system is:

$$
p\begin{bmatrix} Q_{s1} \\ P_{s1} \\ Q_{s2} \\ P_{s2} \\ Q_{s3} \\ P_{s3} \\ \omega_r \\ v_{dc} \\ i_{Lo} \\ v_b \\ v_c \\ SoC \\ \vdots \\ \vdots \end{bmatrix} = \begin{bmatrix} \frac{-3V_m}{2L_\sigma}\begin{pmatrix} -c_9\frac{2}{3}\frac{Q_{s1}}{V_m} - c_3\frac{2}{3}\frac{Q_{s2}}{V_m} - c_{10}\frac{2}{3}\frac{Q_{s3}}{V_m} + L_\sigma(\omega_r - \omega)\frac{2}{3}\frac{P_{s3}}{V_m} + \\ c_7\lambda_{qs1} + c_7\lambda_{qs2} + c_8\lambda_{qs3} + c_2\frac{M_{qs1}V_{dc}}{2} + c_1\frac{M_{qs2}V_{dc}}{2} \\ +c_1\frac{M_{qs3}V_{dc}}{2} \end{pmatrix} \\ \frac{3V_m}{2L_\sigma}\begin{pmatrix} c_9\frac{2}{3}\frac{P_{s1}}{V_m} + c_3\frac{2}{3}\frac{P_{s2}}{V_m} + c_{10}\frac{2}{3}\frac{P_{s3}}{V_m} - L_\sigma(\omega - \omega_r)\frac{2}{3}\frac{Q_{s3}}{V_m} + c_1\omega_r\lambda_{qs1} \\ +c_1\omega_r\lambda_{qs2} - c_6\omega_r\lambda_{qs3} - c_{11}\omega\lambda_{qs1} - c_{12}\omega\lambda_{qs3} + c_2\frac{M_{ds1}V_{dc}}{2} \\ +c_1\frac{M_{ds2}V_{dc}}{2} + c_1\frac{M_{ds3}V_{dc}}{2} \end{pmatrix} \\ \frac{-3V_m}{2L_\sigma}\begin{pmatrix} -c_3\frac{2}{3}\frac{Q_{s1}}{V_m} - c_9\frac{2}{3}\frac{Q_{s2}}{V_m} - c_{10}\frac{2}{3}\frac{Q_{s3}}{V_m} + L_\sigma(\omega_r - \omega)\frac{2}{3}\frac{P_{s3}}{V_m} + c_7\lambda_{qs1} \\ +c_7\lambda_{qs2} + c_8\lambda_{qs3} + c_1\frac{M_{qs1}V_{dc}}{2} + c_2\frac{M_{qs2}V_{dc}}{2} + c_1\frac{M_{qs3}V_{dc}}{2} \end{pmatrix} \\ \frac{3V_m}{2L_\sigma}\begin{pmatrix} c_3\frac{2}{3}\frac{P_{s1}}{V_m} + c_9\frac{2}{3}\frac{P_{s2}}{V_m} + c_{10}\frac{2}{3}\frac{P_{s3}}{V_m} - L_\sigma(\omega - \omega_r)\frac{2}{3}\frac{Q_{s3}}{V_m} + c_1\omega_r\lambda_{qs1} \\ +c_1\omega_r\lambda_{qs2} - c_6\omega_r\lambda_{qs3} + c_{12}\omega\lambda_{qs2} - c_{11}\omega\lambda_{qs3} + c_1\frac{M_{ds1}V_{dc}}{2} \\ +c_2\frac{M_{ds2}V_{dc}}{2} + c_1\frac{M_{ds3}V_{dc}}{2} \end{pmatrix} \\ \frac{-3V_m}{2L_\sigma}\begin{pmatrix} -c_3\frac{2}{3}\frac{Q_{s1}}{V_m} - c_3\frac{2}{3}\frac{Q_{s2}}{V_m} - c_4\frac{2}{3}\frac{Q_{s3}}{V_m} + L_\sigma(\omega_r - \omega)\frac{2}{3}\frac{P_{s3}}{V_m} + c_7\lambda_{qs1} \\ +c_7\lambda_{qs2} + c_8\lambda_{qs3} + c_1\frac{M_{qs1}V_{dc}}{2} + c_1\frac{M_{qs2}V_{dc}}{2} + c_2\frac{M_{qs3}V_{dc}}{2} \end{pmatrix} \\ \frac{3V_m}{2L_\sigma}\begin{pmatrix} c_3\frac{2}{3}\frac{P_{s1}}{V_m} + c_3\frac{2}{3}\frac{P_{s2}}{V_m} + c_4\frac{2}{3}\frac{P_{s3}}{V_m} + L_\sigma(\omega_r - \omega)\frac{2}{3}\frac{Q_{s1}}{V_m} - c_5\lambda_{qs1}\omega_r \\ -c_5\lambda_{qs2}\omega_r - c_6\lambda_{qs3}\omega_r + c_1\frac{M_{ds1}V_{dc}}{2} + c_1\frac{M_{ds2}V_{dc}}{2} + c_2\frac{M_{ds3}V_{dc}}{2} \end{pmatrix} \\ \frac{3P}{4J}\left(-\lambda_{qs1}\frac{2}{3}\frac{P_{s1}}{V_m} - \lambda_{qs2}\frac{2}{3}\frac{P_{s2}}{V_m} - \lambda_{qs3}\frac{2}{3}\frac{P_{s3}}{V_m} - T_j\right), \forall\, j = \begin{cases} m & \text{Gen} \\ L & \text{motor} \end{cases} \\ \frac{1}{C_{dc}}\left(\frac{3}{4}\sum_{k=1}^{3}\left(-M_{qsk}\frac{2}{3}\frac{Q_{sk}}{V_m} + M_{dsk}\frac{2}{3}\frac{P_{sk}}{V_m}\right) - \frac{3}{4}\left(M_{q1}i_{s1q} + M_{d1}i_{s1d}\right) - d_1 i_{Lo}\right) \\ \frac{1}{L_o}\left[d_1 v_{dc} - v_b\right], \forall\, d_1\varepsilon[0,1] \\ \frac{1}{C_b}\left(i_{Lo} - \frac{v_b}{R_s} + \frac{v_c}{R_s} + \frac{V_{oc}}{R_s}\right) \\ \frac{1}{C}\left(\frac{v_b}{R_s} - \left(\frac{1}{R_s} + \frac{1}{R_p}\right)v_c + \frac{1}{R_s}V_{oc}\right) \\ \frac{1}{q_{max}}\left(v_b - \frac{v_c}{R_s} - \frac{V_{oc}}{R_s}\right) \\ \vdots \\ \vdots \end{bmatrix}
$$

$$(A2.16)$$

With the load voltage aligned to the $q-$ axis reference voltage for the load voltage, the

204

Appendix A2. Nine Phase induction machine differential flux modification to current differential

$d-$ axis component is zero.

$$
p \begin{vmatrix} \vdots \\ i_{s1q} \\ i_{s1d} \\ i_{Lq} \\ i_{Ld} \\ i_{1q} \\ i_{1d} \\ v_{qcc} \\ v_{dcc} \end{vmatrix} = \begin{vmatrix} \vdots \\ \frac{1}{L_{l1}}\left(\frac{M_{q1}v_{dc}}{2} - v_{qpcc} - R_{l1}i_{s1q} - L_{s1}\omega i_{s1d}\right) \\ \frac{1}{L_{l1}}\left(\frac{M_{d1}v_{dc}}{2} - R_{l1}i_{s1d} + L_{s1}\omega i_{s1q}\right) \\ \frac{1}{L_l}\left(v_{qpcc} - R_L i_{Lq} - L_l\omega i_{Ld}\right) \\ \frac{1}{L_l}\left(-R_L i_{Ld} + L_l\omega i_{Lq}\right) \\ \frac{\omega}{Q_0}\left(-\frac{2}{3}\frac{P_0^2 + Q_0^2}{v_{qpcc}^2}v_{qpcc} + P_0 i_{1q} - Q_0 i_{1d}\right) \\ \frac{\omega}{Q_0}\left(P_0 i_{1d} + Q_0 i_{1q}\right) \\ \frac{1}{C_{pcc}}\left(i_{s1q} - i_{Lq} - \frac{2}{3}\frac{P_0 v_{qpcc}}{v_{qpcc}^2}\right) \\ \frac{1}{C_{pcc}}\left(i_{s1d} - i_{Ld} - \frac{2}{3}\frac{P_0 v_{qpcc}}{v_{qpcc}^2}\right) \end{vmatrix} \tag{A2.17}
$$

- Steady State Model

The term "steady state" refers to the condition of a system where all transients and disturbances have been resolved. In this state, the differential equations governing the system transform into algebraic equations, simplifying the handling process. Consequently, at steady state, the solution involves simultaneously solving algebraic equations instead of engaging in the more intricate task of solving multiple differential equations. So, at steady state, the left hand side of the model equation (4.21)–(4.22), i.e the differential part is set equal to zero $p = \frac{d}{dt} = 0$. The equation reduce to algebraic

Appendix A2. Nine Phase induction machine differential flux modification to current differential

equations, which can be solved for variables of interest.

$$
\begin{bmatrix} 0 \\ 0 \\ 0 \\ 0 \\ 0 \\ 0 \\ 0 \\ 0 \\ 0 \\ 0 \\ 0 \\ 0 \\ 0 \\ \vdots \\ \vdots \end{bmatrix} =
\begin{bmatrix}
\frac{-3V_m}{2L_\sigma}\left(\begin{array}{c} -c_9\frac{2}{3}\frac{Q_{s1}}{V_m} - c_3\frac{2}{3}\frac{Q_{s2}}{V_m} - c_{10}\frac{2}{3}\frac{Q_{s3}}{V_m} + L_\sigma(\omega_r - \omega)\frac{2}{3}\frac{P_{s3}}{V_m} + \\ c_7\lambda_{qs1} + c_7\lambda_{qs2} + c_8\lambda_{qs3} + c_2\frac{M_{qs1}V_{dc}}{2} + c_1\frac{M_{qs2}V_{dc}}{2} \\ + c_1\frac{M_{qs3}V_{dc}}{2} \end{array} \right) \\
\frac{3V_m}{2L_\sigma}\left(\begin{array}{c} c_9\frac{2}{3}\frac{P_{s1}}{V_m} + c_3\frac{2}{3}\frac{P_{s2}}{V_m} + c_{10}\frac{2}{3}\frac{P_{s3}}{V_m} - L_\sigma(\omega - \omega_r)\frac{2}{3}\frac{Q_{s3}}{V_m} + c_1\omega_r\lambda_{qs1} \\ + c_1\omega_r\lambda_{qs2} - c_6\omega_r\lambda_{qs3} - c_{11}\omega\lambda_{qs1} - c_{12}\omega\lambda_{qs3} + c_2\frac{M_{ds1}V_{dc}}{2} \\ + c_1\frac{M_{ds2}V_{dc}}{2} + c_1\frac{M_{ds3}V_{dc}}{2} \end{array} \right) \\
\frac{-3V_m}{2L_\sigma}\left(\begin{array}{c} -c_3\frac{2}{3}\frac{Q_{s1}}{V_m} - c_9\frac{2}{3}\frac{Q_{s2}}{V_m} - c_{10}\frac{2}{3}\frac{Q_{s3}}{V_m} + L_\sigma(\omega_r - \omega)\frac{2}{3}\frac{P_{s3}}{V_m} + c_7\lambda_{qs1} \\ + c_7\lambda_{qs2} + c_8\lambda_{qs3} + c_1\frac{M_{qs1}V_{dc}}{2} + c_2\frac{M_{qs2}V_{dc}}{2} + c_1\frac{M_{qs3}V_{dc}}{2} \end{array} \right) \\
\frac{3V_m}{2L_\sigma}\left(\begin{array}{c} c_3\frac{2}{3}\frac{P_{s1}}{V_m} + c_9\frac{2}{3}\frac{P_{s2}}{V_m} + c_{10}\frac{2}{3}\frac{P_{s3}}{V_m} - L_\sigma(\omega - \omega_r)\frac{2}{3}\frac{Q_{s3}}{V_m} + c_1\omega_r\lambda_{qs1} \\ + c_1\omega_r\lambda_{qs2} - c_6\omega_r\lambda_{qs3} + c_{12}\omega\lambda_{qs2} - c_{11}\omega\lambda_{qs3} + c_1\frac{M_{ds1}V_{dc}}{2} \\ + c_2\frac{M_{ds2}V_{dc}}{2} + c_1\frac{M_{ds3}V_{dc}}{2} \end{array} \right) \\
\frac{-3V_m}{2L_\sigma}\left(\begin{array}{c} -c_3\frac{2}{3}\frac{Q_{s1}}{V_m} - c_3\frac{2}{3}\frac{Q_{s2}}{V_m} - c_4\frac{2}{3}\frac{Q_{s3}}{V_m} + L_\sigma(\omega_r - \omega)\frac{2}{3}\frac{P_{s3}}{V_m} + c_7\lambda_{qs1} \\ + c_7\lambda_{qs2} + c_8\lambda_{qs3} + c_1\frac{M_{qs1}V_{dc}}{2} + c_1\frac{M_{qs2}V_{dc}}{2} + c_2\frac{M_{qs3}V_{dc}}{2} \end{array} \right) \\
\frac{3V_m}{2L_\sigma}\left(\begin{array}{c} c_3\frac{2}{3}\frac{P_{s1}}{V_m} + c_3\frac{2}{3}\frac{P_{s2}}{V_m} + c_4\frac{2}{3}\frac{P_{s3}}{V_m} + L_\sigma(\omega_r - \omega)\frac{2}{3}\frac{Q_{s1}}{V_m} - c_5\lambda_{qs1}\omega_r \\ - c_5\lambda_{qs2}\omega_r - c_6\lambda_{qs3}\omega_r + c_1\frac{M_{ds1}V_{dc}}{2} + c_1\frac{M_{ds2}V_{dc}}{2} + c_2\frac{M_{ds3}V_{dc}}{2} \end{array} \right) \\
\frac{3P}{4J}\left(-\lambda_{qs1}\frac{2}{3}\frac{P_{s1}}{V_m} - \lambda_{qs2}\frac{2}{3}\frac{P_{s2}}{V_m} - \lambda_{qs3}\frac{2}{3}\frac{P_{s3}}{V_m} - T_j \right), \forall\, j = \begin{cases} m & \text{Gen} \\ L & \text{motor} \end{cases} \\
\frac{1}{C_{dc}}\left(\frac{3}{4}\sum_{k=1}^{3}\left(-M_{qsk}\frac{2}{3}\frac{Q_{sk}}{V_m} + M_{dsk}\frac{2}{3}\frac{P_{sk}}{V_m} \right) - \frac{3}{4}(M_{q1}i_{s1q} + M_{d1}i_{s1d}) - d_1 i_{Lo} \right) \\
\frac{1}{L_o}\left[d_1 v_{dc} - v_b \right], \ \forall\, d_1\varepsilon[0,1] \\
\frac{1}{C_b}\left(i_{Lo} - \frac{v_b}{R_s} + \frac{v_c}{R_s} + \frac{V_{oc}}{R_s} \right) \\
\frac{1}{C}\left(\frac{v_b}{R_s} - \left(\frac{1}{R_s} + \frac{1}{R_p} \right) v_c + \frac{1}{R_s}V_{oc} \right) \\
\frac{1}{q_{max}}\left(v_b - \frac{v_c}{R_s} - \frac{V_{oc}}{R_s} \right) \\
\vdots \\
\vdots
\end{bmatrix}
$$

(A2.18)

206

Appendix A2.   Nine Phase induction machine differential flux modification to current differential

$$
\begin{bmatrix}
\vdots \\
0 \\
0 \\
0 \\
0 \\
0 \\
0 \\
0 \\
0
\end{bmatrix}
=
\begin{bmatrix}
\vdots \\
\frac{1}{L_{l1}}\left(\frac{M_{q1}v_{dc}}{2} - v_{qpcc} - R_{l1}i_{s1q} - L_{s1}\omega i_{s1d}\right) \\
\frac{1}{L_{l1}}\left(\frac{M_{d1}v_{dc}}{2} - R_{l1}i_{s1d} + L_{s1}\omega i_{s1q}\right) \\
\frac{1}{L_l}\left(v_{qpcc} - R_L i_{Lq} - L_l\omega i_{Ld}\right) \\
\frac{1}{L_l}\left(-R_L i_{Ld} + L_l\omega i_{Lq}\right) \\
\frac{\omega}{Q_0}\left(-\frac{2}{3}\frac{P_0^2+Q_0^2}{v_{qpcc}^2}v_{qpcc} + P_0 i_{1q} - Q_0 i_{1d}\right) \\
\frac{\omega}{Q_0}\left(P_0 i_{1d} + Q_0 i_{1q}\right) \\
\frac{1}{C_{pcc}}\left(i_{s1q} - i_{Lq} - \frac{2}{3}\frac{P_0 v_{qpcc}}{v_{qpcc}^2}\right) \\
\frac{1}{C_{pcc}}\left(i_{s1d} - i_{Ld} - \frac{2}{3}\frac{P_0 v_{qpcc}}{v_{qpcc}^2}\right)
\end{bmatrix}
\qquad (A2.19)
$$

Appendix A2. Nine Phase induction machine differential flux modification to current differential

A2.3 Steady State Equations based on VSD approach

$$
p \begin{bmatrix} i_{qs} \\ i_{ds} \\ T_e \\ T_r \\ \lambda_{ss} \\ \omega_r \\ v_{dc} \\ i_{Lo} \\ v_b \\ v_c \\ SoC \\ i_{s1q} \\ i_{s1d} \\ i_{Lq} \\ i_{Ld} \\ i_{1q} \\ i_{1d} \\ v_{qcc} \\ v_{dcc} \end{bmatrix} = \begin{bmatrix} \frac{1}{L_\sigma}\left(-\frac{r_r\lambda_{qs}}{L_m} + \frac{(L_r r_s + L_s r_r)i_{qs}}{L_m} - \frac{L_r V_{qs}}{L_m} + i_{ds}L_\sigma\left(-\omega+\omega_r\right)\right) \\ \frac{1}{L_\sigma}\left(-\frac{(-L_r r_s - L_s r_r)i_{ds}}{L_m} - \frac{L_r V_{ds}}{L_m} - \frac{L_r \omega_r \lambda_{qs}}{L_m} - i_{qs}L_\sigma\left(-\omega+\omega_r\right)\right) \\ \frac{1}{L_\sigma}\left(\begin{array}{c}-\left(L_\sigma i_{ds}\right)k_t V_{qs} + \left(L_\sigma i_{qs} + \lambda_{qs}\frac{L_r}{L_m}\right)k_t V_{ds} + \frac{(L_r r_s + L_s r_r)T_e}{L_m} \\ -L_\sigma \omega_r T_r + \frac{k_t L_r \omega_r \lambda_{ss}}{L_m}\end{array}\right) \\ \frac{1}{L_\sigma}\left(\begin{array}{c}-k_t\left(L_\sigma i_{qs} - \lambda_{qs}\frac{L_r}{L_m}\right)V_{qs} - k_t\left(L_\sigma i_{ds}\right)V_{ds} + k_t\frac{r_r}{L_m}\lambda_{ss} + \frac{(T_r^2 + T_e^2)L_\sigma r_s}{k_t \lambda_{ss}} \\ + \frac{(L_r r_s + L_s r_r)}{L_m}T_r + \omega_r k_t L_\sigma T_e\end{array}\right) \\ \left(2\lambda_{qs}V_{qs} + \frac{2r_s T_r}{k_t}\right) \\ \frac{P}{2J}\left(T_e - T_j\right), \forall\, j = \begin{cases} m & \text{Gen} \\ \\ L & \text{motor} \end{cases} \\ \frac{1}{C_{dc}}\left(\frac{3}{4}\left(M_{qs}i_{qs} + M_{ds}i_{ds}\right) - \frac{3}{4}\left(M_{q1}i_{s1q} + M_{d1}i_{s1d}\right) - d_1 i_{Lo}\right) \\ \frac{1}{L_o}\left[d_1 v_{dc} - v_b\right], \ \forall\, d_1 \varepsilon[0,1] \\ \frac{1}{C_b}\left(i_{Lo} - \frac{v_b}{R_s} + \frac{v_c}{R_s} + \frac{V_{oc}}{R_s}\right) \\ \frac{1}{C}\left(\frac{v_b}{R_s} - \left(\frac{1}{R_s} + \frac{1}{R_p}\right)v_c + \frac{1}{R_s}V_{oc}\right) \\ \frac{1}{q_{max}}\left(v_b - \frac{v_c}{R_s} - \frac{V_{oc}}{R_s}\right) \\ \frac{1}{L_{l1}}\left(\frac{M_{q1}v_{dc}}{2} - v_{qpcc} - R_{l1}i_{s1q} - L_{s1}\omega i_{s1d}\right) \\ \frac{1}{L_{l1}}\left(\frac{M_{d1}v_{dc}}{2} - R_{l1}i_{s1d} + L_{s1}\omega i_{s1q}\right) \\ \frac{1}{L_l}\left(v_{qpcc} - R_L i_{Lq} - L_l \omega i_{Ld}\right) \\ \frac{1}{L_l}\left(-R_L i_{Ld} + L_l \omega i_{Lq}\right) \\ \frac{\omega}{Q_0}\left(-\frac{2}{3}\frac{P_0^2 + Q_0^2}{v_{qpcc}^2}v_{qpcc} + P_0 i_{1q} - Q_0 i_{1d}\right) \\ \frac{\omega}{Q_0}\left(P_0 i_{1d} + Q_0 i_{1q}\right) \\ \frac{1}{C_{pcc}}\left(i_{s1q} - i_{Lq} - \frac{2}{3}\frac{P_0 v_{qpcc}}{v_{qpcc}^2}\right) \\ \frac{1}{C_{pcc}}\left(i_{s1d} - i_{Ld} - \frac{2}{3}\frac{P_0 v_{qpcc}}{v_{qpcc}^2}\right) \end{bmatrix}
$$

(A2.20)

- **Steady state equations**

Appendix A2.   Nine Phase induction machine differential flux modification to current differential

$$
\begin{bmatrix}
0 \\ 0 \\ 0 \\ 0 \\ 0 \\ 0 \\ 0 \\ 0 \\ 0 \\ 0 \\ 0 \\ 0 \\ 0 \\ 0 \\ 0 \\ 0 \\ 0 \\ 0 \\ 0 \\ 0 \\ 0
\end{bmatrix}
=
\begin{bmatrix}
\frac{1}{L_\sigma}\left(-\frac{r_r\lambda_{qs}}{L_m} + \frac{(L_r r_s + L_s r_r)i_{qs}}{L_m} - \frac{L_r V_{qs}}{L_m} + i_{ds}L_\sigma\left(-\omega + \omega_r\right)\right) \\[6pt]
\frac{1}{L_\sigma}\left(-\frac{(-L_r r_s - L_s r_r)i_{ds}}{L_m} - \frac{L_r V_{ds}}{L_m} - \frac{L_r \omega_r \lambda_{qs}}{L_m} - i_{qs}L_\sigma\left(-\omega + \omega_r\right)\right) \\[6pt]
\frac{1}{L_\sigma}\left(
\begin{array}{c}
-(L_\sigma i_{ds})k_t V_{qs} + \left(L_\sigma i_{qs} + \lambda_{qs}\frac{L_r}{L_m}\right)k_t V_{ds} + \frac{(L_r r_s + L_s r_r)T_e}{L_m} \\[4pt]
-L_\sigma \omega_r T_r + \frac{k_t L_r \omega_r \lambda_{ss}}{L_m}
\end{array}
\right) \\[10pt]
\frac{1}{L_\sigma}\left(
\begin{array}{c}
-k_t\left(L_\sigma i_{qs} - \lambda_{qs}\frac{L_r}{L_m}\right)V_{qs} - k_t\left(L_\sigma i_{ds}\right)V_{ds} + k_t \frac{r_r}{L_m}\lambda_{ss} + \frac{(T_r^2 + T_e^2)L_\sigma r_s}{k_t \lambda_{ss}} \\[4pt]
+ \frac{(L_r r_s + L_s r_r)}{L_m}T_r + \omega_r k_t L_\sigma T_e
\end{array}
\right) \\[10pt]
\left(2\lambda_{qs}V_{qs} + \frac{2r_s T_r}{k_t}\right) \\[6pt]
\frac{P}{2J}\left(T_e - T_j\right), \forall\, j = \begin{cases} m & \text{Gen} \\ L & \text{motor} \end{cases} \\[8pt]
\frac{1}{C_{dc}}\left(\frac{3}{4}\left(M_{qs}i_{qs} + M_{ds}i_{ds}\right) - \frac{3}{4}\left(M_{q1}i_{s1q} + M_{d1}i_{s1d}\right) - d_1 i_{Lo}\right) \\[6pt]
\frac{1}{L_o}\left[d_1 v_{dc} - v_b\right], \ \forall\, d_1 \varepsilon [0,1] \\[6pt]
\frac{1}{C_b}\left(i_{Lo} - \frac{v_b}{R_s} + \frac{v_c}{R_s} + \frac{V_{oc}}{R_s}\right) \\[6pt]
\frac{1}{C}\left(\frac{v_b}{R_s} - \left(\frac{1}{R_s} + \frac{1}{R_p}\right)v_c + \frac{1}{R_s}V_{oc}\right) \\[6pt]
\frac{1}{q_{max}}\left(v_b - \frac{v_c}{R_s} - \frac{V_{oc}}{R_s}\right) \\[6pt]
\frac{1}{L_{l1}}\left(\frac{M_{q1}v_{dc}}{2} - v_{qpcc} - R_{l1}i_{s1q} - L_{s1}\omega i_{s1d}\right) \\[6pt]
\frac{1}{L_{l1}}\left(\frac{M_{d1}v_{dc}}{2} - R_{l1}i_{s1d} + L_{s1}\omega i_{s1q}\right) \\[6pt]
\frac{1}{L_l}\left(v_{qpcc} - R_L i_{Lq} - L_l \omega i_{Ld}\right) \\[6pt]
\frac{1}{L_l}\left(-R_L i_{Ld} + L_l \omega i_{Lq}\right) \\[6pt]
\frac{\omega}{Q_0}\left(-\frac{2}{3}\frac{P_0^2 + Q_0^2}{v_{qpcc}^2}v_{qpcc} + P_0 i_{1q} - Q_0 i_{1d}\right) \\[6pt]
\frac{\omega}{Q_0}\left(P_0 i_{1d} + Q_0 i_{1q}\right) \\[6pt]
\frac{1}{C_{pcc}}\left(i_{s1q} - i_{Lq} - \frac{2}{3}\frac{P_0 v_{qpcc}}{v_{qpcc}^2}\right) \\[6pt]
\frac{1}{C_{pcc}}\left(i_{s1d} - i_{Ld} - \frac{2}{3}\frac{P_0 v_{qpcc}}{v_{qpcc}^2}\right)
\end{bmatrix}
$$

A2.4   Steady State Equations based on VSD approach Analysis

$$
\frac{\omega P_o i_d}{Q_0} + \omega i_q = 0
$$
$$
i_q = -\frac{P_o i_d}{Q_0}
$$

(A2.22)

Appendix A2. Nine Phase induction machine differential flux modification to current differential

$$i_q = -\frac{-P_o i_d}{Q_0}$$

$$- i_d + \frac{\omega P_o i_q}{Q_o} - \frac{2\omega \left(P_o^2 + Q_o^2\right)}{3 V_{qpcc} Q_o} = 0$$

$$- i_d + \frac{P_o i_q}{Q_o} - \frac{2}{3}\frac{\left(P_o^2 + Q_o^2\right)}{V_{qpcc} Q_o} = 0$$

$$- i_d - \frac{P_o^2 i_d}{Q_o^2} - \frac{3}{3}\frac{\left(P_o^2 + Q_o^2\right)}{V_{qpcc} Q_o} = 0$$

$$- i_d \left(1 + P_0^2/Q_0^2\right) = \frac{2}{3}\left(\frac{P_0^2 + Q_0^2}{V_{qpcc} Q_0}\right) \tag{A2.23}$$

$$- i_d \left(\frac{Q_o^2 + P_o^2}{Q_o^2}\right) = \frac{2}{3}\left(\frac{P_o^2 + Q_o^2}{V_{qpcc} Q_o}\right)$$

$$- i_d = \frac{2}{3}\left(\frac{\left(P_o^2 + Q_o^2\right)}{V_{qpcc} Q_o}\right) \times \frac{Q_0^2}{\left(Q_o^2 + P_o^2\right)}$$

$$- i_d = \frac{2}{3}\frac{Q_o}{V_{qpcc}}$$

- $R - L$ load steady state model

$$- \frac{R_L i_{Ld}}{L_l} + \omega i_{Lq} = 0$$

$$- i_{Lq}\omega = -\frac{R_L i_{Ld}}{L_l}$$

$$i_{Lq} = \frac{R_L i_{Ld}}{\omega L}$$

$$- \omega i_{Ld} - \frac{R_L i_{Lq}}{L_l} + \frac{V_{qpcc}}{L_l} = 0$$

$$- \omega i_{Ld} - \frac{R_L}{L_l} \times \frac{R_L i_{Ld}}{\omega L_l} + \frac{V_{qpcc}}{L_l} = 0$$

$$- \omega^2 L_l^2 i_{Ld} - R_L^2 i_{Ld} + V_{qpcc} \times \omega L_l = 0 \tag{A2.24}$$

$$- i_{Ld} \left(\omega^2 L_l^2 + R_L^2\right) + V_{qpcc} \cdot \omega L_l = 0$$

$$i_{Ld} = \frac{V_{qpcc} \cdot \omega L_l}{R_L^2 + \omega^2 L_l^2}$$

$$i_{Lq} = \frac{R_L i_{Ld}}{\omega L_l}$$

$$i_{Lq} = \frac{R_L}{\omega L_l} \times \frac{V_{qpcc} \cdot \omega L_l}{R_L^2 + \omega^2 L_l^2}$$

Appendix A2. Nine Phase induction machine differential flux modification to current differential

- $R - L$ Transmission line steady state model

$$\frac{-i_{Lq}}{C_{pcc}} + \frac{i_{s1q}}{C_{pcc}} - \frac{2P_o}{3V_{qpcc}C_{pcc}} = 0$$

$$i_{s1q} = \frac{2P_o}{3V_{qpac}} + i_{Lq} \tag{A2.25}$$

$$i_{s1q} = \frac{2P_o}{3V_{qpcc}} + \frac{R_L i_{Ld}}{\omega L_l}$$

$$-\frac{i_{Ld}}{C_{pcc}} + \frac{i_{s1d}}{C_{pcc}} - \frac{2P_o}{3V_{qpcc}C_{pcc}} = 0$$

$$i_{s1d} = \frac{2}{3}\frac{P_o}{V_{qpcc}} + i_{Ld}$$

$$i_{s1d} = \frac{2}{3}\frac{P_o}{V_{qpcc}} + \frac{V_{qpcc}\omega L_l}{R_L^2 + \omega^2 L_l} \tag{A2.26}$$

- Inveter -Transmission line steady state model

$$\frac{-R_{l1}i_{s1d}}{L_{l1}} + \frac{L_{s1}\omega i_{s1q}}{L_{l1}} + \frac{M_{d1}}{2L_{l1}}v_{dc} = 0$$

$$M_{d1}V_{dc} = 2R_{l1}i_{s1d} - 2L_{s1}\omega i_{s1q}$$

$$\mid M_{d1} = \frac{2R_{l1}i_{s1d} - 2L_{s1}\omega i_{s1q}}{v_{dc}} \mid \quad \begin{array}{l}\text{inverter}\\ \text{modulating}\\ \text{index.}\end{array}$$

$$-\frac{R_{l1}i_{s1q}}{L_{l1}} - \frac{L_{s1}\omega i_{s1d}}{L_{l1}} + \frac{M_{11}V_{dc}}{2L_{l1}} - \frac{V_{\text{ppce}}}{L_{l1}} = 0$$

$$M_{q1}v_{dc} = 2V_{qpcc} + 2L_{s1}\omega i_{s1d} + R_{l1}i_{s1q}$$

$$\mid M_{q1} = \frac{2V_{qpcc} + 2L_{s1}\omega i_{s1d} + 2R_{l_1}i_{s1q}}{v_{dc}} \mid \tag{A2.28}$$

- Battery section Steady State model

$$v_b = v_c - V_{oc} = 0$$

$$v_b = d_1 v_{dc} \qquad d_1 v_{dc} = v_c - V_{oc} \tag{A2.29}$$

$$i_{Lo}R_s - v_b + v_c + V_{oc} = 0$$

$$i_{Lo} = \frac{d_1 v_{dc} - v_c - V_{oc}}{R_s} \tag{A2.30}$$

211

Appendix A2. Nine Phase induction machine differential flux modification to current differential

- Rectifier-inverter and Battery section Steady State model

$$\frac{1}{C_{dc}}\left(\frac{3}{4}\left(M_{qs}i_{qs} + M_{ds}i_{ds}\right) - \frac{3}{4}\left(M_{qs}i_{s1q} + M_{d1}i_{s1d}\right) - d_1 i_{Lo}\right) = 0$$

$$M_{qs}i_{qs} + M_{ds}i_{ds} - M_{q1}i_{s1q} - M_{d1}i_{s1d} - \frac{4}{3}d_1 i_{Lo} = 0$$

$$M_{qs}i_{qs} + M_{ds}i_{ds} = \frac{4}{3}d_1 i_{Lo} + M_{q1}i_{s1q} + M_{ds}i_{s1d}$$

$$M_{rec} = \sqrt{M_{qs}^2 + M_{ds}^2} \cong 1$$

$$M_{inv} = \sqrt{M_{q1}^2 + M_{d1}^2} \cong 1$$

Electromagnetic Relation for Nine phase machine

$$\frac{P}{2J}\left(T_e - T_j\right) = 0 \quad j = \begin{cases} L - \text{ motor} \\ m \rightarrow \text{ generator} \end{cases}$$

$$T_e = T_j$$

Magnitude of the stator flux steady state Relations

$$2\lambda_{qs}V_{qs} + \frac{2r_s T_r}{k_t} = 0$$

$$V_{qs} = \frac{-2r_s T_r}{2\lambda_{qs}k_t}$$

$$V_{qs} = \frac{-r_s T_r}{\lambda_{qs}k_t}$$

$$But \quad V_{qs} = \frac{M_{qs}v_{dc}}{2}$$

$$\frac{M_{qs}v_{dc}}{2} = \frac{-r_s T_r}{\lambda_{qs}k_t}$$

$$M_{qs} = \left| \frac{-2r_s T_r}{v_{dc}\lambda_{qs}k_t} \right|$$

- Nine phase Induction machine rectifier section Steady State model

$$-2L_\sigma L_m i_{ds}\left(\omega - \omega_r\right) - r_r L_m \lambda_{qs} + 2\left(L_r r_s + L_r r_r\right)i_{qs} - L_r M_{qs}v_{dc} = 0$$

$$i_{ds} = \frac{i_{qs}L_r r_s + i_{qs}L_s r_r - r_r \lambda_{qs} - \frac{1}{2}L_r M_{qs}v_{dc}}{-\omega L_m L_\sigma + L_m L_\sigma \omega_r}$$

(A2.31)

- Nine phase Induction machine rectifier section Steady State model

Appendix A2.   Nine Phase induction machine differential flux modification to current differential

$$-\frac{(-L_r r_s - L_s r_r)\, i_{ds}}{L_m} + (\omega L_\sigma - L_\sigma \omega_r)\, i_{qs} - \frac{L_r M_{ds} V_{dc}}{2L_m} - \frac{L_r \omega_r \lambda_{qs}}{L_m} = 0$$

$$2\,(L_r r_s + L_s r_r)\, i_{ds} + 2L_s\,(\omega - \omega_r)\, i_{qs} - L_r M_{ds} V_{dc} - 2L_r \omega_r \lambda_{qs} = 0 \qquad \text{(A2.32)}$$

$$2\,(L_r r_s + L_s r_r)\, i_{ds} + 2L_\sigma\,(\omega - \omega_r)\, i_{qs} = L_r M_{ds} V_{dc} + 2L_r \omega_r \lambda_{qs}$$

$$i_{qs} = \frac{A+B}{2L_m^2 L_\sigma^2 \omega^2 - 4L_m^2 L_\sigma^2 \omega \omega_r + 2L_m^2 L_\sigma^2 \omega_r^2 - 2L_r^2 r_s^2 - 4L_r L_s r_r r_s - 2L_s^2 r_r^2} \qquad \text{(A2.33)}$$

Where:

$A = -2\left(-\frac{1}{2} L_{rr} M_{ds} v_{dc} - L_r \omega_r \lambda_{qs}\right) L_m L_\sigma\,(\omega - \omega_r) - L_r^2 M_{qs} r_s v_{dc}$

$B = -L_r L_s M_{qs} r_r v_{dc} - 2L_r \lambda_{qs} r_r r_s - 2L_s \lambda_{qs} r_r^2$

Appendix B

Nine Phase Induction Machine

B.1 Stator winding Design

This section show a design of a nine phase induction machine. A three phase induction machine geometric quantities is used to re-calculate the new values for a nine phase induction machine [201, 202]. A full detail design procedure for a six phase induction machine type for asymmetric and symmetric machine concept is shown [203]. The winding design of multi-phase induction machines shares the same magnetic framework as the standard three phase machine design.

- The winding is designed for chorded pitch, double layer winding. The full winding layout after the design is as shown in Fig. 1

- Number of slots $Q_s = 36$, number of poles $P = 4$. The number of phases will be group of three phase windings. m will denote the number of phases in one set of three phase windings. Here, it is three.

- Slot/pole $\frac{36}{4} = 9$

- Chord length expressed in pole per circumferential perimeter $y/\tau = 7/9$

- Slot per pole per phase, $q = \frac{36}{(4 \times 3)} = 3$, this value of q obtained will be shared amongst the three set of three phase windings. So, each set of three phase windings will be redistributed in the slots of stator of the induction machine for $q = 1$, (i.e concentrated winding) for each three phase winding sets.

Appendix B. Nine Phase Induction Machine

Table B.1: Winding throw for a 36 slot, four pole, 50Hz, nine phase asymmetrical Induction machine

Phases	$i = 1$	$i = 2$	$i = 3$
A_i	$\begin{cases} + \longmapsto 1 - 8' \\ - \longmapsto 17 - 10' \\ + \longmapsto 19 - 26' \\ - \longmapsto 35 - 28' \end{cases}$	$\begin{cases} + \longmapsto 2 - 9' \\ - \longmapsto 18 - 11' \\ + \longmapsto 20 - 27' \\ - \longmapsto 36 - 29' \end{cases}$	$\begin{cases} + \longmapsto 3 - 10' \\ - \longmapsto 19 - 12' \\ + \longmapsto 21 - 28' \\ - \longmapsto 1 - 30' \end{cases}$
B_i	$\begin{cases} + \longmapsto 7 - 14' \\ - \longmapsto 23 - 16' \\ + \longmapsto 25 - 32' \\ - \longmapsto 5 - 34' \end{cases}$	$\begin{cases} + \longmapsto 8 - 15' \\ - \longmapsto 24 - 17' \\ + \longmapsto 26 - 33' \\ - \longmapsto 6 - 35' \end{cases}$	$\begin{cases} + \longmapsto 9 - 16' \\ - \longmapsto 25 - 18' \\ + \longmapsto 27 - 34' \\ - \longmapsto 7 - 36' \end{cases}$
C_i	$\begin{cases} + \longmapsto 13 - 20' \\ - \longmapsto 29 - 22' \\ + \longmapsto 31 - 2' \\ - \longmapsto 11 - 4' \end{cases}$	$\begin{cases} + \longmapsto 14 - 21' \\ - \longmapsto 30 - 23' \\ + \longmapsto 32 - 3' \\ - \longmapsto 12 - 5' \end{cases}$	$\begin{cases} + \longmapsto 15 - 22' \\ - \longmapsto 31 - 24' \\ + \longmapsto 33 - 4' \\ - \longmapsto 13 - 6' \end{cases}$

Throughout the table, $'$ attached to a slot number, denote coil side placed at the top of slot, and that without prime denote coil side placed at the bottom of a slot in a double layer winding. A_i, B_i, C_i denote phases of a winding set i. $\forall i = 1, 2, 3$ and their respective winding throw.

- The slot angle in elect. degree $\gamma = (\frac{P \times \pi}{Q_s})$, yield $20°$.

- The number of slots g between phases using this expression $g = \frac{2\pi}{m\gamma}$ is 6

- Slot between the adjacent machines windings is obtained, $SM = \frac{g}{2M}$, where M is the number of three phase machine sets. For the case in this paper, the number of machine sets is 3. puting all the earlier obtained parameters together, $SM = 1$.

- The slot angle which is a reflection of the physical layout and winding placement in the slot can be obtained using the relationship between electrical and mechanical angle using pairs of poles, $\xi_{mech} = \frac{2}{p}\xi_{elect}$. This yield $\xi_{mech} = 10°$.

- In some circumstances in this thesis we will denote, the number of pole pairs P' to be $P' = \frac{P}{2}$

215

Table B.2: Winding throw for a 36 slot, four pole, 50Hz, nine phase symmetrical Induction machine

Phases	$i = 1$	$i = 2$	$i = 3$
A_i	$\begin{cases} + \longmapsto 1 - 8' \\ - \longmapsto 17 - 10' \\ + \longmapsto 19 - 26' \\ - \longmapsto 35 - 28' \end{cases}$	$\begin{cases} + \longmapsto 3 - 10' \\ - \longmapsto 19 - 12' \\ + \longmapsto 21 - 28' \\ - \longmapsto 1 - 30' \end{cases}$	$\begin{cases} + \longmapsto 5 - 12' \\ - \longmapsto 21 - 14' \\ + \longmapsto 23 - 30' \\ - \longmapsto 3 - 32' \end{cases}$
B_i	$\begin{cases} + \longmapsto 7 - 14' \\ - \longmapsto 23 - 16' \\ + \longmapsto 25 - 32' \\ - \longmapsto 5 - 34' \end{cases}$	$\begin{cases} + \longmapsto 9 - 16' \\ - \longmapsto 25 - 18' \\ + \longmapsto 27 - 34' \\ - \longmapsto 7 - 36' \end{cases}$	$\begin{cases} + \longmapsto 11 - 18' \\ - \longmapsto 27 - 20' \\ + \longmapsto 29 - 36' \\ - \longmapsto 9 - 2' \end{cases}$
C_i	$\begin{cases} + \longmapsto 13 - 20' \\ - \longmapsto 29 - 22' \\ + \longmapsto 31 - 2' \\ - \longmapsto 11 - 4' \end{cases}$	$\begin{cases} + \longmapsto 15 - 22' \\ - \longmapsto 31 - 24' \\ + \longmapsto 33 - 4' \\ - \longmapsto 13 - 6' \end{cases}$	$\begin{cases} + \longmapsto 17 - 24' \\ - \longmapsto 33 - 26' \\ + \longmapsto 35 - 6' \\ - \longmapsto 15 - 8' \end{cases}$

Throughout the table, $\prime$ attached to a slot number, denote coil side placed at the top of slot, and that without prime denote coil side placed at the bottom of a slot in a double layer winding. A_i, B_i, C_i denote phases of a winding set i. $\forall i = 1, 2, 3$ and their respective winding throw.

Appendix B. Nine Phase Induction Machine

Table B.1 and B.2 shows the winding throw for asymmetrical and symmetrical induction machine. A clock diagram showing the winding distribution layout in the stator slot for asymmetrical and symmetrical induction machine is shown in Figure B.1 and FigureB.2.
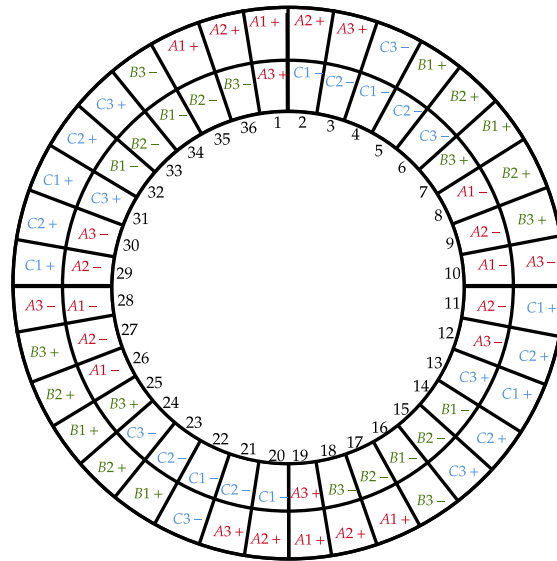
Figure B.1: Double layer winding distribution round a 36 slot stator for an asymmetrical Nine phase induction machine with 20° elect. geometric shit between windings

B.2   Stator Multiphase Inductance Evaluation

This section is designed to calculate the inductances due to air gap fluxes. The self and mutual inductance based on machine geometry can be obtain. The inductances is evaluated based on air gap , slot fluxes and overhang fluxes.
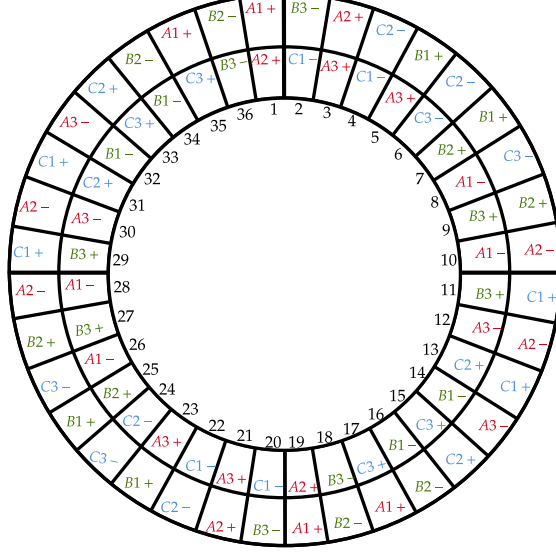
Figure B.2: Double layer winding distribution round a 36 slot stator for an symmetrical Nine phase induction machine with 40° elect. geometric shit between windings

B.2.1 Inductance Component value due to Air-Gap Fluxes

The flux linking N turns of stator winding, given k_{bns} and k_{pns} as the winding factor for the nth harmonic:

$$\lambda_{aa} = \frac{\mu_0 2 l_e N^2}{\pi p} \int_{\lambda - \frac{1}{2}\pi}^{\lambda + \frac{1}{2}\pi} h_2 B_{h2} d\theta = \frac{\mu_0^2 N^2 l_e}{\pi} \sum_{n=1,3}^{\infty} \frac{k_{bns}^2 k_{pns}^2}{n} \left(\frac{h_2^{np} + h_1^{np}}{h_2^{np} - h_1^{np}} \right) \cos n\lambda \quad \text{(B.1)}$$

Here, the angle λ is the exciting winding and chosen reference point. Self inductance due to air gap fluxes for $\lambda = 0$

$$L_{aa(\text{ air-gap})} = \frac{\mu_0 4 N^2 l_e h_2}{\pi g p} \sum_{n=1,3}^{\infty} \left(\frac{k_{bns}^2 k_{pns}^2}{n^2} \right) [= 0.2239\text{H}] \quad \text{(B.2)}$$

For other phases,'b' and 'c' the inductaces is obtained by subtituing in place of λ, the value $\lambda = \pm 120°$. The inductance between phase 'a' and 'b'.

Appendix B. Nine Phase Induction Machine

The equation obtained above did not present practical airgap inductance, as it was calculated based on infinite permeability. To account for a more practical airgap inductance, a correction factor k_μ is used to multiply the expression, to obtained an inductance more close to reality. This factor is adjudged to even out the effect of saturation[*Philip Algar*].

All of this work employs essentially the same definition of Leakage inductance as applied to VSD, though it is only recently that the concept has be formalized and extended to related VSD and multiple $d - q$.

$$L_{ab \text{ (air-gap)}} = \frac{\mu_0 4N^2 l_e h_2}{\pi p g} \sum_{n=1,3}^{\infty} \frac{k_{bns}^2 k_{pns}^2}{n^2} \cos n\lambda \tag{B.3}$$

$$[= -0 \cdot 1069H \text{ for } \lambda = 2\pi/3]$$
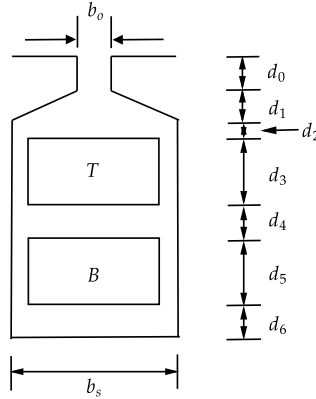
Figure B.3: Slots geometry

B.2.2 Inductance Component value due to Slot Fluxes

Table B.3 list the parameters of the slot dimension used for the calculation of the slot permeance and inductance of a double layer winding of one slot of the figure B.2.

In this section, reference to the geometry shown in FigureB.3. The permeance for

Appendix B. Nine Phase Induction Machine

Table B.3: Table of parameter for the slot geometry show in figure B.3

parameter	value (cm)	parameter	value(cm)	slot index	value
w_1	0.3175	d_2	1.956	δ_1	12
w_2	1.113	d_3	0.381	δ_2	8
d_0	0.0508	d_4	0.3175	δ_3	14
d_1	1.956	d_5	0.0	δ_4	12

δ_i indicates number of slots pertaining to respective cases

each section is calculated. If the conductor for the double layer are of the same phase(i.e Top(T) and bottom (B) conductors), The inductances are calculated due to the current they each carry. Here, n is the number of conductors per slot.

- **Self Inductance** per slot, due to current flowing in same direction in both layers:

$$L'_{aa(\text{ slot flux})} = \frac{\mu_0 n_s^2 l_e}{4} \left[\frac{4d_5}{w_1} + \frac{8d_4}{(w_1+w_2)} + \frac{4d_3+d_2}{w_2} + \frac{4(d_1-d_2)}{3w_2} \right]$$

$$\left[= 2945 \times 10^{-7} \text{H} \right]$$

(B.4)

- **self-inductance** per slot for the **bottom** layer alone carrying current:

$$L''_{aa} \text{ (slot flux))} = \frac{\mu_0 n_s^2 l_e}{4} \left[\frac{d_5}{w_1} + \frac{2d_4}{(w_1+w_2)} + \frac{2(d_1-d_2)+3d_3}{3w_2} \right]$$

$$\left[= 1037 \times 10^{-7} \text{H} \right]$$

(B.5)

- **self-inductance** per slot for the **top** layer alone carrying current:

$$L'''_{aa \text{ (slot flux)}} = \frac{\mu_0 n_s^2 l_e}{4} \left[\frac{d_5}{w_1} + \frac{2d_4}{(w_1+w_2)} + \frac{d_3}{w_2} + \frac{(d_1-d_2)}{6w_2} \right]$$

$$\left[= 576 \cdot 5 \times 10^{-7} \text{H} \right]$$

(B.6)

Then, **The self inductance** per slot.

$$L_{aa(\text{ slot flux})} = L'_{aa}\delta_1 + L''_{aa}\delta_2 + L'''_{aa}\delta_3 [= 0.00247 \text{H}]$$

(B.7)

Here, the δ_1, δ_2 and δ_3, denotes the number of slots pertaining to each respective cases. Proceeding in the similar manner, the **mutual inductance** per slot in top and bottom layers is:

$$L'_{aa(\text{ slot flux})} = -\frac{\mu_0 n_s l_e}{4} \left[\frac{(d_1-d_2)}{4w_2} + \frac{d_3}{w_2} + \frac{2d_4}{(w_1+w_2)} + \frac{d_5}{w_1} \right]$$

$$\left[= 6 \cdot 53 \times 10^{-5} \text{H} \right]$$

(B.8)

Appendix B. Nine Phase Induction Machine

Hence,

$$L_{ab(\text{ slot flux})} = \delta_4 L'_{ab(\text{ slot flux})} \left[= -5.23 \times 10^{-4}\text{H}\right] \qquad \text{(B.9)}$$

Appendix C

Model Equation Parameter Dump

The parameters listed here, are those of equation described in text, that are so lengthy and was moved to this section.

C.1   Parameter of Nine Phase Induction Machine

The parameters for equation (3.29) are defined thus:

Where 'j' is a complex symbol.

$A_{s1} = \frac{f_1}{L_{\sigma 1}}, A_{s2} = \frac{f_2}{L_{\sigma 1}}, A_{s3} = \frac{f_3}{L_{\sigma 1}}, B_{s1} = \frac{f_4}{L_{\sigma 1}}, B_{s2} = \frac{f_5}{L_{\sigma 1}}, B_{s3} = \frac{f_6}{L_{\sigma 1}}, C_{s1} = \frac{f_7}{L_{\sigma 1}}, C_{s2} = \frac{f_8}{L_{\sigma 1}}, C_{s3} = \frac{f_9}{L_{\sigma 1}},$

$L\sigma 1 = 3\left(\left(L_{lm} + L_{lr} + \frac{L_{ls}}{3} \right) L_m + \left(L_{lm} + \frac{L_{ls}}{3} \right) L_{lr} \right) L_{ls}$

$f_{1a} = 3\mathrm{j}L_{lm}L_{lr}\omega_{sl} + 3\mathrm{j}L_{lm}L_m\omega_{sl} + \mathrm{j}L_{lr}L_{ls}\omega_{sl}$

$f_{1b} = 3\mathrm{j}L_{lr}L_m\omega_{sl} + \mathrm{j}L_{ls}L_m\omega_{sl} - 3L_{lm}r_r - L_{ls}r_r - 3L_m r_r$

$f_1 = r_{s1}\left(\left(-L_{lr} - L_{lm} + \frac{L_{ls}L_m r_r}{f_{1a}+f_{1b}} \right) L_m - L_{lm}L_{lr} \right)$

$f_{2a} = 3\mathrm{j}L_{lm}L_{lr}\omega_{sl} + 3\mathrm{j}L_{lm}L_m\omega_{sl} + \mathrm{j}L_{lr}L_{ls}\omega_{sl}$

$f_{2b} = 3\mathrm{j}L_{lr}L_m\omega_{sl} + \mathrm{j}L_{ls}L_m\omega_{sl} - 3L_{lm}r_r - L_{ls}r_r - 3L_m r_r$

$f_2 = r_{s2}\left(\left(-L_{lr} - L_{lm} + \frac{L_{ls}L_m r_r}{f_{2a}+f_{2b}} \right) L_m - L_{lm}L_{lr} \right)$

$f_{3a} = 3\mathrm{j}L_{lm}L_{lr}\omega_{sl} + 3\mathrm{j}L_{lm}L_m\omega_{sl} + \mathrm{j}L_{lr}L_{ls}\omega_{sl}$

Appendix C. Model Equation Parameter Dump

$$f_{3b} = 3\mathrm{j}L_{lr}L_m\omega_{sl} + \mathrm{j}L_{ls}L_m\omega_{sl} - 3L_{lm}r_r - L_{ls}r_r - 3L_m r_r$$

$$f_3 = r_{s3}\left(\left(-L_{lr} - L_{lm} + \frac{L_{ls}L_m r_r}{f_{3a}+f_{3b}}\right)L_m - L_{lm}L_{lr}\right)$$

$$f_{4a} = 3\mathrm{j}L_{lm}L_{lr}\omega_{sl} + 3\mathrm{j}L_{lm}L_m\omega_{sl} + \mathrm{j}L_{lr}L_{ls}\omega_{sl}$$

$$f_{4b} = 3\mathrm{j}L_{lr}L_m\omega_{sl} + \mathrm{j}L_{ls}L_m\omega_{sl} - 3L_{lm}r_r - L_{ls}r_r - 3L_m r_r$$

$$f_4 = r_{s3}\left(\left(-L_{lr} - L_{lm} + \frac{L_{ls}L_m r_r}{f_{4a}+f_{4b}}\right)L_m - L_{lm}L_{lr}\right)$$

$$f_{5a} = 3\mathrm{j}L_{lm}L_{lr}\omega_{sl} + 3\mathrm{j}L_{lm}L_m\omega_{sl} + \mathrm{j}L_{lr}L_{ls}\omega_{sl}$$

$$f_{5b} = 3\mathrm{j}L_{lr}L_m\omega_{sl} + \mathrm{j}L_{ls}L_m\omega_{sl} - 3L_{lm}r_r - L_{ls}r_r - 3L_m r_r$$

$$f_5 = r_{s3}\left(\left(-L_{lr} - L_{lm} + \frac{L_{ls}L_m r_r}{f_{5a}+f_{5b}}\right)L_m - L_{lm}L_{lr}\right)$$

$$f_{6a} = 3\mathrm{j}L_{lm}L_{lr}\omega_{sl} + 3\mathrm{j}L_{lm}L_m\omega_{sl} + \mathrm{j}L_{lr}L_{ls}\omega_{sl}$$

$$f_{6b} = 3\mathrm{j}L_{lr}L_m\omega_{sl} + \mathrm{j}L_{ls}L_m\omega_{sl} - 3L_{lm}r_r - L_{ls}r_r - 3L_m r_r$$

$$f_6 = r_{s3}\left(\left(-L_{lr} - L_{lm} + \frac{L_{ls}L_m r_r}{f_{6a}+f_{6b}}\right)L_m - L_{lm}L_{lr}\right)$$

$$f_{7a} = 3\mathrm{j}L_{lm}L_{lr}\omega_{sl} + 3\mathrm{j}L_{lm}L_m\omega_{sl} + \mathrm{j}L_{lr}L_{ls}\omega_{sl}$$

$$f_{7b} = 3\mathrm{j}L_{lr}L_m\omega_{sl} + \mathrm{j}L_{ls}L_m\omega_{sl} - 3L_{lm}r_r - L_{ls}r_r - 3L_m r_r$$

$$f_7 = r_{s1}\left(\left(2L_{lr} + 2L_{lm} - L_{ls}\left(-\frac{L_m r_r}{f_{7a}+f_{7b}} - 1\right)\right)L_m + 2\left(L_{lm} + \frac{L_{ls}}{2}\right)L_{lr}\right)$$

$$f_{8a} = 3\mathrm{j}L_{lm}L_{lr}\omega_{sl} + 3\mathrm{j}L_{lm}L_m\omega_{sl} + \mathrm{j}L_{lr}L_{ls}\omega_{sl}$$

$$f_{8b} = 3\mathrm{j}L_{lr}L_m\omega_{sl} + \mathrm{j}L_{ls}L_m\omega_{sl} - 3L_{lm}r_r - L_{ls}r_r - 3L_m r_r$$

$$f_8 = r_{s2}\left(\left(2L_{lr} + 2L_{lm} - L_{ls}\left(-\frac{L_m r_r}{f_{8a}+f_{8b}} - 1\right)\right)L_m - 2\left(L_{lm} - \frac{L_{ls}}{2}\right)L_{lr}\right)$$

$$f_{9a} = 3\mathrm{j}L_{lm}L_{lr}\omega_{sl} + 3\mathrm{j}L_{lm}L_m\omega_{sl} + \mathrm{j}L_{lr}L_{ls}\omega_{sl}$$

$$f_{9b} = 3\mathrm{j}L_{lr}L_m\omega_{sl} + \mathrm{j}L_{ls}L_m\omega_{sl} - 3L_{lm}r_r - L_{ls}r_r - 3L_m r_r$$

$$f_9 = r_{s2}\left(\left(2L_{lr} + 2L_{lm} - L_{ls}\left(-\frac{L_m r_r}{f_{9a}+f_{9b}} - 1\right)\right)L_m - 2\left(L_{lm} - \frac{L_{ls}}{2}\right)L_{lr}\right)$$

The table of parameter for the resistance and inductance use for the simulation is given in table [204]:

Table C.1: Table of parameter for the Nine Phase Induction Machine use for simulation in chapter 3

parameter	value	parameter	value
L_m	520mH	r_{s1}	4.85
L_{ls}	18mH	r_{s2}	4.85
L_{lr}	8.6mH	r_{s3}	4.85
P	4	r_r	1.82

$L_{lm} = 0.1789$ H, for this machine
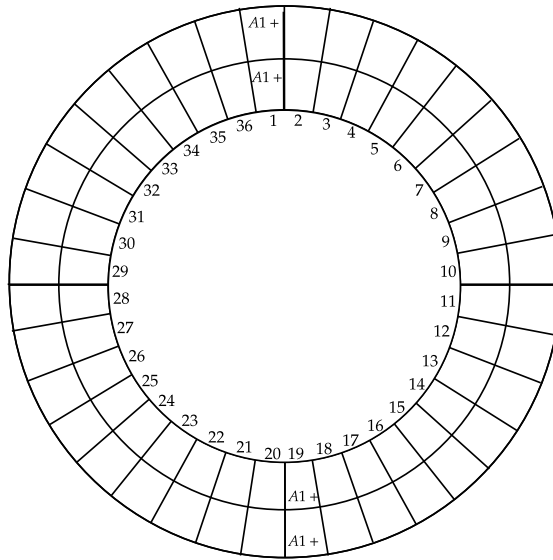
Figure C.1: Clock diagram development template

Bibliography

[1] Majid T Fard, JiangBiao He, Hao Huang, and Yue Cao. Aircraft distributed electric propulsion technologies-a review. *IEEE Transactions on Transportation Electrification*, 2022.

[2] Press Release No: 66/ IATA. Net-zero carbon emissions by 2050, October 2021.

[3] Radu Bojoi, Sandro Rubino, Alberto Tenconi, and Silvio Vaschetto. Multiphase electrical machines and drives: A viable solution for energy generation and transportation electrification. In *2016 International Conference and Exposition on Electrical and Power Engineering (EPE)*, pages 632–639. IEEE, 2016.

[4] Mohab Gaber, SH El-banna, MS Hamad, and Mahmoud Eldabah. Studying the effect of using multi-phases switched reluctance motor to reduce the torque ripple for ship propulsion system. In *2020 IEEE PES/IAS PowerAfrica*, pages 1–5. IEEE, 2020.

[5] Mohamed Amine Frikha, Julien Croonen, Kritika Deepak, Yassine Benômar, Mohamed El Baghdadi, and Omar Hegazy. Multiphase motors and drive systems for electric vehicle powertrains: State of the art analysis and future trends. *Energies*, 16(2):768, 2023.

[6] Ahmed Salem and Mehdi Narimani. A review on multiphase drives for automotive traction applications. *IEEE Transactions on Transportation Electrification*, 5(4):1329–1348, 2019.

Bibliography

[7] Anil Kumar Reddy Siddavatam, Kaushik Rajashekara, Hao Huang, and Fred Wang. A review of distributed electric aircraft propulsion architecture progression. In *AIAA AVIATION 2023 Forum*, page 4429, 2023.

[8] Eunsoo Jung, Hyunjae Yoo, Seung-Ki Sul, Hong-Soon Choi, and Yun-Young Choi. A nine-phase permanent-magnet motor drive system for an ultrahigh-speed elevator. *IEEE Transactions on Industry Applications*, 48(3):987–995, 2012.

[9] Kai Strunz, Khaled Almunem, Christoph Wulkow, Maren Kuschke, Marta Valescudero, and Xavier Guillaud. Enabling 100% renewable power systems through power electronic grid-forming converter and control: System integration for security, stability, and application to europe. *Proceedings of the IEEE*, 2022.

[10] Tao Liu, Yue Song, Lipeng Zhu, and David J Hill. Stability and control of power grids. *Annual Review of Control, Robotics, and Autonomous Systems*, 5:689–716, 2022.

[11] Euan Thomas Andrew. Design and analysis of a new model predictive current controller for grid connected converters. 2022.

[12] Kotb B Tawfiq, Mohamed N Ibrahim, EE EL-Kholy, and Peter Sergeant. Replacing stator of existing three-phase synchronous reluctance machines towards improved multiphase machines performance. In *2020 International Conference on Electrical Machines (ICEM)*, volume 1, pages 2145–2151. IEEE, 2020.

[13] Rajdeep Bondade, Yi Zhang, Bingqing Wei, Taoli Gu, Hai Chen, and D Brian Ma. Integrated auto-reconfigurable power-supply network with multidirectional energy transfer for self-reliant energy-harvesting applications. *IEEE Transactions on Industrial Electronics*, 63(5):2850–2861, 2016.

[14] Phillipe Vilaca Gomes, Joao T Saraiva, Leonel Carvalho, Bruno Dias, and Leonardo W Oliveira. Impact of decision-making models in transmission expansion planning considering large shares of renewable energy sources. *Electric Power Systems Research*, 174:105852, 2019.

Bibliography

[15] Giuseppe Scarcella, Giacomo Scelba, Mario Cacciato, Andrea Spampinato, and Mark M Harbaugh. Vector control strategy for multidirectional power flow in integrated multidrives starter-alternator applications. *IEEE Transactions on Industry Applications*, 52(6):4816–4826, 2016.

[16] Shakil Ahamed Khan, Md Rabiul Islam, Youguang Guo, and Jianguo Zhu. A new isolated multi-port converter with multi-directional power flow capabilities for smart electric vehicle charging stations. *IEEE Transactions on Applied Superconductivity*, 29(2):1–4, 2019.

[17] Ahmad Anad Abduallah, Obrad Dordevic, and Martin Jones. Multidirectional power flow control among double winding six-phase induction machine winding sets. In *IECON 2017-43rd Annual Conference of the IEEE Industrial Electronics Society*, pages 8001–8006. IEEE, 2017.

[18] Haoyuan Yu, Yanbo Wang, Hanwen Zhang, and Zhe Chen. Impedance modelling and stability analysis of triple active bridge converter-based renewable electricity-hydrogen-integrated metro dc traction power system. *IEEE Transactions on Industrial Electronics*, 2023.

[19] Antoine Cizeron, Javier Ojeda, Eric Monmasson, and Olivier Béthoux. Control of a segmented three-phase synchronous motor with highly coupled subwindings. *IEEE Transactions on Industrial Electronics*, 70(5):4405–4415, 2022.

[20] Xiaokang Peng, Zicheng Liu, and Dong Jiang. A review of multiphase energy conversion in wind power generation. *Renewable and Sustainable Energy Reviews*, 147:111172, 2021.

[21] Emil Levi, Radu Bojoi, Francesco Profumo, HA Toliyat, and S Williamson. Multiphase induction motor drives–a technology status review. *IET Electric Power Applications*, 1(4):489–516, 2007.

[22] Susan Rogers. Advanced power electronics and electric motors r&d. *US DOE Presentation, May*, 14, 2013.

227

Bibliography

[23] Utkal Ranjan Muduli, Abdul R Beig, Khaled Al Jaafari, Khalifa Al Hosani, Ameena Saad Al-Sumaiti, and Ranjan Kumar Behera. Dual motor power sharing control for electric vehicles with battery power management. *IEEE Transactions on Industrial Electronics*, 2023.

[24] Radu Bojoi, Andrea Cavagnino, Marco Cossale, and Alberto Tenconi. Multiphase starter generator for a 48-v mini-hybrid powertrain: Design and testing. *IEEE Transactions on Industry Applications*, 52(2):1750–1758, 2015.

[25] Xiaoyan Huang, Andrew Goodman, Chris Gerada, Youtong Fang, and Qinfen Lu. Design of a five-phase brushless dc motor for a safety critical aerospace application. *IEEE transactions on industrial electronics*, 59(9):3532–3541, 2011.

[26] C Gerada, M Galea, and A Kladas. Electrical machines for aerospace applications. In *2015 IEEE workshop on electrical machines design, control and diagnosis (WEMDCD)*, pages 79–84. IEEE, 2015.

[27] C Bassi, Alberto Tessarolo, R Menis, and Giorgio Sulligoi. Analysis of different system design solutions for a high-power ship propulsion synchronous motor drive with multiple pwm converters. In *Electrical Systems for Aircraft, Railway and Ship Propulsion*, pages 1–6. IEEE, 2010.

[28] Mehrzad Mohammadi Bijaieh, Satish Vedula, and Olugbenga Moses Anubi. Low-bandwidth modular mathematical modeling of dc microgrid systems for control development with application to shipboard power systems. In *2021 IEEE Electric Ship Technologies Symposium (ESTS)*, pages 1–7. IEEE, 2021.

[29] Md Alamgir Hossain, Hemanshu Roy Pota, Md Jahangir Hossain, and Frede Blaabjerg. Evolution of microgrids with converter-interfaced generations: Challenges and opportunities. *International Journal of Electrical Power & Energy Systems*, 109:160–186, 2019.

[30] C Chellaswamy, TS Geetha, P Thiruvalar Selvan, and A Arunkumar. 6-phase dfig for wind energy conversion system: A hybrid approach. *Sustainable Energy Technologies and Assessments*, 53:102497, 2022.

Bibliography

[31] Alford Sibanda and Nkosinathi Gule. Modelling of a grid connected nine-phase induction generator. In *2020 International Symposium on Power Electronics, Electrical Drives, Automation and Motion (SPEEDAM)*, pages 799–804. IEEE, 2020.

[32] Zicheng Liu, Yongdong Li, and Zedong Zheng. A review of drive techniques for multiphase machines. *CES Transactions on Electrical Machines and Systems*, 2(2):243–251, 2018.

[33] Ahmed Salem and Mehdi Narimani. A review on multiphase drives for automotive traction applications. *IEEE Transactions on Transportation Electrification*, 5(4):1329–1348, 2019.

[34] Emil Levi, Nandor Bodo, Obrad Dordevic, and Martin Jones. Recent advances in power electronic converter control for multiphase drive systems. In *2013 IEEE Workshop on Electrical Machines Design, Control and Diagnosis (WEMDCD)*, pages 158–167, 2013.

[35] Mohd Faisal Khan and Mohd Rizwan Khan. Analysis of a nine-phase self excited induction generator equipped with optimum excitation capacitances. In *2022 International Conference for Advancement in Technology (ICONAT)*, pages 1–6. IEEE, 2022.

[36] Rishabh Raj, Prithivirajan Subramaniyane, and Luca Peretti. Design of a variable phase-pole induction machine for electric vehicle applications. In *2022 International Conference on Electrical Machines (ICEM)*, pages 976–982. IEEE, 2022.

[37] M. Zabaleta, E. Levi, and M. Jones. Modelling approaches for triple three-phase permanent magnet machines. In *2016 XXII International Conference on Electrical Machines (ICEM)*, pages 466–472, 2016.

[38] Andrea Cervone, Obrad Dordevic, and Gianluca Brando. General approach for modeling and control of multiphase pmsm drives. *IEEE Transactions on Power Electronics*, 36(9):10490–10503, 2021.

Bibliography

[39] Rolf H Loewenherz, Stefan A Koschik, Michael Kruse, and Rik W De Doncker. Modeling of modular multi-phase machines. In *2020 23rd International Conference on Electrical Machines and Systems (ICEMS)*, pages 559–564. IEEE, 2020.

[40] Ayman S Abdel-khalik, Shehab Ahmed, and Ahmed Massoud. A five-phase induction machine model using multiple dq planes considering the effect of magnetic saturation. In *2014 IEEE Energy Conversion Congress and Exposition (ECCE)*, pages 287–293. IEEE, 2014.

[41] Philip L Alger, EH Freiburghouse, and DD Chase. Double windings for turbine alternators. *Transactions of the American Institute of Electrical Engineers*, 49(1):226–244, 1930.

[42] EE Ward and H Härer. Preliminary investigation of an invertor-fed 5-phase induction motor. In *Proceedings of the Institution of Electrical Engineers*, volume 116, pages 980–984. IET, 1969.

[43] EF Fuchs and LT Rosenberg. Analysis of an alternator with two displaced stator windings. *IEEE Transactions on Power Apparatus and Systems*, (6):1776–1786, 1974.

[44] RH Nelson and PC Krause. Induction machine analysis for arbitrary displacement between multiple winding sets. *IEEE Transactions on Power Apparatus and Systems*, (3):841–848, 1974.

[45] Saikat Ghosh and SN Mahato. Modeling and control topology of multiphase induction generator for supplying ac and dc power simultaneously. In *Proceedings of Symposium on Power Electronic and Renewable Energy Systems Control: PERESC 2020*, pages 329–340. Springer, 2021.

[46] Hamid Reza Mohabati, Javad Shokrollahi Moghani, and Samad Taghipour Boroujeni. Complex vector modelling and sequence analysis of the integrated three-phase rotating transformer for design of a symmetrical structure. *IET Electric Power Applications*, 10(7):649–657, 2016.

230

[47] Samad Thaghipour Boroujeni. Complex vector modeling of a doubly fed cascaded cage rotor induction machine. *Electrical Engineering*, 102:1831–1842, 2020.

[48] ASO Ogunjuyigbe, TR Ayodele, and BB Adetokun. Modelling and analysis of dual stator-winding induction machine using complex vector approach. *Engineering Science and Technology, an International Journal*, 21(3):351–363, 2018.

[49] Hajer Kouki, Mouldi Ben Fredj, and Habib Rehaoulia. Vector space decomposition for double star induction machine modeling. In *2014 15th International Conference on Sciences and Techniques of Automatic Control and Computer Engineering (STA)*, pages 581–586. IEEE, 2014.

[50] Alberto Tessarolo. On the modeling of poly-phase electric machines through vector-space decomposition: Theoretical considerations. In *2009 International Conference on Power Engineering, Energy and Electrical Drives*, pages 519–523. IEEE, 2009.

[51] Ayman S Abdel-Khalik, Ahmed M Massoud, and Shehab Ahmed. Nine-phase six-terminal induction machine modeling using vector space decomposition. *IEEE Transactions on Industrial Electronics*, 66(2):988–1000, 2018.

[52] Andrew A Rockhill and TA Lipo. A simplified model of a nine-phase synchronous machine using vector space decomposition. *Electric Power Components and Systems*, 38(4):477–489, 2010.

[53] Ivan Zoric, Martin Jones, and Emil Levi. Vector space decomposition algorithm for asymmetrical multiphase machines. In *2017 International Symposium on Power Electronics (Ee)*, pages 1–6. IEEE, 2017.

[54] Juri Jatskevich, Eric A Walters, and Charles E Lucas. Coupled-circuit modeling of 3, 6, and 9-phase induction machine drive systems. Technical report, SAE Technical Paper, 2006.

Bibliography

[55] Shen Wang, Koji Imai, and Shinji Doki. A novel decoupling control scheme for dual three phase motors. In *2020 23rd International Conference on Electrical Machines and Systems (ICEMS)*, pages 1225–1229. IEEE, 2020.

[56] Carlos A Reusser, Samir Kouro, and Marcelo Perez. Circulating current control scheme for double-star winding induction motor drive based, ship propulsion system. In *IECON 2017-43rd Annual Conference of the IEEE Industrial Electronics Society*, pages 6783–6788. IEEE, 2017.

[57] Djafar Hadiouche, Hubert Razik, and Abderrezak Rezzoug. On the modeling and design of dual-stator windings to minimize circulating harmonic currents for vsi fed ac machines. *IEEE Transactions on industry applications*, 40(2):506–515, 2004.

[58] Sandro Rubino, Fabio Mandrile, Eric Armando, Iustin Radu Bojoi, and Luca Zarri. Fault-tolerant torque controller based on adaptive decoupled multi-stator modeling for multi-three-phase induction motor drives. *IEEE Transactions on Industry Applications*, 58(6):7318–7335, 2022.

[59] Wan Noraishah Wan Abdul Munim, Muhammad Hazizi Ahmad Khairi, Hang Seng Che, and Mahdi Tousizadeh. Analysis of fault-tolerant dual three-phase induction machine using graphical user interface. In *2021 IEEE International Conference in Power Engineering Application (ICPEA)*, pages 167–172. IEEE, 2021.

[60] Ivan Zoric, Martin Jones, and Emil Levi. Arbitrary power sharing among three-phase winding sets of multiphase machines. *IEEE Transactions on Industrial Electronics*, 65(2):1128–1139, 2017.

[61] Sandro Rubino, Radu Bojoi, Andrea Cavagnino, and Silvio Vaschetto. Asymmetrical twelve-phase induction starter/generator for more electric engine in aircraft. In *2016 IEEE Energy Conversion Congress and Exposition (ECCE)*, pages 1–8. IEEE, 2016.

[62] Thomas A Lipo. *Introduction to AC machine design*. John Wiley & Sons, 2017.

Bibliography

[63] Paul C Krause, Oleg Wasynczuk, Scott D Sudhoff, and Steven D Pekarek. *Analysis of electric machinery and drive systems*, volume 75. John Wiley & Sons, 2013.

[64] Yixuan Wu, Gustaf Falk Olson, Luca Peretti, and Oskar Wallmark. Harmonic plane decomposition: An extension of the vector-space decomposition-part i. In *IECON 2020 The 46th Annual Conference of the IEEE Industrial Electronics Society*, pages 985–990. IEEE, 2020.

[65] Gustaf Falk Olson, Yixuan Wu, Luca Peretti, and Oskar Wallmark. Harmonic plane decomposition: An extension of the vector-space decomposition-part ii. In *IECON 2020 The 46th Annual Conference of the IEEE Industrial Electronics Society*, pages 991–996. IEEE, 2020.

[66] Wesam Taha, Peter Azer, Alan Dorneles Callegaro, and Ali Emadi. Multiphase traction inverters: State-of-the-art review and future trends. *IEEE Access*, 10:4580–4599, 2022.

[67] Emil Levi, Martin Jones, Slobodan N Vukosavic, and Hamid A Toliyat. A novel concept of a multiphase, multimotor vector controlled drive system supplied from a single voltage source inverter. *IEEE transactions on Power Electronics*, 19(2):320–335, 2004.

[68] Jorge Rodas. A brief survey of model predictive current control techniques for six-phase induction machines. In *2021 IEEE CHILEAN Conference on Electrical, Electronics Engineering, Information and Communication Technologies (CHILECON)*, pages 1–6. IEEE, 2021.

[69] Martin Jones, Slobodan Vukosavic, Emil Levi, and Drazen Dujic. Current control issues in rotor flux oriented multiphase induction motor drives. In *2008 18th International Conference on Electrical Machines*, pages 1–6. IEEE, 2008.

[70] HS Che, WP Hew, NA Rahim, E Levi, M Jones, and MJ Duran. Current control of a six-phase induction generator for wind energy plants. In *2012 15th International Power Electronics and Motion Control Conference (EPE/PEMC)*, pages LS5b–2. IEEE, 2012.

Bibliography

[71] I Zoric, M Zabaleta, M Jones, and E Levi. Techniques for power sharing between winding sets of multiple three-phase machines. In *2017 IEEE Workshop on Electrical Machines Design, Control and Diagnosis (WEMDCD)*, pages 208–215. IEEE, 2017.

[72] Sandro Rubino, Radu Bojoi, Shafiq Ahmed Odhano, and Pericle Zanchetta. Model predictive direct flux vector control of multi-three-phase induction motor drives. *IEEE Transactions on Industry Applications*, 54(5):4394–4404, 2018.

[73] Liwei Wang, Sina Chini Foroosh, Juri Jatskevich, and Ali Davoudi. Physical variable modeling of multiphase induction machines. In *2008 Canadian Conference on Electrical and Computer Engineering*, pages 000999–001004. IEEE, 2008.

[74] Ivan Zorić. *Multiple three-phase induction generators for wind energy conversion systems*. Liverpool John Moores University (United Kingdom), 2018.

[75] Zicheng Liu, Zedong Zheng, Lie Xu, Kui Wang, and Yongdong Li. Current balance control for symmetrical multiphase inverters. *IEEE Transactions on Power Electronics*, 31(6):4005–4012, 2015.

[76] AA Abduallah, O Dordevic, and M Jones. Synthetic loading for symmetrical and asymmetrical six-phase machines. In *2018 IEEE 18th International Power Electronics and Motion Control Conference (PEMC)*, pages 617–622. IEEE, 2018.

[77] Yifan Zhao and Thomas A Lipo. Space vector pwm control of dual three-phase induction machine using vector space decomposition. *IEEE Transactions on industry applications*, 31(5):1100–1109, 1995.

[78] Michał Janaszek. Extended clarke transformation for n-phase systems. *Prace Instytutu Elektrotechniki*, (274):5–26, 2016.

[79] Alberto Tessarolo, Mauro Bortolozzi, and Alfredo Contin. Modeling of split-phase machines in park's coordinates. part i: Theoretical foundations. In *Eurocon 2013*, pages 1308–1313. IEEE, 2013.

Bibliography

[80] Sandro Rubino, Radu Bojoi, Davide Cittanti, and Luca Zarri. Decoupled torque control of multiple three-phase induction motor drives. In *2019 IEEE Energy Conversion Congress and Exposition (ECCE)*, pages 4903–4910. IEEE, 2019.

[81] Sandro Rubino, Obrad Dordevic, Eric Armando, Iustin Radu Bojoi, and Emil Levi. A novel matrix transformation for decoupled control of modular multiphase pmsm drives. *IEEE Transactions on Power Electronics*, 36(7):8088–8101, 2020.

[82] AA Rockhill and TA Lipo. A generalized transformation methodology for polyphase electric machines and networks. In *2015 IEEE International Electric Machines & Drives Conference (IEMDC)*, pages 27–34. IEEE, 2015.

[83] Ayman S Abdel-Khalik, Mahmoud I Masoud, Shehab Ahmed, and Ahmed M Massoud. Effect of current harmonic injection on constant rotor volume multiphase induction machine stators: A comparative study. *IEEE Transactions on Industry Applications*, 48(6):2002–2013, 2012.

[84] Jano Malvar, Óscar López, Alejandro G Yepes, Ana Vidal, Francisco D Freijedo, Pablo Fernández-Comesaña, and Jesús Doval-Gandoy. Graphical diagram for subspace and sequence identification of time harmonics in symmetrical multiphase machines. *IEEE Transactions on Industrial Electronics*, 61(1):29–42, 2013.

[85] IZ Mohammedi, O Touhami, MO Mahmoudi, C Hénaux, and Y Lefèvre. Transformation by rewinding a stator of a three phase induction machine with squirrel cage to a five-phase induction machine. In *2016 XXII International Conference on Electrical Machines (ICEM)*, pages 619–625. IEEE, 2016.

[86] Pradeep K Sood, Habib Rehaoulia, Donald W Novotny, and Hienas A Lipo. A pulse width controlled three switch exciter for induction generators. In *1985 Annual Meeting Industry Applications Society*, pages 653–661. IEEE, 1985.

[87] Mario J Duran, Emil Levi, and Martin Jones. Independent vector control of asymmetrical nine-phase machines by means of series connection. In *IEEE International Conference on Electric Machines and Drives, 2005.*, pages 167–173. IEEE, 2005.

Bibliography

[88] Emil Levi, Martin Jones, Slobodan N Vukosavic, and Hamid A Toliyat. Operating principles of a novel multiphase multimotor vector-controlled drive. *IEEE Transactions on Energy Conversion*, 19(3):508–517, 2004.

[89] Ivan Subotic, Nandor Bodo, Emil Levi, and Martin Jones. Onboard integrated battery charger for evs using an asymmetrical nine-phase machine. *IEEE Transactions on industrial electronics*, 62(5):3285–3295, 2014.

[90] V Fernão Pires, Armando Cordeiro, Daniel Foito, and J Fernando Silva. A three-phase on-board integrated battery charger for evs with six-phase machine and nine switch converter. In *2019 IEEE 13th International Conference on Compatibility, Power Electronics and Power Engineering (CPE-POWERENG)*, pages 1–6. IEEE, 2019.

[91] S Ranjith, V Vidya, and R Sudharshan Kaarthik. An integrated ev battery charger with retrofit capability. *IEEE Transactions on Transportation Electrification*, 6(3):985–994, 2020.

[92] Syed Qaseem Ali, Diego Mascarella, Geza Joos, and Longcheng Tan. Torque cancelation of integrated battery charger based on six-phase permanent magnet synchronous motor drives for electric vehicles. *IEEE Transactions on Transportation Electrification*, 4(2):344–354, 2018.

[93] Sohit Sharma, Mohan V Aware, and Apekshit Bhowate. Integrated battery charger for ev by using three-phase induction motor stator windings as filter. *IEEE Transactions on Transportation Electrification*, 6(1):83–94, 2020.

[94] Ayman S Abdel-Khalik, Shehab Ahmed, and Ahmed M Massoud. A nine-phase six-terminal concentrated single-layer winding layout for high-power medium-voltage induction machines. *IEEE Transactions on Industrial Electronics*, 64(3):1796–1806, 2016.

[95] Ayman Samy Abdel-Khalik, Mostafa S Hamad, Ahmed M Massoud, and Shehab Ahmed. Postfault operation of a nine-phase six-terminal induction machine under

single open-line fault. *IEEE Transactions on Industrial Electronics*, 65(2):1084–1096, 2017.

[96] Yifan Zhao and Thomas A Lipo. Modeling and control of a multi-phase induction machine with structural unbalance. *IEEE Transactions on energy conversion*, 11(3):578–584, 1996.

[97] Yifan Zhao and Thomas A Lipo. Modeling and control of a multi-phase induction machine with structural unbalance part ii. field-oriented control and experimental verification. *IEEE Transactions on energy conversion*, 11(3):578–584, 1996.

[98] Tamires Santos de Souza, Rodrigo Rodrigues Bastos, and Braz J Cardoso Filho. Synchronous-frame modeling and dq current control of an unbalanced nine-phase induction motor due to open phases. *IEEE Transactions on Industry Applications*, 56(2):2097–2106, 2020.

[99] Mario J Duran, Ignacio Gonzalez-Prieto, Natalia Rios-Garcia, and Federico Barrero. A simple, fast, and robust open-phase fault detection technique for six-phase induction motor drives. *IEEE Transactions on power electronics*, 33(1):547–557, 2017.

[100] Emil Levi. Advances in converter control and innovative exploitation of additional degrees of freedom for multiphase machines. *IEEE Transactions on Industrial Electronics*, 63(1):433–448, 2015.

[101] Taiwo Samuel Ajayi and Olimpo Anaya-Lara. Modeling, analysis of current trajectories of a nine phase induction machine for regenerative capabilities. In *2019 IEEE PES/IAS PowerAfrica*, pages 1–4. IEEE, 2019.

[102] Ivan Subotic, Emil Levi, Martin Jones, and Dušan Graovac. On-board integrated battery chargers for electric vehicles using nine-phase machines. In *2013 International Electric Machines & Drives Conference*, pages 226–233. IEEE, 2013.

[103] Mohamed Y Metwly, Mahmoud S Abdel-Majeed, Ayman S Abdel-Khalik, Ragi A Hamdy, Mostafa S Hamad, and Shehab Ahmed. A review of integrated on-board ev

battery chargers: Advanced topologies, recent developments and optimal selection of fscw slot/pole combination. *Ieee Access*, 8:85216–85242, 2020.

[104] Jiaqi Yuan, Lea Dorn-Gomba, Alan Dorneles Callegaro, John Reimers, and Ali Emadi. A review of bidirectional on-board chargers for electric vehicles. *IEEE Access*, 9:51501–51518, 2021.

[105] Mohamed Yehia Metwly, Fadi Adel Maximos, Ahmed Tarek Ahmed, Ahmed Sarya Hawam, Ahmed Abdel-Moneim Zaki, Amr Abdel-Moneim Helal, Abdel-Rahman Mohamed Mokhtar, Salman Mohamed Abdelghaffar, Rawan Ahmed Taha, Ragi Ali Hamdy, et al. Design case study of a nine-phase integrated on-board battery charger. In *2018 Twentieth International Middle East Power Systems Conference (MEPCON)*, pages 815–821. IEEE, 2018.

[106] Upendra Singh, Yash Pal, Sunil Nagpal, and Gautam Sarkar. Three-phase on-board integrated bidirectional ev battery charger with power factor correction. In *2019 6th International Conference on Signal Processing and Integrated Networks (SPIN)*, pages 335–340. IEEE, 2019.

[107] Harish Karneddi and Deepak Ronanki. Reconfigurable battery charger with a wide voltage range for universal electric vehicle charging applications. *IEEE Transactions on Power Electronics*, 2023.

[108] Mario J Duran, Ignacio González-Prieto, Angel González-Prieto, and Federico Barrero. Multiphase energy conversion systems connected to microgrids with unequal power-sharing capability. *IEEE Transactions on Energy Conversion*, 32(4):1386–1395, 2017.

[109] Judith M Apsley. Derating of multiphase induction machines due to supply imbalance. *IEEE Transactions on Industry Applications*, 46(2):798–805, 2010.

[110] Angel Gonzalez-Prieto, Juan J Aciego, Ignacio Gonzalez-Prieto, and Mario J Duran. Automatic fault-tolerant control of multiphase induction machines: A game changer. *Electronics*, 9(6):938, 2020.

Bibliography

[111] Hugo Guzman, Ignacio Gonzalez, Federico Barrero, and Mario Durán. Open-phase fault operation on multiphase induction motor drives. *Induction Motors—Applications, Control and Fault Diagnostics*, page 328, 2015.

[112] Zicheng Liu, Yongdong Li, and Zedong Zheng. A review of drive techniques for multiphase machines. *CES Transactions on Electrical Machines and Systems*, 2(2):243–251, 2018.

[113] Jakub Kellner, Slavomír Kaščák, Michal Praženica, Patrik Resutík, and Želmíra Ferková. Implementation of new fault tolerant control for five-phase induction motor in fault operation. In *2022 ELEKTRO (ELEKTRO)*, pages 1–6. IEEE, 2022.

[114] Roland Ryndzionek, Krzysztof Blecharz, Filip Kutt, Michal Michna, and Grzegorz Kostro. Fault-tolerant performance of the novel five-phase doubly-fed induction generator. *IEEE Access*, 10:59350–59358, 2022.

[115] Fazlli Patkar and Martin Jones. Performance of an asymmetrical six-phase induction machine in single-and two-neutral point configurations. In *2013 48th International Universities' Power Engineering Conference (UPEC)*, pages 1–6. IEEE, 2013.

[116] Amirreza Poorfakhraei, Mehdi Narimani, and Ali Emadi. A review of modulation and control techniques for multilevel inverters in traction applications. *IEEE Access*, 9:24187–24204, 2021.

[117] Endika Robles, Markel Fernandez, Jon Andreu, Edorta Ibarra, Jordi Zaragoza, and Unai Ugalde. Common-mode voltage mitigation in multiphase electric motor drive systems. *Renewable and Sustainable Energy Reviews*, 157:111971, 2022.

[118] Gabriele Grandi, Giovanni Serra, and Angelo Tani. Space vector modulation of a six-phase vsi based on three-phase decomposition. In *2008 International Symposium on Power Electronics, Electrical Drives, Automation and Motion*, pages 674–679. IEEE, 2008.

Bibliography

[119] Reza Kianinezhad, B Nahid, Franck Betin, and G-A Capolino. Multi-vector svm: A new approach to space vector modulation control for six-phase induction machines. In *31st Annual Conference of IEEE Industrial Electronics Society, 2005. IECON 2005.*, pages 6–pp. IEEE, 2005.

[120] Keliang Zhou and Danwei Wang. Relationship between space-vector modulation and three-phase carrier-based pwm: a comprehensive analysis [three-phase inverters]. *IEEE transactions on industrial electronics*, 49(1):186–196, 2002.

[121] Wenxi Yao, Haibing Hu, and Zhengyu Lu. Comparisons of space-vector modulation and carrier-based modulation of multilevel inverter. *IEEE transactions on Power Electronics*, 23(1):45–51, 2008.

[122] Waheed Ahmed and Syed M Usman Ali. Comparative study of svpwm (space vector pulse width modulation) & spwm (sinusoidal pulse width modulation) based three phase voltage source inverters for variable speed drive. In *IOP Conference Series: Materials Science and Engineering*, volume 51, page 012027. IOP Publishing, 2013.

[123] Li Zhao, Shoudao Huang, Jian Zheng, and Yuan Gao. A harmonic suppression svpwm strategy for the asymmetric six-phase motor fed by two-level six-phase vsi operating in the overmodulation region. *Energies*, 15(20):7589, 2022.

[124] BS Umesh and Keerthipati Sivakumar. Dual-inverter-fed pole-phase modulated nine-phase induction motor drive with improved performance. *IEEE Transactions on Industrial Electronics*, 63(9):5376–5383, 2016.

[125] Prasoon Chandran Mavila and PP Rajeevan. A five level dtc scheme for dual inverter-fed five phase open-end winding induction motor drives with single dc source. In *2019 IEEE Industry Applications Society Annual Meeting*, pages 1–6. IEEE, 2019.

[126] Peng Han, Greg Heins, Yibin Zhang, and Dan M Ionel. Integrated modular motor drives based on multiphase axial-flux pm machines with fractional-slot

Bibliography

concentrated windings. In *2021 IEEE International Electric Machines & Drives Conference (IEMDC)*, pages 1–6. IEEE, 2021.

[127] Kan Akatsu and Keita Fukuda. Advanced control method of 5-phase dual concentrated winding pmsm for inverter integrated in-wheel motor. *World Electric Vehicle Journal*, 12(2):61, 2021.

[128] B Prathap Reddy and Sivakumar Keerthipati. Distributed short-pitch winding for multi-phase pole-phase modulated induction motor drives. In *2018 IEEE International Conference on Power Electronics, Drives and Energy Systems (PEDES)*, pages 1–6. IEEE, 2018.

[129] Mohamed Y Metwly, Ayman S Abdel-Khalik, Mostafa S Hamad, Shehab Ahmed, and Noha A Elmalhy. Multiphase stator winding: New perspectives, advanced topologies, and futuristic applications. *IEEE Access*, 10:103241–103263, 2022.

[130] Sandro Rubino, Radu Bojoi, Davide Cittanti, and Luca Zarri. Decoupled and modular torque control of multi-three-phase induction motor drives. *IEEE Transactions on Industry Applications*, 56(4):3831–3845, 2020.

[131] Mohamed A Abu-Seif, Mohamed Ahmed, Mohamed Y Metwly, Ayman S Abdel-Khalik, Mostafa S Hamad, Shehab Ahmed, and Noha Elmalhy. Data-driven-based vector space decomposition modeling of multiphase induction machines. *IEEE Transactions on Energy Conversion*, 2023.

[132] R Bojoi, E Levi, F Farina, Alberto Tenconi, and Francesco Profumo. Dual three-phase induction motor drive with digital current control in the stationary reference frame. *IEE Proceedings-Electric Power Applications*, 153(1):129–139, 2006.

[133] Martin Jones, Slobodan N Vukosavic, Drazen Dujic, and Emil Levi. A synchronous current control scheme for multiphase induction motor drives. *IEEE Transactions on Energy Conversion*, 24(4):860–868, 2009.

[134] Guojia Peng, Kai Ni, Chun Gan, Ronghai Qu, and Yihua Hu. A direct starting method of doubly-fed induction machine for shipboard propulsion system applica-

tion. In *2021 24th International Conference on Electrical Machines and Systems (ICEMS)*, pages 949–954. IEEE, 2021.

[135] Angelo Tani, Giovanni Serra, Michele Mengoni, Luca Zarri, Giancarlo Rini, and Domenico Casadei. Dynamic stator current sharing in quadruple three-phase induction motor drives. In *IECON 2013-39th Annual Conference of the IEEE Industrial Electronics Society*, pages 5173–5178. IEEE, 2013.

[136] Atif Iqbal, Sheikh Moinuddin, M Rizwan Khan, and Imtiaz Ashraf. Indirect rotor flux oriented control of a seven-phase induction motor drive. In *2006 IEEE International Conference on Industrial Technology*, pages 440–445. IEEE, 2006.

[137] Najmeh Rezaei, Calum Cossar, and Kamyar Mehran. Modelling and analysis of indirect field-oriented control of svpwm-driven induction motor drive based on a voltage source inverter. In *2018 IEEE Canadian Conference on Electrical & Computer Engineering (CCECE)*, pages 1–6. IEEE, 2018.

[138] Hang Seng Che, Emil Levi, Martin Jones, Wooi-Ping Hew, and Nasrudin Abd. Rahim. Current control methods for an asymmetrical six-phase induction motor drive. *IEEE Transactions on Power Electronics*, 29(1):407–417, 2014.

[139] Ignacio Gonzalez-Prieto, Mario J Duran, HS Che, Emil Levi, Mario Bermúdez, and Federico Barrero. Fault-tolerant operation of six-phase energy conversion systems with parallel machine-side converters. *IEEE Transactions on Power Electronics*, 31(4):3068–3079, 2015.

[140] Ignacio Gonzalez, Mario J Duran, Hang Seng Che, Emil Levi, and Federico Barrero. Fault-tolerant control of six-phase induction generators in wind energy conversion systems with series-parallel machine-side converters. In *IECON 2013-39th Annual Conference of the IEEE Industrial Electronics Society*, pages 5276–5281. IEEE, 2013.

[141] Ivan Subotic, Obrad Dordevic, J Barry Gomm, and Emil Levi. Active and reactive power sharing between three-phase winding sets of a multiphase induction machine. *IEEE Transactions on Energy Conversion*, 34(3):1401–1410, 2019.

Bibliography

[142] I-G Park, S-Y Park, and J-K Park. An analysis of boost rectifier. In *Proceedings IECON'91: 1991 International Conference on Industrial Electronics, Control and Instrumentation*, pages 519–524. IEEE, 1991.

[143] Aakash Singh and Aftab Alam. A new mathematical technique and analysis of a three-phase voltage source rectifier. In *2017 International Conference on Innovations in Information, Embedded and Communication Systems (ICIIECS)*, pages 1–5. IEEE, 2017.

[144] Mittapalli Abhishek, K Sudarsana Reddy, C Shanthini, and V S Kirthika Devi. Comparative analysis of boost and quadratic boost converter for wind energy conversion system. In *2022 International Conference on Electronics and Renewable Systems (ICEARS)*, pages 283–287. IEEE, 2022.

[145] Roland Greul, Simon D Round, and Johann W Kolar. Analysis and control of a three-phase, unity power factor y-rectifier. *IEEE Transactions on Power Electronics*, 22(5):1900–1911, 2007.

[146] Xinmeng Zhang, Ziying Liu, Xiangtao Wang, and Zhiyong Ji. Analysis of control strategy of three-phase bridge fully controlled rectifier circuit based on pid principle. In *2023 IEEE 2nd International Conference on Electrical Engineering, Big Data and Algorithms (EEBDA)*, pages 703–709. IEEE, 2023.

[147] M Mehrasa and M Ahmadigorji. Input/output feedback linearization control for three level/phase npc voltage-source rectifier using its dual lagrangian model. In *2012 11th International Conference on Environment and Electrical Engineering*, pages 712–718. IEEE, 2012.

[148] Tongying Li and Hongbo Zhu. Three-phase voltage-type pwm rectifier controller design based on feedback linearization. In *2019 Chinese Automation Congress (CAC)*, pages 1872–1875. IEEE, 2019.

[149] Ounis Rabiaa, Ben Hamed Mouna, Dhaoui Mehdi, and Sbita Lassaad. Modeling of a dual-three-phase induction motor including the effect of stator mutual leakage

Bibliography

inductance. In *2017 International Conference on Green Energy Conversion Systems (GECS)*, pages 1–5. IEEE, 2017.

[150] Hang Seng Che, Emil Levi, Martin Jones, Wooi-Ping Hew, and Nasrudin Abd Rahim. Current control methods for an asymmetrical six-phase induction motor drive. *IEEE Transactions on Power Electronics*, 29(1):407–417, 2013.

[151] Remus Teodorescu, Frede Blaabjerg, Marco Liserre, and P Chiang Loh. Proportional-resonant controllers and filters for grid-connected voltage-source converters. *IEE Proceedings-Electric Power Applications*, 153(5):750–762, 2006.

[152] Zhiyong Chen, Boyi Wang, and Bin Li. A digital proportional-resonant controller with desired tracking-error convergence. *IEEE Transactions on Industrial Electronics*, 2023.

[153] Changjin Liu, Frede Blaabjerg, Wenjie Chen, and Dehong Xu. Stator current harmonic control with resonant controller for doubly fed induction generator. *IEEE transactions on power electronics*, 27(7):3207–3220, 2011.

[154] Ayman S Abdel-Khalik, Mahmoud S Abdel-Majeed, and Shehab Ahmed. Effect of winding configuration on six-phase induction machine parameters and performance. *IEEE Access*, 8:223009–223020, 2020.

[155] Chong Di, Ilya Petrov, and Juha J Pyrhönen. Design of a high-speed solid-rotor induction machine with an asymmetric winding and suppression of the current unbalance by special coil arrangements. *IEEE Access*, 7:83175–83186, 2019.

[156] Yixuan Wu, Gustaf Falk Olson, Luca Peretti, and Oskar Wallmark. Harmonic plane decomposition: An extension of the vector-space decomposition - part i. In *IECON 2020 The 46th Annual Conference of the IEEE Industrial Electronics Society*, pages 985–990, 2020.

[157] Yifan Zhao and T.A. Lipo. Space vector pwm control of dual three-phase induction machine using vector space decomposition. *IEEE Transactions on Industry Applications*, 31(5):1100–1109, 1995.

Bibliography

[158] Angel Gonzalez-Prieto, Ignacio Gonzalez-Prieto, Alejandro G Yepes, Mario J
Duran, and Jesus Doval-Gandoy. Symmetrical six-phase induction machines: A
solution for multiphase direct control strategies. In *2021 22nd IEEE International
Conference on Industrial Technology (ICIT)*, volume 1, pages 1362–1367. IEEE,
2021.

[159] Tapani Jokinen, Valeria Hrabovcova, and Juha Pyrhonen. *Design of rotating
electrical machines*. John Wiley & Sons, 2013.

[160] Ahmad Abduallah. Five-phase sensorless induction motor drives with lc filter for
high power applications. In *Qatar Foundation Annual Research Forum Volume
2013 Issue 1*, volume 2013, pages EESP–036. Hamad bin Khalifa University Press
(HBKU Press), 2013.

[161] Nagi F Ali Mohamed, Osama M Al Gali, and Abdussalam Khamis. A novel
approach for catching the flux leakage in induction machines using wireless power
transfer. In *2022 IEEE 2nd International Maghreb Meeting of the Conference
on Sciences and Techniques of Automatic Control and Computer Engineering
(MI-STA)*, pages 798–801. IEEE, 2022.

[162] Hang Seng Che, Ayman Samy Abdel-Khalik, Obrad Dordevic, and Emil Levi.
Parameter estimation of asymmetrical six-phase induction machines using modified
standard tests. *IEEE Transactions on Industrial Electronics*, 64(8):6075–6085,
2017.

[163] Yang Lu, Jian Li, and Kai Yang. Study on winding design of dual three-phase
electrical machines for circulating current harmonics and vibration suppression.
IEEE Transactions on Industrial Electronics, 2023.

[164] Alberto Tessarolo and D Giulivo. Analytical methods for the accurate computation
of stator leakage inductances in multi-phase synchronous machines. In *SPEEDAM
2010*, pages 845–852. IEEE, 2010.

[165] Bharti Srivastava and Christopher Roger Lines. Effect of slot leakage flux on
winding inductance and ac resistance in an axial flux machine with distributed

Bibliography

windings. In *2023 IEEE Workshop on Electrical Machines Design, Control and Diagnosis (WEMDCD)*, pages 1–5. IEEE, 2023.

[166] Pedro Salas-Biedma, Ignacio Gonzalez-Prieto, and Mario J Duran. Current imbalance detection method based on vector space decomposition approach for five-phase induction motor drives. In *IECON 2019-45th Annual Conference of the IEEE Industrial Electronics Society*, volume 1, pages 975–980. IEEE, 2019.

[167] Sathyanarayanan Nandagopal, Hemantha Kumar Ravi, and Lenin Natesan Chokkalingam. Harmonics study of five phase induction machine with different winding approaches for traction. In *2019 IEEE Transportation Electrification Conference (ITEC-India)*, pages 1–4. IEEE, 2019.

[168] Karl J Åström and Björn Wittenmark. *Computer-controlled systems: theory and design*. Courier Corporation, 2013.

[169] Chirag Rohit, Pranav B Darji, and HR Jariwala. A stability assessment and estimation of equivalent damping gain for ssr stability by nyquist stability criterion in dfig-based windfarms. In *2021 31st Australasian Universities Power Engineering Conference (AUPEC)*, pages 1–6. IEEE, 2021.

[170] EI Jury. A simplified stability criterion for linear discrete systems. *Proceedings of the IRE*, 50(6):1493–1500, 1962.

[171] T Nigel Lucas. The bilinear method: a new stability-preserving order reduction approach. *Proceedings of the Institution of Mechanical Engineers, Part I: Journal of Systems and Control Engineering*, 216(5):429–436, 2002.

[172] Jing Ma. *Power system wide-area stability analysis and control*. John Wiley & Sons, 2018.

[173] Adrian Ioinovici. *Power Electronics and Energy Conversion Systems: Fundamentals and Hard-switching Converters. Volume 1*. Wiley Online Library, 2013.

[174] Ahmed AS Mohamed, Alberto Berzoy, and Osama A Mohammed. Experimental validation of comprehensive steady-state analytical model of bidirectional

wpt system in evs applications. *IEEE Transactions on Vehicular Technology*, 66(7):5584–5594, 2016.

[175] Jung-Soo Bae, Tae-Hyun Kim, Seong-Ho Son, Hyoung-Suk Kim, Chan-Hun Yu, and Sung-Roc Jang. Series stacked modular dc–dc converter using simple voltage balancing method. *IEEE Transactions on Power Electronics*, 36(3):2471–2475, 2020.

[176] Lorrana Faria da Rocha, Hans Anders Faraasen, Hendrik Vansompel, and Pål Keim Olsen. Investigation of power electronics converters and architecture for modular hvdc wind generators. In *2022 IEEE International Conference on Power Systems Technology (POWERCON)*, pages 1–6. IEEE, 2022.

[177] Jonas Steffen, Sebastian Lengsfeld, Marco Jung, Bernd Ponick, Mercedes Herranz Gracia, Aristide Spagnolo, Markus Klöpzig, Klaus Schleicher, and Klaus Schäfer. Design of a medium voltage generator with dc-cascade for high power wind energy conversion systems. *energies*, 14(11):3106, 2021.

[178] Martina Baumann and Johann W Kolar. Parallel connection of two three-phase three-switch buck-type unity-power-factor rectifier systems with dc-link current balancing. *IEEE Transactions on Industrial Electronics*, 54(6):3042–3053, 2007.

[179] Ricardo Vidal-Albalate, R Pena, Salvador Añó-Villalba, Enrique Belenguer, and R Blasco-Gimenez. Hybrid full bridge-half bridge mml power converter for hvdc diode rectifier connection of large off-shore wind farms. In *2018 IEEE International Conference on Industrial Technology (ICIT)*, pages 994–999. IEEE, 2018.

[180] Amanda P Monteiro, Cursino B Jacobina, Filipe AC Bahia, and Reuben PR Sousa. Ac-dc power conversion systems for open-end winding pmsm based on vienna rectifiers. In *2019 IEEE Energy Conversion Congress and Exposition (ECCE)*, pages 2156–2163. IEEE, 2019.

[181] Endusa Billy Muhando, Tomonobu Senjyu, Aki Uehara, Toshihisa Funabashi, and Chul-Hwan Kim. Lqg design for megawatt-class wecs with dfig based on

functional models' fidelity prerequisites. *IEEE transactions on energy conversion*, 24(4):893–904, 2009.

[182] Zainab Jamal Mohammed, Saad Enad Mohammed, and Mohammad Obaid Mostafa. Improving the performance of pitch angle control of variable speed wind energy conversion systems using fractional pi controller. In *2022 Iraqi International Conference on Communication and Information Technologies (IICCIT)*, pages 209–215. IEEE, 2022.

[183] Haseeb Rehman, Syed Ali Mohsin, and Abdullah Mughees. Pitch angle control for wind turbines using optimum torque control and real time wind speed. In *2020 IEEE 23rd International Multitopic Conference (INMIC)*, pages 1–6. IEEE, 2020.

[184] Hadi Banakar, Changling Luo, and Boon-Teck Ooi. Steady-state stability analysis of doubly-fed induction generators under decoupled p–q control. *IEE Proceedings-Electric Power Applications*, 153(2):300–306, 2006.

[185] M Ben Slimene. Performance analysis of six-phase induction machine-multilevel inverter with arbitrary displacement. , (4 (eng)):12–16, 2020.

[186] Ayman S Abdel-Khalik, Ahmed M Massoud, and Shehab Ahmed. An improved torque density pseudo six-phase induction machine using a quadruple three-phase stator winding. *IEEE Transactions on Industrial Electronics*, 67(3):1855–1866, 2019.

[187] Pablo Jaen-Sola, Alasdair S McDonald, and Erkan Oterkus. Dynamic structural design of offshore direct-drive wind turbine electrical generators. *Ocean Engineering*, 161:1–19, 2018.

[188] Olorunfemi Ojo. Dynamics and system bifurcation in autonomous induction generators. In *Proceedings of 1994 IEEE Industry Applications Society Annual Meeting*, volume 1, pages 31–37. IEEE, 1994.

[189] Jacek F Gieras. *Electrical machines: fundamentals of electromechanical energy conversion*. Crc Press, 2016.

Bibliography

[190] A Jan Melkebeek. *Electrical machines and drives: fundamentals and advanced modelling.* Springer, 2018.

[191] Alfredo R Muñoz and Thomas A Lipo. Dual stator winding induction machine drive. *IEEE Transactions on Industry Applications*, 36(5):1369–1379, 2000.

[192] Renato OC Lyra and Thomas A Lipo. Torque density improvement in a six-phase induction motor with third harmonic current injection. *IEEE transactions on industry applications*, 38(5):1351–1360, 2002.

[193] O Mykhailiuk. Magnetic field analysis of an induction machine with multiphase stator winding through finite element method. *International Journal of Mechanical Engineering and Technology*, 9(11):789–801, 2018.

[194] Zhiqiao Wu and Olorunfemi Ojo. Optimal magnetic design of the stator windings of dual stator winding squirrel-cage induction machines. In *2009 IEEE Energy Conversion Congress and Exposition*, pages 256–261. IEEE, 2009.

[195] Ignacio Gonzalez-Prieto, Mario J Duran, Federico Barrero, Mario Bermudez, and Hugo Guzmán. Impact of postfault flux adaptation on six-phase induction motor drives with parallel converters. *IEEE Transactions on Power Electronics*, 32(1):515–528, 2016.

[196] Mansour Ojaghi and Vahid Bahari. Rotor damping effects in dynamic modeling of three-phase synchronous machines under the stator interturn faults—winding function approach. *IEEE Transactions on Industry Applications*, 53(3):3020–3028, 2017.

[197] Martin Ćalasan, Mihailo Micev, Ziad M Ali, Ahmed F Zobaa, and Shady HE Abdel Aleem. Parameter estimation of induction machine single-cage and double-cage models using a hybrid simulated annealing–evaporation rate water cycle algorithm. *Mathematics*, 8(6):1024, 2020.

[198] Thomas A Lipo. *Analysis of synchronous machines.* CRC press, 2017.

Bibliography

[199] Angel González-Prieto, Ignacio González-Prieto, Alejandro G Yepes, Mario J Duran, and Jesus Doval-Gandoy. On the advantages of symmetrical over asymmetrical multiphase ac drives with even phase number using direct controllers. *IEEE Transactions on Industrial Electronics*, 69(8):7639–7650, 2021.

[200] Taiwo Samuel Ajayi, Grain Adam, David Campos Gaona, and Olimpo Anaya-Lara. Determination of an asymmetrical nine phase induction machine stator and rotor inductances using winding function approach. In *2023 IEEE Workshop on Electrical Machines Design, Control and Diagnosis (WEMDCD)*, pages 1–6. IEEE, 2023.

[201] Anvar Khamitov and Eric L Severson. Analysis and design of multi-phase combined windings for bearingless machines. In *2021 IEEE energy conversion congress and exposition (ECCE)*, pages 3949–3956. IEEE, 2021.

[202] Ariel Fleitas, Magno Ayala, Osvaldo González, Larizza Delorme, Carlos Romero, Jorge Rodas, and Raul Gregor. Winding design and efficiency analysis of a nine-phase induction machine from a three-phase induction machine. *Machines*, 10(12):1124, 2022.

[203] Archana Nanoty and AR Chudasama. Design and control of multiphase induction motor. In *2011 IEEE International Electric Machines & Drives Conference (IEMDC)*, pages 354–358. IEEE, 2011.

[204] Ahmad Anad Abduallah. *Independent power flow control of multiple energy sources using a single electric machine.* Liverpool John Moores University (United Kingdom), 2019.